



HAL
open science

Biocompatibility improvement conferred by the immobilization of a CD31 peptide on endovascular stents

Charlotte Rasser

► **To cite this version:**

Charlotte Rasser. Biocompatibility improvement conferred by the immobilization of a CD31 peptide on endovascular stents. Biochemistry, Molecular Biology. Université Sorbonne Paris Cité, 2017. English. NNT : 2017USPCC317 . tel-02385280

HAL Id: tel-02385280

<https://theses.hal.science/tel-02385280>

Submitted on 2 Dec 2019

HAL is a multi-disciplinary open access archive for the deposit and dissemination of scientific research documents, whether they are published or not. The documents may come from teaching and research institutions in France or abroad, or from public or private research centers.

L'archive ouverte pluridisciplinaire **HAL**, est destinée au dépôt et à la diffusion de documents scientifiques de niveau recherche, publiés ou non, émanant des établissements d'enseignement et de recherche français ou étrangers, des laboratoires publics ou privés.

Thèse de doctorat
de l'Université Sorbonne Paris Cité

Préparée à l'Université Paris Diderot

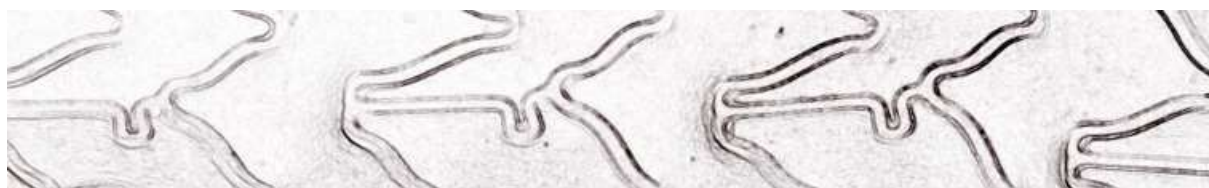
École doctorale 562 – BioSPC

Laboratory for Vascular Translational Science (Inserm U1148)

**Biocompatibility improvement conferred by the
immobilization of a CD31 peptide on endovascular stents**

Par Charlotte Rasser

Thèse dirigée par Giuseppina Caligiuri



Soutenue publiquement à Paris le 27 novembre 2017 devant un jury composé de :

Président	Dr Yves Colin-Aronovicz	CNRS, UMR S 1134
Rapporteur	Pr Imo Hoefler	University Medical Center Utrecht
Rapporteur	Dr Nicolas Blanchemain	Université Lille 2, Inserm U1008
Examineur	Pr Didier Léonard	Université Lyon 1, UMR 5280
Directrice de thèse	Dr Giuseppina Caligiuri	LVTS (Inserm U1148)
Invité	Dr Cédric Guyon	Chimie Paris, UMR 8247

Mes travaux de thèse ont été menés au sein du laboratoire :

Inserm U1148, Laboratory for Vascular Translational Science (LVTS)

Équipe 1, « Cardiovascular Immunobiology »

Hôpital Bichat-Claude Bernard

46 rue Henri Huchard

75018 Paris

FRANCE

Résumé

Au cours des dernières décennies, les stents coronaires et les stents déviateurs de flux intracrâniens ont révolutionné le traitement endovasculaire de deux pathologies artérielles différentes : la maladie coronarienne et les anévrismes intracrâniens. Ces deux types d'endoprothèses métalliques ont des mécanismes de fonctionnement différents, mais ils sont tous deux associés à des complications qui découlent de problèmes de biocompatibilité. En particulier, la couverture rapide de ces endoprothèses par des cellules endothéliales présentant un phénotype anti-inflammatoire et anti-thrombotique est cruciale pour leur intégration à l'interface vaisseau/sang. Par conséquent, le développement de solutions visant à améliorer l'endothélialisation et l'intégration de ces deux types de stents dans la paroi vasculaire représenterait un progrès majeur dans leur domaine respectif.

Dans ce contexte, cette thèse porte sur l'immobilisation d'une molécule bioactive à la surface de stents coronaires et de stents déviateurs de flux, afin de résoudre leurs problèmes de biocompatibilité. La molécule bioactive utilisée est un peptide synthétique, appelé P8RI, qui promeut les fonctions régulatrices de la glycoprotéine transmembranaire CD31 : l'inhibition de l'activation des plaquettes et des leucocytes, ainsi que l'amélioration de la survie, de la migration et de la fonction de barrière des cellules endothéliales.

La première partie de ce travail de thèse a consisté à développer un procédé d'immobilisation du P8RI sur des stents métalliques. Nous avons successivement adopté trois approches : l'immobilisation directe du peptide sur des surfaces d'alliage fonctionnalisées par plasma ; le dépôt chimique en phase vapeur assisté par plasma d'une couche intermédiaire de polymère ; et le dépôt d'une couche de polydopamine par auto-polymérisation, suivi de l'immobilisation d'un bras d'ancrage et de la liaison du P8RI par chimie click sans cuivre.

Nous avons ensuite réalisé une évaluation *in vitro* de la biocompatibilité des surfaces d'alliage ainsi revêtues, en termes de propriétés anti-thrombotiques, anti-inflammatoires et pro-endothélialisation. Les surfaces sur lesquelles le P8RI avait été immobilisé ont montré une tendance à diminuer l'adhésion plaquettaire, à améliorer l'adhérence et la fonction de barrière de cellules endothéliales vasculaires humaines, et à promouvoir un phénotype anti-inflammatoire et anti-thrombotique chez ces dernières.

Enfin, nous avons évalué *in vivo* des stents coronaires et déviateurs de flux recouverts de P8RI. Les stents coronaires ont été implantés dans des artères coronaires de porcs, et les résultats préliminaires ont montré une endothélialisation plus complète et une moindre densité de leucocytes adhérents sur les stents recouverts de P8RI que sur les témoins. Quant aux stents déviateurs de flux recouverts de P8RI, implantés dans un modèle d'anévrisme carotidien induit par incubation d'élastase chez le lapin, ils ont été associés à la formation d'une néointima plus épaisse et mieux organisée que sur les témoins, en particulier au niveau du collet anévrismal, ce qui implique de moindres risques de persistance du flux sanguin et de rupture d'anévrisme.

Abstract

Over the last decades, coronary stents and intracranial flow diverting stents have revolutionized the endovascular treatment of two different arterial pathologies: coronary artery disease and intracranial aneurysms. The working mechanisms of these metallic endoprotheses are different but both are associated with complications stemming from biocompatibility issues. In particular, the rapid covering by endothelial cells presenting an anti-inflammatory and anti-thrombotic phenotype is key to the integration of the endoprosthesis at the blood/vessel interface. Thus, the development of solutions to improve the endothelialization and the integration of these two types of stents in the vessel wall would represent a major progress in their respective field.

In this context, this thesis work deals with the immobilization of a bioactive molecule on coronary stents and flow diverting stents in order to solve their biocompatibility issues. The bioactive molecule that we used is a synthetic peptide, named P8RI, which promotes the regulatory functions of the transmembrane glycoprotein CD31: the inhibition of platelets and leukocytes activation, as well as the enhancement of endothelial cell survival, migration and barrier function.

The first part of this thesis work consisted in the development of a process for the immobilization of P8RI on metallic stents. We adopted three successive approaches: the direct immobilization of the peptide on plasma-functionalized alloy surfaces; the plasma-enhanced chemical vapor deposition of an intermediate polymeric layer; and the deposition of a polydopamine coating by self-polymerization, followed with the immobilization of a linker and the binding of P8RI by copper-free click chemistry.

We then carried out an *in vitro* evaluation of the biocompatibility of the resulting coated alloy surfaces, in terms of anti-thrombotic, anti-inflammatory, and pro-endothelialization properties. The surfaces on which P8RI had been immobilized were shown to exhibit a tendency to decrease platelet adhesion, increase endothelial cell adhesion and barrier function, and promote an anti-inflammatory and anti-thrombotic phenotype in human vascular endothelial cells.

Finally, coronary stents and flow diverting stents were evaluated *in vivo*. Coronary stents were implanted in the coronary arteries of farm pigs, and preliminary results showed a more complete endothelialization and a lesser density of adherent leukocytes on 'P8RI-coated' stents than on the controls. 'P8RI-coated' flow diverting stents were implanted in a rabbit elastase-induced carotid aneurysm model. Compared with the controls, they were associated with the formation of a thicker and better organized neointima, in particular on the stent struts in front of the aneurysm neck, which implies lesser risks of persistence of blood flow and aneurysm rupture.

Acknowledgements

I would like to offer my sincere thanks to the members of the jury, who have kindly agreed to examine my work: Yves Colin Aronovicz, Didier Léonard, and in particular my '*rapporteurs*' Nicolas Blanchemain and Imo Hoefler. I am very grateful to the four of you for the valuable and complementary perspectives that you have accepted to bring on my work.

Je remercie également chaleureusement Didier Letourneur, directeur du LVTS, qui a été mon premier contact au laboratoire et qui m'a orientée vers ma future directrice de thèse. Merci de m'avoir accueillie au sein de l'unité, et merci de ton engagement à en faire un lieu de travail de qualité, mais aussi convivial et humain.

Mille mercis à Pina, ma directrice de thèse. Ton enthousiasme, ta disponibilité, tes encouragements, et la clarté que tu prends toujours soin d'apporter à tes explications, font de toi une encadrante hors pair. Tu m'as énormément appris sur la manière de présenter un projet, d'en prioriser les étapes, d'étayer un raisonnement, d'envisager et de justifier tous les aspects d'une manip, bref, de mener un projet scientifique. Je suis très heureuse d'avoir été encadrée par toi, et je tiens à t'en remercier du fond du cœur.

Merci également à Tony, qui dirige notre équipe au sein du LVTS. Comme tous mes collègues et camarades du quatrième, j'ai énormément de respect pour tes connaissances et ton jugement scientifiques, et je te suis très reconnaissante de la bienveillance et de la disponibilité avec lesquelles tu assumes tes fonctions de chef d'équipe. Merci de supporter nos taquineries chroniques sur ta technophilie (en particulier, je pense qu'on peut qualifier de courageuse ta décision d'utiliser OneNote en réunion d'équipe pour la première fois), d'encourager les discussions, scientifiques et autres, au sein de l'équipe, et d'avoir écouté avec amusement mes occasionnels jugements lapidaires sur tel ou tel film, écrivain ou homme politique.

Merci à tous les membres du quatrième évidemment, qui êtes devenus pour moi au cours de ces trois ans quelque chose comme une entité hybride, située quelque part entre collègues, famille et amis sur la carte des relations humaines :

Alexia, dont le rire trop fort me manquera tellement. Je suis certaine que ta passion et ton intelligence te mèneront où tu auras envie d'aller. J'espère juste que ce sera dans un labo et pas

derrière un bar en Australie, parce que la recherche a besoin de gens comme toi (peut-être que la mixologie aussi mais là-dessus je ne saurais pas dire).

Guillaume, pilier du quatrième (et certainement du futur bar d'Alexia si elle en ouvre un mais là n'est pas la question), que ferions-nous sans tes compétences, ta bonne volonté, et surtout, surtout, ton indéfectible bonne humeur ? Bon vent, Guigui, comme on dit dans ta chère région d'adorateurs du beurre !

Julie, grande maîtresse de la technique du Ver de Terre (et accessoirement des dosages par billes, de la culture cellulaire, des manips en flux...), merci pour ton énergie, ta conscience professionnelle et tes Minutes On s'en Fout !

Anh, dont j'ai admiré les doigts de fée (ou plutôt de microchirurgienne) et le caractère bien trempé, merci pour ton aide sur les manips in vivo !

Merci à Marion pour tes marquages, et pour m'avoir montré il y a maintenant longtemps les rudiments de la culture cellulaire !

Merci à Lele, qui a connu les joies de la préparation de dizaines de petits disques pour le recouvrement par polydopamine. On aurait aimé te garder plus longtemps avec nous, mais on est heureux que tu te plaisés dans ton nouveau travail !

Kévin, qui a mis la barre tellement haut avec le contenu de sa thèse conclue quelques mois après mon arrivée, merci pour nos quelques longues discussions du soir et pour toutes tes vanes !

Merci à Varouna pour les manips sur les souris, je te souhaite de faire une super thèse, tu la mérites largement par tes capacités de travail impressionnantes !

Merci à Francesco, qui lui vient d'achever une super thèse méritée par ses longues heures de travail et sa persévérance. Félicitations pour ce que tu as accompli et bonne chance dans ta carrière de chercheur !

Aurélié, qui soutiendra juste après moi, bravo pour le très beau travail que tu as réussi à faire en thèse tout en assurant tes fonctions d'anapath, et merci pour ton humour acide !

Merci à Jamila pour ses recettes maison de gels de collagène, à Greg pour ses conseils avisés, à Sandrine pour son initiation à la culture microbiologique, à Devy pour son aide indispensable sur l'IRM (et à Sandrine et Devy pour leurs organisations spontanées de soirées au bar), à Marie pour nous faire rire des bêtises de son bébé sumo, et à Alice à qui je souhaite bonne chance dans la voie qu'elle s'est choisie !

Merci à Véronique O., qui m'a appris tant de choses quand je ne savais encore rien. C'est toujours un plaisir de travailler avec quelqu'un d'aussi efficace, dynamique et compétent que toi – et de déjeuner avec quelqu'un d'aussi vivant et sympathique.

Merci à Christine, l'experte du MEB, pour ses longues heures passées à acquérir de magnifiques images d'artères de cochons (et autres disques trempés dans le sang). Merci aussi pour ton travail de responsable hygiène et sécurité !

Je remercie Jean-Baptiste Michel, ex-directeur du LVTS et de l'ancien U698, sans qui les expériences sur les lapins n'auraient pas été possibles à l'unité.

Merci à Aymeric et Jildaz, les neuroradiologues à qui nous devons toutes les expériences sur les lapins, pour leur irremplaçable contribution au projet P8RI.

Merci à Corinne, Asma et Hanine, vous qui faites tourner l'unité et sans qui aucun projet ne pourrait être mené. Merci pour l'énorme travail que vous abattez tout en répondant à nos demandes intempestives de feutres et autres cahiers de labo – sans parler des courses DHL d'urgence.

Je remercie tous les membres de l'unité que j'ai eu l'occasion de côtoyer au cours de ces trois années, et avec lesquels j'ai pu avoir des échanges – scientifiques ou non – qui m'ont beaucoup apporté : Frédéric Chaubet, à qui l'on doit l'idée originelle d'immobiliser le P8RI sur des stents, Benoît Ho-Tin-Noé, qui m'a entre autres appris à utiliser le microscope, Martine Jandrot-Perrus, Liliane, Stéphane, Catherine, Yael, Marie-Anne, Lucas, Maya, Jessica, Audrey, Louis, Joana, Teresa...

Tous mes remerciements à Michael Tatoulian, pour m'avoir accueillie dans son laboratoire 2PM, et conseillée pendant toute la première partie de ma thèse.

Un grand merci à Cédric, qui m'a encadrée à Chimie Paris sur toute la partie « plasma » de ma thèse, avec compétence et bonne humeur, et dont je suis très heureuse qu'il puisse assister à ma soutenance en tant qu'invité.

Merci à tous les membres de 2PM :

Fred, à l'humour si léger qu'il en ferait passer un menu Quick pour une gaufrette sans sucre, merci pour tes montages photo et la bonne ambiance que tu contribues à créer.

Alex, merci pour nos innombrables discussions du temps où tu n'étais encore qu'un vieux thésard dont je partageais le bureau, et bonne chance dans ta carrière (de volleyeur, bien sûr).

ACKNOWLEDGEMENTS

Kader, dernier membre du trio du bureau des courants d'air, merci également pour nos discussions au labo et au billard, et pour les private jokes glissées dans des thèmes de spectacles d'impro. À bientôt à Paris (probablement) ou à Palaiseau (moins probablement) !

Erick ! Ton départ pour le Mexique a laissé un grand vide derrière toi, dans les couloirs de 2PM comme dans l'arrière-salle du Hurling Pub. Merci pour ton amitié et ton irremplaçable folie !

Merci à Mengxue pour son implication dans l'école de Chimie Paris et dans 2PM, et bonne chance dans ta jeune carrière de chercheuse !

Merci à Olivier et ses réparties du tac au tac, à Bradley, Inès, Rafik, Guillaume Schelcher, Stéphanie Ognier, Siméon Cavadias, Daniel Morvan et tous ceux grâce à qui 2PM reste un labo où il fait bon (bien) travailler.

Enfin, une pensée pour la (plus si) nouvelle génération, P.-A., Julien, Jonathan, Aurélien, qui a su installer dans les nouveaux locaux de l'IPGG le même genre d'ambiance de travail agrémenté de « pauses humour » que ce que nous connaissions dans les anciens bureaux de Chimie Paris.

Je tiens à remercier chaleureusement Diego Mantovani, pour sa collaboration tout au long de ce projet et pour m'avoir accueillie au LBB à Québec durant les trois mois que j'y ai passés.

Tous mes remerciements également à Pascale, qui m'a appris les bases de l'analyse XPS et a réalisé la plupart des acquisitions de spectres XPS de ce projet. Tu as rendu notre collaboration à la fois utile et agréable par ton efficacité, et j'ai pu apprécier lors de mon séjour au LBB à quel point tu étais précieuse au laboratoire, par ta compétence, ton dynamisme, ton humour et l'attention que tu portes à l'encadrement des projets des étudiants.

Merci à Sergio, qui m'a accueillie avec amitié au LBB et m'a patiemment montré le fonctionnement des nombreux appareils dont j'ai eu besoin. Merci de m'avoir aidée durant tout ce séjour, notamment pendant nos longues et minutieuses sessions de ponçage de supports en résine, et merci de m'avoir fait découvrir dès mon arrivée l'un des plus beaux sites des alentours de Québec !

Merci à tous les membres du LBB et du LIS, Carlo, Stéphane, Lucie, Andrée-Anne, Ranna, Ludivine, Héloïse, Laurence, Caroline, Stéphanie, Vanessa, Éléonore, Daniele, Alfredo, Nina, Livia, Désirée, et tous les autres. Merci pour votre aide, et surtout pour votre accueil, au sein du labo et dans les nombreuses sorties que j'ai eu la chance de faire avec vous.

Merci à Éric Largen et Marie Pauchard, chez Balt, pour votre implication dans le projet et les liens de collaboration étroite que nous avons pu nouer.

Je remercie Bijan Ghaleh, qui nous a ouvert les portes de son laboratoire à l'école vétérinaire d'Alfort, et Romain Gallet, Alain Bizé et Lucien Sambin, qui y ont effectué les implantations de stents chez des cochons, et ont réussi à s'adapter à toutes les contraintes d'organisation et aux modifications du programme devenues nécessaires en cours de route.

Tous mes remerciements à Sylvie Bay, à qui nous devons l'idée d'utiliser un bras d'ancrage basé sur la chimie click sans cuivre pour immobiliser le peptide sur la polydopamine. Merci beaucoup pour la rapidité et la précision de vos réponses à nos nombreuses questions.

Merci à tous ceux qui ont bien voulu accorder du temps et de l'intérêt à mon projet : Julie Le Faouder, pour le temps qu'elle a volontiers accepté de consacrer aux analyses en MALDI-ToF de mes échantillons, Nadège Anizan, qui nous a aidés à utiliser la TEP/IRM, Graciela, qui a transmis à Christine et Guillaume la technique d'inclusion des artères stentées en PMMA, ainsi qu'Armelle Babonneau (Abbott), Dorothée Faille, Laurent Feldman, Erwann Guenin, Josette Legagneux, Gérard Partouche, François Rouzet, Laurent Spelle, Olivier Thibaudeau, et ceux que j'oublie de nommer ici.

Je tiens également à remercier les organismes qui ont financé ce projet : l'AMX, l'ANR, la FRM. Merci aussi à l'école doctorale BioSPC, au service de ressources humaines de Paris Diderot, au CFDip et à ses intervenants (Pierre Girard en particulier), à qui je dois la partie « scolarité » de ma thèse. Je remercie également les personnes impliquées dans le concours « Ma Thèse en 180 secondes », à Paris 7, SPC (Cécile Draï, Sofia Nadir, et Fabienne Berriau en particulier) et au niveau national, pour m'avoir permis de participer à cette expérience exceptionnelle et très formatrice.

J'adresse un grand merci aux quatre stagiaires avec lesquels j'ai eu la chance de travailler au cours de ma thèse :

Caroline, qui a réussi à faire avancer les manip à Chimie Paris et au LVTS même pendant mon séjour au Québec. Ça a été un plaisir de travailler avec toi, et je ne me fais aucun souci pour la fin de tes brillantes études et ta future carrière professionnelle.

Sylvain, qui a lui aussi dû se montrer très autonome, alors que je passais l'essentiel de mon temps au LVTS et lui chez 2PM, et dont j'ai pu apprécier le sérieux, la motivation et la grande facilité à s'intégrer. Bonne chance pour ta thèse !

Pierluigi, qui m'en a largement autant appris sur la chimie organique que ce que j'ai pu lui transmettre en matière d'expériences biologiques sur les plaquettes et les cellules endothéliales – c'est à lui que nous devons le développement de l'immobilisation du P8RI sur la polydopamine.

ACKNOWLEDGEMENTS

Je sais que tu as profité à fond de ton expérience parisienne, et je suis sûre que tu sauras mettre ta maturité et ta détermination au service de ton projet de thèse.

Neïla, qui a passé d'innombrables heures à manipuler, avec patience et humour, des dizaines de petits disques de cobalt-chrome, avant de participer enfin à l'implantation de stents coronaires chez des cochons. Félicitations pour ton mémoire très bien écrit, merci beaucoup pour ton implication dans le projet au-delà de ton stage, qui a rendu possibles les manip *in vivo* pendant ma rédaction de thèse, et bonne continuation !

Enfin, je tiens à remercier ma famille, mes amis (les quelques très vieux et d'autant plus précieux, les ex-taupins et/ou X et/ou improvisateurs, et les autres), et le petit espace entre les deux, de leur soutien, de leur humour, mais aussi de leurs intérêts respectifs pour les sujets les plus divers et les plus éloignés de la recherche sur les stents.

Table of contents

RÉSUMÉ	5
ABSTRACT	7
ACKNOWLEDGEMENTS	9
LIST OF ABBREVIATIONS	18
LIST OF FIGURES	20
LIST OF TABLES	23
INTRODUCTION	25
I. STENTS	27
I.1. CORONARY STENTS	27
I.1.a. Origins and evolution of coronary artery disease	27
I.1.b. Endovascular treatment of coronary artery disease: balloons and scaffolds	31
I.1.c. Current challenges for coronary stents	33
I.2. FLOW DIVERTING STENTS	34
I.2.a. Intracranial aneurysms	34
I.2.b. Historical treatments of intracranial aneurysms	36
I.2.c. Design and performances of flow diverting stents	37
I.2.d. Towards better flow diverting stents	39
II. CD31 AND AGONIST PEPTIDES	41
II.1. GENERAL PRESENTATION OF CD31	41
II.2. CD31 ACTIVATION AND SIGNALING PATHWAYS	42
II.3. CELLULAR FUNCTIONS OF CD31	43
II.3.a. CD31 in platelets	44
II.3.b. CD31 in leukocytes	44
II.3.c. CD31 in endothelial cells	45
II.4. CD31 SHEDDING AND IDENTIFICATION OF RESCUE AGONIST PEPTIDES	46
II.4.a. CD31 shedding	46
II.4.b. CD31 agonist peptides	47
III. RATIONALE OF THE THESIS WORK	49
IV. STENT COATING WITH BIOACTIVE MOLECULES	50
IV.1. ELUTION VS IMMOBILIZATION	50
IV.2. POLYMER COATINGS	51
IV.2.a. Usefulness and drawbacks of polymer coatings	51
IV.2.b. Plasma-polymerized HMDSN	51
IV.2.c. Polydopamine	52
IV.3. COATING TECHNIQUES	52
IV.3.a. Plasma-assisted treatments	53
IV.3.b. Polydopamine deposition	54
OBJECTIVES OF THE THESIS WORK	55
EXPERIMENTAL WORK	57
I. IMMOBILIZATION OF THE CD31 AGONIST PEPTIDE ON ALLOY SURFACES	59
I.1. DIRECT AMINATION BY LOW PRESSURE PLASMA	59

I.1.a. N ₂ -H ₂ low-pressure plasma treatment increases the nitrogen content of CoCr samples but also introduces surface contaminations	61
I.2. DIRECT AMINATION BY ATMOSPHERIC PRESSURE PLASMA	67
I.2.a. N ₂ -H ₂ APPJ treatment increases the nitrogen content of CoCr samples with high variability	68
I.2.b. An optimized electropolishing treatment removes the zinc contamination and smoothens the surface of the CoCr samples	71
I.2.c. Derivatization provides no evidence of amines on the surface of CoCr disks after N ₂ -H ₂ atmospheric pressure plasma treatment	76
I.3. HMDSN FILM DEPOSITION BY ATMOSPHERIC PRESSURE PLASMA	77
I.3.a. Characterization of the PP-HMDSN coatings	78
I.3.b. Thickness estimation of the PP-HMDSN coatings	82
I.3.c. The coating does not withstand 7 days of ageing test in flow conditions	83
I.4. POLYDOPAMINE-BASED COATINGS	86
I.4.a. Polydopamine self-assembly	86
I.4.b. Direct immobilization of the peptide	89
I.4.c. Immobilization of the peptide with the help of a linker	92
I.4.d. Immobilization of P8RI azide on PDA coatings with the help of the BCN-amine linker	94
I.4.e. Stability of the PDA-linker-P8RI coating in one-month ageing test in liquid medium	97
II. <i>IN VITRO</i> EVALUATION OF THE BIOCOMPATIBILITY OF P8RI-COATED SURFACES	98
II.1. HEMOCOMPATIBILITY	98
II.1.a. The bare and coated CoCr surfaces do not cause hemolysis	98
II.1.b. The “PDA+P8RI” coating tends to reduce platelet adhesion	101
II.2. ENDOTHELIALIZATION	105
II.2.a. The “PDA + P8RI” coating favors rapid and functional endothelialization of CoCr surfaces	108
II.2.b. The “PDA + P8RI” coating tends to induce an anti-inflammatory and anti-thrombotic phenotype in endothelial cells	109
III. <i>IN VIVO</i> EVALUATION OF THE BIOCOMPATIBILITY OF P8RI-COATED SURFACES	111
III.1. IMPLANTATION OF CORONARY STENTS IN FARM PIGS	111
III.2. IMPLANTATION OF FLOW DIVERTING STENTS IN A RABBIT ELASTASE ANEURYSM MODEL	117
DISCUSSION	125
I. STRATEGIC CHOICES AND CHARACTERISTICS OF THE P8RI COATINGS	127
I.1. DIRECT BINDING OF P8RI ON THE ALLOY OR USE OF AN INTERMEDIATE LAYER?	127
I.2. WHY CHOOSE PDA RATHER THAN POLYMERS ALREADY USED FOR STENTS?	127
I.3. CHOICE OF THE STRATEGY FOR THE IMMOBILIZATION OF P8RI ON PDA	129
I.4. IMPORTANCE OF THE THICKNESS OF THE COATING IN THE “PDA-P8RI” STRATEGY	130
I.5. ADHESION AND STABILITY OF THE “PDA + P8RI” COATING	131
II. TECHNICAL CONSIDERATION: CELL-BASED ASSAYS ON METALLIC SAMPLES	132
III. SCIENTIFIC AND INDUSTRIAL CONTEXT OF THE PROJECT	133
III.1. ALTERNATIVE APPROACHES TO IMPROVE STENTS ENDOTHELIALIZATION	133
III.2. NEXT GENERATION STENTS: A HIGHLY COMPETITIVE MARKET	134
IV. PERSPECTIVES	136
IV.1. “PDA+P8RI”-BASED DUAL STENT COATING	136
IV.2. WHAT WILL THE STENT OF THE FUTURE BE?	137
GENERAL CONCLUSION	139
BIBLIOGRAPHY	141
ANNEX	163

List of abbreviations

AFM	Atomic force microscopy
APPJ	Atmospheric-pressure plasma jet
ATR	Attenuated total reflection
BCN	Bicyclo[6.1.0]nonyne
BCR	B cell receptor
BMS	Bare metal stent
BSA	Bovine serum albumin
CAD	Coronary Artery Disease
CCP	Capacitively coupled plasma
CoCr	Cobalt-chromium alloy
DES	Drug-eluting stents
DIPH	Delayed intraparenchymal hemorrhage
EC	Endothelial cell
ECM	Extracellular matrix
EDC	1-ethyl-3-(3-dimethylaminopropyl) carbodiimide hydrochloride
FDS	Flow diverting stent
FITC	Fluorescein isothiocyanate
FTIR	Fourier transform infrared spectroscopy
HCAEC	Human coronary artery endothelial cell
HMDSN	Hexamethyldisilazane
HMDSN	Hexamethyldisilazane
HPS	Hematoxylin-phloxine-saffron stain
HUVEC	Human umbilical vein endothelial cell
ICP	Inductively coupled plasma
Ig	Immunoglobulin
ISR	In-stent restenosis
ITAM	Immunoreceptor Tyrosine-Based Activation Motif
ITIM	Immunoreceptor tyrosine-based inhibitory motif

LDL	Low-density lipoproteins
PAI-1	Plasminogen Activator Inhibitor-1
PBS	Phosphate buffer saline
PCI	Percutaneous coronary intervention
PDA	Polydopamine
PECAM-1	Platelet-Endothelial Cell Adhesion Molecule-1 (CD31)
PECVD	Plasma-enhanced chemical vapor deposition
PEG	Polyethylene glycol
PMMA	Poly(methyl methacrylate)
POBA	'Plain old' balloon angioplasty
PP	Plasma-polymerized
PtCr	Platinum-chromium alloy
SEM	Scanning Electron Microscopy
SH2	Src homology 2
SHP	SH2-containing phosphatases
SIA	N-Succinimidyl iodoacetate
SKF	Src family kinase
SMC	Smooth muscle cell
s-NHS	N-hydroxysulfosuccinimide
SPAAC	Strain-promoted alkyne-azide cycloaddition
SPANC	Strain-promoted alkyne-nitrone cycloaddition
TCR	T cell receptor
TEOS	Tetraethyl orthosilicate
TFPI	Tissue Factor Pathway Inhibitor
VCAM-1	Vascular Cell Adhesion Molecule-1
VSMC	Vascular smooth muscle cell
XPS	X-ray photoelectron spectroscopy
αSMA	Alpha-smooth muscle actin

List of figures

Figure 1. Structure of an artery wall.....	27
Figure 2. Progression of atherosclerosis.	28
Figure 3. Schematic representations of positive and negative arterial remodeling.....	30
Figure 4. Coronary arteries.	30
Figure 5. Stent deployment	32
Figure 6. Schematic drawings of aneurysms.....	34
Figure 7. Major localization of intracranial aneurysms.....	35
Figure 8. Most common treatments of intracranial aneurysms.....	36
Figure 9. Schematic representation of a flow diverting stent in an artery.....	37
Figure 10. Schematic structure of CD31.....	41
Figure 11. CD31 activation and signaling pathway	43
Figure 12. The CD31-derived peptide maintains a cluster of shed CD31.	47
Figure 13. Representation of the structures of P8RI and P8F.	48
Figure 14. Immobilization reaction of P8RI on an aminated alloy surface.	59
Figure 15. Schematic drawing of an ICP-RF plasma reactor.....	61
Figure 16. Photograph of the ICP-RF low-pressure plasma reactor used in this study.	61
Figure 17. Example of deconvolution of an XPS high-resolution spectrum.....	63
Figure 18. C/O ratio and nitrogen percentage of CoCr disks after different plasma treatments.	65
Figure 19. Representative high-resolution XPS spectra of nitrogen peaks on N ₂ -H ₂ plasma-treated CoCr samples.	66
Figure 20. Schematic drawing of the atmospheric-pressure plasma jet.	67
Figure 21. Photograph of the atmospheric-pressure plasma reactor.....	68
Figure 22. Schematic diagram of the trajectory of the APPJ nozzle above a 20 mm diameter CoCr disk.....	69
Figure 23. Nitrogen surface percentage of CoCr disks after different N ₂ -H ₂ treatments by APPJ.70	
Figure 24. Principle of electropolishing.	71
Figure 25. Photograph of a CoCr disk after excessively intensive electropolishing	72
Figure 26. SEM pictures of the edges of CoCr disks.....	73
Figure 27. SEM pictures of CoCr samples after different surface treatments.	73
Figure 28. AFM pictures of CoCr disks.....	75
Figure 29. Representation of the derivatization reaction between the SIA and the aminated CoCr surface.....	76
Figure 30. Surface atomic percentages of CoCr disks.....	77

Figure 31. Structure of the HMDSN molecule.....	77
Figure 32. ATR principle.....	79
Figure 33. SEM pictures of PP-HMDSN-coated CoCr disk.....	79
Figure 34. AFM pictures of PP-HMDSN-coated CoCr disk.....	80
Figure 35. Representative FTIR spectrum of a PP-HMDSN coating.....	81
Figure 36. Elemental composition of PP-HMDSN-coated CoCr disks.....	81
Figure 37. Schematic view of the dynamic test bench.....	83
Figure 38. SEM pictures of a PP-HMDSN-coated CoCr disk after a 7-day ageing test in flow conditions.....	85
Figure 39. Photographs of dopamine solution and PDA.....	87
Figure 40. Representative FTIR spectra of bare and PDA-coated CoCr disks.....	88
Figure 41. XPS survey spectra of bare and PDA-coated CoCr disks.....	89
Figure 42. Schematic representation of the binding of the peptide to the PDA coating.....	90
Figure 43. Unmodified and iodinated L-tyrosines.....	91
Figure 44. XPS survey spectra of PDA-coated and 'PDA + iodinated P8RI' CoCr disks.....	91
Figure 45. Cycloaddition with azide (SPAAC) or nitrene (SPANAC).....	93
Figure 46. Linker-mediated immobilization of P8RI on PDA.....	94
Figure 47. Detection of the immobilized fluorescent P8RI by fluorescence microscopy.....	95
Figure 48. O/C and N/C surface ratios of coated CoCr disks.....	96
Figure 49. Elemental composition of PDA-linker-P8RI" coated samples after ageing in PBS.....	97
Figure 50. Quantification of soluble molecules in the supernatants of endothelial cells cultured on coated CoCr samples.....	98
Figure 51. Visual summary of the protocol used for the hemolysis assay.....	99
Figure 52. Photograph of a microplate filled with platelet-poor plasma at the end of a hemolysis assay.....	100
Figure 53. Hemolysis ratios after 1h or 24h incubation.....	100
Figure 54. Visual summary of the platelet adhesion assay protocol.....	101
Figure 55. Principle of immunofluorescence.....	101
Figure 56. Fluorescence microscopy photographs of adherent platelets on CoCr disks.....	104
Figure 57. Visual summary of the endothelial cell growth assay.....	105
Figure 58. Principle of the multiplex bead array assay.....	106
Figure 59. Immunostained HCAEC after 2 days of culture on CoCr disks.....	108
Figure 60. Results of a multiplex assay analysis of cell culture supernatants from a representative experiment.....	109
Figure 61. Results of multiplex assay analyses of cell culture supernatants.....	110
Figure 62. Coronary arteries.....	113

LIST OF FIGURES

Figure 63. Angiograms of a stent implantation procedure 113

Figure 64. Photograph of a stented porcine coronary artery..... 114

Figure 65. SEM images of a “PDA-P8RI” stent in a porcine coronary artery 115

Figure 66. SEM images of a “Plasma-P8RI” stent in a porcine coronary artery. 115

Figure 67. SEM images of a drug eluting stent in a porcine coronary artery 116

Figure 68. SEM images of a bare metal stent in a porcine coronary artery. 116

Figure 69. Creation of the rabbit elastase aneurysm model..... 117

Figure 70. Photograph of an explanted stented artery embedded in PMMA. 119

Figure 71. SEM images of a FDS implanted in the subclavian artery of a rabbit..... 120

Figure 72. Histological sections of implanted FDSs stained with Masson’s trichrome. 122

Figure 73. Histological sections of implanted FDSs immunostained for α SMA..... 123

Figure 74. Thickness evolution of PDA coating on Si as measured by AFM of patterned surfaces.
..... 130

Figure 75. Evolution of the prices of the BMSs and DESs reimbursed by the French social security
system between 2003 and 2017..... 136

List of tables

Table 1. Flow diverting stents currently in use in Europe.	39
Table 2. Parameters used for the plasma treatments.....	62
Table 3. Surface atomic percentages of CoCr disks after different treatments.....	64
Table 4. Elemental composition of the L-605 CoCr alloy.....	64
Table 5. Parameters of the plasma treatments performed by APPJ for the direct amination of CoCr samples.	69
Table 6. Surface atomic percentages of ultrasound cleaned CoCr disks, after different atmospheric-pressure N ₂ -H ₂ plasma treatments.	70
Table 7. Composition of the electropolishing solution used in this study.	72
Table 8. Surface atomic percentages of ultrasound cleaned and electropolished CoCr samples.	74
Table 9. Parameters used for the plasma-enhanced chemical vapor deposition of HMDSN by APPJ.	78
Table 10. Comparison between the parameters used for the deposition of the PP-HMDSN coatings presented in this thesis work, and the PP-TEOS coatings on which thickness measurements were performed by ellipsometry.	82
Table 11. Properties of the different liquid media considered for ageing tests.	84
Table 12. Average surface atomic percentages of bare and PDA-coated CoCr disks	89
Table 13. Surface atomic percentages of coated CoCr disks.....	91
Table 14. Theoretical and experimental elemental ratios of coatings.	96
Table 15. Reagents used in the immunofluorescence protocol.....	102
Table 16. Drug-eluting stents included in the list of products reimbursed by the French social security system.....	128

Introduction

I. Stents

This work aims at improving the biocompatibility of two types of arterial endoprostheses: the balloon-inflatable coronary stents and the self-expanding intracranial flow diverting stents. In order to set the stage for the presentation of my experimental work, the pathologies that led to the development of these stents will be briefly presented, and the current challenges associated with the use of these medical devices will be detailed.

I.1. Coronary stents

I.1.a. Origins and evolution of coronary artery disease

Coronary stents are used for the revascularization of obstructed coronary arteries. The obstruction of the coronary lumen area, called “stenosis” is caused by atherosclerosis, a chronic and multifactorial pathologic process of the arterial wall.

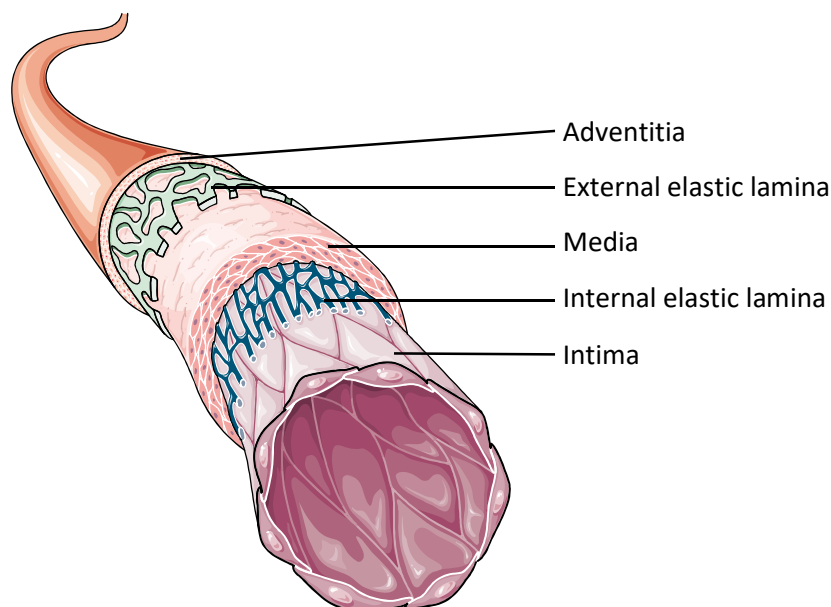


Figure 1. Structure of an artery wall. Picture from Servier Medical Art image bank.

The arterial wall is made of three layers, as shown on Figure 1. The innermost layer is the tunica intima (or simply ‘intima’). It contains a monolayer of endothelial cells (ECs) attached to a basal lamina that they produce, and an elastic membrane, the ‘internal elastic lamina’, which separates the intima from the tunica media (also called just ‘media’). The media, which is responsible for the contractility of the arteries, is composed of vascular smooth muscle cells (VSMCs), collagen and elastic fibers. The external elastic lamina separates the media from the

outermost layer, the *tunica adventitia* (or 'adventitia'), made of fibroblasts, fibrous connective tissue, feeding adventitial vessels, draining lymphatics, and terminal nervous motor fibers.

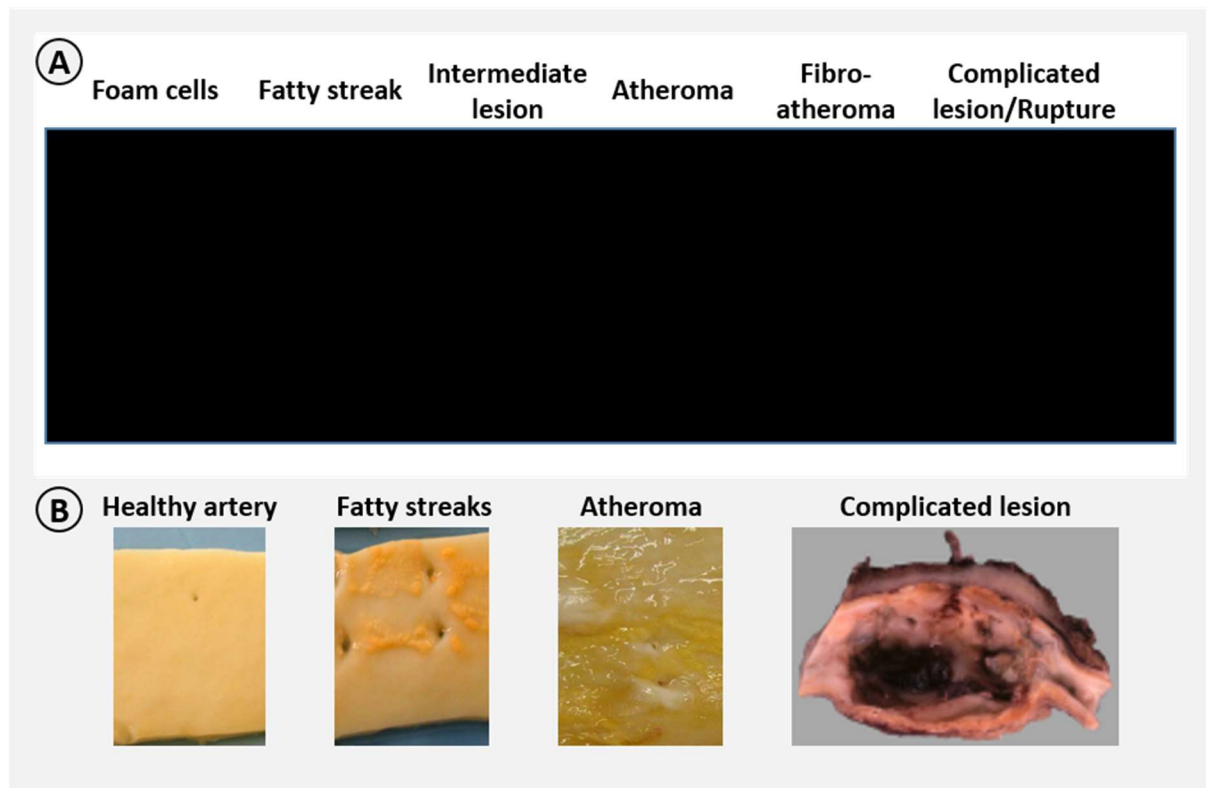


Figure 2. Progression of atherosclerosis. A. Figure adapted from Koenig and Khuseyinova (2007). B. Photographs of human samples from our biobank at the LVTS (Inserm U1148).

Figure 2 shows the different stages of atherosclerosis evolution, which are detailed below.

According to the current paradigm, atherosclerosis is initiated by the deposition and the accumulation of low-density lipoproteins (LDLs) in the sub-intimal space, under the endothelium. This accumulation is enhanced by high concentrations of circulating LDLs (Steinberg 1983; Schwenke and Carew 1989; Nievelstein et al. 1991), and it occurs preferentially at the sites where blood flow is turbulent (Caro et al. 1969; Zarins et al. 1983; Moore et al. 1992), which might increase endothelial permeability. In particular, an association between low shear rate and high concentration of atherosclerosis has been identified in some areas of the coronary arteries (Sabbah et al. 1986).

The LDLs that accumulate in the subendothelial space undergo several biochemical modifications, and notably, oxidation (Henriksen et al. 1981; Morel et al. 1984; Palinski et al. 1989; Steinberg 1997). Oxidized LDLs are known to induce leukocyte recruitment (Steinberg et al. 1989; Frostegård et al. 1990; Lehr et al. 1991), in particular through the release of oxidation products such as lysophosphatidylcholine, which is a chemoattractant for monocytes (Quinn et

al. 1988) and induces the expression of various leukocyte adhesion molecules and chemokines in ECs (Kume et al. 1992; Takahara et al. 1996; Takabe et al. 2004).

As a result, monocytes and T lymphocytes are recruited (Gerrity et al. 1979; Jonasson et al. 1986; Babaev et al. 1993). Once they have infiltrated the subendothelial space, monocytes differentiate into macrophages and take up oxidized LDLs (Poole and Florey 1958; Schaffner et al. 1980; Gerrity 1981). The ingestion of oxidized LDLs by the macrophages, mediated by the "scavenger receptors", is not regulated and leads to the transformation of the macrophages into lipid-laden 'foam cells', so named because of their histological aspect (de Villiers and Smart 1999). The accumulation of foam cells in the subendothelial space results in the formation of the so-called 'fatty streaks'. These macroscopically visible, clinically harmless lesions are already present in the arteries of newborns and children (Klotz and Manning 1911; Napoli et al. 1997). A photograph of fatty streaks is shown on Figure 2B. Some fatty streaks regress, while others progress to intermediate lesions (as summarized on Figure 2A).

The progression of atherosclerosis is marked by the formation of a necrotic lipid core, resulting from macrophage necrosis (Tabas 2005). The lipid core contains extracellular lipids and pro-coagulant and inflammatory factors released by necrotic macrophages. It also contains calcium deposits, which accumulate with time (Stary 2001). In parallel with the formation of foam cells and the lipid core, VSMCs migrate towards the subendothelial space, proliferate and synthesize extracellular matrix (ECM) components, in response to cytokines and growth factors released by leukocytes and ECs (Dzau et al. 2002). Thereby, they create a 'fibrous cap' between the lipid core and the endothelium.

The resulting 'fibrofatty' plaque tends to grow with the persistent accumulation of LDLs and inflammatory cells. This growth is often accompanied by arterial remodeling: the external elastic membrane can either shrink and drive vessel restriction (this is called 'negative remodeling') or expand ('positive remodeling') (Schoenhagen et al. 2001). A sketch of these situations is shown on Figure 3. Thus, the size of the plaque itself does not directly determine the degree of stenosis, but the progressive growth of the plaque along with a negative remodeling causes increasing stenosis of the atherosclerotic arteries. When the process is situated in a coronary artery (shown on Figure 4), this progressive luminal narrowing causes a reduction of blood flow ('ischemia') in the myocardium, and the first symptoms of coronary artery disease (CAD) appear: chest pain ('angina') and short breath are experienced first during exertion, and then, as the occlusion progresses, also at rest.

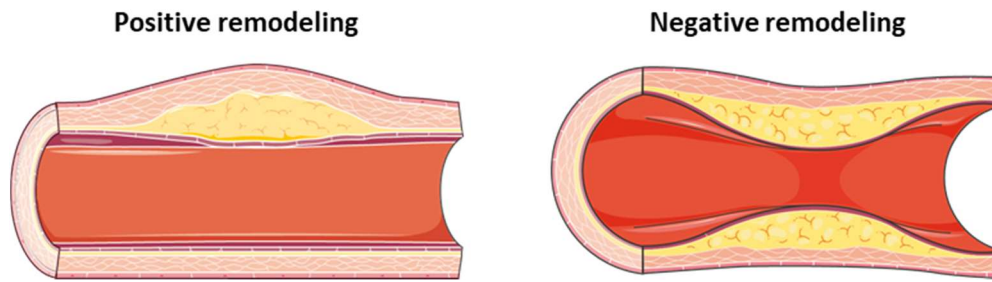


Figure 3. Schematic representations of positive and negative arterial remodeling. Pictures from Servier Medical Art image bank.

Besides this progressive stenosis process, full stenosis can be achieved acutely on lesions that were clinically silent. This acute obstruction results from the formation of a luminal thrombus forming on eroded or ruptured atherosclerotic lesions. The exact causes of plaque erosion and plaque rupture are not yet known. Concerning plaque rupture, a large body of evidence suggests a role for the matrix proteinases produced by leukocytes infiltrated within the plaque. The rupture of the plaque causes the exposure of the procoagulant factors contained in the necrotic core (such as tissue factor) to the circulating blood, resulting in the formation of a thrombus (Libby 2002). Still, this event can be asymptomatic, as thrombolysis also takes place, and the plaque 'heals' through the formation a thicker fibrous cap.

However, when the lumen of the artery is already largely reduced by the plaque, the thrombus created after the rupture of the lesion can cause a total occlusion of the artery. When the lesion is situated in a coronary artery, this results in acute myocardial infarction (commonly known as 'heart attack'). Myocardial infarction (MI) is the final and most severe manifestation of CAD, and it requires emergency treatment in order to prevent the death of the patient.

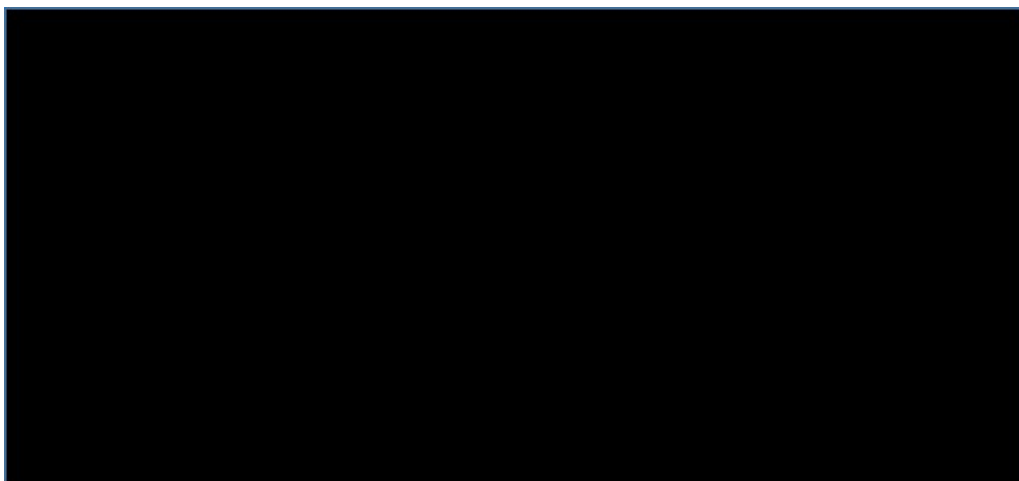


Figure 4. Coronary arteries.The coronary arteries surround the myocardium, which they supply in oxygen.

I.1.b. Endovascular treatment of coronary artery disease: balloons and scaffolds

An estimated 15.9 million people suffered from myocardial infarction worldwide in 2015 (Hay et al. 2017), and cardiovascular diseases are the first cause of death in Western countries such as the United States (Thom et al. 2006). CAD is therefore a major health concern. Tremendous progress has been made in the treatment of this disease over the past decades. The decrease in mortality rates after hospitalization for myocardial infarction reflects this progress. For instance, a Danish nationwide cohort study showed that the 30-day mortality after myocardial infarction dropped from about 30% in the period 1984-1988 to 15% in 2004-2008 (Schmidt et al. 2012). This progress was correlated to the generalization of the use of medications such as beta-blockers and thrombolytics (as reported by Gheorghiadu and colleagues (1996)), and is also due to two successive 'revolutions' in the treatment of CAD: the revascularization of the stenotic coronary arteries by balloon angioplasty, next followed by intravascular stenting techniques.

A more detailed description of the historical evolution and current challenges of percutaneous transluminal coronary angioplasty can be found in a review that I co-authored (Caligiuri et al. 2017). This review is presented in annex.

Balloon angioplasty without stents (also called 'plain old balloon angioplasty' or POBA) was first performed by Andreas Gruntzig in 1977 (Gruntzig 1978). It consists in inserting a deflated balloon in the occluded artery (by percutaneous intervention) and inflating it in order to mechanically restore the luminal diameter. It is a minimally invasive technique, requiring only the insertion of a catheter at a peripheral entry point. As it demonstrated high success rates (de Feyter et al. 1991), its use became general over the years, and it became a gold standard treatment for myocardial infarction (Iannone et al. 1993; Zijlstra 1995). However, the clinical efficiency of POBA was limited by elastic recoil and post-angioplasty restenosis, with rates as high as 30 to 60% (Bauters et al. 1996). Coronary stents were developed in order to solve this issue.

Coronary stents are metallic endoprostheses that are mounted on a deflated angioplasty balloon. When the balloon is inflated, they expand, and they remain in place after the balloon is removed, thus acting as a scaffold for the artery and maintaining open the lumen. The deployment of a coronary stent is represented on Figure 5.



Figure 5. Stent deployment. A. The stent, mounted on a deflated balloon, on a catheter, is placed in the occluded artery segment. B. The balloon is inflated, which causes the stent to expand and the atheromatous plaque to be compressed against the artery wall. C. After retraction of the catheter, the stent stays in place in order to maintain the lumen diameter. Figure from the Encyclopædia Britannica.

A coronary stent was implanted in a human for the first time in 1986 (Sigwart et al. 1987). Several models were developed by different companies in the early 1990s, and the results of two major clinical trials, BENESTENT and STRESS (Fischman et al. 1994; Serruys et al. 1994), established the efficiency of stents in preventing restenosis after balloon angioplasty. Stents became more and more common, and in 1999, they were used in nearly 85% of the percutaneous coronary interventions (PCIs) (Serruys et al. 2006). PCIs are either primary (performed in emergency to treat acute myocardial infarction) or elective (performed to treat CAD that has not yet led to acute myocardial infarction).

The incidence rate of in-stent restenosis in the 6 months following the implantation of these 'bare metal stents' (BMSs) was considerable, at 20 to 30% (Fischman et al. 1994; Serruys et al. 1994; Ijsselmuiden et al. 2003). In-stent restenosis (ISR) is a result of a 'neointimal' formation. The injury caused by the stent to the vascular wall triggers an inflammatory reaction involving platelets and leukocytes. This inflammatory reaction causes smooth muscle cells to migrate in the plaque towards the lumen, proliferate and produce ECM matrix components (Virmani and Farb 1999; Mitra and Agrawal 2006). The resulting neointimal hyperplasia covers the stent struts and obstructs the arterial lumen. In addition, our laboratory has recently shown that local peristrut microhemorrhages, cholesterol accumulation, and oxidation, trigger together in-stent neoatherosclerosis (Terzian et al. 2017).

The high rate of in-stent restenosis associated with BMSs prompted the development of a new type of stents: drug-eluting stents (DESs), which are coated with a polymer matrix containing an antimetabolic or cytostatic drugs. The drugs aim at inhibiting the local inflammation process and the

VSMCs proliferation that lead to restenosis. The first generation of DESs, launched in 1999, were the Taxus stent (produced by Boston Scientific) and the Cypher stent (manufactured by Cordis), eluting paclitaxel and sirolimus respectively. Their use led to a major decrease in restenosis rate compared with BMSs (Morice et al. 2002; Colombo et al. 2003). However, it appeared that, compared with BMSs, they both induced a higher rate of 'late' thrombosis, that is to say thrombosis that happened several months after stent implantation, generally after the discontinuation of the recommended anti-platelet therapy (Pfisterer et al. 2006; Lagerqvist et al. 2009; Stone et al. 2011). This increased risk of late stent thrombosis, which resulted in higher mortality and target lesion revascularization rates, was correlated with a local hypersensitivity reaction provoked by the polymer (or possibly the drugs) (Virmani et al. 2004) and delayed stent strut endothelialization (Joner et al. 2006). The delay in stent endothelialization can be explained by the cytostatic effect of the drugs, which do not only impact leukocytes and VSMCs, but also endothelial cells (Pasquier et al. 2004; Prasad et al. 2005; Reineke et al. 2015).

During the last fifteen years, BMSs and DESs have evolved. Cobalt-chromium alloys (CoCr) and, more recently, platinum-chromium alloys (PtCr) have largely replaced 316L stainless steel as stents core material (Foin et al. 2014). The superior mechanical properties of these new alloys made it possible to increase the flexibility of the stents and decrease stent strut thickness, which resulted in lower restenosis rates (Briguori et al. 2002; Pache et al. 2003).

As regards DESs, their second generation is characterized by the use of sirolimus-derived drugs (everolimus, zotarolimus, novolimus, Biolimus A9) and new polymer coatings, in order to avoid the hypersensitivity reactions associated with the coatings of first-generation stents. A third generation of DESs, coated with bioresorbable poly(lactic acid)-based polymers, was later developed.

The superiority of second-generation DESs over first-generation DESs in terms of late thrombosis risk and myocardial infarction incidence was shown by a meta-analysis (Navarese et al. 2013) and the study of a registry of more than 18000 patients (Tada et al. 2013). However, two meta-analyses showed no superiority of third-generation DESs over second-generation DESs, in terms of stent thrombosis, myocardial infarction and mortality (Navarese et al. 2013; Pandya et al. 2016).

1.1.c. Current challenges for coronary stents

The biological complications currently associated with coronary stents (thrombosis and restenosis) stem from biocompatibility issues. The stent surface induces pro-thrombotic and pro-inflammatory reactions in the cells that contact it: platelets and leukocytes at first, then migrating endothelial cells. Indeed, the phenotype of the endothelial cells that cover the stent struts is not

physiological, since they display defective intercellular junctions and decreased expression of antithrombotic molecules (Otsuka et al. 2012).

New stent coatings are needed to address this issue. A great part of the current research and development in coronary stents actually focuses on strategies to improve stents endothelialization, either by promoting endothelial cells migration through the immobilization of ECM-derived components (Li et al. 2011; Joner et al. 2012; Castellanos et al. 2017; Montaña-Machado et al. 2017), or by recruiting endothelial progenitor cells (Kutryk et al. 2008; Lin et al. 2010; van Beusekom et al. 2012; Li et al. 2016). Only one of these approaches has already been transferred to a commercially available stent: a coating with anti-CD34 antibodies, which aims at capturing circulating endothelial progenitor cells, on OrbusNeich's Genous and Combo stents.

The strategy that we propose aims at improving stents endothelialization, in terms of both shortening of the delay before complete covering and induction of a physiologic EC phenotype, in order to prevent biological complications.

A similar strategy can also be applied to another type of arterial stent, the 'flow diverting stents', used for the treatment of intracranial aneurysms. The pathology and clinical challenges associated with this type of stent differ from those seen with the use of balloon-expandable stents. Thus, prior to discussing the stent improving strategy used in this work, I will introduce the challenges associated with the use of flow diverting stents.

1.2. Flow diverting stents

Flow diverting stents were developed for the endovascular treatment of intracranial aneurysms. The following section presents the medical context for the use of these stents.

1.2.a. Intracranial aneurysms

Aneurysms are abnormal bulges of a blood vessel. There are two main types of aneurysms: saccular (or 'berry') aneurysms, which protrude on one side of a vessel, and fusiform aneurysms, which consist in a symmetrical enlargement of the vessel diameter. A drawing of the two types of aneurysms is provided on Figure 6.

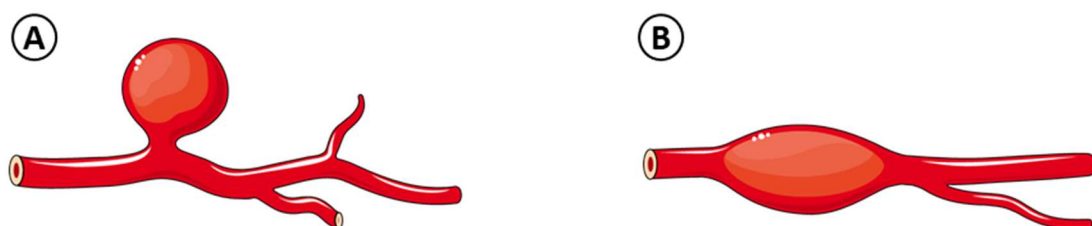


Figure 6. Schematic drawings of aneurysms. A. Saccular aneurysm. B. Fusiform aneurysm. Pictures from Servier Medical Art image bank.

Aneurysms can form in both arteries and veins, but are far more common in arteries (Gillespie et al. 1997). In particular, most aneurysms are found in the aorta or in intracranial arteries (Ruigrok et al. 2008). We will henceforth focus on intracranial aneurysms, since flow diverting stents were developed for their treatment. Most intracranial aneurysms are saccular, and are situated in the subarachnoid space at the base of the brain, as shown on Figure 7.

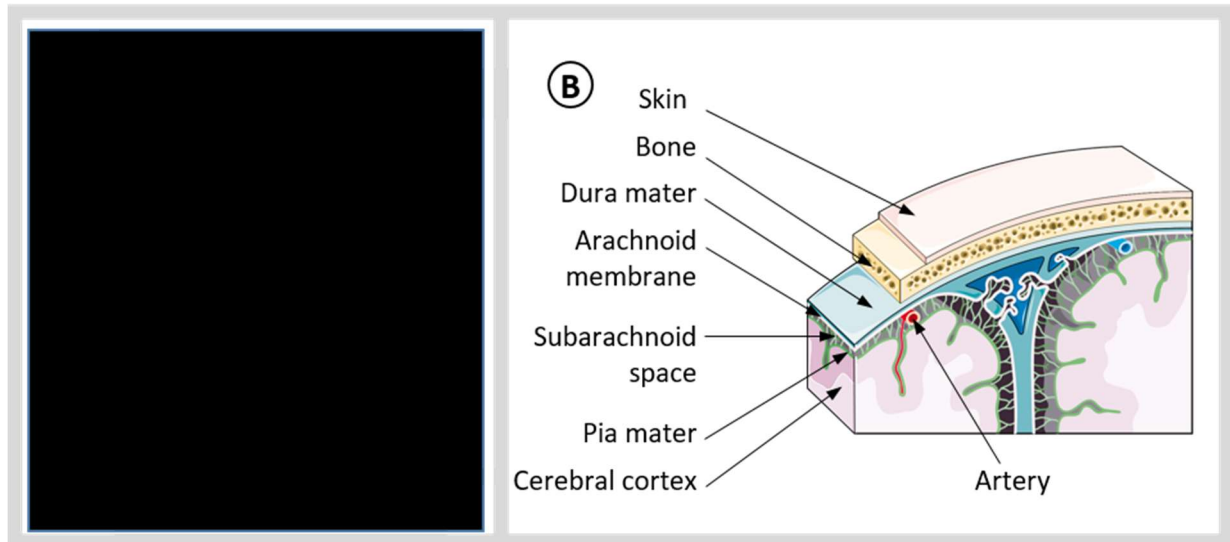


Figure 7. Major localization of intracranial aneurysms. A. Sketch of the base of the brain, with the most common sites of aneurysms evidenced by blue circles. Picture from van Gijn et al. (2007). B. Tissue layers surrounding the brain. The arteries in which most intracranial aneurysms occur are localized in the subarachnoid space. Picture from Servier Medical Art image bank.

The pathogenesis of intracranial aneurysms is not well understood. They may result from a deformation of the vessel wall under the effect of arterial blood flow. However, the initial mechanisms which can lead to excessive local blood pressure and vessel wall weakening are very diverse, and as a consequence, intracranial aneurysms are a common manifestation of many different diseases (Krings et al. 2011). Genetic connective-tissue disorders, smoking and hypertension are the most important risk factors associated with intracranial aneurysms (Schievink 1997).

Aneurysms are generally asymptomatic until a catastrophic event happens: the rupture of the arterial wall at the apex of the aneurysm. Most of the aneurysms never rupture: according to a systematic review (Rinkel et al. 1998), the prevalence of intracranial aneurysms in adults without specific risk factors is 2%, and they have an annual risk of rupture of approximately 2%. However, when intracranial aneurysms do rupture, it results in subarachnoid haemorrhage, a form of stroke which has a fatality rate of 30-40%, and causes the individual to become functionally dependent in 10-20% of the cases (Nieuwkamp et al. 2009). Today, the treatment of ruptured and unruptured intracranial aneurysms is a public health priority.

1.2.b. Historical treatments of intracranial aneurysms

The first developed method to treat intracranial aneurysms was microsurgical clipping. As shown on Figure 8A, it consists in pinching the aneurysm neck with a metallic clip. Thus, the aneurysm is isolated from blood flow, and cannot cause hemorrhages. This procedure involves general anesthesia and craniotomy, which is why it is generally not recommended in patients with a weak health status.



Figure 8. Most common treatments of intracranial aneurysms. A. Clipping. B. Coiling. C. Stent-assisted coiling. Note: the aneurysms represented here are unruptured, but these treatments are also applied to ruptured aneurysms. Pictures from Mayfield Clinic.

An endovascular treatment of intracranial aneurysms was developed in the 1990s: ‘aneurysm coiling’ (cf Figure 8B). This method consists in inserting a catheter in the aneurysm neck, and filling the aneurysm with thin radio-opaque platinum coils, so as to allow the formation of a stable thrombus, isolated from the circulation. In the ISUIA study (Wiebers 2003), which included more than 2000 patients who had undergone either open surgical or endovascular treatment of unruptured aneurysms, coiling demonstrated similar or better outcomes for patients in terms of morbidity and mortality at 30 days and 1 year, compared with clipping. The ATENA study (Pierot et al. 2008) later confirmed the feasibility and low morbidity and mortality rates associated with coiling of unruptured aneurysms. As for the treatment of ruptured intracranial aneurysms, the multi-center, randomized ISAT study (Molyneux et al. 2015) showed better outcomes for coiling than clipping, in terms of mortality and dependency at 10 years.

Aneurysm coiling was not recommended for wide-neck aneurysms, due to the risk of the coils obstructing the parent artery rather than the aneurysm. In the 2000s, ‘stent-assisted coiling’ was developed in order to overcome this limitation. As shown in Figure 8C, it consists in deploying a stent in the parent artery before filling the aneurysm with coils, in order to insure the proper positioning of the coils. Although there are some concerns about the complications associated with stent-assisted coiling, the demonstration of its efficacy in terms of recurrence rate has led to the generalization of its use (Piotin et al. 2010; Chalouhi et al. 2013; Hong et al. 2014).

Today, surgical clipping and endovascular coiling (stent-assisted or not) are the two main treatment options for intracranial aneurysm. However, a third option has emerged in the last decade and brought a revolution to the treatment of complex aneurysms: flow diverting stents.

I.2.c. Design and performances of flow diverting stents

Flow diverting stents (FDSs) are self-expanding, low porosity stents, which are positioned in the parent artery, in front of the aneurysm neck (as shown on Figure 9). As their name implies, they keep the blood in the parent artery, thus isolating the aneurysm from the circulation. After a local inflammatory response, thrombosis and remodeling take place in the aneurysm, while the aneurysm neck is progressively occluded by the endothelialization of the FDS and the subsequent neointimal proliferation (Kadirvel et al. 2013).

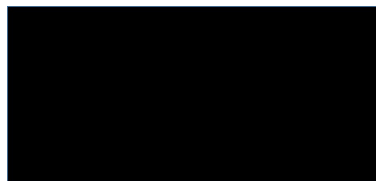


Figure 9. Schematic representation of a flow diverting stent in an artery. Picture from Mayfield Clinic.

FDSs perform very well in terms of aneurysmal occlusion: a systematic review of the literature, which included 1451 patients implanted with FDSs, reported an aneurysmal occlusion rate of 76% at 6 months (Brinjikji et al. 2013), while a clinical study on 633 patients reported occlusion rates of 90% at 1 year and 100% at 8 years (Lundquist et al. 2016). However, the morbidity rate is not negligible: 5.9% at 30 days and 9% at 6 months, according to the same studies by Lundquist et al. and Brinjikji et al. respectively. It is partially due to the two most common non-technical complications associated with FDS implantation: delayed aneurysm rupture and delayed intraparenchymal hemorrhage.

The occurrence rate of delayed aneurysm rupture was reported to be 1.9% in a retrospective study (Kulcsár and Szikora 2012). The causes of delayed aneurysm rupture have yet to be identified. The most plausible hypotheses are the persistence of flow inside the aneurysm and the

degradation of the aneurysm wall by proteases from the inflamed aneurysmal thrombus (Fontaine et al. 2002; Carrell et al. 2006; Cebal et al. 2011; Kulcsár et al. 2011; Rajah et al. 2017).

Concerning delayed intraparenchymal hemorrhages (DIPHS), their occurrence rate is reported to be 3% in a meta-analysis grouping 1451 patients (Brinjikji et al. 2013), and 2.4% in a retrospective study on 793 patients (Kallmes et al. 2015). Like for delayed aneurysm rupture, the mechanisms behind DIPH are not understood yet. However, the vast majority (80%) of DIPHS were reported to occur in the arterial segment containing the FDS, which suggests that they are caused by the stent or the procedure itself. The remaining 20% of DIPHS occur far from the FDS, which points to the involvement of antiplatelet therapy in this complication (Rouchaud et al. 2016a). Antiplatelet therapy is systematically administered to the patients after FDS implantation in order to prevent in-stent thrombosis.

It is worth noting that, unlike in coronary stents, in-stent restenosis is not a major issue in FDSs despite the fact that small studies reported in-stent stenosis occurrences to be between 10 and 40% in the first months after implantation (Pierot 2011; Cohen et al. 2014; John et al. 2016). Indeed, almost all in-stent stenoses were asymptomatic, and later angiographic follow-up showed their partial regression (John et al. 2016).

The primary indication of FDSs is the treatment of unruptured anatomically complex aneurysms (e.g. wide-neck or giant saccular aneurysms, fusiform aneurysms). However, the promising results of the first clinical studies in terms of clinical outcomes and aneurysm occlusion rates (Fiorella et al. 2009; Szikora et al. 2010; de Barros Faria et al. 2011; Nelson et al. 2011; Fischer et al. 2012; Martin et al. 2012; McAuliffe et al. 2012; Narata et al. 2012; Cruz et al. 2013) have led to a progressive extension of their use to other types of aneurysms, including ruptured aneurysms (Brouillard et al. 2016).

Thus, although the flow diverters market is relatively small today (414 FDSs were implanted in France between October 2012 and February 2014, according to the *Société Française de Neuroradiologie* (2016), it is quickly expanding.

The various models of FDSs currently in use in Europe are listed in Table 1. Contrary to the coronary stents, which are mostly produced by laser cutting (Martinez and Chaikof 2011), FDSs consist of braided wires. Most wires are made of either CoCr or 'nitinol', a shape-memory, super-elastic alloy composed of nickel and titanium in approximately equal atomic percentages. A few platinum, platinum-tungsten or tantalum wires are added in order to increase the radio-opacity of the devices.

CE marking	Manufacturer	Model	Alloy
2008	Balt	Silk	Nitinol + Pt
2008	Medtronic	Pipeline	CoCr + PtW
2011	Stryker Neurovascular	Surpass	CoCr + PtW
2012	Phenox	p64	Nitinol + Pt
2013	MicroVention	FRED	Nitinol + Ta

Table 1. Flow diverting stents currently in use in Europe. Pt: Platinum. W: Tungsten. Ta: Tantalum. Similar models of the same line (e.g.: Pipeline and Pipeline Flex) have been omitted.

I.2.d. Towards better flow diverting stents

Flow diverting stents have not yet celebrated the tenth anniversary of their first CE marking, and the evaluation of their performances and potential complications still lacks some precision. The results of several ongoing randomized clinical trials (FIAT, LARGE and EVIDENCE trials) are therefore eagerly awaited. However, as detailed in the previous section, FDSs have largely proven their value as a treatment option for various types of aneurysms, and the issues that the next generation of FDSs should address can already be identified. Indeed, although the precise mechanisms behind the main complications of FDSs (delayed aneurysm rupture and DIPH) have not been elucidated, three types of biological causes have been isolated: the persistence of blood flow in the supposedly occluded aneurysm, the effect of antiplatelet therapy, and the degradation of the aneurysmal wall by proteases released from the thrombus.

The aneurysm occlusion and healing have been shown to depend on the endothelialization and the subsequent formation of an ‘impermeable’ neointima on the stent struts in front of the aneurysm neck (Kadirvel et al. 2013). Therefore, both the persistence of blood flow in the aneurysm and the proteolytic activity of the thrombus should decrease if the stent could promote the fast formation of a functional neointima. As for the antiplatelet therapy, its use is required to prevent in-stent thrombosis, which is caused by the pro-thrombotic action of the FDS on the cells that contact it (blood circulating cells first, then ECs and SMCs).

Thus, the issues identified with intracranial FDSs are similar to the ones associated with coronary stents: they concern the biocompatibility of the devices towards the cells present in their *in vivo* environment. The solution developed for one device can therefore be applicable to the other, provided that it is adapted to the materials and the mechanical properties of both stents.

Medtronic, the world leader of the FDS market, is currently studying a phosphorylcholine coating (called ‘Shield Technology’) to reduce the thrombogenicity of its FDS (Pipeline).

INTRODUCTION

Medtronic's French competitor, Balt, was involved in the current study, which aimed at developing a coating that would decrease platelet adhesion, but also promote stent endothelialization and favor a physiological, anti-thrombotic phenotype in the endothelial cells.

The bioactive molecule that we chose to immobilize on both balloon-inflatable and auto-expandable stents, in order to improve their biocompatibility, is derived from the CD31 protein. The reasons for this choice are explained in the next section.

II. CD31 and agonist peptides

II.1. General presentation of CD31

CD31 is a transmembrane glycoprotein which is constitutively and exclusively expressed on platelets, leukocytes and endothelial cells (Ohto et al. 1985; Goyert et al. 1986; Stockinger et al. 1990). The sequence of human CD31 contains 738 amino acid residues, including a 27-residue signal peptide which is cleaved during the maturation of the protein in the endoplasmic reticulum (Newman et al. 1990; Stockinger et al. 1990). This sequence corresponds to a molecular weight of 83 kDa. However, CD31 is heavily glycosylated, so the molecular weight of the mature glycoprotein is actually 130 kDa (Newton et al. 1999).

As shown on Figure 10, CD31 consists of six extracellular immunoglobulin-like (Ig-like) domains (characterized by a specific arrangement of 100-residue long β strands stabilized by a disulfide bridge), a transmembrane region, and a cytoplasmic tail containing two immunoreceptor tyrosine-based inhibitory motifs (ITIMs).

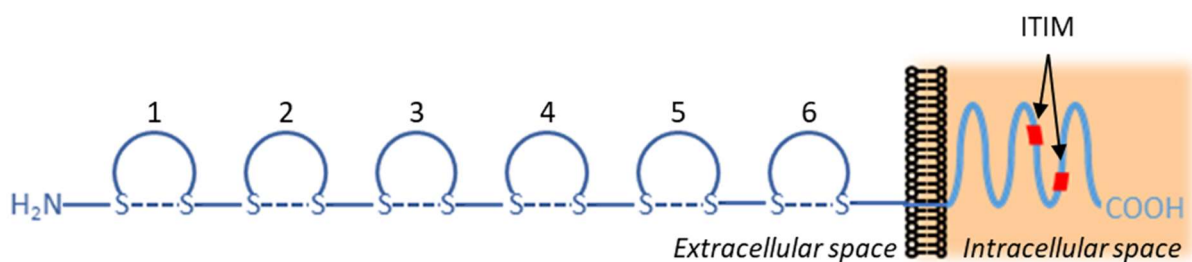


Figure 10. Schematic structure of CD31. The six loops of the extracellular region represent the Ig-like domains. By convention, they are numbered from the most distal to the most proximal, relatively to the membrane. The dash lines represent the disulfide bridges that stabilize the Ig-like domains.

Because of its Ig-like extracellular domains, CD31 was first classified within the Immunoglobulin Cell Adhesion Molecule (IgCAM) family. Since it was expressed on both platelets and endothelial cells, it was named Platelet-Endothelial Cell Adhesion Molecule-1 (PECAM-1). Its function was thought to primarily mediate the adhesion between platelets and endothelial cells (Newman et al. 1990).

However, a few years later, the discovery that PECAM-1 possessed two ITIMs on its cytoplasmic tail led to its switching to the Ig-ITIM family (Newman 1999). The Ig-ITIMs drive inhibitory signaling cascades and henceforth, CD31 was not considered as a cell adhesion molecule anymore, but as an inhibitory receptor which performs regulatory functions in the cells that express it (Newman and Newman 2003).

II.2. CD31 activation and signaling pathways

The regulatory functions of CD31 act primarily through the recruitment and activation of phosphatases by the phosphorylated ITIMs of its cytoplasmic tail. ITIMs are short residue sequences of the form: S/I/V/L - x - Y - x - x - I/V/L. Upon phosphorylation of their central tyrosine (Y), they become a binding motif for the Src homology 2 (SH2) domains of protein tyrosine phosphatases (Unkeless and Jin 1997).

The activation of these ITIMs requires the clustering of CD31 and the presence of neighboring activated tyrosine kinases. The following explanation of the activation and signaling mechanisms of CD31 is summarized on Figure 11.

Two mechanisms are involved in the clustering of CD31: a trans-homophilic interaction involving the distal domains 1 and 2 (Sun et al. 1996; Paddock et al. 2016) and a cis-homophilic engagement at the domain 6 (Newton et al. 1997). The two ITIMs on the cytoplasmic tails of the clustered CD31 molecules are then phosphorylated by tyrosine kinases. Several research groups have identified members of the Src kinase family (the Src family kinases, or SFKs) as the kinases which phosphorylate the ITIMs of CD31 (Lu et al. 1997; Cao et al. 1998; Cicmil et al. 2000; Newman et al. 2001).

It is important to note that CD31 is not endowed with autocatalytic properties and its ITIM motifs are not phosphorylated in resting cells. The stimulation of cell signaling through other receptors is needed and, as reported by P. Newman (1999), various cellular stimuli can lead to CD31 ITIM phosphorylation in the different types of cells which express it. These stimuli include platelet aggregation (Jackson et al. 1996), shear stress (Osawa et al. 1997), oxidative stress (Wang et al. 1998), exposure to lysophosphatidylcholine (Ochi et al. 1998), cross-linking of the Fcε receptor (Sagawa et al. 1997) and cross-linking of CD31 itself (Varon et al. 1998).

Once phosphorylated, the ITIMs recruit and activate SH2-containing phosphatases (SHPs), SHP-2 in particular (Cao et al. 1998; Pumphrey et al. 1999; Henshall et al. 2001). The subsequent effects downstream of SHPs activation greatly vary depending on the type of cell considered and the activation stimuli it has received. Like all ITIM receptors, CD31 negatively regulates the activation pathway of ITAM (Immunoreceptor Tyrosine-Based Activation Motif) receptors, thereby lowering the activation threshold of immune cells (Ravetch and Lanier 2000). However, as detailed in the next paragraph, CD31 is far from just being an ITIM-bearing receptor (Newman and Newman 2003). The main known functions of CD31 in different cell types are detailed in the next section.

For instance, CD31 appears to be involved in serine/threonine signalization pathways. Serine residues of CD31's cytoplasmic tail are known to undergo phosphorylation, at levels increasing with activation (Newman et al. 1992; Ilan et al. 2000). The effects of this phosphorylation have

not yet been elucidated. CD31 was also shown to bind to elements of the cytoskeleton such as actin filaments, and to be functionally involved in their assembly (Matsumura et al. 1997). Finally, CD31 was also shown to engage in heterophilic interactions, in particular with CD177 and CD38 (Dianzani et al. 1994; Deaglio et al. 1998; Fedele et al. 2004; Sachs et al. 2007; Bayat et al. 2010). However, the *in vivo* effects of these interactions have not been clearly evidenced, contrary to the effects of homophilic CD31 interactions and ITIM-driven cellular functions.

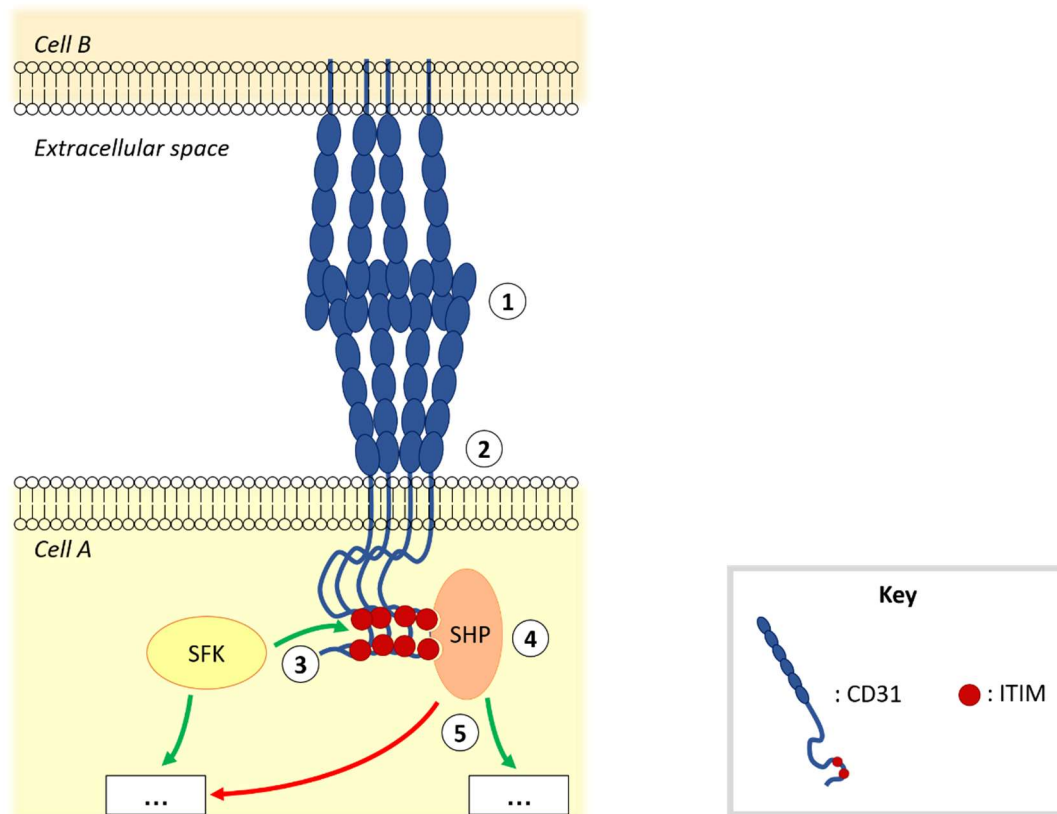


Figure 11. CD31 activation and signaling pathway. 1) Clustering of CD31 by trans-homophilic engagement of the distal domains 1 and 2. 2) Consolidation of the cluster by cis-homophilic engagement of the proximal domain 6. 3) Phosphorylation of the ITIMs of the cytoplasmic tail by SFKs (Src family kinases). 4) Recruitment and activation of SHPs (SH2-containing phosphatases) by the phosphorylated ITIMs. 5) Signaling cascade of the SHPs: inhibition of ITAM-dependent cascades, and other actions depending on the cell type.

II.3. Cellular functions of CD31

CD31 is constitutively expressed on endothelial cells, as well as on platelets, monocytes, neutrophils, eosinophils, basophils, mast cells, lymphocytes, that is to say on all hematopoietic cells except for red blood cells. CD31 levels of expression differ depending on the cells: there are approximately 5000 CD31 molecules per platelet, 50 000 per T cell, 100 000 per neutrophil and

1 000 000 per endothelial cell (Newman 1994). CD31 regulatory functions are also very different in endothelial cells, platelets and leukocytes.

II.3.a. CD31 in platelets

It is globally agreed upon that CD31 functions in platelets are mainly inhibitory. CD31 engagement has been shown to induce ITIMs phosphorylation and to inhibit aggregation, degranulation and intracellular calcium mobilization in platelets activated *in vitro* with specific agonists, namely collagen, collagen-related peptide and convulxin (Jones et al. 2001; Cicmil 2002; Jones et al. 2009). Besides, platelets from CD31 KO mice are more prone to aggregation and α -granule secretion than platelets from wild-type mice, when stimulated with collagen (Patil et al. 2001). *In vitro* and *in vivo* studies also showed that CD31 engagement inhibits thrombus growth (Jones et al. 2001; Rathore et al. 2003; Falati 2006).

II.3.b. CD31 in leukocytes

In **T lymphocytes**, the crosslinking of CD31 with the T cell receptor (TCR) was shown to inhibit TCR-dependent activation (Newton-Nash and Newman 1999). CD31 engagement with a recombinant CD31 was also shown to decrease the production of pro-inflammatory cytokines and to inhibit the proliferation of TCR-stimulated T cells (Prager et al. 2001).

In **B cells**, the co-ligation of the B cell receptor with CD31 chimeras attenuates downstream mechanisms such as calcium mobilization (Henshall et al. 2001). On the contrary, B cells from CD31 KO mice were shown to exhibit increase calcium mobilization and proliferation in response to BCR ligation (Wilkinson et al. 2002).

For **mast cells**, an *in vivo* study showed that, in response to anaphylaxis, CD31 KO mice exhibited higher serum histamine concentrations than wild-type mice. This points to an inhibitory function of CD31 in the regulation of mast cells activation in allergic diseases (Wong et al. 2002).

The function of CD31 in **polymorphonuclear cells** is not well known yet. However, several studies point at the involvement of CD31 in neutrophil migration and transmigration (Berman and Muller 1995; Miller et al. 2001; Wu et al. 2005; Bayat et al. 2010). Recent work carried out in our laboratory, by Francesco Andreatta and colleagues, expands upon the role of CD31 in neutrophil transmigration, suggesting that CD31 signaling is essential for controlling neutrophil oxidative burst and degranulation at sites of inflammation (abstract presented at the International Immunology Congress, Melbourne 21-26 August 2016, manuscript in preparation).

CD31 was shown to perform inhibitory functions in **macrophages**: its engagement regulates negatively Toll-like receptor 4 signaling and decreases pro-inflammatory cytokines production

by LPS-activated macrophages (Rui et al. 2007). CD31 also inhibits phagocytosis by transmitting 'detachment' signals between a healthy cell and a contacting macrophage, through homophilic engagement (Brown et al. 2002).

II.3.c. CD31 in endothelial cells

CD31 has been shown to play many different roles in endothelial cells. We will present here the best known functions and the ones that are most relevant to the issues of stent endothelialization. The following description partly relies on a review written by Privratsky and Newman (2014).

CD31 is known to localize at the intercellular junctions of endothelial cells as they become confluent (Muller et al. 1989; Newman et al. 1990). It plays a role in the initial formation of endothelial intercellular junctions, since the blocking of CD31 by antibodies prevents the formation of these contacts (Albelda et al. 1990). Moreover, CD31 was shown to localize at the cell-cell junctions between fibroblast-like or enteroendocrine cells which had been transfected with CD31 cDNA. On the contrary, the CD31 surface distribution remained homogeneous when a CD31-transfected cell contacted a cell that did not express CD31 (Albelda et al. 1991). These results point at an involvement of CD31 in intercellular junctions through trans-homophilic engagement. The homophilic nature of CD31 engagement at intercellular junctions was later confirmed by further studies (Sun et al. 1996; Newton et al. 1997).

In vitro and *in vivo* experiments also showed that the endothelium permeability to macromolecules was much increased in the presence of anti-CD31 antibodies (Ferrero et al. 1995), thus evidencing the involvement of CD31 in the maintenance of the vascular barrier function. Biswas et al. (2006) proved that CD31 plays a key role in the reconstitution of endothelial intercellular junctions after a breach. Besides, the CD31-dependent promotion of endothelial cell survival has been extensively reported (Evans et al. 2001; Ferrero et al. 2003; Gao et al. 2003; Limaye et al. 2005).

CD31 is also involved in angiogenesis, and in particular in promoting endothelial cells migration (DeLisser et al. 1997; Zhou et al. 1999; RayChaudhury et al. 2001; Cao et al. 2002; Wu and Sheibani 2003; Kondo et al. 2007).

Finally, numerous *in vitro* and *in vivo* studies also showed the involvement of CD31 in the regulation of leukocyte extravasation through the endothelial barrier (Muller et al. 1993; Vaporciyan et al. 1993; Newman 1994).

In summary, CD31 performs different roles in platelets, leukocytes and endothelial cells. In platelets and leukocytes, its functions are essentially inhibitory, whereas in endothelial cells, it

promotes migration and survival of the cells, as well as the formation and maintenance of the intercellular junctions responsible for the integrity of the vessel barrier function.

These characteristics correspond to the properties wanted on the surface of coronary stents and FDSs. Thus, it seems desirable for a stent coating to promote CD31 regulatory functions.

II.4. CD31 shedding and identification of rescue agonist peptides

II.4.a. CD31 shedding

Upon cell activation or stressful condition, CD31 has been shown to undergo cleavage in its extracellular domain, and thus shedding, in several types of cells.

In endothelial cells, Ilan et al. (2001) discovered that CD31 is shed during starving-induced apoptosis. A 100 kDa soluble protein is released during this process; this fragment consists of the extracellular domain of CD31. A truncated protein, which comprises the cytoplasmic and transmembrane domains of CD31, remains anchored to the plasma membrane.

CD31 was also shown to be shed in platelets treated with an inhibitor of the cytosolic calmodulin (Wong et al. 2004), in HIV-infected leukocytes (Eugenin et al. 2006), and in T lymphocytes following TCR activation (Fornasa et al. 2010).

In the cases where it was investigated, the effect of CD31 shedding on the cells was the loss of the regulatory functions of CD31 (Ilan et al. 2001; Fornasa et al. 2010). This result is no surprise, since the primary signaling pathway of CD31 requires its clustering, which is maintained by homophilic interactions in the extracellular domain (as detailed in section II.2).

The mechanisms of CD31 shedding – in particular, the identity of the proteases responsible for the cleavage – have not been elucidated. Besides, most studies which report a decrease of CD31 surface expression in a given context have not looked for soluble CD31 fragments that could have been released. Thus, CD31 shedding is probably a much more common phenomenon than what might be inferred from the few cases that have been reported with certainty so far.

A previous work from our laboratory, by Giulia Fornasa and colleagues (Fornasa et al. 2010), showed that, contrary to what previous studies had implied, CD31 does not completely disappear from the cell surface. Instead, it is shed and after its shedding, a CD31 fragment remains anchored to the membrane. The truncated CD31 that remains anchored to the cell includes the cytoplasmic domain, the transmembrane segment, and a portion of the extracellular domain consisting of a part of the membrane-proximal Ig-like domain 6.

This observation paved the way for the use of synthetic CD31 peptides, targeting the membrane-proximal sequence of the extracellular domain, as bioactive molecules for the restoration of CD31 regulatory functions, as detailed in the following section.

II.4.b. CD31 agonist peptides

Fifteen years before the work published by Fornasa and colleagues, Zehnder et al. (Zehnder et al. 1995) had discovered that a synthetic peptide, corresponding to the 23 most membrane-proximal extracellular residues of CD31, was able to inhibit T cell proliferation in a mixed lymphocyte reaction, in a specific and dose-dependent manner. Surprisingly, this inhibition, which was known to be associated with CD31 engagement, was observed even on 'CD31 low' T cells. At the time, the authors hypothesized that the CD31 peptide had interacted with a heterotypic ligand.

However, in light of the findings of Fornasa et al., the 'CD31 low' cells that were responding to the 23 aa synthetic peptide were indeed cells in which CD31 had been shed. This re-interpretation led to the proposal that the CD31 peptide had engaged in homophilic interactions with the remaining portion of the extracellular domain of CD31, as shown on Figure 12. This hypothesis was confirmed by the direct observation of the contacts between the CD31 peptide and the remaining portion of CD31 extracellular domain by TIRF microscopy (Fornasa et al. 2010).

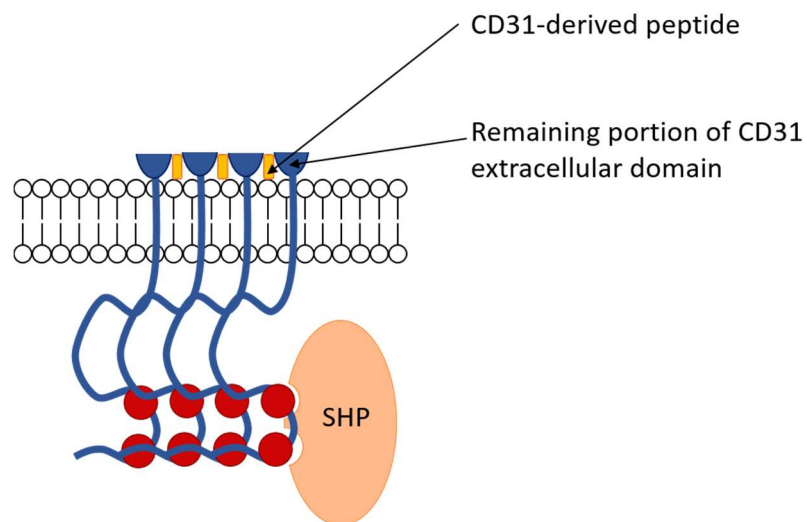
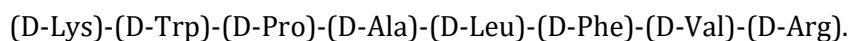


Figure 12. The CD31-derived peptide maintains a cluster of shed CD31. The homophilic engagement of the peptide with the remaining extracellular portion of the shed CD31 molecules stabilizes the CD31 cluster. The signaling cascade of CD31, including the recruitment of SHPs, is maintained.

Thus, the cleavage site of CD31 shedding leaves an extracellular therapeutic target which can be used to restore CD31 regulatory functions thanks to a CD31-derived peptide. Such a peptide could be used for the promotion of CD31 functions in the various contexts where cell activation leads to CD31 shedding.

In the years following this finding, our laboratory developed different CD31-derived peptides. An 8-residue long sequence, included in the original 23-residue long peptide, was finally chosen

because it is highly conserved among species and because it showed high specificity towards CD31 in *in vitro* assays (unpublished work). Since it is known that dextrorotatory amino acids exhibit better stability against enzymatic degradation than the natural levorotatory enantiomers (Tugyi et al. 2005), the CD31 peptide was designed with D-amino acids. Thus, the peptidic sequence was assembled in reverse order so as to retain the original spatial orientation and the chirality of the side chains. The resulting peptide was named 'P8RI', where P stands for peptide, 8 is the number of amino acids, and RI means retro-inverso. The sequence of P8RI is:



The structure of P8RI is shown on Figure 13, along with that of the original, non-inverted sequence (called P8F).

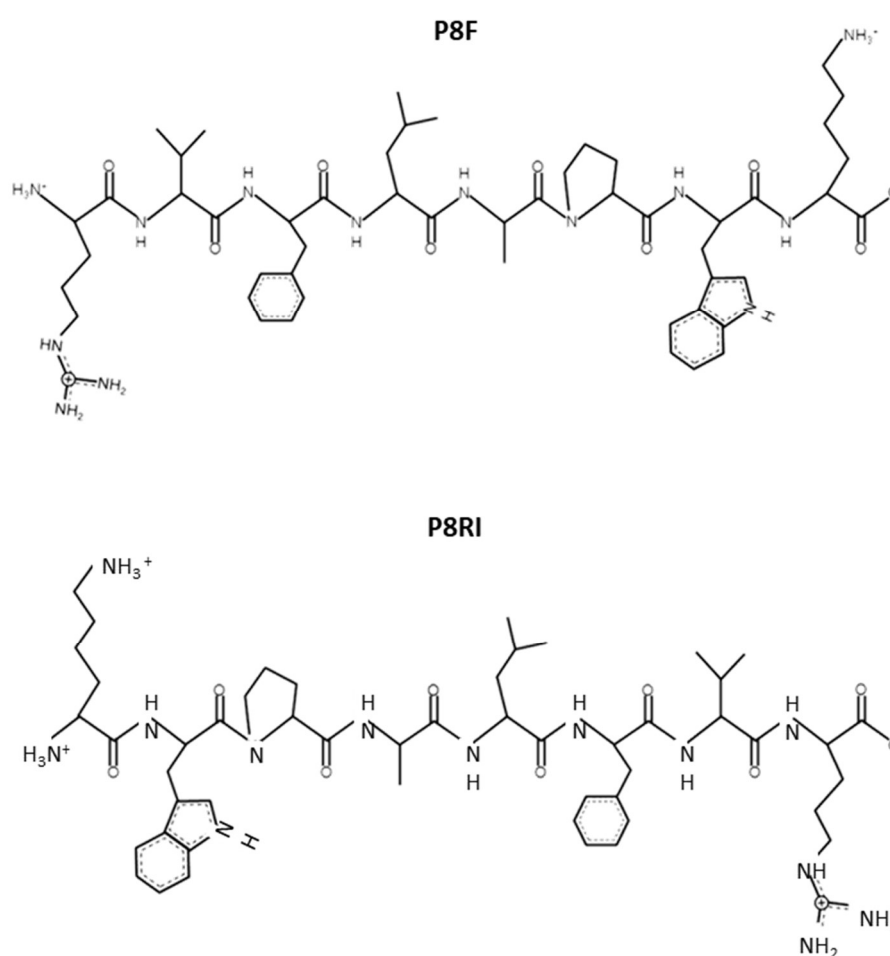


Figure 13. Representation of the structures of P8RI and P8F. 'P8F' designates the original sequence from the CD31 molecule, in forward sense, whereas P8RI is the retro-inverso sequence, where both the order and the chirality of the residues are inverted. Drawings realized with the software Pepdraw.

III. Rationale of the thesis work

Coronary stents and intracranial flow diverting stents were developed in the past decades for the endovascular treatment of two different arterial pathologies: coronary artery disease (stenosis of the artery) and intracranial aneurysms (enlargement of the artery). The working mechanisms of these devices is different but both are associated with complications stemming from biocompatibility issues. In particular, the rapid covering by endothelial cells presenting an anti-inflammatory and anti-thrombotic phenotype is key to the integration of the endoprosthesis at the blood/vessel interface. Thus, the implementation of solutions to improve their endothelialization and integration in the vessel wall would represent a major progress in their respective field.

My thesis work deals with the immobilization of a bioactive molecule on these stents in order to solve their biocompatibility issues. We propose to use a peptide which promotes CD31 regulatory functions: the inhibition of platelets and leukocytes activation, as well as the enhancement of endothelial cell survival, migration and barrier function.

IV. Stent coating with bioactive molecules

The idea to coat medical devices such as stents with bioactive molecules is not new: the most common examples are drug eluting stents. However, the mechanism of action of a peptide such as P8RI differs from that of small-molecule drugs, and this must be taken into account in the design of the coating method. The first challenge thus consists in developing a process to immobilize this peptide, named P8RI, on the surface of metallic endoprostheses.

IV.1. Elution vs immobilization

All the drugs in current DESs are eluted. Most derive from sirolimus and target the mTOR pathway which regulates cell growth (Tsang et al. 2007). They aim at preventing restenosis by inhibiting SMC proliferation. For this application, it is highly desirable that the drug should diffuse in the tissue surrounding the stent struts, in order to increase its efficacy. Therefore, the current design of the DESs coatings, which allows the release of the drug over the course of a few months, is perfectly adapted to their needs.

Our approach to the issue of stent biocompatibility is quite different, since we chose to promote the regulatory functions of CD31 in the cells that directly enter in contact with the stent. Thus, the CD31 coating would confer anti-thrombotic and anti-inflammatory properties to the surface, and, above all, it would promote the rapid formation of a functional endothelium on the stent struts. The CD31 agonist P8RI peptide is designed to achieve this goal by targeting the CD31 sequence involved in the cis-homophilic engagement which naturally occurs when endothelial cells, leukocytes, or platelets enter in contact with each others, and which is essential for the intracellular CD31 signaling.

Since our aim was to target the cells that directly contact the stent, the elution of the peptide did not fit our purpose. Instead, the biological mechanism of action of our bioactive molecule required its immobilization on the surface. Its anchoring needed to be strong enough to withstand *in vivo* flow conditions, which is why we chose to immobilize the peptide by covalent binding, rather than simple surface adsorption. Therefore, we designed a stent coating which would support the covalent immobilization of P8RI, rather than its elution.

For optimal biological efficacy, P8RI should stay on the stents at least during the period needed for complete endothelialization. This period was estimated to be one week for BMSs in healthy farm pigs (Pérez de Prado et al. 2011), and a few months for BMSs in humans (Joner et al. 2006).

IV.2. Polymer coatings

IV.2.a. Usefulness and drawbacks of polymer coatings

Coronary stents and FDSs are metallic devices, whose surfaces do not display the chemical functions required for the conjugation of biomolecules. Thus, their surface must be 'functionalized' for the subsequent covalent immobilization of a bioactive molecule such as the P8RI peptide. A possible approach that allows the direct immobilization of the peptide on an alloy is the plasma-assisted surface functionalization, which was the subject of the first part of this study. However, the use of this technique on metallic surfaces is challenging, and alternative polymer-based solutions had to be considered.

The use of polymer coatings as intermediate layers for the immobilization of bioactive molecules has several advantages. The first one is that, unlike almost all other types of materials, most polymers either contain functional groups that can react with bioactive molecules, or are easy to functionalize with such groups. The second one is that polymers are generally inexpensive and easy to process into coatings. Finally, there exists a very broad range of polymers, which allows for the fine-tuning of the chemical properties of the coatings. For these reasons, the use of polymer films is generally considered as an optimal solution for the immobilization of bioactive molecules and has been the preferred system in the design of coated stents.

However, polymer films do have some limitations, especially in their application as biomaterials coating. Their adhesion to the metal, their resistance to stent deployment, and their stability properties must be adapted to the intended use, in order to prevent the deleterious biological effects of delamination (the detachment of the film from its substrate) and uncontrolled degradation. Above all, the biocompatibility of the polymer coatings and of their degradation products is key to the biological performances of coated stents. We kept these considerations in mind when we chose the intermediate layers that we used for the immobilization of the P8RI peptide.

IV.2.b. Plasma-polymerized HMDSN

The first coating that we developed in this study was plasma-polymerized hexamethyldisilazane (PP-HMDSN). Indeed, when it came to the choice of a precursor monomer for the atmospheric pressure plasma deposition system we used, we had to consider, besides the requirements outlined above, the compatibility of the precursor with our technique. In that regard, HMDSN had the advantage that its successful deposition by atmospheric pressure plasma had already been largely reported (Kim and Lee 1997; Gengenbach and Griesser 1999; Yang et al. 2009; Hody et al. 2010). Moreover, it had been shown to exhibit appropriate adhesion properties in scratch tests (Kuo and Yang 2000; Nowling et al. 2005), and it was known to be compatible

with the culture of various types of cells (Li and Ho 2008; Krasteva et al. 2009; Radeva et al. 2009). PP-HMDSN thus appeared to fulfil the required conditions for its use as a biomaterials coating.

IV.2.c. Polydopamine

Polydopamine (PDA) is a bio-inspired, self-assembling polymer which was discovered in 2007 by Messersmith and colleagues. This discovery originated from their investigations on the adhesive proteins of marine mussels. They found that the proteins that allow mussels to adhere strongly on any type of substrate are very rich in quinone and amine groups (Lee et al. 2006). This led them to study dopamine, a small molecule previously known for its biological role as a neurotransmitter, which combines an amine and a catechol group (which is converted into quinone by oxidation). They discovered that, when dissolved in an aqueous buffer at a slightly basic pH, dopamine self-polymerizes into a very adherent film, on various types of substrates. Besides, PDA exhibits latent reactivity towards amine and thiol groups, which makes it a very attractive substrate for bioactive molecule immobilization (Lee et al. 2007).

PDA capitulates the outstanding adhesive properties of mussel adhesion proteins, as demonstrated by tape peel tests (Zhu and Edmondson 2011). This has led several groups to use it as an intermediate layer to improve the adhesion of other films (Ou et al. 2011; Beckford and Zou 2014; Sobocinski et al. 2014). Moreover, PDA coatings have been shown to be stable in aqueous medium for at least one month (Yang et al. 2012; Saidin et al. 2013). As for the biocompatibility properties of PDA, they appeared to be very adapted to its application as a stent coating application: it was shown to promote endothelial cell adhesion and proliferation, to decrease platelet adhesion and to reduce SMC proliferation (Ku et al. 2010; Yang et al. 2012; Luo et al. 2013b).

For all these reasons, the final coating that we developed in this study for the immobilization of the P8RI peptide contained polydopamine as an intermediate layer. Indeed, since PDA seems an attractive choice for biomaterials coating, many research groups have proposed its use as an intermediate layer for stent coatings (Kim et al. 2009; Bae et al. 2012; Ding et al. 2014; Liu et al. 2014; Sobocinski et al. 2014; Wang et al. 2014; Liu et al. 2015a; Song et al. 2015; Chen et al. 2016; Kim et al. 2016).

IV.3. Coating techniques

Polymer films can be deposited through a multitude of coating methods. The objective of this section is not to provide a comprehensive review of all the available techniques, but rather to present the coating techniques that were used in this study, and to outline the essential considerations that should be taken into account when developing a process for the deposition of

a polymer-based coating for an application in biomaterials. Reproducibility, scalability and limited cost are essential requirements for any process developed for an industrial application, and coating methods for medical devices are no exception. In addition, processes used in the manufacturing of medical devices need to meet some extra criteria regarding the safety and sterility of the end product, stated by the authorities in the “Good Manufacturing Practices”.

IV.3.a. Plasma-assisted treatments

The first part of the experimental work conducted in this study concerned low-pressure and atmospheric-pressure cold plasma treatments.

Plasma, often referred to as ‘the fourth state of matter’, is a gas medium in which part of the species are ionised. Most technological applications rely on ‘cold’, or ‘non-thermal’ plasmas, in which the temperature of the electrons is higher than that of the heavy species (neutral and ionic atoms and molecules).

Cold plasma are obtained by applying an electric or electromagnetic field to a gas. This causes the ionisation of the gas and the acceleration of the resulting electrons. The plasma is characterized by a high number of collisions between the electrons and the heavy species, which essentially results in ionization, dissociation and excitation of the species. Excited species emit photons of different energies, from infrared to ultraviolet wavelengths. Since only a small part of the gas is ionized, the macroscopic temperature of the gas remains close to the ambient temperature, while many reactive species (free radicals, ions and excited atoms) are produced.

These characteristics (low macroscopic temperature and generation of reactive species) make plasma processes well adapted to the deposition and the surface functionalization of polymers.

The plasma-assisted deposition of polymer coatings is called ‘PECVD’ (plasma-enhanced chemical vapor deposition). It consists in generating a plasma, containing gaseous or nebulized monomers, above a substrate, in a reactor. The resulting polymer coatings generally exhibit high levels of cross-linking, low permeability and good adhesion on the substrate, compared with conventional wet polymerization techniques.

The surface functionalization of substrates can be performed in a similar way, in the same reactors as those designed for PECVD, without the addition of monomers in the gas.

Most cold plasma reactors operate at low pressure, and thus require closed chambers in order to establish a partial vacuum, but atmospheric-pressure cold plasma reactors also exist. These last ones involve much higher gas flows, but also shorter treatment times. As they do not operate under vacuum, cold plasma sources can even be integrated into continuous production processes. They are therefore of great interest for industrial surface treatment processes, including the coating of medical devices.

Both low-pressure and atmospheric-pressure cold plasma reactors have been used in the present study, for the surface functionalization or the coating of alloy substrates.

IV.3.b. Polydopamine deposition

The second type of coating process that we used was the self-polymerization of polydopamine, by dip-coating of the substrates in an aqueous medium. The extreme simplicity and versatility of this method are great advantages for its potential future applications in the coating of medical devices.

Objectives of the thesis work

This thesis work is based on the hypothesis that a CD31-mimicking coating could improve the biocompatibility of two types of metallic stents (coronary and flow-diverting stents), regarding in particular the endothelialization of the stent struts, in terms of delay, extent, and of anti-inflammatory and anti-thrombotic phenotype of the endothelial cells.

To address this issue, we chose to use a synthetic peptide termed P8RI, which acts as a CD31 agonist peptide, for the coating of the surface of stents.

Thus, the first objective of this thesis work was to develop a process for the immobilization of P8RI on alloy surfaces.

The second objective was to perform an *in vitro* assessment of the P8RI-coated surfaces, in terms of anti-thrombotic, anti-inflammatory, and, above all, pro-endothelialization properties.

The third and last objective was the *in vivo* evaluation of P8RI-coated flow diverting stents and coronary stents, in two relevant animal models.

Experimental work

This approach would result in the direct immobilization of the P8RI peptide on the alloy surface, without any intermediate polymeric layer. As there have been concerns about the biocompatibility of several polymers used in stents coatings (this will be further detailed in the discussion), the direct immobilization of P8RI appears as a very attractive solution. In addition, this should minimize the loss of the coated molecules during stent deployment.

The other side of the coin is that the optimization of the direct amination process is necessarily substrate-dependent. In particular, this technique, if developed for the functionalization of L-605 CoCr alloy, might not be applied to FDSs made of nitinol. However, since the use of coronary stents made of CoCr L-605 alloy is by far more frequent than that of FDSs, we considered that it was worth evaluating extensively this approach, in spite of this limitation.

The direct plasma amination of different polymers and carbon-based materials (for instance graphene or carbon nanotubes) has been performed by many research groups, and its mechanisms are partially known (Chevallier et al. 2001; Klages and Grishin 2008; Borris et al. 2009; Lachmann et al. 2009; Sharma and Mutharasan 2012; Artemenko et al. 2015; Yang et al. 2015; Motrescu and Nagatsu 2016; Alam et al. 2017). On the contrary, the literature on direct amination of metallic oxides is scarce (Wang et al. 2012; Ciolan et al. 2014), which made the empirical optimization of the plasma parameters all the more necessary.

The first experiments of plasma amination of CoCr samples were performed with an inductively coupled low-pressure radio frequency plasma reactor (ICP-RF low-pressure plasma reactor). As can be seen on the schematic diagram of an ICP-RF reactor provided on Figure 15, the electric field necessary for the creation of the plasma derives from the magnetic field created by the RF current circulating in the coil that surrounds the reaction chamber. Contrary to the setup of capacitively coupled plasma reactors (CCP reactors), where the electric field is created between two electrodes inside the reactor, the ICP-RF setup has the advantage of preventing possible contaminations from electrodes inside the reactor chamber.

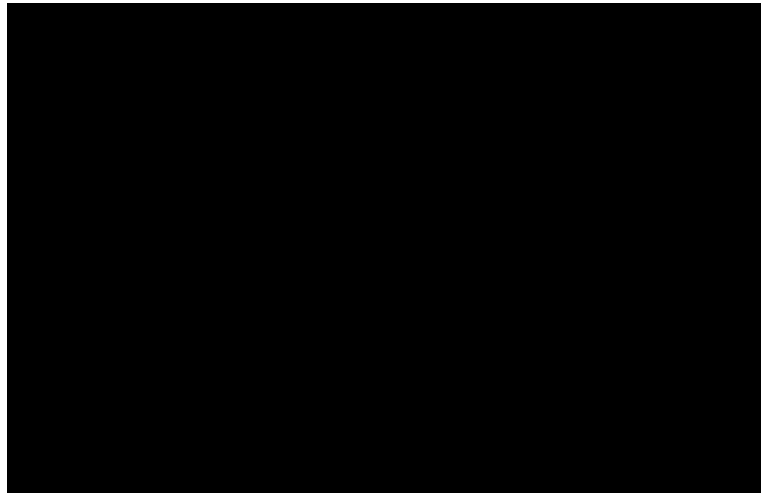


Figure 15. Schematic drawing of an ICP-RF plasma reactor.
Reproduced from Gao et al., 2009.

The ICP-RF plasma reactor that was used in this study was the FLR-300 model manufactured by Plasmionique. A picture of the reactor is shown on Figure 16.

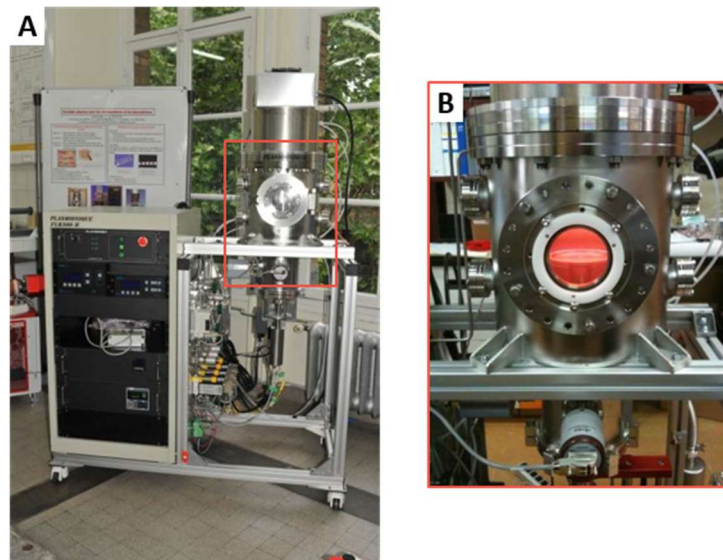


Figure 16. Photograph of the ICP-RF low-pressure plasma reactor used in this study. A: general view. B: close-up of the reactor chamber with the plasma discharge on.

I.1.a. N₂-H₂ low-pressure plasma treatment increases the nitrogen content of CoCr samples but also introduces surface contaminations

All the experiments were performed on polished CoCr L-605 disks, with a thickness of 250 μm and a diameter of either 5 or 20 mm, purchased from Goodfellow Cambridge Ltd (UK). In

order to remove surface organic contaminants, the CoCr disks were systematically ultrasound cleaned in three successive 10-minute baths of acetone, ethanol and deionized water before further treatment. This cleaning process was applied before all the treatments presented in sections II and III.

After the introduction of the CoCr samples in the reactor, the reactor chamber was purged under high vacuum ($2 \pm 1 \times 10^{-3}$ Pa) for 30 minutes. The first gas mixture was then introduced in the chamber and the operating frequency of the vacuum pump was adjusted in order to reach the desired pressure inside the chamber. Once the pressure and the composition of the outlet gas (monitored by mass spectrometry) were stabilized, the plasma discharge was started.

When the plasma treatment involved two successive discharges with different gas mixtures, the previous step was repeated.

After the last plasma discharge had ended, the reactor chamber was purged one last time under high vacuum. Nitrogen gas was then introduced in the chamber until atmospheric pressure was reached and the samples could be retrieved.

Two types of plasma treatment were consecutively used:

- a 50% argon, 50% dioxygen mixture was used to further clean the surface of the samples by physical and chemical etching, by removing organic contaminants in the form of gaseous H_2O and CO_2 (Choi et al. 2003). This type of discharge will be referred to below as "Ar- O_2 pretreatment".

- a mixture of dinitrogen and dihydrogen gases in variable proportions was used for the amination process. This treatment will be designated hereafter as "N₂-H₂ treatment".

The parameters used for these treatments are listed in Table 2.

	Total gas flow rate	Gases ratios	Duration	RF power	Pressure
Ar- O_2 pretreatment	50 sccm	1:1	5 min	100 W	4.5 ± 0.5 Pa
N ₂ -H ₂ treatment	100 sccm	3:1 to 97:3	20 min	100 W	45 ± 5 Pa

Table 2. Parameters used for the plasma treatments. sccm: standard cubic centimeters.

Quantitative information on the chemical composition of the plasma-treated CoCr samples was obtained by X-ray Photoelectron Spectroscopy (XPS). In this technique, the sample is illuminated with monochromatic X-rays, which cause the atoms of the surface (top 1-10 nm) to emit core electrons (named "photoelectrons"). The kinetic energy of these photoelectrons is measured by a detector. The original binding energy of each photoelectron is easily deduced by the following formula: $E_{binding} = E_{X-rays} - E_{kinetic}$. A spectrum of the number of electrons detected versus the binding energy is thus obtained. The atomic composition of the sample is

determined by associating each peak of the spectrum with the corresponding atomic orbital. The relative quantity of the atoms is calculated by measuring the relative area of the peaks and correcting with atomic sensitivity factors.

It is worth noting that XPS cannot detect hydrogen atoms, as they do not have core electrons when they form compounds.

Information on the chemical bonds of the surface of the sample can also be obtained by analyzing the shape of specific atomic peaks on high-resolution spectra. Since the binding energy of the electrons slightly varies according to the chemical bonds the atom is involved in, atomic peaks can be separated in several components by deconvolution. The relative areas of the component peaks are correlated to the relative frequency of each type of chemical bond. An example of peak deconvolution is shown on Figure 17.

XPS spectra were recorded on treated and untreated CoCr disks, using a PHI 5600-CI spectrometer (Physical Electronics). Survey spectra were acquired with a monochromatic aluminum X-ray source (300 W) whereas high-resolution spectra were recorded with a monochromatic magnesium X-ray source (300 W). The detection angle was set to 45°. The analysis was done on three spots per disk to assess the homogeneity of the coating.

We analyzed the spectra with the software MultiPak (Physical Electronics).

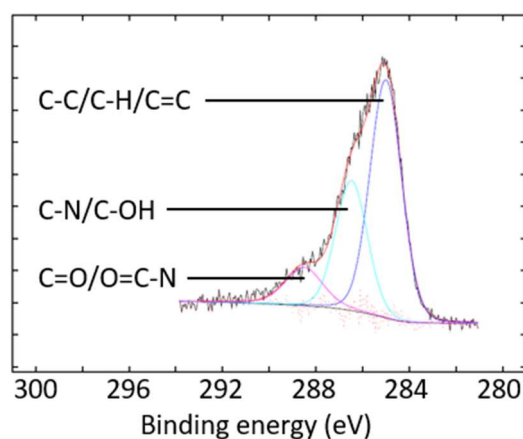


Figure 17. Example of deconvolution of an XPS high-resolution spectrum. The C1s region is deconvoluted in three component peaks. The chemical bonds attributed to each peak are indicated.

The surface atomic percentages calculated from the XPS spectra of the samples are presented on Table 3. As this XPS analysis was the first we performed on the CoCr disks, an “as received” sample (which had not been submitted to any cleaning procedure in our laboratory) was included as well as an ultrasound cleaned sample in order to assess the efficiency of the cleaning procedure and the original level of surface organic contamination of the disks.

CoCr sample	O 1s	C 1s	N 1s	Co 2p3	Cr 2p3	W 4f	Zn 2p	Si 2p	F 1s
As received	20.3	73.7	1.3	0.3	1.5	-	3.0	-	-
Ultrasound cleaned	38.6	50.1	2.3	2.3	4.1	-	2.7	-	-
N₂-H₂ plasma 3% H ₂	40.2	28.2	1.8	6.3	7.7	-	1.6	6.2	7.9
without Ar-O₂ 10% H ₂	41.8	28.4	2.8	3.6	7.6	-	4.5	6.4	5.0
pretreatment 75% H ₂	39.8	28.7	5.5	4.6	6.7	-	3.7	5.5	5.5
Ar-O₂ pretreatment	48.5	21.7	0.9	9.8	2.7	-	4.5	7.2	4.7
N₂-H₂ plasma 3% H ₂	45.5	29.2	1.7	2.1	2.8	1.9	2.9	-	13.8
after Ar-O₂ 10% H ₂	37.4	21.5	1.6	15.0	2.8	-	1.0	8.8	11.9
pretreatment 75% H ₂	38.6	25.0	3.0	9.4	1.7	0.1	4.7	5.5	12.0

Table 3. Surface atomic percentages of CoCr disks after different treatments.

As Table 3 contains a great amount of qualitative and quantitative information, we will first discuss the nature of the detected elements, before focusing on some key quantitative values.

Oxygen and carbon were detected on all samples. This is explained by the presence of metal oxides and (to a lesser extent) carbides, as well as residual surface organic contaminants. Nitrogen was also detected on all samples, including the ones that had not undergone N₂-H₂ plasma treatment. On the untreated samples, nitrogen most probably originated from organic contaminants. Cobalt, chromium, and sometimes tungsten were identified, which was expected as these are the main elements that compose the L-605 CoCr alloy (see Table 4).

Cobalt (Co)	Chromium (Cr)	Tungsten (W)	Nickel (Ni)	Iron (Fe)	Manganese (Mn)
50	20	15	10	3	2

Table 4. Elemental composition of the L-605 CoCr alloy(in %).

Unexpectedly, zinc, silicon and fluorine were detected in significant proportions (1-5% zinc, 5-12% silicon and fluorine). The L-605 alloy does not contain zinc or fluorine, and contains only 0.4% silicon, which cannot explain the detected amounts. Zinc was present on all samples, whereas silicon and fluorine were detected only on the samples that had been treated in the plasma reactor (either by Ar-O₂ pretreatment or by N₂-H₂ treatment). Therefore, the most probable explanation was that zinc contaminated the surface of the samples during their manufacturing process (the disks had been cut out of L-605 sheets in a not particularly clean industrial workshop, probably using galvanized workbenches and tools), whereas silicon and

fluorine were adsorbed on the inner walls of the plasma reactor (silicon- and fluorine-containing precursor gases had been previously used in the reactor by other researchers) and had possibly contaminated the surface of the samples during the plasma treatments.

The measures that were taken to eliminate these contaminations were the electropolishing of the samples (as detailed in I.2) and the cleaning of the low-pressure plasma reactor by prolonged Ar-O₂ plasma discharge.

With the quantitative information obtained from the XPS analysis, we focused on the two most significant values:

- the nitrogen percentage, as it is of course correlated to the success of the amination process
- the carbon/oxygen ratio, which is an indicator of the level of organic contamination, and thus of the efficiency of the cleaning procedure.

These values are plotted on Figure 18. The “as received” disk exhibited a high C/O ratio (around 3.5), which was greatly decreased by the ultrasound cleaning, indicating the successful removal of most of the organic contaminants. Plasma treatments further eliminated organic contaminants, reducing the C/O ratio to about 0.6 with Ar-O₂ pretreatment, and 0.7 without pretreatment.

For both pretreated and not pretreated samples, the amount of nitrogen on the surface increased with increasing H₂ content in the N₂-H₂ plasma discharge. Higher nitrogen percentages were obtained on not pretreated disks compared to the pretreated ones. This observation might be explained by the fact that the C/O ratio of pretreated disks is lower than that of the others, and that nitrogen bonding is most efficient on carbon atoms in organic compounds than on metal oxide.

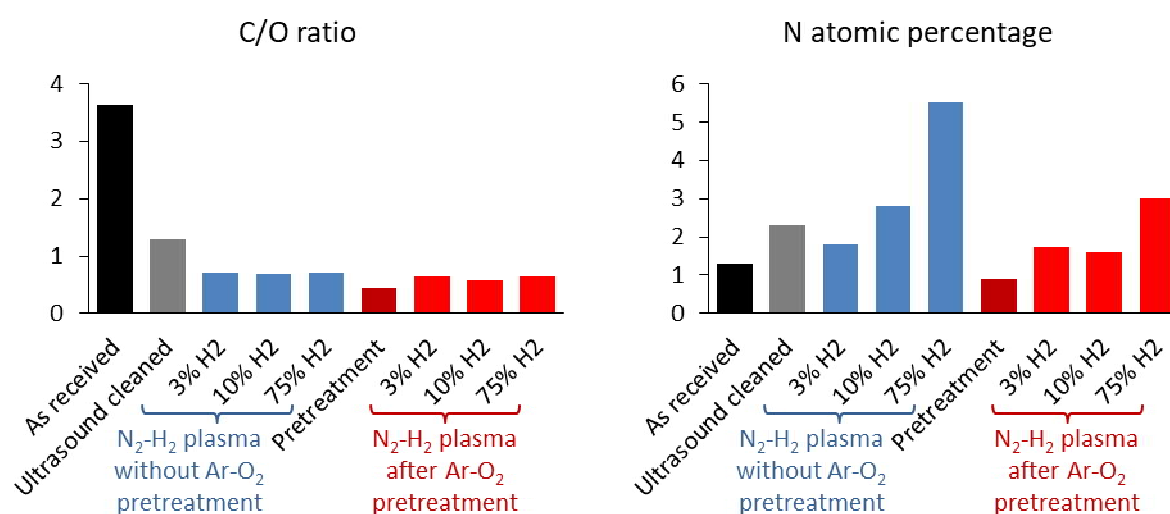


Figure 18. C/O ratio and nitrogen percentage of CoCr disks after different plasma treatments.

The highest measured nitrogen percentage was obtained after a 25% N₂ - 75% H₂ plasma discharge. It was more than twice as high as the nitrogen surface amount of the cleaned sample (5.5% against 2.3%), which proves that the plasma treatment successfully incorporated nitrogen compounds at the surface of the CoCr samples. However, the immobilization of the peptide on these surfaces by carbodiimide chemistry would be possible only if a significant part of the nitrogen atoms were under the form of amine functions. Deconvoluting high-resolution XPS spectra of the N1s region would give information on the chemical state of the nitrogen atoms. However, as shown on Figure 19, the signal/noise ratio of the high-resolution spectra of N1s peaks was too low to allow for a reliable deconvolution. Thus, the surface density of amine functions on plasma-treated CoCr samples could not be determined from this XPS analysis.

After this experience, we used another method for the identification of amine functions on plasma-treated surfaces: derivatization, as detailed below in I.2.

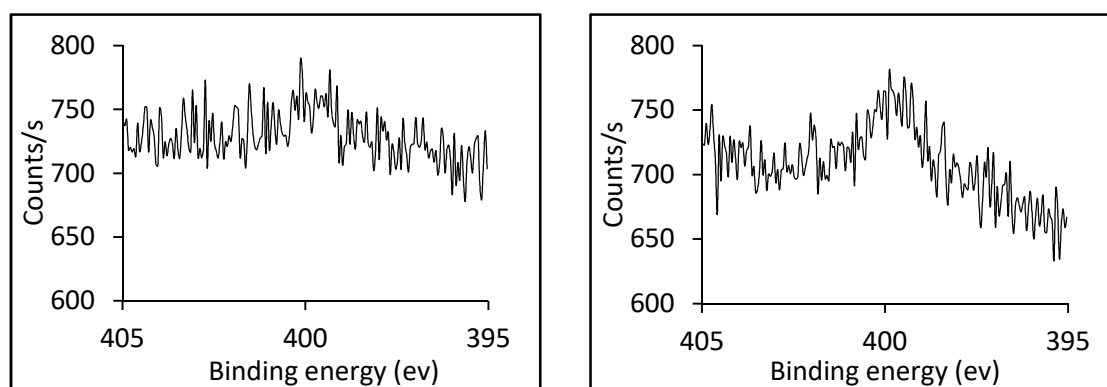


Figure 19. Representative high-resolution XPS spectra of nitrogen peaks on N₂-H₂ plasma-treated CoCr samples. Left: Sample after 3% H₂ - 97% N₂ plasma treatment, without Ar-O₂ pretreatment. Right: Sample after 75% H₂ - 25% N₂ plasma treatment, without Ar-O₂ pretreatment. As the nitrogen percentage is low (a few percent), the spectra appear very noisy.

Despite repeated attempts to eliminate the residual contaminants from the walls of the reactor chamber by argon and oxygen-based plasma treatments, later XPS analyses of samples treated in the reactor still showed significant silicon and fluorine contaminations. These contaminations were a major obstacle for a reliable amination of CoCr samples in the FLR-300 reactor. Thus, the decision was taken to stop the low-pressure plasma treatments with this reactor. This part of the work was pursued with a low-pressure microwave plasma reactor at the Laboratory for Biomaterials and Bioengineering (LBB, Université Laval, Québec City, Canada), where I later spent a two-month period as a visiting scientist during my PhD program, in the framework of a research collaboration.

The direct plasma amination of CoCr samples in a low-pressure microwave plasma reactor was developed at the LBB by Sergio Díaz-Rodríguez, a PhD student under the supervision of Dr

Pascale Chevallier and Pr Diego Mantovani, whose PhD work focuses on the surface treatments and uses P8RI as a model peptide. He subsequently immobilized a PEG (Polyethylene glycol) linker with two carboxylic acid extremities on the aminated surfaces and covalently bonded the P8RI peptide to the linker, by carbodiimide chemistry. I later undertook the *in vitro* and *in vivo* assessment of the biological properties of these surfaces covered with P8RI at the Laboratory for Vascular Translational Science.

In the meanwhile, I pursued the plasma amination approach in Paris using another type of reactor: an atmospheric-pressure plasma jet, as detailed in the following section.

I.2. Direct amination by atmospheric pressure plasma

In parallel with the experiments performed with the low-pressure ICP-RF reactor, N₂-H₂ plasma treatments of CoCr samples were performed with an atmospheric-pressure plasma jet (APPJ). As can be seen on the schematic drawing presented on Figure 20, the samples treated by APPJ are not directly in contact with the plasma but only with the afterglow, a few centimeters away from the core of the plasma. As the afterglow carries the reactive species created in the plasma, this setup allows for the surface modification of all types of samples, including temperature-sensitive polymers.

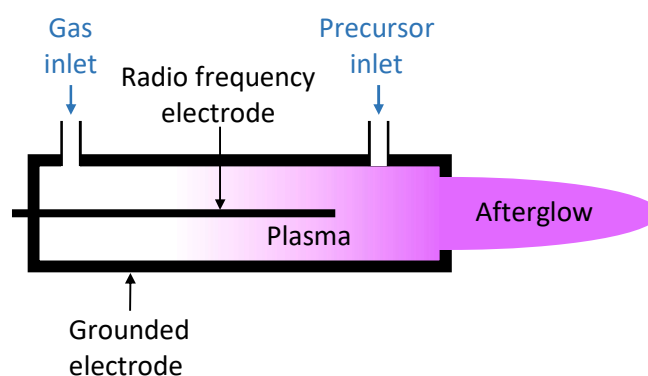


Figure 20. Schematic drawing of the atmospheric-pressure plasma jet.

The main differences between APPJ and ICP-RF low pressure plasma reactors are the pressure at which the reactions occur (10⁵ Pa against 1-100 Pa) and the gas flows involved (about 40 L/min against 0.1 L/min). The power density of the discharge is also much lower, as the APPJ operates at about 700 W for 40 L/min, whereas the ICP-RF operates at 100 W for 0.1 L/min. In addition, the surface modifications of samples in an ICP-RF low-pressure reactor take place in a controlled atmosphere, in a closed reaction chamber, whereas, with an APPJ, the afterglow and the substrate surface are in contact with atmospheric air. Another important difference between

the two reactors is the area of the surface of contact between the plasma (or the afterglow) and the sample. In the ICP-RF reactor, the plasma covers the entire surface of the substrate holder (about 100 cm²), whereas the projected area of the afterglow of an APPJ is only a few square millimetres. Thus, the APPJ nozzle is mounted on a motorized xyz table, so that it can sweep the surface of the sample at constant speed in order to deliver a homogeneous treatment. Finally, since it operates at high flow rates and at atmospheric pressure, the APPJ treatment is much faster and more scalable than the low-pressure plasma treatment. A photograph of the atmospheric pressure plasma reactor used in this study, which was manufactured by AcXys Technologies, is shown on Figure 21.



Figure 21. Photograph of the atmospheric-pressure plasma reactor.

As the plasma is generated at atmospheric pressure and in contact with air, safety precautions have to be taken regarding the use of gases such as dioxygen (which is highly oxidizing) or dihydrogen (highly flammable). Thus, dioxygen and dihydrogen cannot be used in their pure form but only as diluted mixtures with inert gases. As the process generator was not yet suitable for argon discharges at the time of the experiments, Ar-O₂ pretreatment was not performed with the APPJ. A dinitrogen-dihydrogen mixture containing 3% dihydrogen was used for the N₂-H₂ treatments. This concentration ensured the safety of the experiments, since the lower flammability limit for hydrogen in air, with nitrogen as a diluent, is 5.7% at room temperature and atmospheric pressure (*CHEMSAFE database*).

I.2.a. N₂-H₂ APPJ treatment increases the nitrogen content of CoCr samples with high variability

As the first APPJ treatments were performed in parallel with the low-pressure plasma treatments exposed in the previous section, the CoCr disks used for both types of treatments were

submitted to the same cleaning procedure: ultrasound baths in different solvents, without electropolishing, as detailed in section II.1. After ultrasound cleaning, the CoCr disks were stuck on the motorized table with double-sided carbon tape. A small piece of tape was stuck in the centre of each sample, so that the surface of the tape would not be exposed and etched by the APPJ and thus contaminate the surface of the samples.

In order to ensure that the plasma nozzle would sweep the whole surface of the sample at constant speed, its trajectory was defined in a zigzag pattern, as shown on Figure 22. The parameters used for the APPJ treatments are presented on Table 5. XPS spectra were recorded as detailed in the previous section.

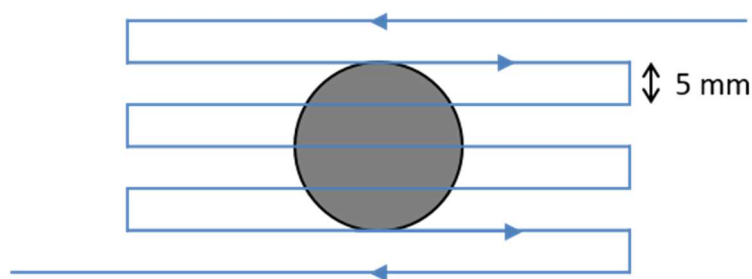


Figure 22. Schematic diagram of the trajectory of the APPJ nozzle above a 20 mm diameter CoCr disk. The width of the zigzag pattern was adjusted so that the nozzle would sweep the sample's surface at constant speed.

Gas flow rate	N ₂ :H ₂ ratio	RF power	Sample-surface distance	Nozzle speed	Number of passes
45 L/min	97:3	600 W	10 mm	25-50 mm/s	1-6

Table 5. Parameters of the plasma treatments performed by APPJ for the direct amination of CoCr samples.

The surface atomic percentages calculated from the XPS spectra of the samples are presented on Table 6. As in the analysis of low-pressure plasma treated samples (I.1), oxygen, carbon and nitrogen were detected on all samples, as well as the main elements constitutive of the L-605 alloy (cobalt, chromium, and tungsten in lower proportions), and zinc, that had contaminated the samples during manufacturing processes.

Silicon was also identified on three plasma-treated samples. This contamination most probably originated from silicon-based coatings previously deposited on the motorized table during experiments performed by other users of the APPJ reactor. A more careful cleaning of the motorized table was thus carried out before later experiments.

	O 1s	C 1s	N 1s	Co 2p3	Cr 2p3	W 4f	Zn 2p3	Si 2s
Ultrasound cleaned	46.1 ± 1.4	36.4 ± 0.5	0.6 ± 0.6	7.2 ± 1.1	5.5 ± 0.9	-	4.3 ± 0.6	-
N₂-H₂ plasma treated	50 mm/s - x1	49.4 ± 0.6	33.5 ± 0.5	1.3 ± 0.1	7.2 ± 1.0	5.6 ± 1.1	-	2.8 ± 0.2
	50 mm/s - x2	49.5 ± 2.0	34.1 ± 2.3	0.4 ± 0.7	6.8 ± 1.0	5.1 ± 0.5	0.3 ± 0.5	2.2 ± 0.1
	50 mm/s - x4	52.9 ± 0.8	25.4 ± 2.2	2.7 ± 0.3	6.4 ± 0.6	2.2 ± 0.1	0.8 ± 0.1	1.0 ± 0.1
	50 mm/s - x6	50.9 ± 3.1	28.7 ± 4.1	2.2 ± 0.6	8.9 ± 0.9	2.3 ± 0.5	0.5 ± 0.2	0.7 ± 0.0
	25 mm/s - x1	55.4 ± 4.0	26.3 ± 6.8	1.6 ± 0.4	8.6 ± 3.5	5.6 ± 1.1	0.8 ± 0.1	1.7 ± 0.5
	25 mm/s - x2	53.9 ± 0.6	24.4 ± 2.1	2.1 ± 0.8	12.8 ± 0.8	4.1 ± 0.6	0.8 ± 0.2	1.8 ± 0.5

Table 6. Surface atomic percentages of ultrasound cleaned CoCr disks, after different atmospheric-pressure N₂-H₂ plasma treatments. For each plasma treated sample, the value in mm/s is the plasma nozzle displacement speed, while the value preceded by an “x” is the number of passes of the nozzle over the sample. Standard deviations were calculated between three measurement points for each sample.

The nitrogen atomic percentages measured on the samples are plotted on Figure 23. There was a general increase of the nitrogen content on the plasma-treated samples, especially on the ones that had been submitted to the most intensive treatments (with the highest number of passes and lowest nozzle speed). However, no consistent trend was observed. This might be attributed to the variability of the initial organic and zinc contamination of the samples, as well as the silicon-based contaminations that occurred during the plasma treatments.

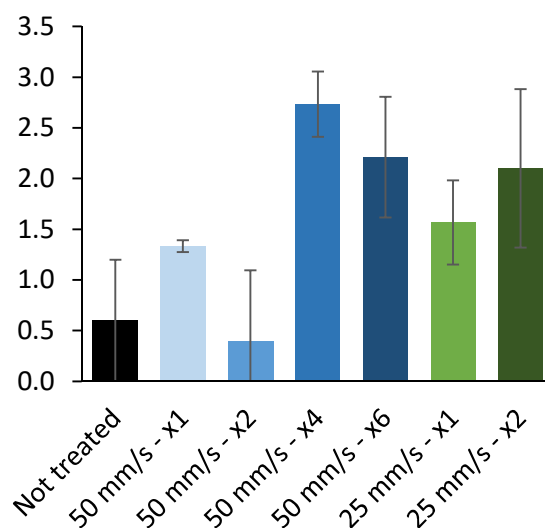


Figure 23. Nitrogen surface percentage of CoCr disks after different N₂-H₂ treatments by APPJ. The N₂-H₂ plasma treatment resulted in an increase of the nitrogen content of the surface on all samples but one. The variability between measurement points was high, and the influence of the number of passages of the plasma nozzle and of its displacement speed did not result in a consistent trend. Error bars: Standard deviations between three measurement points.

Overall, these first analyses revealed that the surface condition of the CoCr disks was not satisfactory, as significant amounts of contaminants were still present on the surface after the ultrasound cleaning procedure. Therefore, an electropolishing procedure was developed to provide a controlled surface status of the samples before the plasma treatments.

I.2.b. An optimized electropolishing treatment removes the zinc contamination and smoothens the surface of the CoCr samples

The development of the electropolishing procedure presented in this section was carried out during a research period at the Laboratory for Biomaterials and Bioengineering of the University of Laval, at Québec City (Canada).

A schematic view of the electropolishing setup is presented on Figure 24. A. The metallic sample is integrated in an electric circuit as the anode, thus leading to the release of metal ions from the surface into an electrolyte solution, usually composed of a mixture of acids such as sulfuric and phosphoric acids. As protruding regions of the sample are submitted to a higher current density, the treated surface is smoothed, as illustrated on Figure 24. B. Controlled electropolishing thus results in the dissolution of the original oxide layer, and the formation of a smoother and cleaner oxide layer. However, an excessive applied voltage provokes an oxygen evolution reaction at the anode ($2 \text{H}_2\text{O} \rightarrow \text{O}_2 + 4 \text{H}^+ + 4 \text{e}^-$), which causes pits of the anode surface (Watanabe 2004).

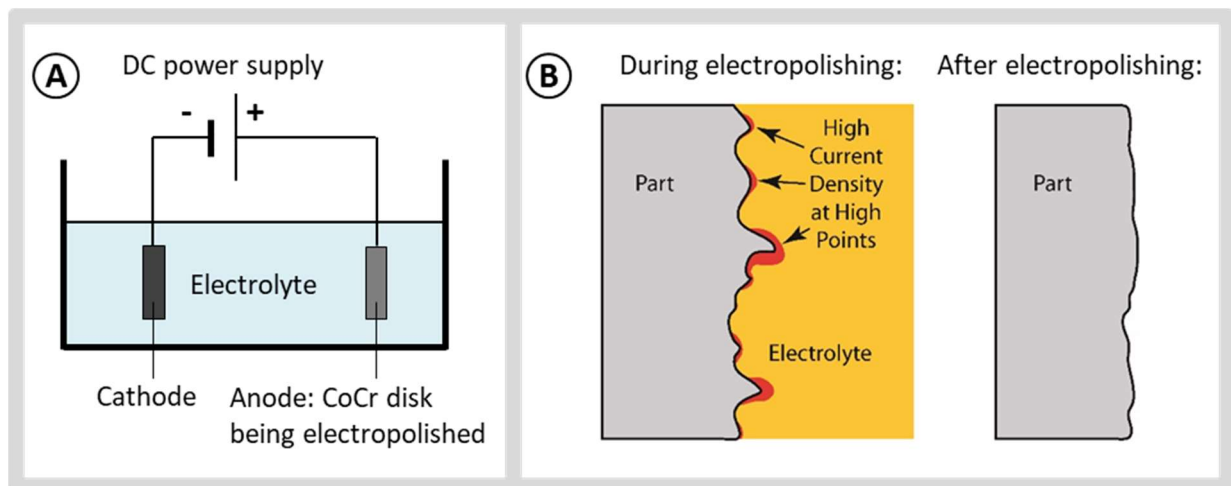


Figure 24. Principle of electropolishing. A. Schematic view of the electropolishing system. B. Principle of surface smoothing by electropolishing. Image reproduced from the website of Cleaning Technologies Group.

The electropolishing protocol used in this study was adapted from a protocol previously developed by other researchers at the Laboratory for Biomaterials and Bioengineering. The CoCr sample to be electropolished was ultrasound cleaned as previously described. After drying by

medical grade compressed air, it was connected to the electric circuit by a crocodile clip. A similar CoCr disk was used as the cathode. Both disks were immersed in a beaker containing the electrolyte solution, surrounded by ice. The composition of the electrolyte solution is presented in Table 7. The electropolishing current intensity and duration was experimentally adjusted, as detailed below. At the end of each electropolishing cycle, the sample was extensively rinsed with deionized water. After the electropolishing treatment, three successive ultrasound baths in deionized water / NaOH 2N / deionized water were carried out in order to neutralize any remaining acid and rinse the surface of the sample.

Component	H ₃ PO ₄	H ₂ SO ₄	HF	Glycerol	Water
Concentration (% v/v)	57	20	1.5	1	20.5

Table 7. Composition of the electropolishing solution used in this study.

The samples were analyzed by scanning electron microscopy, atomic force microscopy and XPS. Scanning electron microscopy (SEM) was carried out in Secondary Electrons mode, at 15 kV, on a JMS-35CF (JEOL). Atomic force microscopy (AFM) was performed in tapping mode on a DimensionTM 3100 (Digital Instrument). XPS spectra were recorded as detailed in section II.1.

In order to obtain a smooth, mirror-bright surface, without pits, the electropolishing current intensity and duration were experimentally optimized. To that end, the treated samples were analyzed by visual inspection and scanning electron microscopy. An example of macroscopically damaged sample is provided on Figure 25, whereas the microscopic effects of moderate and excessively intense electropolishing are shown on Figure 26.



Figure 25. Photograph of a CoCr disk after excessively intensive electropolishing (two 2-minute cycles at 9.4A). The surface appears mirror-bright, but the edges of the sample are visibly etched. The marks at the top of the image were produced by the crocodile clip that held the sample during the electropolishing process.

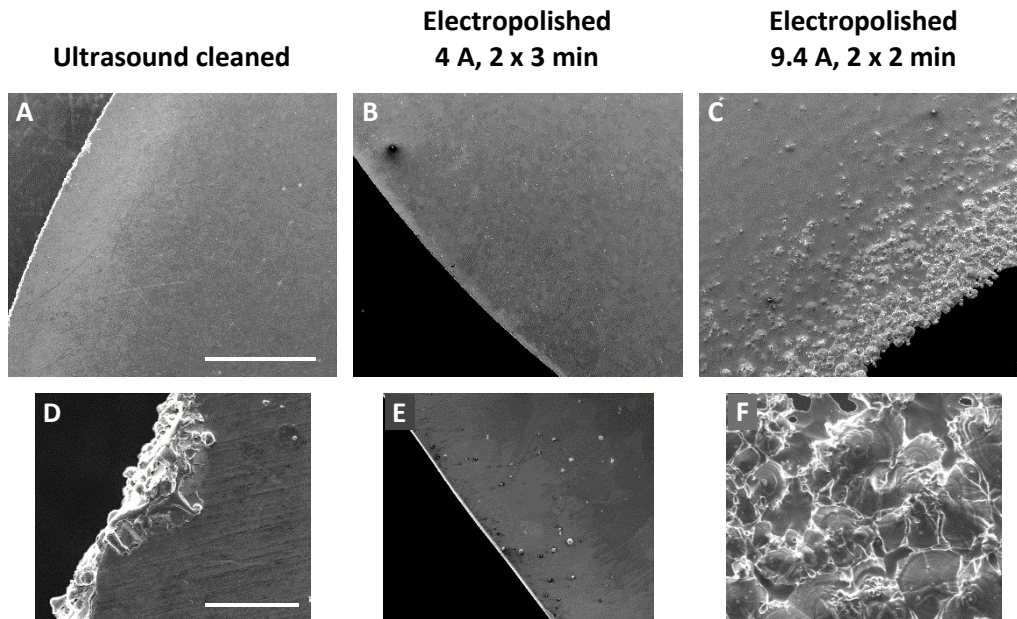


Figure 26. SEM pictures of the edges of CoCr disks. A, B, C: Scale bar = 1 mm. D, E, F: Scale bar = 100 μm . Moderate electropolishing smoothens the surface and the edges (B, E), whereas excessively intense electropolishing roughens the edges (C, F).

The optimal electropolishing treatment was found to be two cycles of 3 minutes, with a current intensity of 4 A. The samples treated with these parameters will be referred to simply as “electropolished” from now on. As shown on Figure 27, the surface of the samples after this treatment appeared flat, free from organic contaminants and scratching grooves, when observed by SEM. The inclusions that were revealed by the electropolishing are most probably chromium and tungsten carbides, which are known to form in L-605 alloy (Tiwari and Nordin 2014).

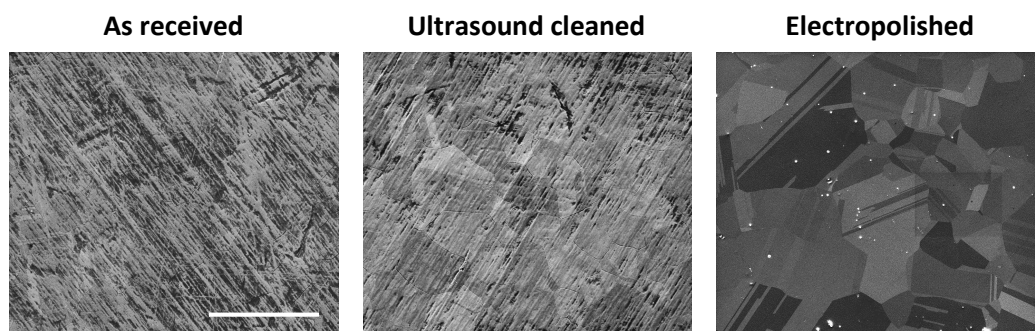


Figure 27. SEM pictures of CoCr samples after different surface treatments. Scale bar = 100 μm . Scratching grooves are visible on the “as received” and ultrasound cleaned samples, as a result of the mechanical polishing performed by the manufacturer. Black streaks, identified as organic contaminants, are present in the grooves, in particular on the “as received” sample. The grain structure is weakly visible on the ultrasound cleaned sample, and indiscernible on the “as received” sample. On the electropolished sample, the surface appears perfectly flat and free from grooves and organic contaminants. The grain structure is revealed, as well as some inclusions.

The visual characterization of CoCr samples before and after electropolishing was completed by AFM analysis, as presented on Figure 28. The images taken by AFM at intermediate magnification (10 μm -wide pictures) are consistent with the observations made by SEM: the ultrasound cleaning removes most of the surface organic contaminants, and electropolishing flattens the surface by eliminating scratching grooves. Higher magnification (1 μm -wide images) reveals a change in the nanometric roughness of the samples after electropolishing.

Finally, the surface chemical composition of an electropolished sample was analyzed by XPS. The resulting surface atomic percentages are presented on Table 8. Zinc was eliminated from the electropolished sample, and the cobalt/chromium ratio was modified. The presence of fluorine and sodium contamination (from hydrofluoric acid and sodium hydroxide respectively) on the electropolished samples points to the necessity of a more extensive rinsing.

	O 1s	C 1s	N 1s	Co 2p3	Cr 2p3	Zn 2p3	Na 1s	F 1s
Ultrasound cleaned	46.0 \pm 0.5	35.5 \pm 0.4	0.7 \pm 0.9	7.1 \pm 0.9	6.7 \pm 0.9	3.9 \pm 0.7	-	-
Electropolished	44.5 \pm 3.3	32.7 \pm 5.9	-	3.5 \pm 0.6	10.1 \pm 0.9	-	5.3 \pm 1.5	3.7 \pm 0.1

Table 8. Surface atomic percentages of ultrasound cleaned and electropolished CoCr samples, measured from XPS spectra. Standard deviations were calculated between three measurement points for each sample. Electropolishing results in an elimination of the zinc surface contamination and an inversion of the Co/Cr ratio. The sodium and fluorine detected on the electropolished sample were adsorbed from the etching and neutralizing solutions.

In conclusion, after optimization of the duration and current intensity of the process, electropolishing resulted in smooth, mirror-bright and zinc contamination-free CoCr samples. Thus, the subsequent plasma treatments were carried out on electropolished CoCr samples.

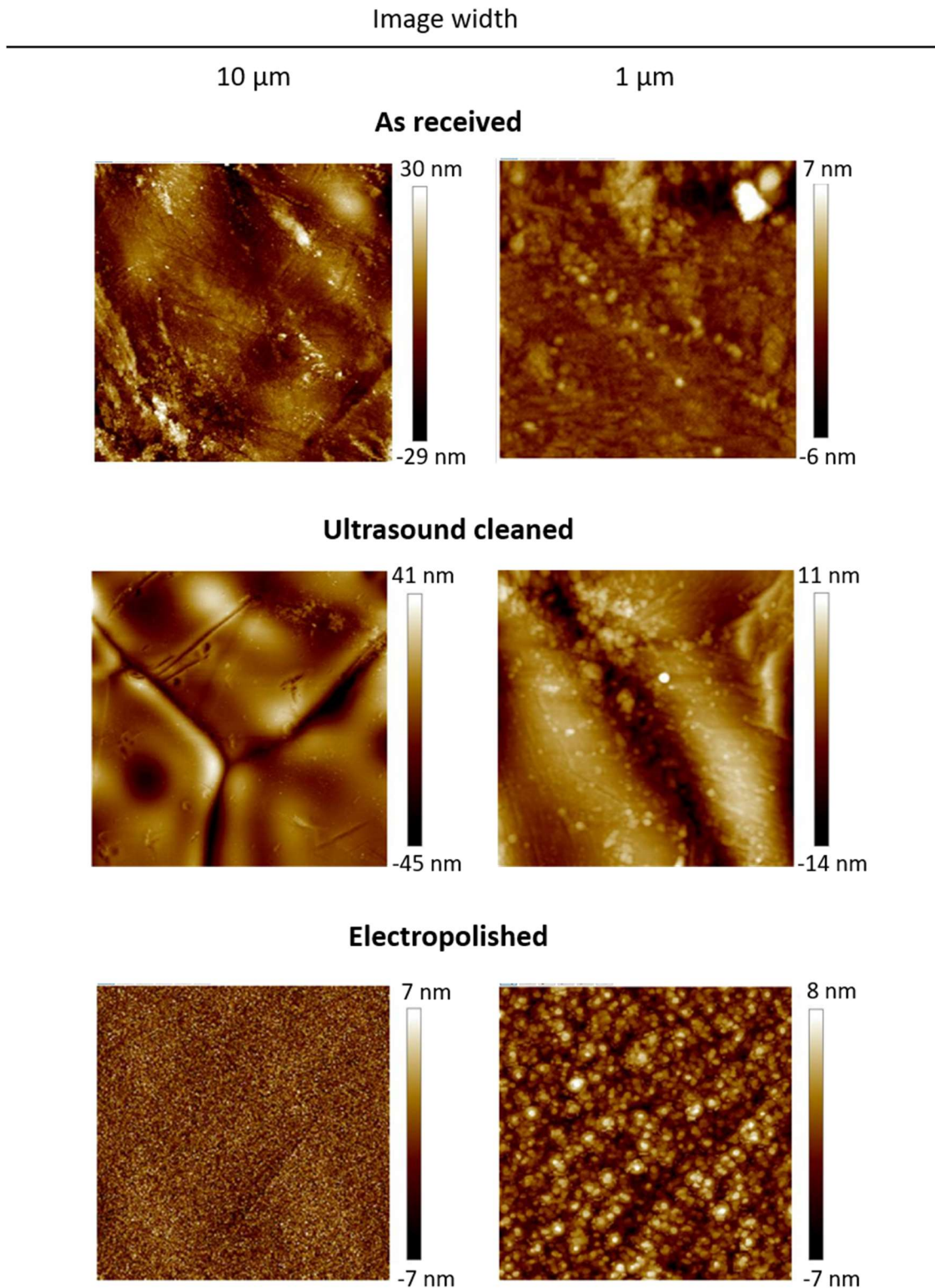


Figure 28. AFM pictures of CoCr disks. The “as received” sample appears covered with irregular particles, identified as organic contaminants. On the ultrasound cleaned samples, some irregular particles are also visible, but the grain boundaries are clearly revealed. The electropolished sample appears much flatter than the other ones at low magnification (on the 10 μm -wide images, the amplitude of altitude variation is 14 nm for the electropolished sample against 59 and 86 nm for the other two samples). At higher magnification (on the 1 μm -wide picture), nanometric asperities are visible on the surface of the electropolished sample.

I.2.c. Derivatization provides no evidence of amines on the surface of CoCr disks after N₂-H₂ atmospheric pressure plasma treatment

As detailed above, the first XPS analyses of CoCr samples treated by N₂-H₂ plasma with the APPJ reactor had shown an increase of the surface nitrogen concentration, depending on the nozzle speed and number of passes. In order to determine whether a significant proportion of this nitrogen was under the form of amines, we decided to carry out a more specific analysis of such samples: the derivatization of primary amines. Succinimidyl iodoacetate (SIA) was chosen because it fulfils the two requirements of a derivatization reactive:

- as a succinimidyl ester, it reacts specifically with primary amines (Wong 1991) (reaction shown on Figure 29);
- it contains iodine, an element which is absent from the surface of treated CoCr samples, and highly detectable by XPS (relative sensitivity factor: 20).

Therefore, if iodine was detected on CoCr surfaces after SIA derivatization, it would demonstrate the presence of amines.

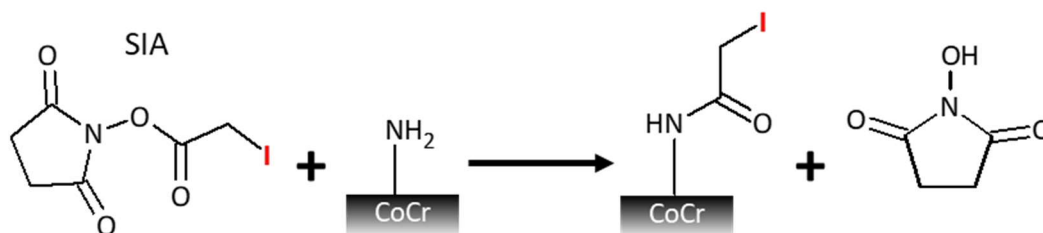


Figure 29. Representation of the derivatization reaction between the SIA and the aminated CoCr surface.

An ultrasound cleaned, electropolished CoCr disk was treated by N₂-H₂ plasma with the APPJ reactor, as detailed on page 68. The plasma nozzle speed and number of passes that had resulted in the highest nitrogen concentration in the first experiments were selected (50 mm/s, 4 passes).

Immediately after the plasma treatment, the sample was incubated for 2h in a 3 mg/mL solution of SIA, diluted in PBS with 1% DMSO, protected from light. It was then extensively rinsed with PBS. XPS spectra were recorded on the sample as detailed previously. Figure 30 presents the surface atomic percentages calculated from the XPS analysis of an electropolished sample and the sample which had been submitted to electropolishing, N₂-H₂ atmospheric-pressure plasma and SIA derivatization. On the derivatized sample, the nitrogen surface concentration was only 1.0%. Phosphorus and chlorine contaminations from the derivatization buffer were detected, but no iodine could be identified. Therefore, the derivatization procedure failed to evidence the presence of amines on the plasma-treated surface.

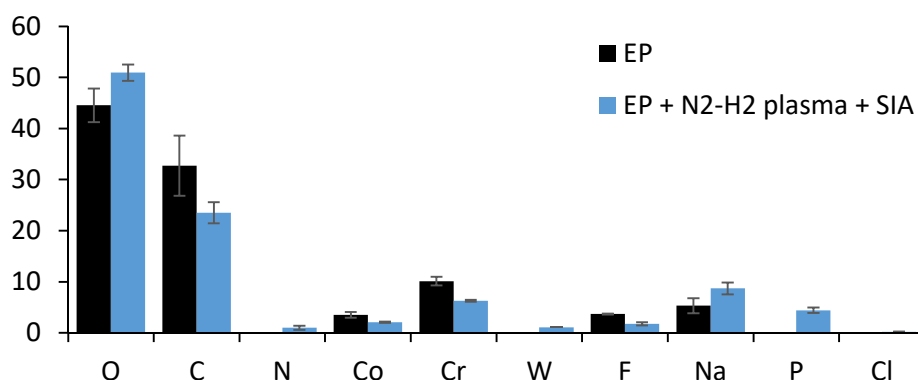


Figure 30. Surface atomic percentages of CoCr disks. “EP”: electropolished sample. “EP+N₂-H₂ plasma + SIA”: sample that had been submitted to electropolishing, N₂-H₂ atmospheric-pressure plasma and succinimidyl iodoacetate derivatization. Error bars: SD between three measurement points. No iodine was detected on the “EP+N₂-H₂ plasma +SIA” sample, meaning that the derivatization procedure failed to evidence the presence of amines on the plasma-treated surface.

Therefore, despite the great attractiveness of direct amination by APPJ in terms of process scalability, and, above all, as a means to avoid potential biocompatibility issues associated with the use of polymers, we did not pursue this approach. We switched to a more common approach: the use of an intermediary plasma-deposited polymeric coating, on which amines would be grafted by a second plasma treatment. This approach was considered to bear higher chances of success, since the amination of polymers is highly documented (Chevallier et al. 2001; Klages and Grishin 2008; Borris et al. 2009; Lachmann et al. 2009; Sharma and Mutharasan 2012; Artemenko et al. 2015; Yang et al. 2015; Motrescu and Nagatsu 2016).

1.3. HMDSN film deposition by atmospheric pressure plasma

As detailed in the introduction, hexamethyldisilazane (HMDSN, structure shown on Figure 31) was chosen as the precursor for the plasma-deposited polymer for its compatibility with our deposition system and its reported biocompatibility and adhesion properties.

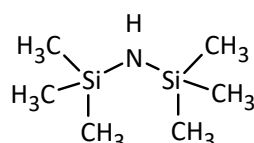


Figure 31. Structure of the HMDSN molecule.

I.3.a. Characterization of the PP-HMDSN coatings

The first depositions of atmospheric pressure plasma-polymerized HMDSN coatings (PP-HMDSN) took place before the development of the electropolishing procedure. Therefore, the CoCr disks used for the deposition of PP-HMDSN were submitted to ultrasound cleaning, without electropolishing (procedure detailed in section II.1). The APPJ deposition was then performed as described in section II.2, with the addition of the HMDSN precursor being brought to the plasma nozzle by a carrier gas. Pure N₂ was used both for the generation of the plasma and as the carrier gas. The parameters used for the HMDSN deposition by APPJ are presented on Table 9.

Carrier gas (N ₂) flow rate	Precursor (HMDSN) flow rate	Total N ₂ flow rate	RF power	Sample-surface distance	Nozzle speed	Number of passes
15 L/min	25-100 µL/min	50 L/min	550-800 W	10 mm	50 mm/s	3

Table 9. Parameters used for the plasma-enhanced chemical vapor deposition of HMDSN by APPJ.

XPS, SEM and AFM analyses of bare and coated CoCr disks were performed as described in the previous sections. The chemical composition of the PP-HMDSN coatings was analyzed by Fourier Transform Infrared (FTIR) spectroscopy. This technique relies on the principle that chemical bonds absorb infrared radiations at particular wavelengths, corresponding to vibrational transitions. In FTIR spectroscopy, a polychromatic infrared light goes through an interferometer and is then shone on the sample. After contacting the sample, the partially absorbed beam is directed to a detector, which records an interferogram. The interferogram is then converted to an absorbance spectrum as a function of wavelength by Fourier transform. The peaks in that spectrum give qualitative information on the chemical composition of the sample.

There are different possible techniques to bring the infrared beam in contact with the sample and detect it afterwards. We used the most common one: Attenuated Total Reflectance (ATR). In this method, represented on Figure 32, infrared radiations go through a crystal with high refractive index and undergo a total internal reflection when they reach the crystal/sample interface. That creates an evanescent wave with a penetration depth on the order of the wavelength. In this way, absorbance from the top 1-10 micrometers of the sample is measured.

FTIR spectra were recorded on bare and coated CoCr disks, using a Cary 660 FTIR spectrometer (Agilent Technologies) equipped with a GladiATR module (Pike Technologies) with a diamond crystal.

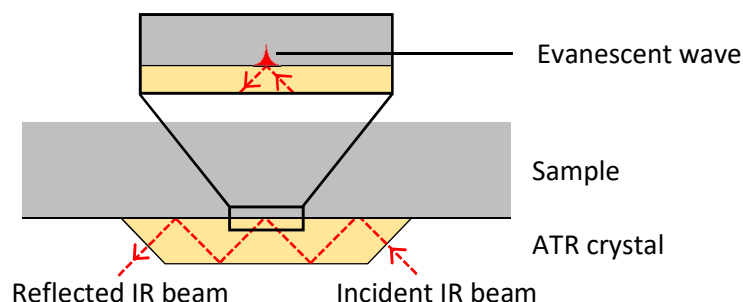


Figure 32. ATR principle. IR: infrared. The incident IR beam undergoes multiple reflections at the sample-crystal interface between exiting the crystal.

Representative pictures of a PP-HMDSN-coated CoCr disk, taken by SEM, are shown on Figure 33. The coating appeared uniform at low magnification, and covered with round-shaped asperities at higher magnification.

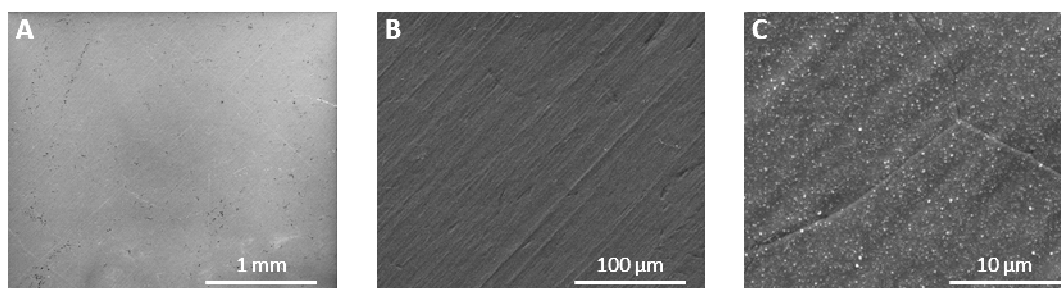


Figure 33. SEM pictures of PP-HMDSN-coated CoCr disk. (Deposition parameters: 550 W, 50 $\mu\text{l}/\text{min}$.) The coating appears homogeneous at low magnification (A, B). The underlying scratching grooves and grain boundaries are discernable (B, C). At higher magnification (C), asperities are visible on the surface of the coating.

The AFM pictures (see Figure 34) were consistent with the observation of these spherical asperities. Other groups have reported the presence of such clusters (Grimoldi et al. 2009; Gonzalez-Macia et al. 2010) and have attributed their formation to the roughness of the underlying substrate, which would limit the lateral diffusion of the precursor (Grimoldi et al. 2009).

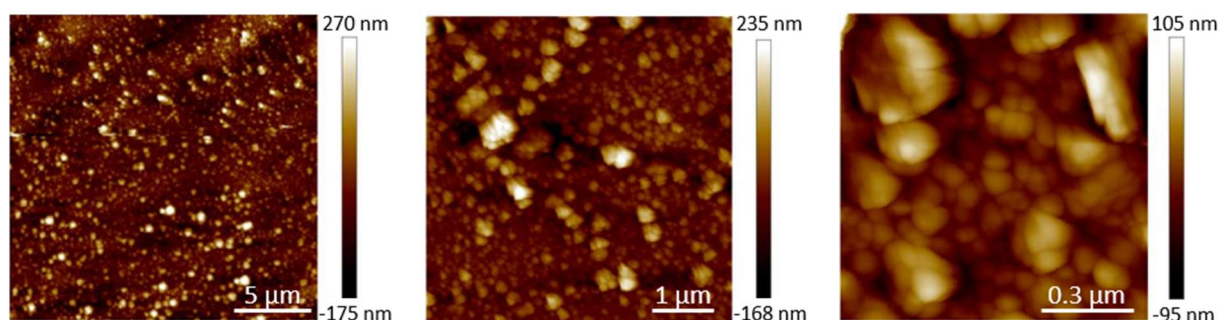


Figure 34. AFM pictures of PP-HMDSN-coated CoCr disk. (Deposition parameters: 550 W, 50 $\mu\text{l}/\text{min}$.) Spherical asperities measuring a few tens of nanometers in diameter are visible on the coating.

Representative spectra of a bare CoCr disk and a PP-HMDSN-coated CoCr sample are shown on Figure 35. The attribution of the peaks was done in accordance with the literature on such coatings (Huang et al. 2010; Guruvenket et al. 2012; Ivashchenko et al. 2014). The main peaks corresponded to Si-O and Si-C peaks. There was no evidence of Si-N peak (which, if present, would be around 950 cm^{-1}), suggesting that there had been no significant integration of nitrogen in the coating. No clear difference was observed between the FTIR spectra of CoCr samples on which HMDSN had been plasma polymerized with different deposition parameters (generator power, number of passes, nozzle speed, precursor flow rate).

The absence of nitrogen was confirmed by the XPS analysis of several PP-HMDSN-coated CoCr disks (see Figure 36), which showed almost no nitrogen on the surface. No metal from the underlying substrate was detected, as expected from the uniformity of the coatings when observed by SEM or AFM. A high level of oxygen incorporation from the surrounding atmospheric air was observed. The silicon concentration remained constant with the variations of generator power and HMDSN flow rate. However, the oxygen/carbon ratio increased with increasing generator power/precursor flow rate ratio. Given that the HMDSN molecule does not contain oxygen atoms, this observation can be explained by the fact that, a higher power/precursor flow rate ratios, the dissociation of the HMDSN molecules is more complete, and therefore less carbon is integrated in the coating.

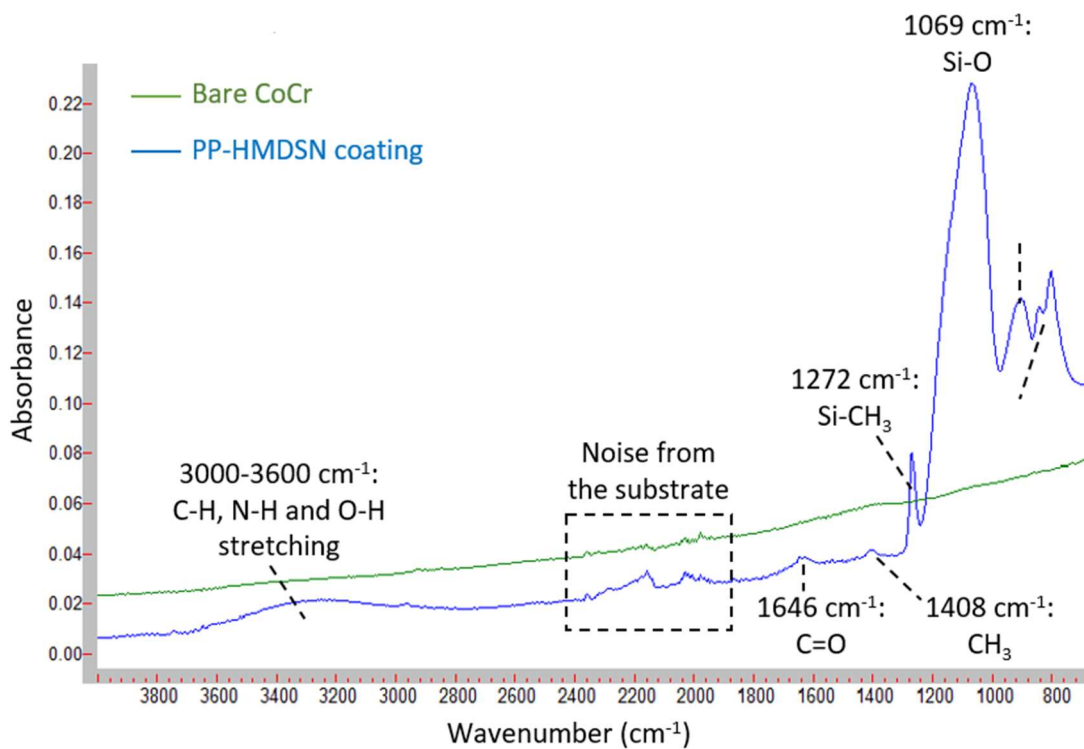


Figure 35. Representative FTIR spectrum of a PP-HMDSN coating. Si-O is the preponderant peak. Si-C peaks are also clearly visible. The Si-N peak was not identifiable.

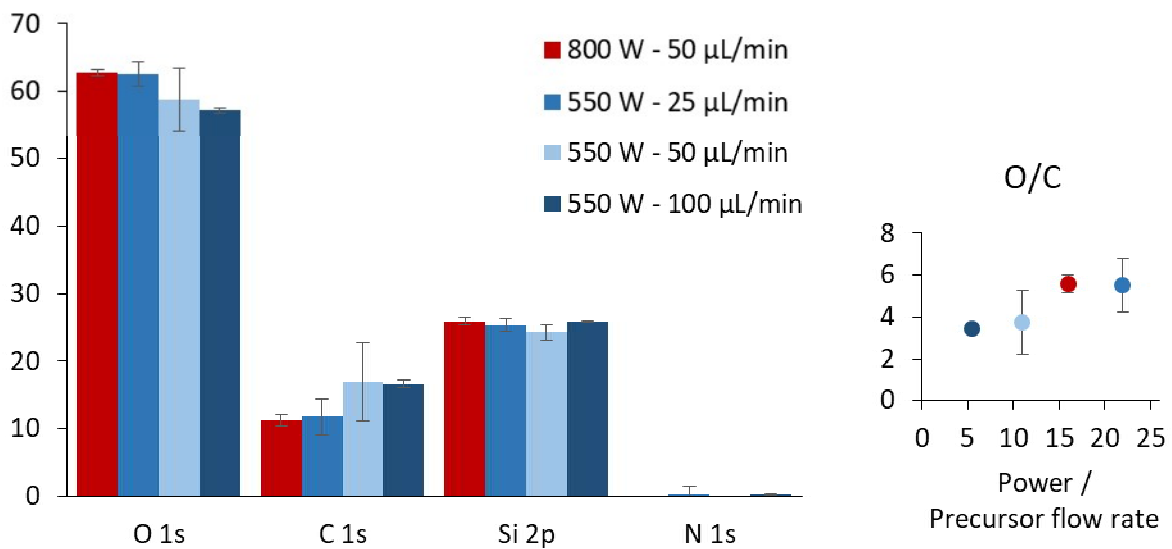


Figure 36. Elemental composition of PP-HMDSN-coated CoCr disks. Left: surface atomic percentages. The legend indicates the generator power and the precursor flow rate used during the treatment. Right: oxygen/carbon ratio of the same samples, as a function of the generator power / precursor flow rate ratio.

I.3.b. Thickness estimation of the PP-HMDSN coatings

The thickness of the PP-HMDSN coatings deposited with an APPJ reactor, at the laboratory 2PM, was not measured during this study. However, other researchers of this laboratory performed ellipsometry measurements on coatings deposited with the same reactor, but with a different precursor: tetraethyl orthosilicate (TEOS). The deposition rates of PP-HMDSN and PP-TEOS coatings by atmospheric pressure RF plasma have been shown to be almost identical (Moravej and Hicks 2005). Thus, the thicknesses of PP-HMDSN and PP-TEOS coatings deposited in similar conditions can be expected to be very close.

A comparison between the deposition parameters used for the PP-HMDSN coatings and the PP-TEOS coatings is presented on Table 10. The precursor flow rate and the nozzle sweep speed of the PP-TEOS were higher than that of the PP-HMDSN. An increase of the precursor flow rate resulted in increased deposition rates (Moravej and Hicks 2005), while an increase of the nozzle sweep speed resulted in a decreased residence time of the plasma, and thus a decreased deposition rate. Therefore, there are sound reasons to believe that the thickness measured on the PP-TEOS coatings is close to that of the PP-HMDSN coatings.

The experimental ellipsometry measurements performed on PP-TEOS films yielded a thickness of 27 ± 2 nm. This value can therefore be considered as a rough estimate of the thickness of PP-HMDSN films.

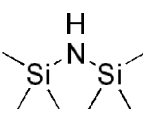
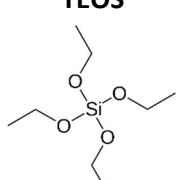
Precursor	HMDSN 	TEOS 
Precursor flow rate	25-100 $\mu\text{L}/\text{min}$	200 $\mu\text{L}/\text{min}$
Nozzle sweep speed	50 mm/s	300 mm/s
RF power	550-800 W	800 W
Main gas	N_2 , 35 L/min	Air, 35 L/min
Carrier gas	N_2 , 15 L/min	N_2 , 5 L/min
Sample-surface distance	10 mm	10 mm
Number of passes	3	3

Table 10. Comparison between the parameters used for the deposition of the PP-HMDSN coatings presented in this thesis work, and the PP-TEOS coatings on which thickness measurements were performed by ellipsometry. Besides the nature of the precursor, the main differences are the precursor flow rate and the nozzle sweep speed.

However, it must be noted that ellipsometry can only provide an average value of the thickness. The observation of PP-HMDSN coatings by AFM (Figure 34) revealed the presence of irregular clusters of about 10 nm diameter on the surface, and the RMS roughness calculated from these images was approximatively 50 nm.

In conclusion, the PP-HMDSN films can be considered to have a very rough profile, with an average thickness of the order of several tens of nanometers. This is much less than the typical thickness of polymeric coatings on stents, which range between 5 and 15 μm (Stefanini et al. 2014). In the context of biomaterials coating, the thinness of the PP-HMDSN films can be considered as an advantage since it means that the total amount of PP-HMDSN present on the device is very small; thus, should the films release potentially toxic degradation products *in vivo*, the effects of these products would be limited by their minute quantity.

I.3.c. The coating does not withstand 7 days of ageing test in flow conditions

As the stability of the coating in aqueous medium is critical for its target *in vivo* application, it was assessed by an ageing test in flow conditions. The dynamic test bench is shown on Figure 37. It had been developed in the Laboratory for Biomaterials and Bioengineering specifically for the testing of degradable or coated samples in laminar, pseudo-arterial flow.

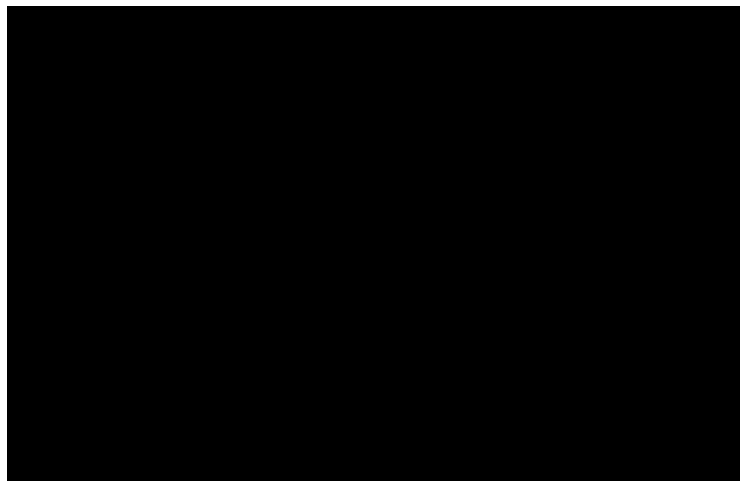


Figure 37. Schematic view of the dynamic test bench, from Lévesque et al. (2008)

Different types of ageing media were considered, as summarized in Table 11. The objective was to choose a medium comparable to blood (in which stents are placed *in vivo*) and free of compounds that would adsorb on the surface of the samples and distort the XPS analysis at the

end of the test. PBS was chosen, as it exhibits a physiological pH and contains no organic compounds, which means that it would not bring carbon or nitrogen to the coating.

<i>Liquid medium</i>	<i>Isotonicity</i>	<i>Physiological pH</i>	<i>Absence of organic compounds</i>	<i>Ionic composition close to that of human plasma</i>
<i>Deionized water</i>	x	x	✓	x
<i>Normal saline</i>	✓	x	✓	x
<i>PBS</i>	✓	✓	✓	x
<i>Pseudo-phys. solutions</i>	✓	✓	x	✓
<i>HBSS</i>			<i>Glucose</i>	
<i>m-SBF</i>			<i>HEPES</i>	
<i>DMEM</i>			<i>HEPES, glucose, amino acids</i>	

Table 11. Properties of the different liquid media considered for ageing tests. Normal saline: 0.9% NaCl in water. Pseudo-phys.: Pseudo-physiological. HBSS: Hank's Balanced Salt Solution. m-SBF: modified Simulated Body Fluid. DMEM: Dulbecco's Modified Eagle's Medium

The dynamic ageing test was performed on two PP-HMDSN-coated CoCr disks (deposition parameters: 550 W, 50 $\mu\text{L}/\text{min}$), in two separate test benches. Each disk was fitted in a custom sample holder designed to expose its coated surface to the laminar flow. The test benches were filled with sterile PBS and placed in a thermostat bath at 37°C (human core body temperature) for one week. After the test, the disks were removed from their holders, thoroughly rinsed with deionized water, and dried with medical-grade compressed air.

They were then examined by SEM, in Secondary Electrons mode, at 6 kV, on a JMS-35CF (JEOL). At the end of the seven-day ageing test, visual inspection of the coated samples showed that large areas of the surface were bared. This observation was confirmed by SEM, as shown on Figure 38: large delamination zones appeared.

As the conclusion of the test was clear, XPS was finally not carried out on the samples.

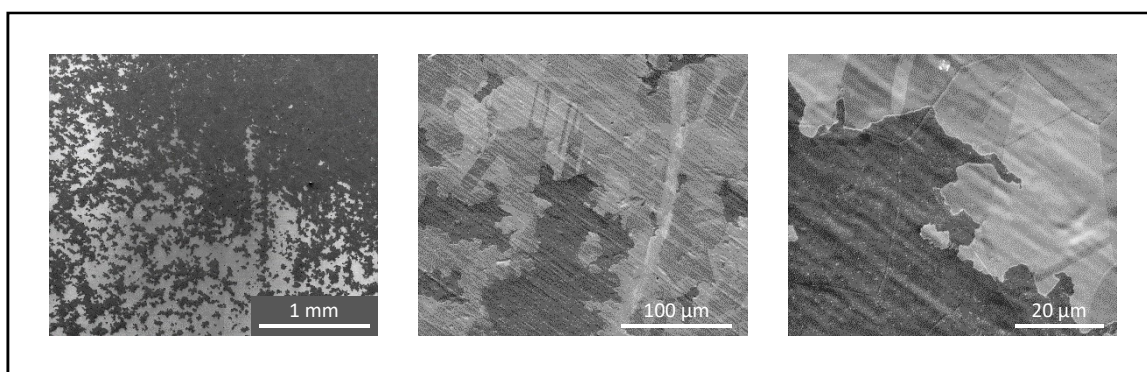


Figure 38. SEM pictures of a PP-HMDSN-coated CoCr disk after a 7-day ageing test in flow conditions. Extensive delamination of the coating took place.

The poor adhesion of the PP-HMDSN coatings in flow conditions can seem surprising, since the adhesion properties of these coatings on various substrates are generally considered as satisfactory, as demonstrated by scratch tests of low-pressure PP-HMDSN (Kuo and Yang 2000) and atmospheric-pressure PP-HMDSN (Nowling et al. 2005). A first remark to be made is that these tests are carried out on dry coatings. Thus, contrary to the dynamic test bench, they do not take into account the possible softening and swelling of the coatings upon exposure to aqueous media, which can favor delamination. Another important point is the surface condition of the substrates. The ageing test in flow conditions was performed on PP-HMDSN coatings that had been deposited on non electropolished coated samples. The substrates thus presented a rough surface, which is beneficial for the coatings adhesion (Amada and Hirose 1998), but also a poorly controlled chemical composition, due to surface contaminations (as shown above on Table 6). As the surface chemical properties of the substrate play a key role in film adhesion (Lewis 2009), electropolishing and plasma pretreatments could drastically improve the adhesion of the PP-HMDSN coatings. Indeed, argon, dinitrogen and ammonia plasma pretreatments have been shown to increase adhesion of SiO_2 films on stainless steel (Bertrand et al. 1998). Thus, further work on PP-HMDSN coatings for stent applications would first require an optimization of the substrates pretreatment.

As the successful immobilization of the peptide was critical for the second part of the project (the assessment of the biological properties of the coated surfaces), it was decided to stop the optimization of the atmospheric pressure plasma processes, and to switch to a well-documented dip-coating process: the deposition of a polydopamine coating.

In parallel, the work on the deposition of organosilicon precursors by APPJ was continued by other researchers at the laboratory 2PM. Thin films were deposited from (3-Aminopropyl)trimethoxysilane (APTMS). XPS analyses of the chemical composition of these films

revealed that they were composed of approximately 6% of nitrogen. Derivatization recently showed that they contained a significant proportion of amine functions. Future work will tell whether these films can serve as an intermediate layer for the immobilization of bioactive molecules.

I.4. Polydopamine-based coatings

Based on the results of series of pilot studies exploring the opportunities and difficulties carried by the different tested approaches, we chose to pursue our work using the polydopamine-based technique for the immobilization of the peptide on the stent surface.

I.4.a. Polydopamine self-assembly

The first step was the deposition of a self-assembled polydopamine layer on the L-605 CoCr samples.

The CoCr disks used in the work presented in this section were different from the ones used for the plasma treatments. The dimensions of the disks were unchanged, but the new batch was made from mirror-polished L-605 sheets processed by the manufacturer (Goodfellow Cambridge Ltd), whereas the first batch had been cut into disks in an uncontrolled industrial workshop, from roughly polished sheets. Thus, the new CoCr disks were free of zinc contaminations, and presented a very flat surface. Therefore, the electropolishing procedure (which had been shown to introduce sodium and fluorine contaminations, see Table 8) was replaced with a simple acidic bath.

The CoCr disks were ultrasound cleaned in three successive 10-minute baths of acetone, ethanol and deionized water. This cleaning procedure ensured the removal of organic contaminants. They were then put in an acid bath (40% HNO₃) for 40 minutes, in order to remove any ionic deposits from the alloy surface and to passivate it. After extensive washing with deionized water, the disks were sterilized by a 10-minute incubation in 70% ethanol. All subsequent steps were performed in sterile conditions, in a laminar flow hood. Solutions were filtered before use. The samples were rinsed several times with water, and, for the last wash, with the Tris buffer used for the dopamine solution.

The following coating protocol was adapted from the work by Lee and colleagues (Lee et al. 2007). A 2mg/mL dopamine solution was prepared just before use from lyophilized dopamine hydrochloride (Alfa Aesar A11136) dissolved in a 10 mM Tris-HCl aqueous buffer with a pH adjusted to 8.5. The solution was added to the wells of a sterile multi-well plate containing the individual experimental samples. The plate containing the samples and the dopamine solution was thereafter covered with a sterile lid and incubated at room temperature for 22 ± 2h, under

orbital shaking and protected from light. According to the literature (Lee et al. 2007), this incubation time results in a uniform coating, approximately 45 nm thick. The samples were then thoroughly rinsed with deionized water, placed in an ultrasound bath for 5 minutes in order to remove polydopamine aggregates from the surface, and further rinsed with deionized water.

The chemical composition of the PDA (polydopamine) coating was analyzed by Fourier Transform Infrared (FTIR) spectroscopy. This technique has been described in section 0.

Quantitative information on the elemental composition of the PDA coating was obtained by XPS (please refer to section 0 which for the description of this technique). XPS spectra were recorded on bare and PDA-coated CoCr disks, using a PHI 5600-CI spectrometer (Physical Electronics). Survey spectra were acquired with a monochromatic aluminum X-ray source (300 W) whereas high-resolution spectra were recorded with a monochromatic magnesium X-ray source (300 W). The detection angle was set to 45°. The analysis was done on three spots per disk to assess the homogeneity of the coating. We analyzed the spectra with the software MultiPak (Physical Electronics).

As reported in the literature (Lee et al. 2007; Zhu and Edmondson 2011), the dopamine solution is originally clear and turns light pink and finally black, as the polymerization process takes place and polydopamine aggregates form. The aspect of the solution after 22h of polymerization is displayed on Figure 39 A. PDA-coated CoCr disks also exhibit a dark brown color, as shown on Figure 39 B-C.

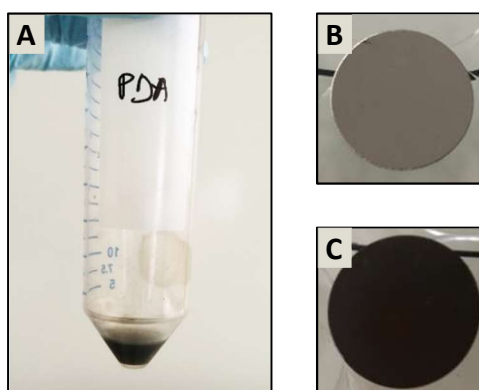


Figure 39. Photographs of dopamine solution and PDA. A. Dopamine solution after 22h of incubation. Polydopamine aggregates have formed in the solution, causing it to turn black. B. Bare CoCr disk. C. Polydopamine-coated CoCr disk, exhibiting a dark-brown surface.

FTIR spectra of bare and PDA-coated CoCr disks are presented on Figure 40. Several peaks and one band were found on the PDA spectrum and not on the bare CoCr spectrum. As shown by the annotations on the figure, they were all attributed to vibrations of chemical bonds that are

present in polydopamine. Those attributions are in agreement with the literature (Xi et al. 2009; Yu et al. 2010; Zhou et al. 2011; Luo et al. 2013a) and evidence the successful deposition of a polydopamine coating on the disks.

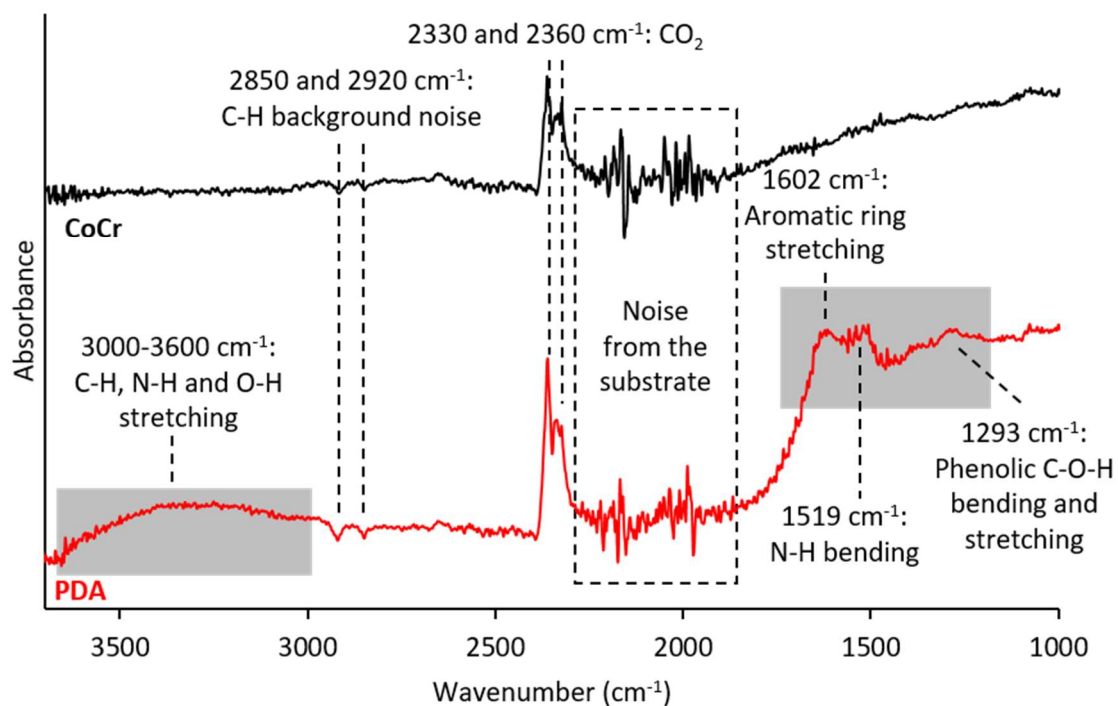


Figure 40. Representative FTIR spectra of bare and PDA-coated CoCr disks. The greyed areas of the PDA spectrum highlight the peaks and bands associated with the PDA coating.

XPS survey spectra of bare and PDA-coated CoCr disks are shown on Figure 41, and the surface atomic percentages calculated from these spectra are presented on Table 12. On the bare samples, the main elements that compose the L-605 alloy were detected (chromium, cobalt, tungsten and nickel). The presence of oxygen and carbon can be explained by the presence of metal oxides and (to a lesser extent) carbides, as well as residual surface organic contaminants.

On the PDA-coated disks, no metallic element was detected. That indicates that the PDA coating covered the surface in a uniform and complete manner. The only elements that were detected were oxygen, carbon and nitrogen, which compose the dopamine molecule. They were found in proportions close to those of the dopamine molecule (18% oxygen, 73% carbon, 9% nitrogen). These results therefore confirm the results obtained with the FTIR characterization.

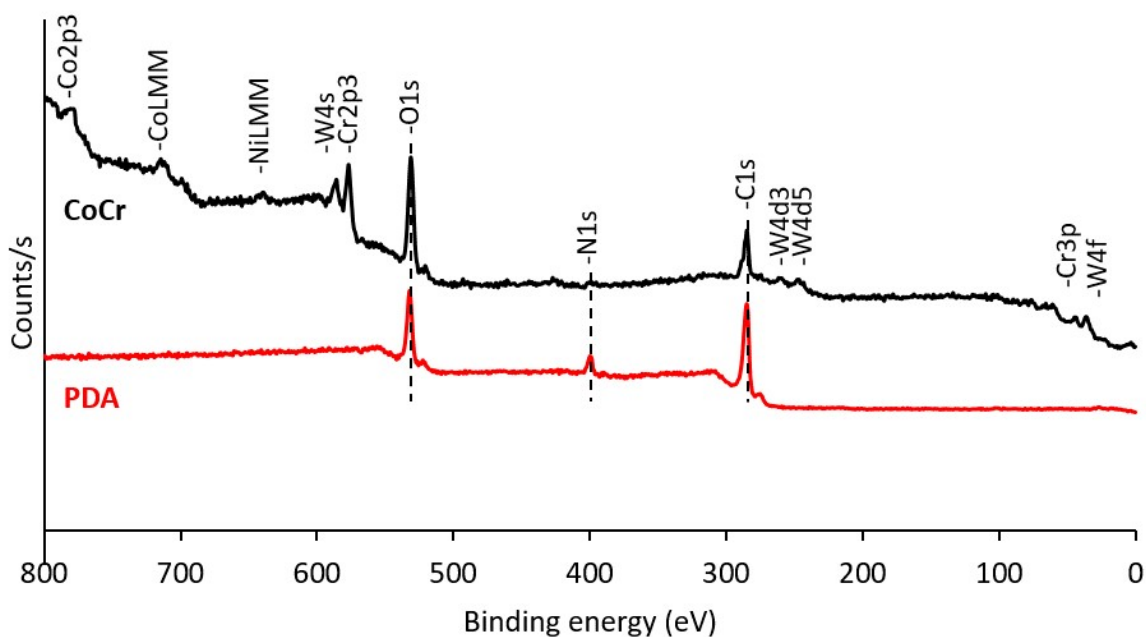


Figure 41. XPS survey spectra of bare and PDA-coated CoCr disks.

	O 1s	C 1s	N 1s	Cr 2p3	Co 2p3	W 4f	Ni 2p3
CoCr	44.3 ± 1.1	41.9 ± 0.8		10.4 ± 0.5	1.8 ± 0.2	1.4 ± 0.1	0.3 ± 0.3
PDA	21.1 ± 0.3	71.1 ± 0.7	7.8 ± 0.5				

Table 12. Average surface atomic percentages of bare and PDA-coated CoCr disks. Standard deviation between three replicates.

1.4.b. Direct immobilization of the peptide

As detailed in the introduction, polydopamine coatings exhibit a latent reactivity towards amine and thiol functions. Therefore, covalent immobilization of amine-containing molecules, such as peptides, can be performed by simple incubation. The latter is the first method we used to bind P8RI on polydopamine-coated CoCr samples. The reaction is shown on Figure 42.

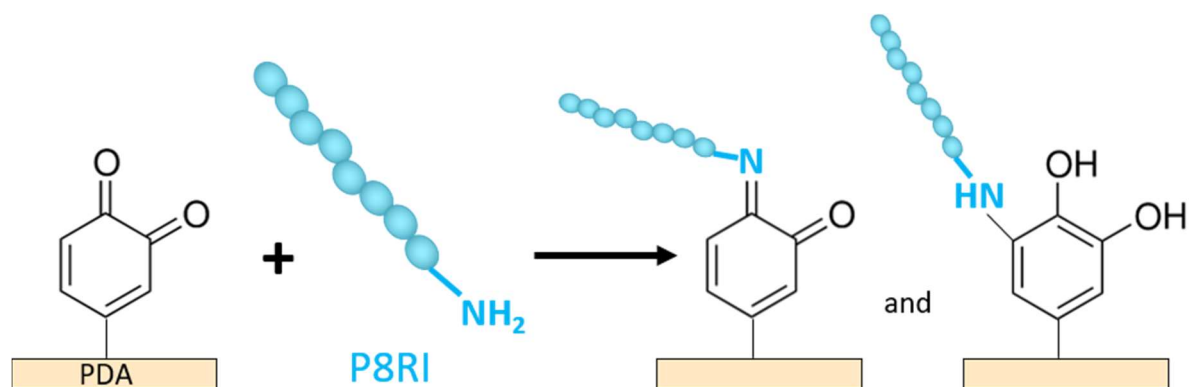


Figure 42. Schematic representation of the binding of the peptide to the PDA coating. The reaction takes place between an o-quinone of the polydopamine and an amine of the peptide, by Schiff base reaction (left) or Michael addition (right). Figure adapted from Lynge et al. (2011)

P8RI binding was carried out on CoCr disks immediately after the polydopamine coating procedure, in a laminar flow hood. A solution containing 0.2 mg/mL P8RI (custom synthesis from Proteogenix) diluted in Tris buffer (10 mM Tris, pH adjusted to 8.5) was added to the wells containing the PDA-coated samples. They were left to incubate for 22 ± 2 h under orbital shaking. They were then thoroughly rinsed with deionized water. This protocol was adapted from the work by Lee and colleagues previously cited (Lee et al. 2007).

To assess the presence of P8RI on the samples after the binding procedure, we considered two analysis techniques: fluorescence microscopy and XPS. Fluorescence microscopy requires the use of a fluorescently labelled peptide. The insertion of a fluorescent tag is a common modification for custom-synthesized peptides. However, it must be noted that, given the small size of P8RI (molar mass: 1016 g/mol), the addition of a fluorophore such as FITC (Fluorescein isothiocyanate) or TAMRA (carboxytetramethylrhodamine), that have molar masses around 400 g/mol, constitutes a significant modification of the molecule. XPS can be used either with unmodified or tagged peptide. As P8RI only contains elements that are also present in polydopamine (carbon, oxygen, nitrogen and hydrogen), the detection of unmodified P8RI immobilized on a PDA coating by XPS would not be straightforward. It would require the analysis of the ratios between elements and the deconvolution of atomic peaks in high resolution spectra, in order to identify amide bonds specific of the peptide. A more direct and accurate technique is provided by the use of P8RI with an “XPS tag”. This tag must be an element that is absent from polydopamine and the underlying CoCr substrate, and that has a high relative sensitivity factor so that it can be easily detected by XPS. Iodine fulfils both those requirements. In addition, it can easily be integrated in a peptide sequence, since some peptide manufacturers can use iodinated tyrosine amino acids, as shown on Figure 43. This peptide modification implies only a minor increase of the molecular mass, and, as the iodinated tyrosine can be inserted several residues

away from the terminal amine, it should not interfere with the binding of the peptide to the PDA coating. Therefore, we opted for that method to detect the immobilized peptide with certainty and with minimal interference in the binding mechanism.

We used a modified P8RI, in which the phenylalanine was replaced by a di-iodinated tyrosine (custom synthesized by Thermo Fisher Scientific), in the immobilization protocol described above, and later analyzed the surface by XPS, as detailed in I.4.a. The PDA-coated CoCr disks on which iodinated P8RI had been immobilized will be designated as “PDA + iodinated P8RI”.

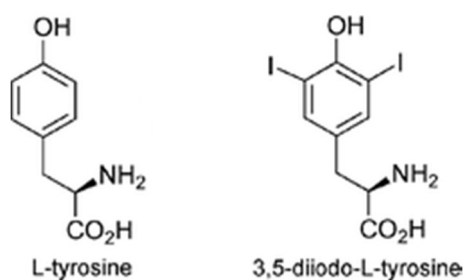


Figure 43. Unmodified and iodinated L-tyrosines.

The surface atomic percentages measured by XPS on PDA-coated and “PDA + iodinated P8RI” CoCr disks are presented in Table 13. On the PDA-coated sample, the results were similar to those analyzed in I.4.a. On the “PDA + iodinated P8RI”, an increase in the relative quantity of nitrogen was noted, as expected after the immobilization of P8RI, which is richer in nitrogen than polydopamine is. A small percentage of iodine was detected, as evidenced on the survey spectra on Figure 44. Therefore, the immobilization of iodinated P8RI on the PDA coating was proven.

Disk	C 1s	O 1s	N 1s	I 3d5
PDA	72.9	20.3	6.8	0.0
PDA + iodinated P8RI	72.3	19.1	8.2	0.5

Table 13. Surface atomic percentages of coated CoCr disks.

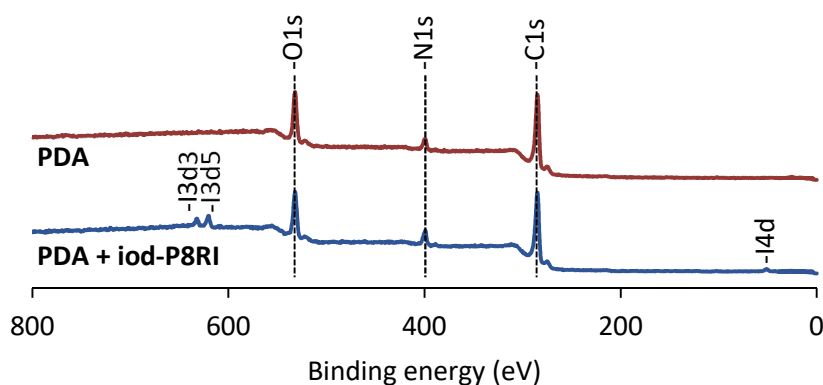


Figure 44. XPS survey spectra of PDA-coated and ‘PDA + iodinated P8RI’ CoCr disks.

Although the direct immobilization of P8RI on PDA coatings was successful, that method has two possible flaws. The first one is that, as the immobilization reaction takes place between the o-quinone functions of the surface and an amine function of the peptide, it could involve not only the terminal amine but also the amines present in the side chain of two amino acids in the P8RI sequence: lysine and arginine. As the pKa of these two side chain amines is significantly higher than that of the terminal amine (respectively 10.79 and 12.48 against 8.95), they are essentially in the protonated form at pH 8.5 (at which the immobilization reaction takes place), and thus much less susceptible to react, compared with the terminal amine. However, a small fraction of the soluble P8RI will bind by a side chain amine. This will modify its orientation in the space, making it potentially less prone to bind to the CD31 molecules exposed by the cells that come into contact with the coated surface.

Another concern with this method is that the immobilization is performed directly between the PDA coating and the P8RI, which implies that some of the amino acids of the peptide are so close to the surface that they might be inaccessible for their putative ligand on contacting cells. Both these concerns were addressed with a second immobilization technique relying on the use of a linker, as detailed in the following section.

I.4.c. Immobilization of the peptide with the help of a linker

In order to better control the orientation of the immobilized P8RI and to render it readily accessible to its ligands at the surface of the cells contacting the coated surface, we used a flexible linker as an intermediary between the peptide and the PDA coating. The linker needed to have: 1) either an amine or a thiol function at one extremity, to be able to react with the o-quinone functions of the polydopamine coating, 2) a flexible chain to improve the accessibility of the bound P8RI and 3) a function at the second extremity that would specifically bind to the peptide N-terminus. As regards that last point, we opted for a bioorthogonal reaction so as to avoid any interference from the side chains of the peptide and the amine functions of the polydopamine. We chose to use copper-free click chemistry, as it allows for a fast reaction in aqueous solution, without the addition of cytotoxic catalysts such as copper.

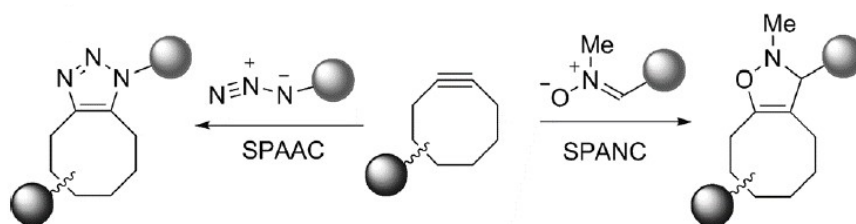
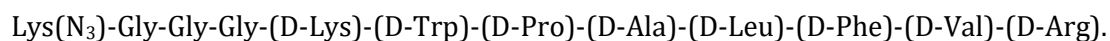


Figure 45. Cycloaddition with azide (SPAAC) or nitronium (SPANC). Diagram from Dommerholt et al. (2010)

The two main types of copper-free click chemistry are strain-promoted azide-alkyne cycloaddition (SPAAC) and strain-promoted alkyne-nitronium cycloaddition (SPANC). They are represented on Figure 45. Numerous SPAAC and SPANC reactions have been described. However, they often involve the use of reactants that are difficult to synthesize, and thus not commercially available (Debets et al. 2011). In addition, as they are bioorthogonal, these reactions involve the use of a modified peptide, with one of the two chemical functions involved in the reaction added at the N-terminus. We searched the literature for an efficient reaction involving a commercially available linker and a peptide modification provided by our peptide manufacturer. We chose a SPAAC reaction with an azide on the peptide and a bicyclo[6.1.0]nonyne (BCN) on the linker, as described by Dommerholt and colleagues (2010). A “P8RI azide” was custom-synthesized, using a modified lysine with an azide instead of the side chain amine was introduced at the N-terminus of the peptide, and separated from the P8RI sequence by three glycines. The sequence of the “P8RI azide” was therefore:



Concerning the linker, we opted for a short PEG chain between the BCN at one end and an amine at the other end. PEG was chosen for its high flexibility and biocompatibility. The resulting linker (Sigma 745073) will be called “BCN-amine” throughout this thesis. The two-step immobilization of the P8RI azide on the PDA coating through the BCN-amine linker is represented on Figure 46.

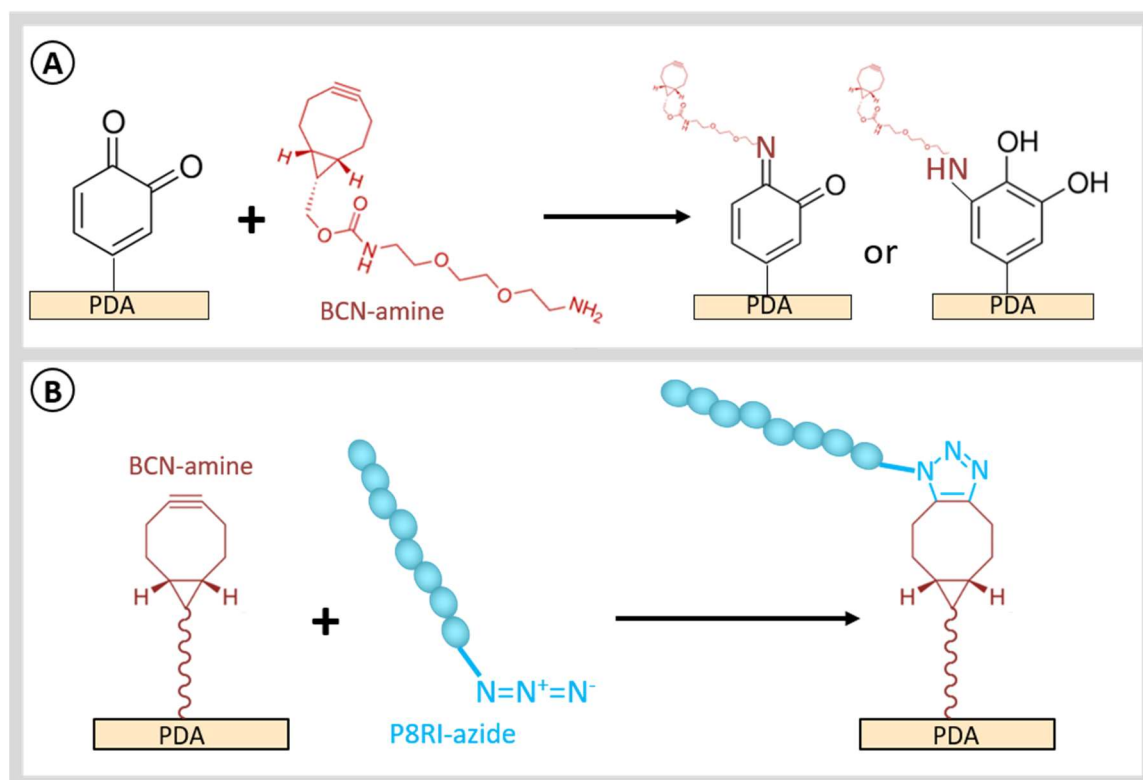


Figure 46. Linker-mediated immobilization of P8RI on PDA. A. Binding of the BCN-amine linker to the PDA coating by Schiff base reaction (left) or Michael addition (right). B. Binding of the peptide to the immobilized BCN-amine linker by click chemistry.

I.4.d. Immobilization of P8RI azide on PDA coatings with the help of the BCN-amine linker

BCN-amine binding was carried out on CoCr disks immediately after the polydopamine coating procedure, in a laminar flow hood. A solution containing 0.1 mg/mL BCN-amine (Sigma 745073) diluted in Tris buffer (10 mM Tris, pH adjusted to 8.5) was added to the wells containing the PDA-coated samples. They were incubated for 22 ± 2 h under orbital shaking. After thorough rinsing with deionized water, a solution containing 0.2 mg/mL “P8RI azide” (custom synthesis, subcontracted to Proteogenix) in deionized water was added to the samples. The samples were then thoroughly rinsed with deionized water. That protocol was adapted from the work by Messersmith’s group and van Delft’s group (Lee et al. 2007; Dommerholt et al. 2010) by Pierluigi Tosi at the Laboratory for Vascular Translational Science.

As detailed in the previous section, three types of surface analysis were relevant for assessing the success of the immobilization of the peptide: fluorescence microscopy (with the use of a fluorescently tagged peptide), XPS with an untagged peptide and XPS with the use of an “XPS-tagged” peptide. For practical reasons (lengthy delivery time of “XPS-tagged” peptides by the

manufacturer), the latter could not be used. Fluorescence microscopy and XPS analysis of untagged peptide immobilized on the surface were thus performed.

For the XPS analysis, unmodified “P8RI azide” was immobilized on CoCr disks as described above. The coated samples were then analyzed by XPS as detailed in I.4.a. Three points were analyzed on each sample.

For the fluorescence microscopy analysis, a “P8RI azide” with an additional C-terminal lysine conjugated to a FITC fluorophore was custom synthesized by the manufacturer Proteogenix. The pseudo-peptidic sequence of that “P8RI-FITC azide” thus was:

Lys(N₃)-Gly-Gly-Gly-(D-Lys)-(D-Trp)-(D-Pro)-(D-Ala)-(D-Leu)-(D-Phe)-(D-Val)-(D-Arg)-Lys(FITC).

The “P8RI-FITC azide” was immobilized on a BCN-amine linker on PDA-coated CoCr disks as described for the “P8RI azide”. The coated samples were then placed face down in imaging dishes to prepare their observation through an inverted microscope and covered with mounting medium (ProLong Gold Antifade Mountant, Thermo Fisher P36930). This medium has a refractive index close to that of the material through which the samples are observed (glass or plastic), so that light transmission is optimized. The ProLong Gold mounting medium also has antifading properties that minimize photobleaching, thus allowing the preservation of fluorescent samples for longer times. Digital photographs of the samples were acquired on an Axio Observer inverted fluorescence microscope (Zeiss), equipped with the software Zen (Zeiss).

As shown on Figure 47, CoCr disks on which the “P8RI-FITC azide” had been immobilized (following the protocol described above) emitted a green fluorescence of much higher intensity than the PDA-coated disks. These results prove the presence of the fluorescent peptide at the surface of the disks after the immobilization protocol.

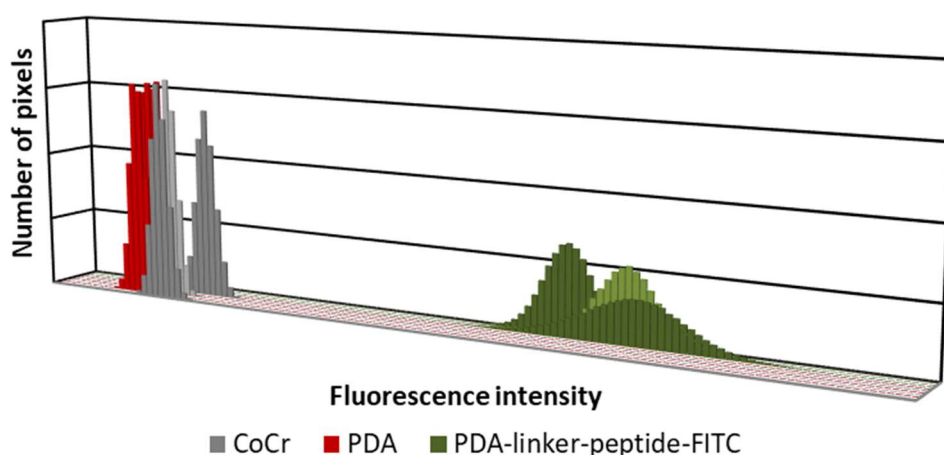


Figure 47. Detection of the immobilized fluorescent P8RI by fluorescence microscopy. Fluorescence intensity histograms of photographs taken on coated CoCr disks. 3 disks per condition.

The XPS analysis of the surface of coated CoCr disks revealed only the presence of the three elements nitrogen, oxygen and carbon on the three types of coating: PDA only, PDA + BCN-amine linker, PDA + linker + P8RI azide. This was consistent with the previous analyses of PDA coatings, which had appeared to be homogeneous. Atomic ratios of nitrogen and oxygen over carbon were calculated from the XPS spectra. They are presented in Table 14, along with the theoretical values of these ratios for the molecules involved in the coatings. A graphical representation is also provided on Figure 48 for greater clarity. The O/C ratio of the polydopamine samples is slightly higher, and the N/C ratio slightly lower, than the values of the pure dopamine molecule. The evolution of the ratios with the addition of the linker and the P8RI to the coatings follows the tendency of the theoretical values: a constant decrease of the O/C ratio, and a slight decrease followed by a larger increase of the N/C ratio. Therefore, these results point to the successful immobilization of the BCN-amine linker and of the P8RI azide.

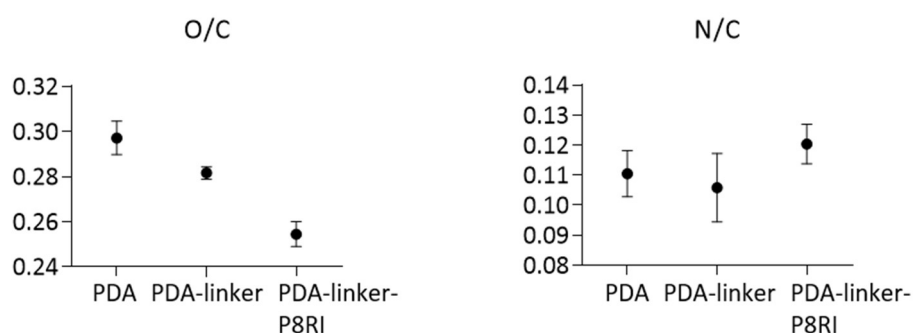


Figure 48. O/C and N/C surface ratios of coated CoCr disks. Error bars: Standard deviation between three replicates. These ratios of surface atomic percentages were derived from XPS analysis. The decrease of the O/C ratio and the increase of the N/C ratio are a strong indicator of the presence of P8RI on the PDA-linker-P8RI coating.

		O/C	N/C
Values measured by XPS on coated CoCr disks	PDA	0.297 ± 0.007	0.111 ± 0.008
	PDA-linker	0.282 ± 0.003	0.106 ± 0.011
	PDA-linker-P8RI	0.254 ± 0.006	0.120 ± 0.007
Values calculated from the molecular formulas	Dopamine	0.250	0.125
	Linker	0.235	0.118
	P8RI azide	0.211	0.316

Table 14. Theoretical and experimental elemental ratios of coatings. The ratios of surface atomic percentages of coated CoCr disks are derived from XPS analysis and are compared with the theoretical ratios of pure dopamine, BCN-amine linker and P8RI azide. Standard deviation between three replicates.

I.4.e. Stability of the PDA-linker-P8RI coating in one-month ageing test in liquid medium

In order to have its full effect *in vivo*, the “PDA-linker-P8RI” coating needs to maintain its integrity for the time necessary for stent endothelialization (about one week). The ageing behavior of the coating was assessed by an *in vitro* static ageing test in liquid medium. PBS was chosen as the liquid medium, for the same reasons as those explained in section I.4.e. Each CoCr disk was fitted in a custom sample holder designed to expose only its coated surface to PBS. The floating sample holder was placed in a beaker filled with PBS and stored in an incubator at 37°C (human core body temperature) for 1 or 4 weeks. Before the test, the beakers and sample holders were sterilized by autoclave to prevent bacterial proliferation during the study. The samples were manipulated in sterile conditions, under a laminar flow hood. After ageing, the disks were removed from their holders, thoroughly rinsed with deionized water, and dried with medical-grade compressed air. They were then analyzed by XPS as detailed in section I.4.a. Three coated disks and one bare CoCr disk were tested for each time point (1 or 4 weeks).

The ageing test was carried out by our collaborators Pascale Chevallier and Sergio Rodriguez-Diaz, directed by professor Diego Mantovani at the Laboratory for Biomaterials and Bioengineering (Université Laval, Québec City).

The surface atomic percentages of the coatings measured by XPS are presented on Figure 49. A. The N/C ratio was considered as the most reliable indicator of the potential degradation of the coating since it is not influenced by oxidation or water adsorption on the coating. As shown on Figure 49. B, the N/C ratio of the “PDA-linker-P8RI” coating was unmodified after 4 weeks of ageing in PBS at 37°C, thus demonstrating that the coating did not undergo any significant degradation.

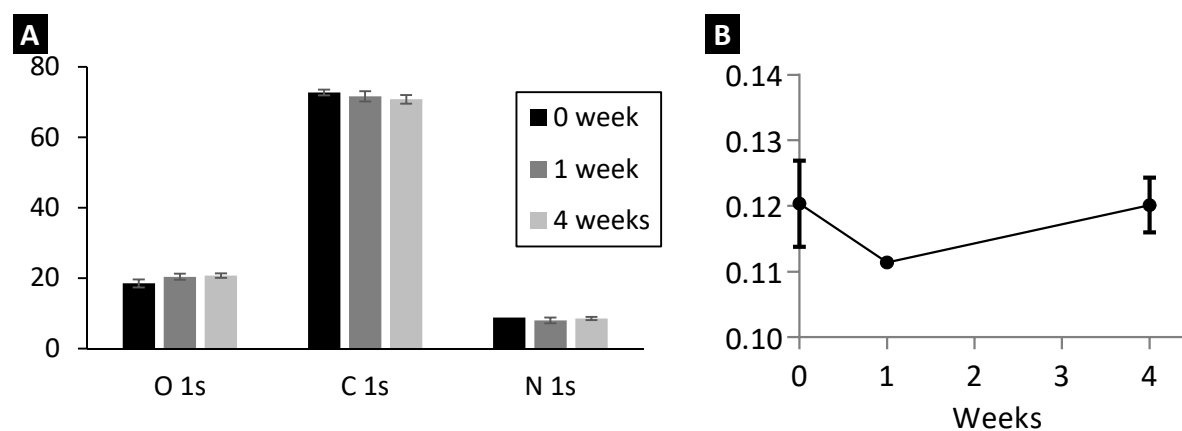


Figure 49. Elemental composition of PDA-linker-P8RI” coated samples after ageing in PBS. A. Surface atomic percentages. B. N/C ratio of the samples. Error bars: standard deviation over 3 replicates.

II. *In vitro* evaluation of the biocompatibility of P8RI-coated surfaces

Note: For the sake of simplicity, in the subsequent section, 'CoCr' designates bare L-605 CoCr disks, 'PDA' means polydopamine-coated CoCr disks, and 'P8RI' are CoCr disks with a polydopamine-linker-P8RI coating.

The concentration of P8RI used during the last step of the polydopamine-linker-P8RI coating process was chosen on the basis of a dose-effect curve obtained using 4-fold dilutions between 6 and 200 $\mu\text{g/mL}$. In preliminary experiments, the concentration of 50 $\mu\text{g/mL}$ yielded the least pro-inflammatory (as detected by the production of soluble IL-6 and VCAM-1) and the most anti-thrombotic (based on the levels of soluble TFPI) phenotype of primary human endothelial cells cultured on the coated surfaces (see Figure 50). The method used for such analysis is detailed below, in section II.2. The concentration of 50 $\mu\text{g/mL}$ was therefore used for coating the CoCr samples in the *in vitro* experiments presented in this section, and the stents in the preclinical studies presented in section III. The definitive choice for the development of the stents intended for clinical use shall be based on repeated *in vitro* experiments, using different endothelial cell donors.

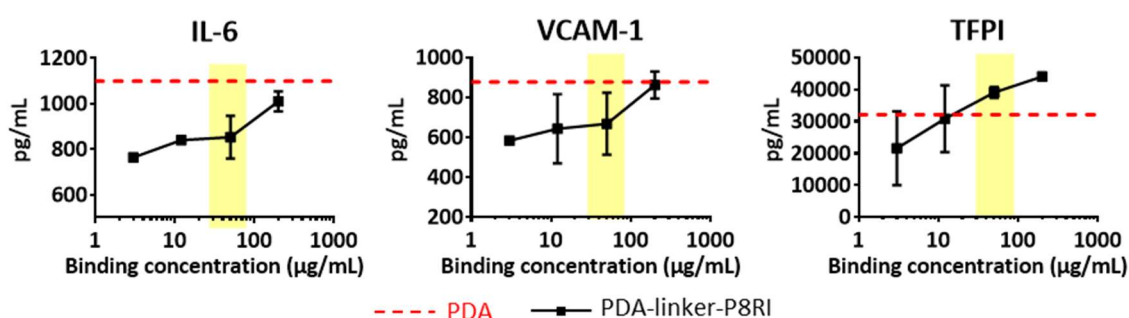


Figure 50. Quantification of soluble molecules in the supernatants of endothelial cells cultured on coated CoCr samples. Different binding concentrations had been used for the immobilization of P8RI on the PDA-coated samples. A binding concentration of 50 $\mu\text{g/mL}$ yielded a decrease in IL-6 and VCAM-1 production, and an increase in TFPI production, compared to the control (PDA coating without P8RI).

II.1. Hemocompatibility

II.1.a. The bare and coated CoCr surfaces do not cause hemolysis

The hemolysis assay is a required biocompatibility test for all blood-contacting devices. It shows whether a given material causes erythrocyte lysis (either by contact or by the release of toxic molecules). The hemolysis assay protocol we used was adapted from the one used by Bae and coworkers (Bae et al. 2012). It is sketched on Figure 51 and detailed below.

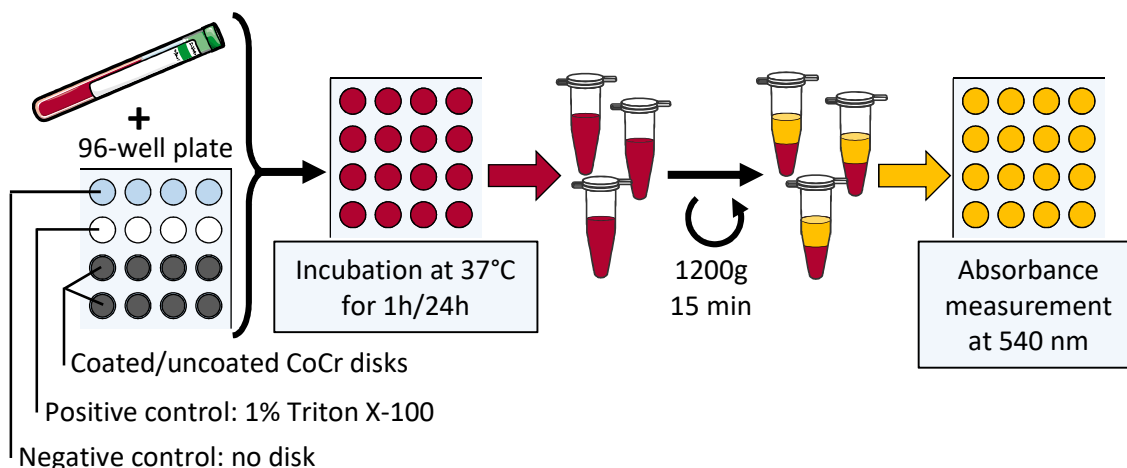


Figure 51. Visual summary of the protocol used for the hemolysis assay.

Coated and bare CoCr disks were placed in the wells of a 96-well plate and sterilized by a ten minute incubation in 70° ethanol. This common laboratory sterilization technique was chosen because the bactericidal properties of concentrated ethanol are well known, and its use does not induce chemical changes in peptides (Huebsch et al. 2005). The disks were rinsed several times in water prior to a final wash in physiological saline solution (0.9% NaCl). Human peripheral whole blood collected in lithium heparin (18 UI/mL) was then gently layered on each disk and the plate was incubated at 37°C during either 1h or 24h. Heparin was chosen for anticoagulation because it does not interfere with the hemolysis assays (Unger et al. 2007).

Disk-free wells were used as negative controls and 1% Triton X-100 (which causes the lysis of most erythrocytes through the dissolution of their plasma cell membrane) was added in blood-containing positive control wells. At the end of the incubation period, the blood was transferred from each well to an individual polypropylene tube (Eppendorf, 1.5ml) and centrifuged at 1200 g for 15 minutes. 50 μ L of platelet-poor plasma were collected at the top of all centrifuged tubes and transferred to a new 96-well plate. Absorbance was measured at 540 nm in a plate reader spectrophotometer (Infinite 200 PRO, TECAN). 540 nm corresponds to the absorbance peak of free hemoglobin, which is released by hemolysis from the erythrocytes. The value of the absorbance at 540 nm is therefore directly proportional to the extent of hemolysis caused by the sample disks in the experimental wells.

The experiment was performed in technical quadruplicates and repeated three times using the blood of different healthy blood donors.

A photograph of the microplate taken just before the measurement of the absorbance at the end of a hemolysis assay is shown on Figure 52. The platelet-poor plasma from whole blood incubated with Triton X-100 appears dark red, reflecting the effective hemolysis in these wells

(positive controls). No macroscopic difference in color is apparent between wells containing the negative control (No disk) and the three experimental groups of plasma.

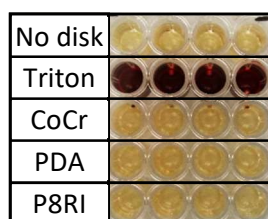


Figure 52. Photograph of a microplate filled with platelet-poor plasma at the end of a hemolysis assay. The positive control wells ('Triton') are the only ones which appear colored in red, as a result of hemoglobin release during hemolysis.

For each experiment, these observations were quantified by absorbance reading at 540 nm, and the measurements were normalized using the values obtained with the positive and negative controls, according to the following formula:

$$R(x) = \frac{A_{540\text{nm}}(x) - A_{540\text{nm}}(\text{No disk})}{A_{540\text{nm}}(\text{Triton}) - A_{540\text{nm}}(\text{No disk})}$$

wherein $R(x)$ is the normalized ratio of group x , and $A_{540\text{nm}}(x)$ is the average absorbance of the wells from group x . The measured ratios are presented on Figure 53.

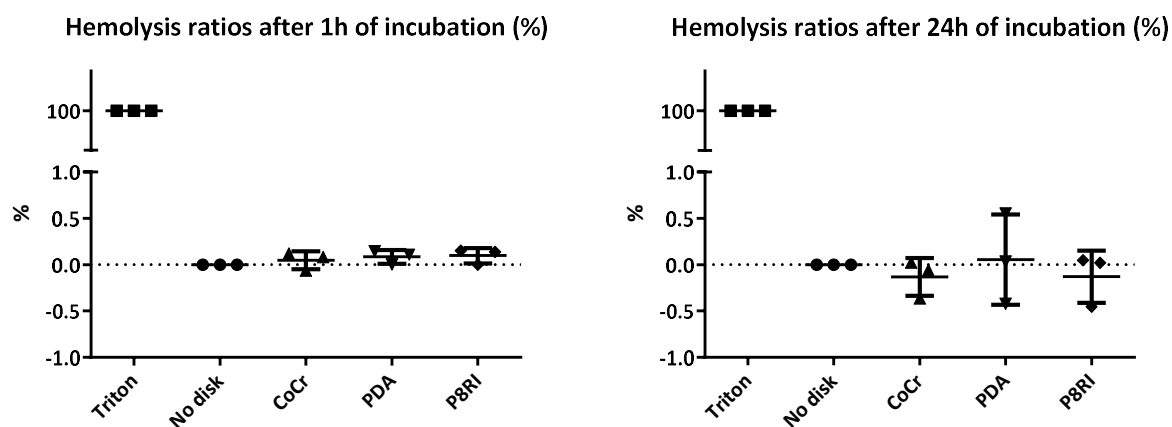


Figure 53. Hemolysis ratios after 1h or 24h incubation. No significant difference appear between the negative control and the bare and coated disks, after 1h or 24h of incubation.

In the three experimental groups (blood incubated with the CoCr disks), after 1h or 24h or incubation, the hemolysis ratios were not significantly different from the negative controls.

Therefore, we conclude that neither the bare CoCr surface nor the coated CoCr surfaces that we used were evidenced to cause hemolysis when contacted with human whole blood.

II.1.b. The “PDA+P8RI” coating tends to reduce platelet adhesion

As thrombosis is one of the two main complications associated with stenting, evaluating the thrombogenicity of each novel stenting material is essential. To this aim, we performed a platelet adhesion assay, visually summarized on Figure 54.

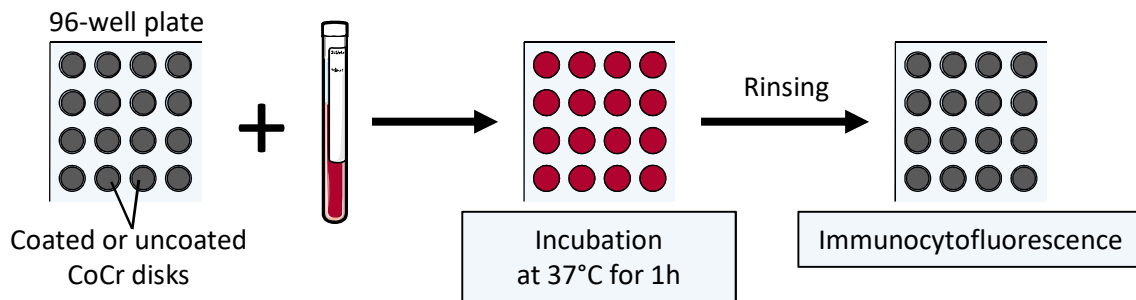


Figure 54. Visual summary of the platelet adhesion assay protocol.

Coated and bare CoCr disks were incubated in 70° ethanol and rinsed, as detailed above. Human whole blood collected in PPACK (75 mM PPACK + 0.1% D-mannitol, Haemtech SCAT-875B) was then deposited on the disks and they were incubated at 37°C for 1h. PPACK (Phe-Pro-Arg-chloromethylketone) is a peptidomimetic thrombin inhibitor that inhibits the coagulation cascade without affecting the physiological concentration of ionized calcium. This is important in a functional test such as platelet adhesion, which is a Ca^{++} dependent process. At the end of the incubation period, the disks were taken out of the wells using delicate tweezers and rinsed by gently stirring in a beaker full of physiological saline solution at room temperature. They were then placed in a new 96-well microplate and rinsed twice in physiological saline solution, prior to fixation with paraformaldehyde. The disks were then processed for immunocytofluorescence. The general principle of this staining technique is illustrated on Figure 55.

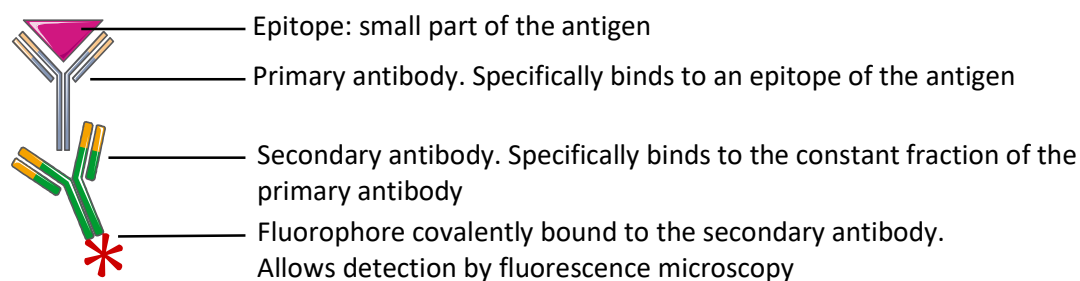


Figure 55. Principle of immunofluorescence

In order to visualize all adherent platelets, we chose to immunostain two antigens that are constitutively expressed by platelets: CD41 and von Willebrand Factor (vWF). CD41, also known as Integrin alpha-IIb, is the most abundant platelet adhesion receptor (Leclerc 2002), and is thus present on the surface of the platelets. vWF is a glycoprotein which plays a major role in blood coagulation (Peyvandi et al. 2011). As it is stored in intracellular compartments of platelets (the α -granules), its immunostaining requires the permeabilization of the platelet membrane. Since this “platelet adhesion assay” was performed with whole blood, leukocyte adhesion was also possible. Hoechst staining of cell nuclei was used to identify leukocytes (which, contrary to platelets, possess a cell nucleus).

Designation	Reference	Concentration
Bovine serum albumin	Jackson ImmunoResearch 001-000-173	5% m/v
Fish gelatin	Sigma-Aldrich F7041	0.1% m/v
Mouse anti-human CD41 primary antibody	Beckman-Coulter IM045	2 μ g/mL
Rabbit anti-human vWF primary antibody	Dako A0082	30 μ g/mL
Goat anti-mouse IgG, Cyanine3 secondary antibody	Jackson ImmunoResearch 115-166-071	3.75 μ g/mL
Goat anti-rabbit IgG, Alexa Fluor 488 secondary antibody	Jackson ImmunoResearch 111-546-046	3.75 μ g/mL
Hoechst 33342	Invitrogen H3570	10 μ g/mL
Prolong Gold Antifade Mountant	Thermo Fisher P36930	

Table 15. Reagents used in the immunofluorescence protocol.

The reagents used in the following protocol are presented on Table 15. The experimental samples were fixed in 4% paraformaldehyde at 4°C for 10 minutes, then rinsed 3 times in Dulbecco’s phosphate buffered saline (PBS). Fixation protects biological samples from decay by cross-linking the proteins. The samples were then permeabilized by a 10-minute incubation in a solution containing 100 mM glycine and 0.5% Triton X-100 in PBS. Triton X-100, being a non-ionic detergent, creates pores in the cell membranes without denaturing proteins, while glycine

was used to quench the formaldehyde. After PBS rinsing, blocking was then performed by a 30-minute incubation in a solution of 5% bovine serum albumin and 0.1% fish gelatin in PBS, in order to reduce unspecific antibody binding, and thus decrease background noise.

The two primary antibodies were diluted in a solution containing 1% bovin serum albumin (BSA) and 0.02% fish gelatin in PBS, and incubated overnight at 4°C with the samples. The samples were then rinsed with PBS and the secondary antibodies, diluted in a similar fashion, were added and incubated for 1 hour at room temperature. After PBS rinsing, the nuclei of the cells were stained by incubation in Hoechst solution. Finally, the samples were placed face down in imaging dishes (to prepare their observation by inverted microscope) and covered with Prolong Gold mounting medium. Digital photographs of the immunostained samples were then acquired on an Axio Observer inverted fluorescence microscope (Zeiss), equipped with the software Zen (Zeiss). The surface of the disks covered by platelets was identified by positive CD41 and vWF staining and quantified on the digital images using the “Analyze particles” function of the open source software Fiji.

The observation of the resulting photographs showed that very few leukocytes had adhered to the surface of the samples (where they were easily identified by their Hoechst positive nuclei). Representative photographs of immunostained samples are shown on Figure 56. Globally, the surface density of platelets (identified by positive CD41 and vWF staining) appeared lower on PDA than on bare CoCr, and even lower on “P8RI” disks as compared to the “PDA” ones. However, high variability can be noted between different disks of the same group, and this was reflected by the values obtained by computer-assisted quantification. Therefore, the significance of the differences observed between the experimental groups is questionable. The experiment was repeated several times, but, as intra-group variability was always high, no significant difference in the adhered platelets density was found between the three groups.

It can be concluded from these experiments that the “PDA” and “P8RI” coatings do not increase but rather tend to reduce platelet adhesion on the surface of CoCr samples.

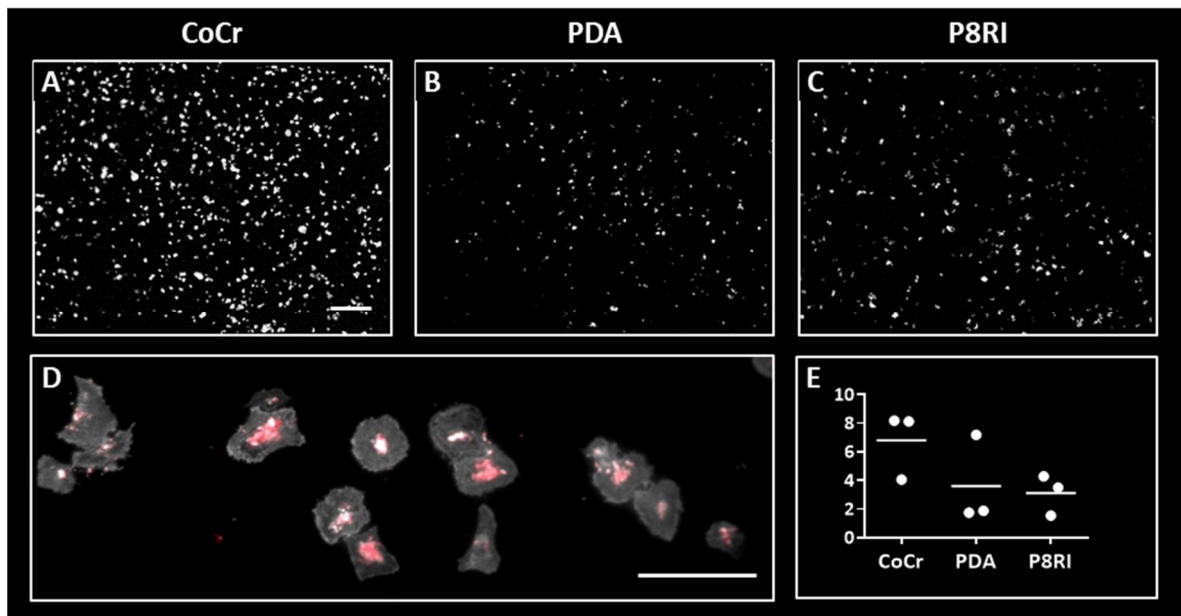


Figure 56. Fluorescence microscopy photographs of adherent platelets on CoCr disks. A-C: CD41 in grey. Bar=100 μ m. D: Higher magnification photograph of a bare CoCr disk. CD41 in grey, von Willebrand factor in red. Bar=20 μ m. E: Quantification of the disks surface coverage by platelets (in percents) based on photographs like A-C.

II.2. Endothelialization

We sought to perform a functional evaluation of coronary artery endothelial cells upon their contact with the experimental (bare and coated) CoCr disks described before. Attachment and survival were evaluated by computer-assisted analysis of digital images after immunofluorescent staining whereas the pro-inflammatory and pro-thrombotic phenotypes were assessed through quantitative analysis of soluble biomarkers in cell culture supernatants. A sketch of the experimental protocol used in these studies is provided on Figure 57.

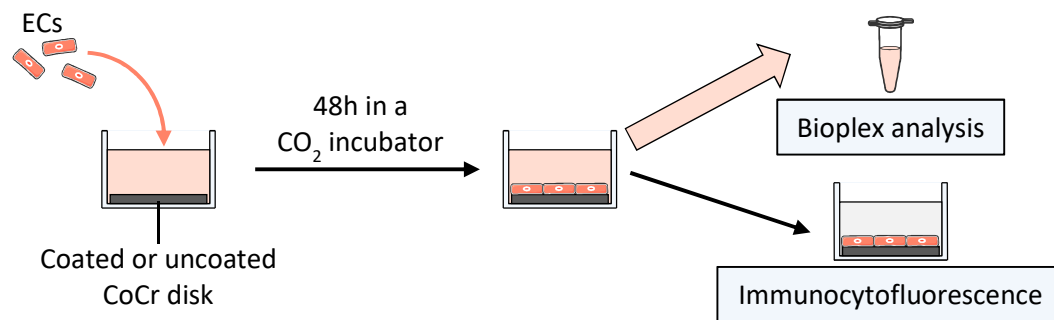


Figure 57. Visual summary of the endothelial cell growth assay. ECs: endothelial cells.

For practical reasons, the first experiments were performed with human umbilical vein endothelial cells (HUVECs, from PromoCell). Human coronary artery endothelial cells from three different individual donors (HCAECs, purchased from Lonza) were then used, in order to better reproduce the environment of coronary stents. The cells were cultured in Endothelial cells Growth Medium MV2 (Promocell), which contained the nutrients and growth factors needed by ECs. Antibiotic, antifungal and antimycoplasma reagents (penicillin, streptomycin, amphotericin B, plasmocin and primocine) were added to the medium in order to prevent contaminations. The cells were used at passages 3 to 5.

Coated and uncoated CoCr disks were placed in the wells of a 96-well plate and sterilized as described above. 100 000 endothelial cells suspended in their growth medium were seeded on each disk. After a 48h incubation at 37°C and 5% CO₂, the cell culture supernatants were collected for multiplex assay analysis, while the adherent cells were processed for immunocytofluorescence.

We chose to immunostain CD31 and VE-Cadherin, because these proteins clusters together at the adherens junction in functional endothelial monolayers (Lampugnani and Dejana 1997). CD31 is known to be truncated and miss the first, most membrane-distal, extracellular domains on stressed endothelial cells (Ilan and Madri 2003). Thus, to detect intact (functional) CD31 molecules we used the mouse monoclonal antibody JC70A (Dako, #M0823) as this antibody

typically fails to stain cells that express a truncated CD31 (Clement et al. 2015). The fact that a monoclonal antibody was available has possibly contributed to the success of this task. Unfortunately, the identification of VE-cadherin came out to be more difficult to standardize, likely due to the lack of a good monoclonal antibody. The use of the polyclonal antibody provided by Abcam (ref 33168) yielded good results in pilot experiments but the replacement vials we bought afterwards never gave satisfactory staining.

The staining protocol was the same as described in the previous section for adherent platelets, except that the permeabilization step was not performed, and that the following antibodies were used:

- primary antibody: mouse anti-human CD31 (10 µg/mL, Dako M0823)
- secondary antibody: goat anti-mouse IgG, A488 (5 µg/mL, Invitrogen A11029).

The measure of pro-inflammatory and pro-coagulant endothelial biomarkers in the cell culture supernatants was achieved using a custom multiplexed cytometric bead assay (Luminex technology). The principle of the multiplex bead array assay is presented on Figure 58. Each bead contains two different types of fluorophores. This makes it possible to detect several types of beads in the same well: each type of bead is identified by different fluorescence intensities at two emission wavelengths. Each type of capture antibody is associated with one type of bead. The quantity of captured antigen on each bead is measured by the fluorescence intensity of the phycoerythrin (PE) bound to detection antibodies. Thus, the concentration of several antigens can be determined in the same well.

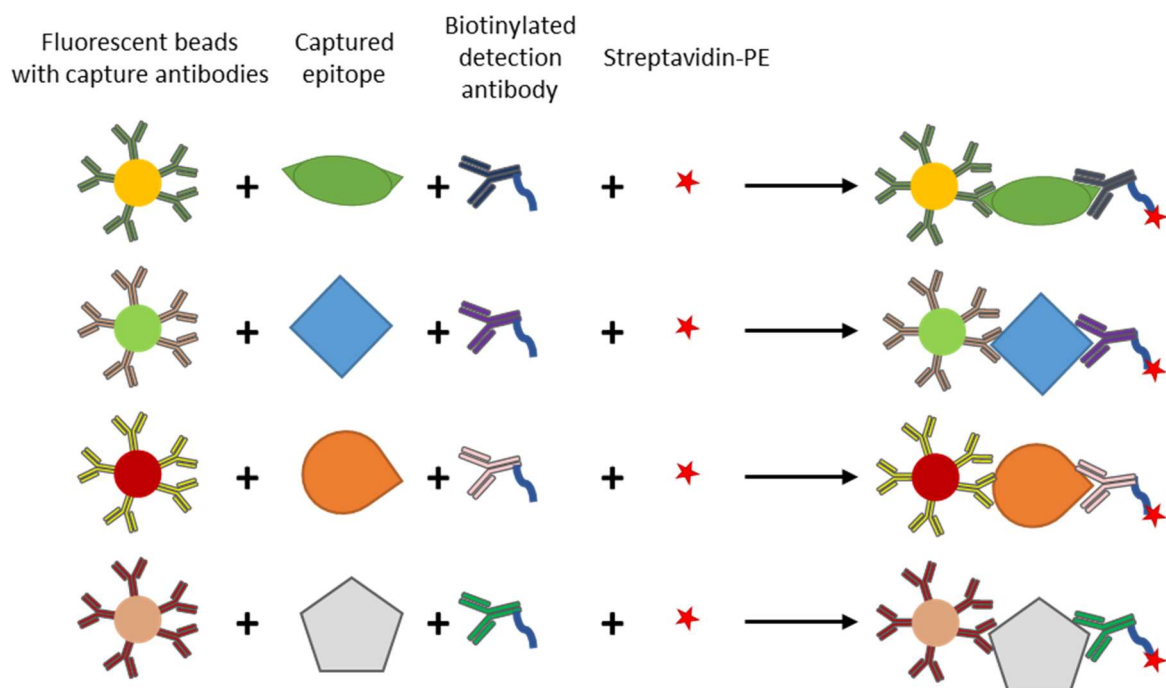


Figure 58. Principle of the multiplex bead array assay.

In order to analyze the influence of “PDA” and “P8RI” coatings on the phenotype of cultivated endothelial cells, we quantified different types of soluble proteins produced by activated endothelial cells. A range of soluble molecules considered as markers of EC pro-inflammatory and pro-thrombotic phenotype were quantified in preliminary experiments. After discarding the ones that were present in undetectable amounts, we chose to focus on five proteins. IL-6, a pro-inflammatory cytokine involved in lymphocyte growth and differentiation, acute phase reaction and fever, and IL-8, a chemokine that induces granulocytes migration and phagocytosis, but also promotes angiogenesis, are both known to be released by endothelial cells in response to inflammatory stimuli, such as LPS and TNF α (Chi et al. 2001; Oude Nijhuis et al. 2003). They were therefore selected as markers of EC pro-inflammatory phenotype. CD62E and VCAM-1 (Vascular Cell Adhesion Molecule-1) are transmembrane glycoproteins of the CAM (cell adhesion molecules) family and are responsible for leukocyte adhesion on ECs. Thus, they are not primarily expressed as soluble molecules. However, cytokine activated endothelial cells are known not only to exhibit increased surface expression of CD62E and VCAM-1, but also to produce soluble forms of these proteins, as a result of unidentified cleavage of shedding processes (Pigott et al. 1992; Constans and Conri 2006; Navasiolava et al. 2010). For this reason, CD62E and VCAM-1 were also chosen as markers of EC pro-inflammatory phenotype. The pro-thrombotic phenotype of the ECs was assessed by the quantification of PAI-1 (Plasminogen Activator Inhibitor-1), a serine protease inhibitor directed against tissue plasminogen activator (tPA) and urokinase (uPA). Since tPA and uPA activate plasminogen and are therefore the main initiators of fibrinolysis, the action of PAI-1 is pro-thrombotic. These five proteins were quantified in cell culture supernatants in several experiments, performed with cells from different donors. Each experiment included eight technical replicates.

The endothelial cell culture supernatants were centrifuged at high speed in order to remove any dead cell and debris, then they were transferred to polypropylene 96-well plates, sealed and stored at - 80°C until the day of the assay. They were then thawed and diluted in staining buffer. The optimal concentration was determined according to previous experiments. The diluted supernatants were transferred to a flat-bottom 96-well plate containing a mix of the capture beads. A standard range was added to the same plate by serial dilution of standard solutions (Bio-Rad), containing a known concentration of each antigen. The plate was incubated on an orbital shaker for 1h, in order for the capture antibodies to bind their antigens. The plate was then rinsed with wash buffer on an automatic wash station, which rinses the wells while holding the magnetic beads at the bottom of the wells. The biotinylated detection antibodies, diluted according to the manufacturer’s instructions, were then incubated with the beads for 30 minutes. Finally, after rinsing, streptavidin-PE was added to each well and incubated for 10 minutes, so that the streptavidin could bind to the detection antibody’s biotin. After a last rinsing step, the beads were

resuspended in assay buffer and analyzed on an assay reader (Bio-Plex 200, Bio-Rad). The statistical analysis of the results was performed with Kruskal-Wallis test. This nonparametric test was chosen as the number of replicates was too low to assess their Gaussian distribution, and hence to fulfill the conditions for an ANOVA test. Differences were considered significant for $p < 0.05$.

II.2.a. The “PDA + P8RI” coating favors rapid and functional endothelialization of CoCr surfaces

Representative images of immunostained endothelial cells are presented on Figure 59. The major difference between the three groups is that the adhesion of endothelial cells appears much lesser on bare CoCr surfaces than on “PDA” and “P8RI” surfaces, since the ECs detached only from the bare surfaces. The “PDA” and “P8RI” coatings on experimental CoCr disks both allowed the formation of a functional confluent layer of endothelial cells, as evidenced by the distribution of CD31 at intercellular junctions.

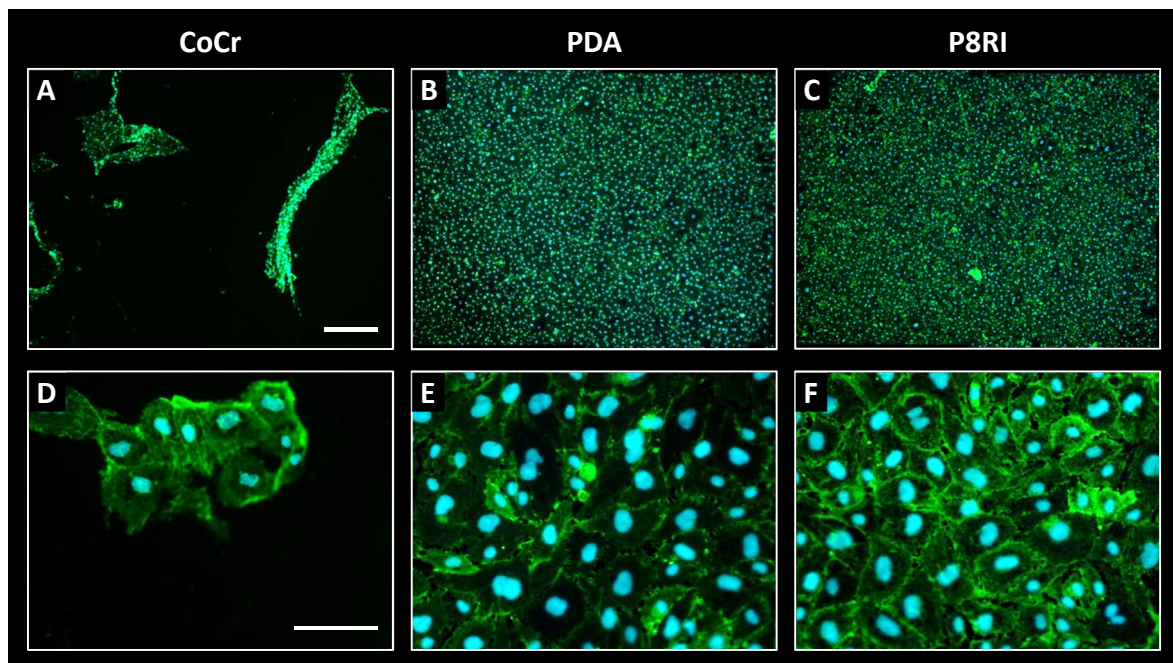


Figure 59. Immunostained HCAEC after 2 days of culture on CoCr disks. Green: CD31. Blue: Hoechst. A-C: low magnification (bar = 500 μm). D-F: higher magnification (bar = 100 μm). Pictures A and D show that the layer of endothelial cells was detached from bare CoCr disks during the process of immunostaining. This was not the case on “PDA” and “P8RI” disks.

II.2.b. The “PDA + P8RI” coating tends to induce an anti-inflammatory and anti-thrombotic phenotype in endothelial cells

As can be seen on Figure 60, the variability between the technical replicates of the multiplex assays was generally low, and clear differences between groups (cells cultivated on bare CoCr, “PDA” or “P8RI” surfaces) were found within one experiment. In particular, a tendency consistently appeared in IL-6, IL-8, CD62E and VCAM-1: concentrations on “PDA” were lower than on “CoCr”, and concentrations on “P8RI” lower than on “PDA”. This experiment thus suggested an anti-inflammatory effect of the PDA coating compared to bare CoCr, and a further effect of P8RI immobilization.

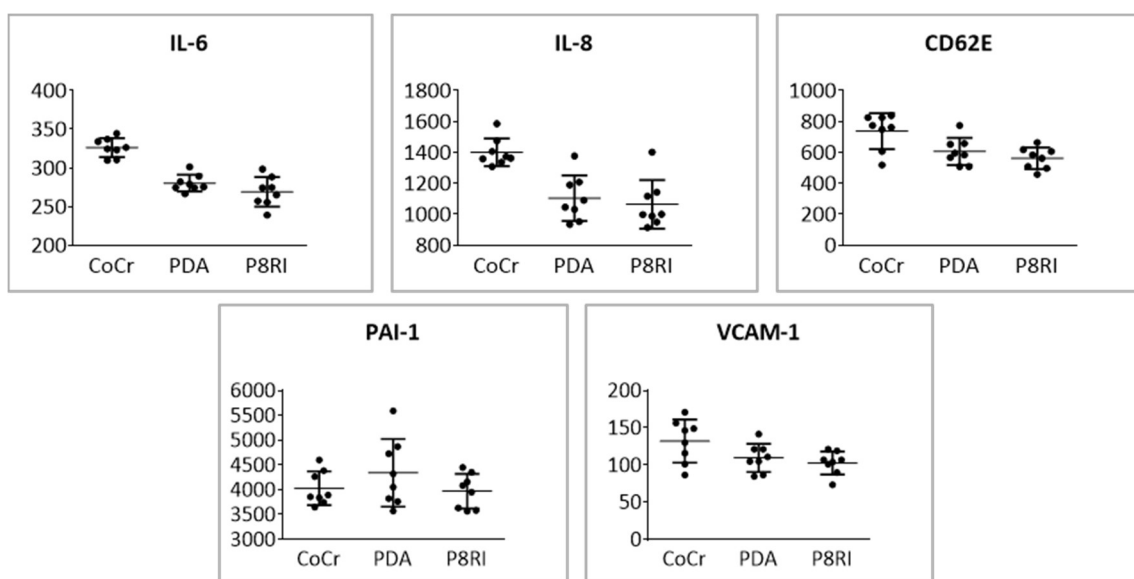


Figure 60. Results of a multiplex assay analysis of cell culture supernatants from a representative experiment performed with HUVECs. Absolute concentrations (in pg/mL) are expressed. *: $p < 0.05$. **: $p < 0.01$. ***: $p < 0.001$.

The synthesis of the results obtained from all cell culture supernatant analyses is presented on Figure 61. The multiplex assay was performed on five biological replicates (endothelial cells from five different donors). Each point on the graphs of Figure 61 represents the average of the technical replicates for one experiment. As in the experiment presented on Figure 60, the concentrations of IL-6, IL-8, CD62E and VCAM-1 are lower in the “PDA” and “P8RI” groups than in the “CoCr” group. An additional effect of P8RI immobilization is observed on IL-8, but also on PAI-1 concentrations, suggesting a slight anti-thrombotic effect of the P8RI coating. However, given the low number of replicates and high variability between experiments, the differences did not reach the statistical significance according to the Kruskal-Wallis test.

Therefore, the apparent anti-thrombotic and anti-inflammatory effects of “PDA” and “P8RI” coatings can only be expressed in terms of tendency.

The same experiment was performed on CoCr disks on which P8RI had been immobilized on a PEG linker, after plasma functionalization of the surface, by our collaborators in Québec (as described in section I.1.a). The multiplex assay carried out on the supernatants of the HCAECs cultured on these disks gave similar results to the ones presented here.

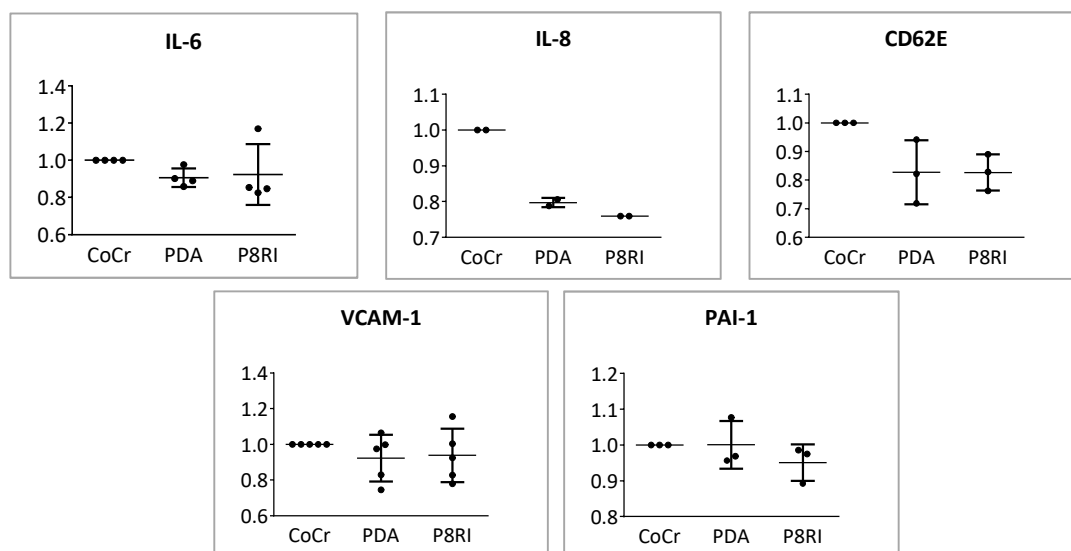


Figure 61. Results of multiplex assay analyses of cell culture supernatants. Each point is a biological replicate. For each analyte and each experiment, concentrations were normalized with respect to “CoCr” group.

III. *In vivo* evaluation of the biocompatibility of P8RI-coated surfaces

Bare and “PDA+P8RI”-coated coronary stents and FDSs were implanted in animal models in order to assess the effect of the coating on the stents’ *in vivo* environment. Large and medium animals (pigs and rabbits) were used for the implantation of coronary stents and FDSs respectively, since the arteries of these animals are large enough to be compatible with the size of stents designed for human use.

We applied the coating strategy that we had developed to commercially available stents. The biocompatibility of the “PDA+P8RI” coating could hence be evaluated also *in vivo*, by comparing the performance of the “PDA+P8RI”-coated stents with that of the parent bare metal or active device, made of the same alloy.

The Multilink BMS, made of CoCr, was suitable for both P8RI immobilization strategies developed during this study (the PDA-P8RI coating and the direct immobilization of P8RI on plasma-functionalized CoCr), whereas only the PDA-based strategy could be applied to the nitinol Silk FDS. Thus, BMSs (Multilink, Abbott) and DESs (Xience) were compared to “Plasma-P8RI” and “PDA-P8RI” coronary stents, whereas commercially available nitinol FDSs (Silk) were compared only to “PDA-P8RI” FDSs.

P8RI-coated and control coronary stents were implanted in the coronary arteries of farm pigs, whereas P8RI-coated and control FDSs were implanted in the right carotid arteries of rabbits, after creation of elastase-induced saccular aneurysms. Due to the size of the target arteries in these animals, which are large enough to be compatible with the size of stents designed for human use, these models are widely used for the issue of *in vivo* stent biocompatibility (Schwartz et al. 2008; Brinjikji et al. 2016).

III.1. Implantation of coronary stents in farm pigs

The primary objective of this first set of *in vivo* experiments was the evaluation of the effect of surface-immobilized P8RI on early stent strut endothelialization and on local inflammation. For this reason, the experimental and control stents were implanted in the three coronary arteries of healthy animals and the stented arteries were evaluated 7 days after stent implantation. According to a study by Pérez de Prado and colleagues (Pérez de Prado et al. 2011), this period is sufficient for the complete endothelialization of BMSs, but not DESs. Thus, it was deemed to be suitable for the comparison of the performances of BMSs, DESs, and P8RI-coated stents *in vivo*.

Four groups of Multilink (Abbott) stents, with different coatings, were implanted in the coronary arteries of 9 male farm pigs: bare metal stents (unmodified), everolimus-eluting stents (Xience, Abbott), “PDA-P8RI” stents (that had been coated with the PDA-based strategy) and “Plasma-P8RI” stents, on which P8RI had been immobilized on a PEG linker after plasma amination of the oxide surface. These last stents were prepared at the Laboratory for Biomaterials and Bioengineering (Québec) by the PhD student Sergio-Augustin Diaz Rodriguez, under the supervision of Dr Pascale Chevallier and Pr Diego Mantovani (as part of a research collaboration on the present project).

The four groups of stents were sterilized by beta radiations (25 kGy) by Ionisos (Chaumesnil, France), a service provider. This sterilization technique was chosen because it was reported not to induce changes in irradiated proteins (Silva et al. 2004), contrary to the ethylene oxide sterilization technique that is commonly used for the sterilization of commercial stents (Starbuck and Busch 1963; Pekkarinen et al. 2005; Dias et al. 2009).

The protocol for the study of the coronary stents in farm pigs was in accordance with the Guide for the Care and Use of Laboratory Animals (National Institutes of Health 1985) and the European Directive 2010/63/EU, and was approved by the local ethic committee (Agence nationale de sécurité sanitaire de l'alimentation, de l'environnement et du travail, 14 rue Pierre et Marie Curie, 94701 Maisons-Alfort Cedex, n° APAFiS : 2017032116276884). The pigs were housed at the Centre de Recherche Biomédicale (CRBM) at the veterinary school of Alfort, where all the *in vivo* experiments were conducted by Dr Romain Gallet assisted by the chief of the experimental surgery animal department, Dr Alain Bizé, and by Lucine Sambin, in Bijan Ghaleh's team.

After a “pre-load” with ticagrelor (180mg) and aspirin (75mg) and an overnight fast, the animals were sedated, intubated (endotracheal intubation) and connected to a ventilator; anesthesia was maintained with gas anesthetics throughout the procedure. After administration of heparin (intravenous bolus, 5000 UI) and antibiotic prophylaxis, arterial access was obtained under sterile conditions by femoral or carotid artery cutdown. Thereafter, coronary angiography was performed to select the part of the coronary tree in which to leave the implant as previously described (van der Giessen et al. 1991). Briefly, on the basis of the angiograms, at least one segment, with a diameter of 2.5-3.0 mm, was selected (except when the anatomical characteristics of the animal did not allow it) in each of the three epicardial coronary arteries (left anterior interventricular, left circumflex artery and right coronary artery). The location of these arteries on the myocardium is shown on Figure 62. Thereafter, an angioplasty catheter with the stent crimped on its deflated balloon was advanced to the selected site for implantation over a standard guidewire. The balloon was inflated to a maximal pressure of 8 atm for 30 seconds, deflated, and slowly withdrawn, leaving the stent in place. A total of 5 to 9 stents per group were

implanted, in 2 to 3 animals per group. After repeated angiography of the stented coronary arteries to confirm patency, the arteriotomy was repaired, the skin closed, and the animals allowed to recover from anesthesia. Aspirin (75mg/day) and ticagrelor (90mg, twice a day) were pursued until the termination of the study.

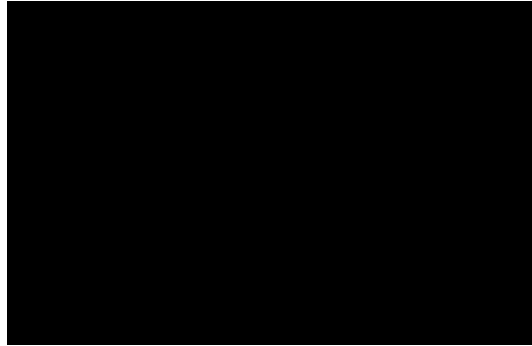


Figure 62. Coronary arteries. The arteries in which stents were implanted are highlighted in bold characters.

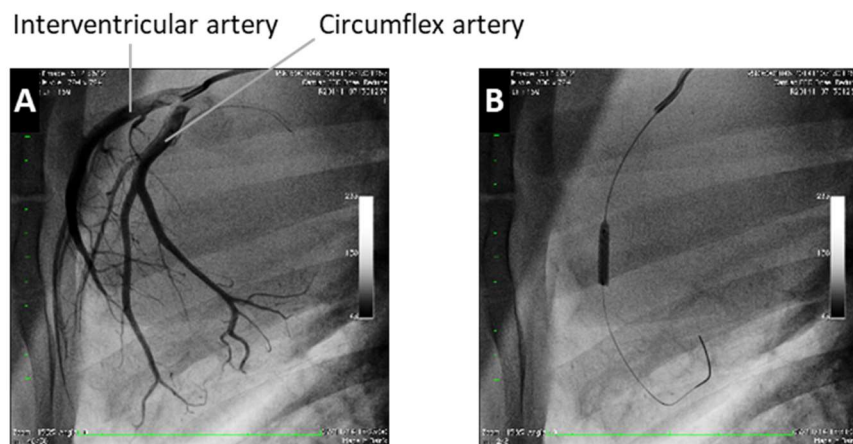


Figure 63. Angiograms of a stent implantation procedure. A. Visualization of the left coronary arteries by contrast agent injection. B. Stent deployment by balloon inflation.

The stents were implanted under angiographic monitoring, as shown on Figure 63. Seven days after stent implantation, the animals were terminated under anesthesia. The stented arteries were explanted, thoroughly rinsed with PBS and fixed in 2.5% glutaraldehyde at 4°C for at least 48h. Before being processed for scanning electron microscope (SEM) observation, they were cut longitudinally into halves, so as to expose their luminal side, as shown on Figure 64. As electron microscopes operate under vacuum, samples dehydration is indispensable. Just before imaging, they were washed in deionized water and dehydrated in ethanol baths of increasing

concentration. They were then coated by gold sputtering. Metallization is a necessary step for biological samples imaging by SEM, as this technique requires an electrically conductive surface in order to avoid the accumulation of electrons on the surface. The metallized samples were then imaged with a scanning electron microscope in secondary electrons imaging mode.



Figure 64. Photograph of a stented porcine coronary artery. The luminal side is exposed by cutting the artery longitudinally after explantation. The stent struts are clearly visible to the naked eye.

These experiments were performed very recently, and the quantitative analysis of the endothelialization on the stented arteries is currently ongoing. Figure 65 shows a representative example of SEM imaging of the luminal side of a circumflex artery implanted with a “PDA+P8RI”-coated stent. The degree of stent strut endothelialization can be evaluated on pictures taken at intermediate magnification (see Figure 65B), and adherent leukocytes can be identified on high magnification images. On this “PDA+P8RI”-coated stent, the endothelialization appears complete, the density of adherent leukocytes is low and their appearance is spheric (non activated), and there are no thrombi. Similar features can be observed on the Plasma-P8RI stent shown in Figure 66.

At variance, the stent struts were so weakly covered by the endothelium in the case of the artery implanted with the DES that the metal structure readily got off the arterial wall at the time of SEM examination, as shown in Figure 67. Furthermore, the morphology of the endothelial cells was altered with loose junctions and the appearance of several microvesicles at their luminal side. The shape of the adherent leukocytes was spheric (non activated), in agreement with the immunosuppressive effect of the eluted drug (everolimus), but platelets and fibrin filaments were readily visible in these specimen (same figure), in spite of the double anti-platelet therapy administered to the pigs during the study period.

The endothelialization was not an issue with BMSs, as shown in Figure 68, but there again striking differences could be detected in terms of platelet/fibrin deposition as compared to P8RI-coated stents. Moreover, the shape of the leukocytes was granular and distorted by the presence of several pseudopods, suggesting an activated phenotype of the adherent leukocytes on these stents.

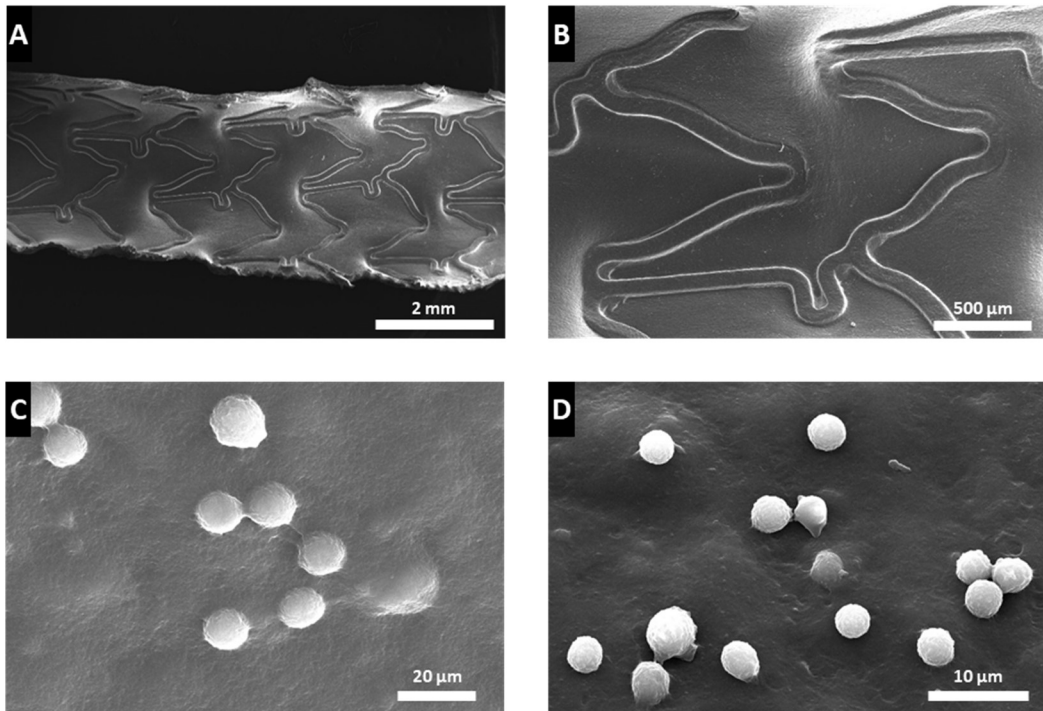


Figure 65. SEM images of a “PDA-P8RI” stent in a porcine coronary artery. A. Global view of the internal surface of the half-artery. The stent struts are clearly visible. B. Higher magnification view of stent struts. The struts endothelialization is complete. C-D. A few round-shaped adherent leukocytes can be seen.

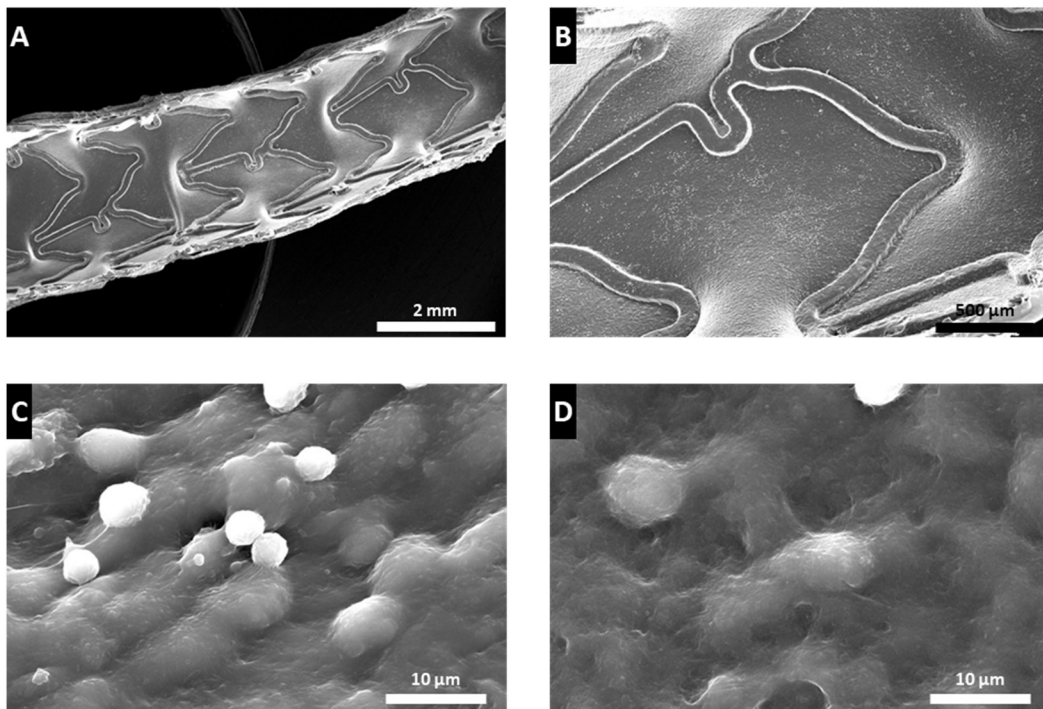


Figure 66. SEM images of a “Plasma-P8RI” stent in a porcine coronary artery. A, B: lower magnification views. C, D: details of adherent cells.

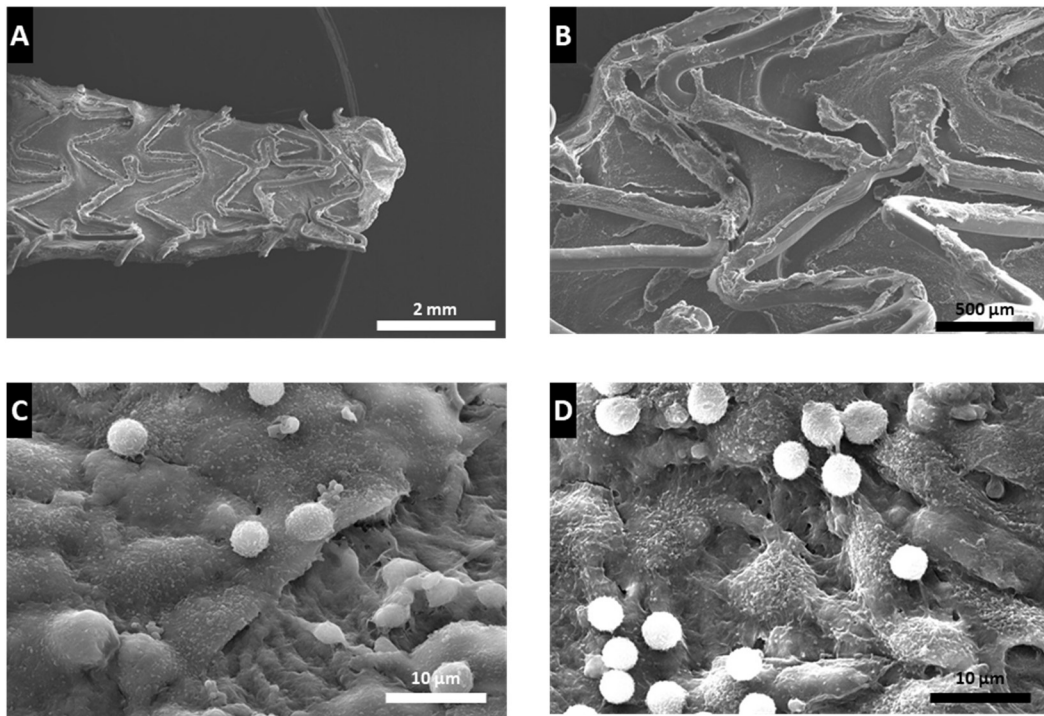


Figure 67. SEM images of a drug eluting stent in a porcine coronary artery. A, B: lower magnification views. C, D: details of adherent cells.

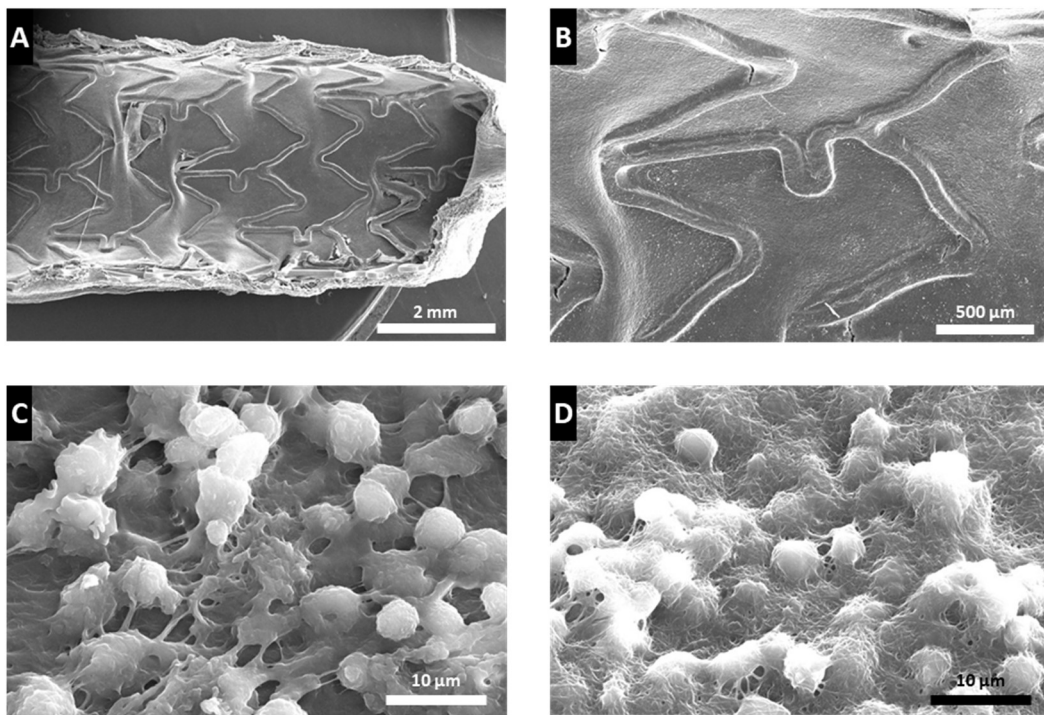


Figure 68. SEM images of a bare metal stent in a porcine coronary artery. A, B: lower magnification views. C, D: details of adherent cells.

These observations can be quantitatively assessed by image analysis on the different groups of stents, in terms of degree of stent strut endothelialization, platelet and fibrin deposits and leukocytes adherence and morphology. A custom computer program is being prepared and the analysis will be performed in the coming weeks.

III.2. Implantation of flow diverting stents in a rabbit elastase aneurysm model

In order to assess the effect of the “PDA+P8RI” coating on the performances of FDSs in terms of aneurysm occlusion and integration at the blood/vessel interface, we conducted *in vivo* experiments with bare and P8RI-coated FDSs, in a rabbit elastase aneurysm model.

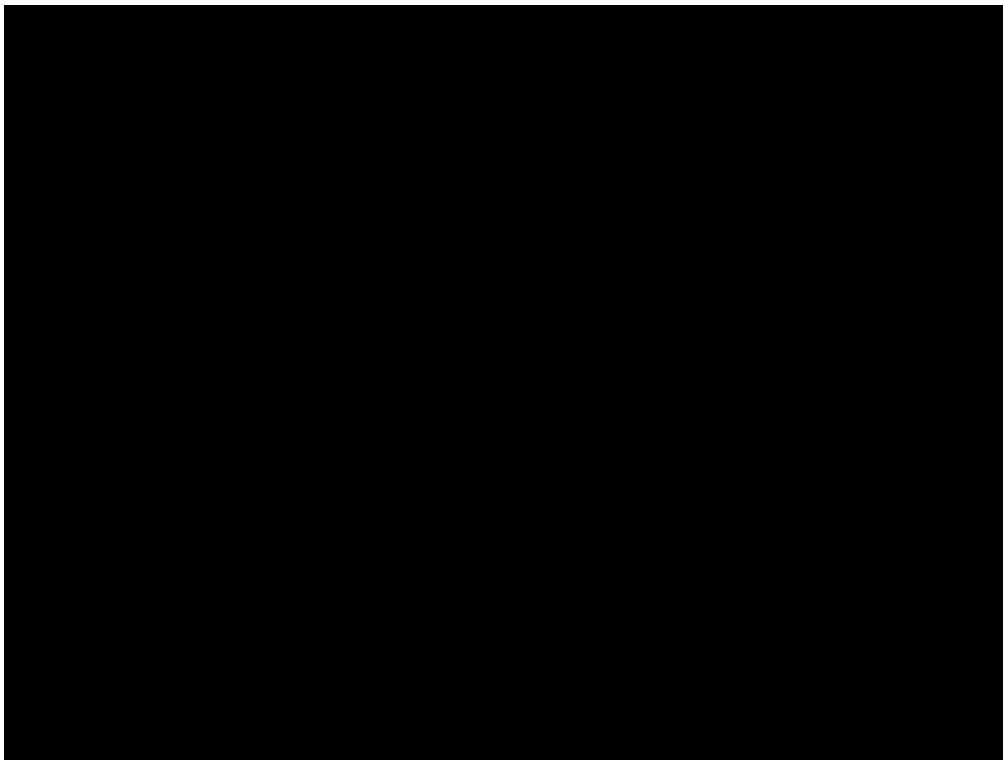


Figure 69. Creation of the rabbit elastase aneurysm model. Following exposure of the right carotid sheath and creation of a small arteriotomy, a sheath is introduced into the right common carotid artery. A balloon is introduced through the sheath and placed at the origin of the right common carotid artery and inflated. The right common carotid artery is ligated. Following this, elastase is introduced into the artery and allowed to incubate for 20 min. The sheath and balloon are then withdrawn and the superior aspect of the aneurysm is cinched off. The aneurysm continues to grow and then generally stabilizes at 1 month due to a combination of elastin digestion and hemodynamic forces. Figure reproduced from Brinjikji et al. (2016).

The FDSs used in this study were Silk stents, supplied by the manufacturer, Balt, who was a research partner, co-funded by the national agency for its participation to the present project (ANR Project IMPLANTS, ref ANR-14-CE17-0014)

P8RI-coated Silk FDS stents were prepared following the procedure described in section I.4.d. and sterilized by beta radiations prior to their implantation *in vivo*.

The rabbit elastase aneurysm is one of the most commonly used models for the testing of FDSs. As shown on Figure 69, it consists in creating an artificial aneurysm in the proximal segment of the right common carotid artery, by incubating elastase in the ligated artery for 20 minutes, so that this protease can hydrolyze elastin in the artery wall and promote its dilative remodeling. The aneurysm then grows over the course of a few weeks. Despite its extracranial location, this procedure results in a stable aneurysm with hemodynamic, morphological and histological features similar to those of human intracranial aneurysms (Sekhar and Heros 1981; Altes et al. 2000; Short et al. 2001; Hoh et al. 2004; Brinjikji et al. 2016).

All the *in vivo* experimental procedures described in this section were performed in our laboratory (Inserm U1148) by the interventional neuroradiologists Dr Aymeric Rouchaud and Dr Jildaz Caroff, who have practiced the rabbit saccular intracerebral aneurysm induced by elastase treatment under the supervision of Dr Laurent Spelle and run it routinely for research study purposes (Rouchaud et al. 2016b; Caroff et al. 2017).

The elastase aneurysm model was run in three separate sets of experiments. The first two were run in the absence of anti-platelet treatment. The presence of a healing thrombus in the stented arteries of these series prevented the analysis of the luminal endothelialization. We therefore performed a third series of experiments for which we created the model in 8 male New Zealand rabbits. Three weeks after the creation of the aneurysms, unmodified (n=4) and P8RI-coated (N=4) FDSs were implanted in the native right subclavian artery of each animal, so as to occlude the experimental saccular aneurysm. The SEM analysis was not suitable for the evaluation of the biocompatibility of the device in this model, due to the asymmetric positioning of the saccular aneurysm which prevented its longitudinal opening and observation on the luminal side. Thus, in two rabbits, an additional FDS was implanted further in the contralateral subclavian artery, in order to assess the integration of the devices in the vessel wall by scanning electron microscopy (SEM) observation of its luminal side.

The animals were administered 75mg of aspirin daily and terminated 4 weeks after FDS implantation. This duration was chosen because it had been shown that the inflammatory reaction in aneurysms created with this model is stopped 4 weeks after endovascular treatment, thus resulting in an aneurysm filled with acellular connective tissue, resembling the stable aneurysms seen in humans (Dai et al. 2006; Brinjikji et al. 2016). Immediately after the sacrifice of each animal, the subclavian artery segment containing the FDS was explanted, together with

the aneurysm. The explanted arteries were then processed for histology. After paraformaldehyde fixation, they were dehydrated by successive incubations in ethanol baths of increasing concentration. Then, they were impregnated with a methyl methacrylate solution. Finally, the polymerization of the methyl methacrylate monomers was triggered by the addition of benzoyl peroxide and N, N-dimethyl-p-toluidine.

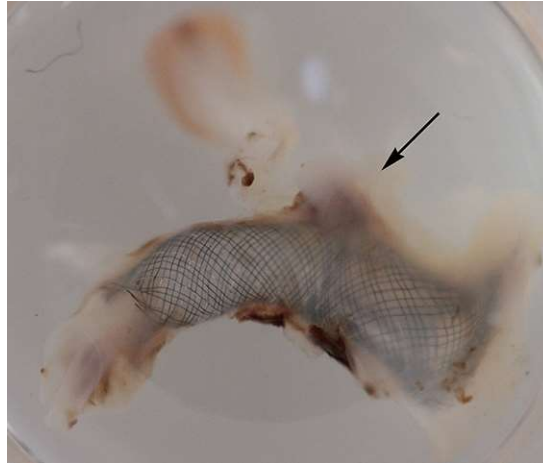


Figure 70. Photograph of an explanted stented artery embedded in PMMA. The arrow points to the aneurysm, which is occluded by the stent in the native artery.

This process resulted in the embedding of the explanted arteries in a poly(methyl methacrylate) (PMMA) resin, as shown on Figure 70. Although it is more complex than the usual histology techniques (paraffin embedding and cryosection), PMMA embedding is necessary for the sectioning of soft tissues, such as arteries, containing hard materials, like metallic stents. Indeed, the PMMA resin greatly decreases the difference in hardness between the stent struts and the surrounding tissue, which makes it possible to section the sample into thin slices without tearing off the tissue.

The embedded arteries were then sectioned transversally in a microtome equipped with a tungsten carbide blade, which is harder than the steel blade used for the sectioning of usual paraffin-embedded tissues. The resulting histology slides were stained by Masson's trichrome, which colors the connective tissues in blue, the cytoplasm in pink and the nuclei in purple. In order to better distinguish the smooth muscle cells, alpha-smooth muscle actin (α SMA) was stained by immunofluorescence in serial sections.

The two extra FDSs which had been implanted in the subclavian arteries of the rabbits, distally from the aneurysm, were processed for SEM observation, as detailed in the previous section. The processing of the explanted arteries was performed by Guillaume Even, Marion Morvan and Christine Choqueux (all staff members at our laboratory).

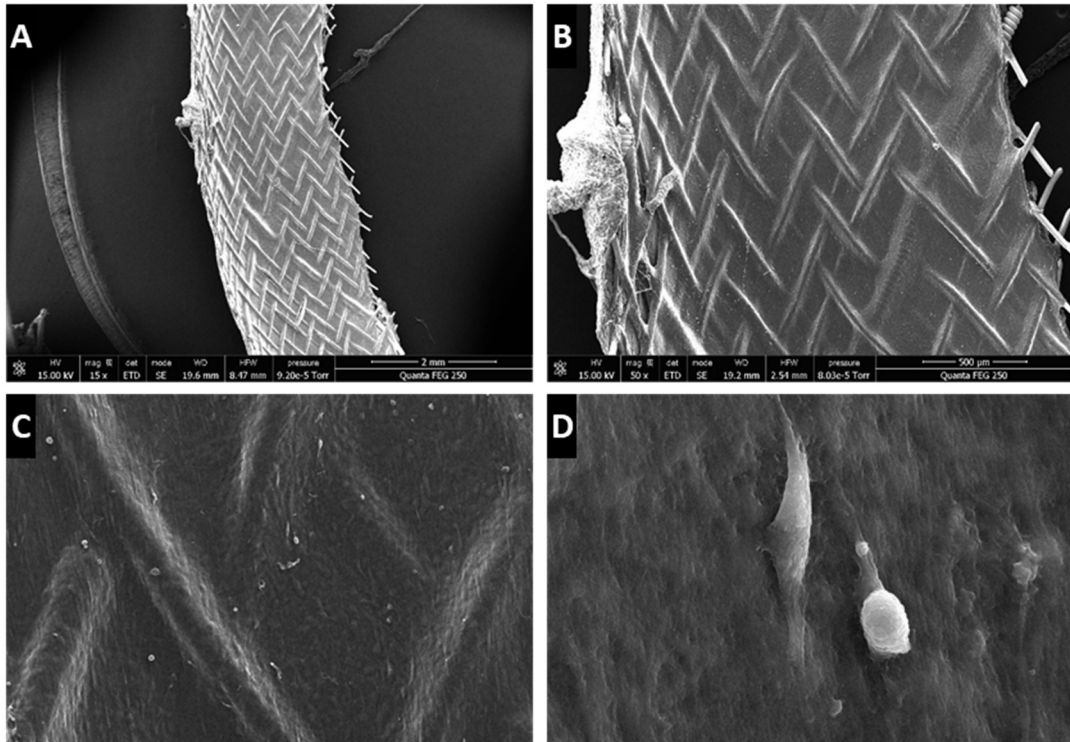


Figure 71. SEM images of a FDS implanted in the subclavian artery of a rabbit. The luminal side of the half-artery is shown. B, C, D are high magnification pictures of the region shown in A. 1 month after implantation, the FDS is entirely covered with arterial tissue. A small number of adherent leukocytes, such as the ones shown in D, can be seen on pictures B and C.

At the present time, the imaging of the stained slides has just been achieved, and we have not yet completed the analysis of the results. Thus, the following observations should be considered as preliminary.

Figure 71 shows SEM images of a P8RI-coated stent implanted in the contralateral, untouched subclavian artery of a rabbit, remotely from the aneurysm. Over its 4 week-period of implantation, the FDS has been entirely covered by neointimal growth, which yields the appearance of a velvet cover over the stent struts. A few adherent cells, identified as non-activated leukocytes because of their round shape, can be seen at the luminal surface of the vessel.

Representative examples of the transversal resin sections of implanted bare and P8RI-coated stents, stained by Masson's trichrome and immunofluorescence, are shown on Figure 72 and Figure 73 respectively. The struts of both types of stents have been covered by neointimal formation over the entire circumference of the vessel. However, the characteristics of the tissue that covers the stent struts strikingly differ with the type of stents. On the P8RI-coated stent the struts are way back in the arterial wall, covered by a thick, organized neointima, with layers of SMCs (see Figure 73 B and F) and oriented sheets of ECM, and exhibit a continuous endothelial monolayer (well visible on Figure 72 D and F). This organization is seen both in front of the aneurysmal neck and away from it. Contrastingly, on the bare stent, the struts are barely covered

by a thin neointima which appears poorly organized, devoid of SMCs (see Figure 73 A and E) and covered with a discontinuous endothelium (see Figure 72 C and E). The better organization and the presence of SMCs and a continuous endothelium on the neointima that covers the P8RI-coated stent constitute promising results, since the impermeability of the neointima covering the stent structure, especially in front of the aneurysmal neck, is key to successful aneurysm occlusion and stable arterial healing. Besides, the media of the aneurysmal wall (Figure 72 A and B) also appears less organized in the animal treated with a bare FDS, since it does not exhibit the layers of oriented SMCs seen in the other animal. Moreover, red blood cells and infiltrated leukocytes (identified by white and yellow arrows respectively on Figure 72 A) are visible in the aneurysmal wall of the animal treated with a bare FDS. Their presence indicates that neoangiogenesis and inflammation take place in the aneurysm wall, making it more susceptible to rupture. These phenomena are not seen in the aneurysmal wall of the animal treated with a "PDA-P8RI"-coated FDS. These observations thus represent another promising result. The careful examination of the images from the other animals of the same series will tell us whether these observations are consistent.

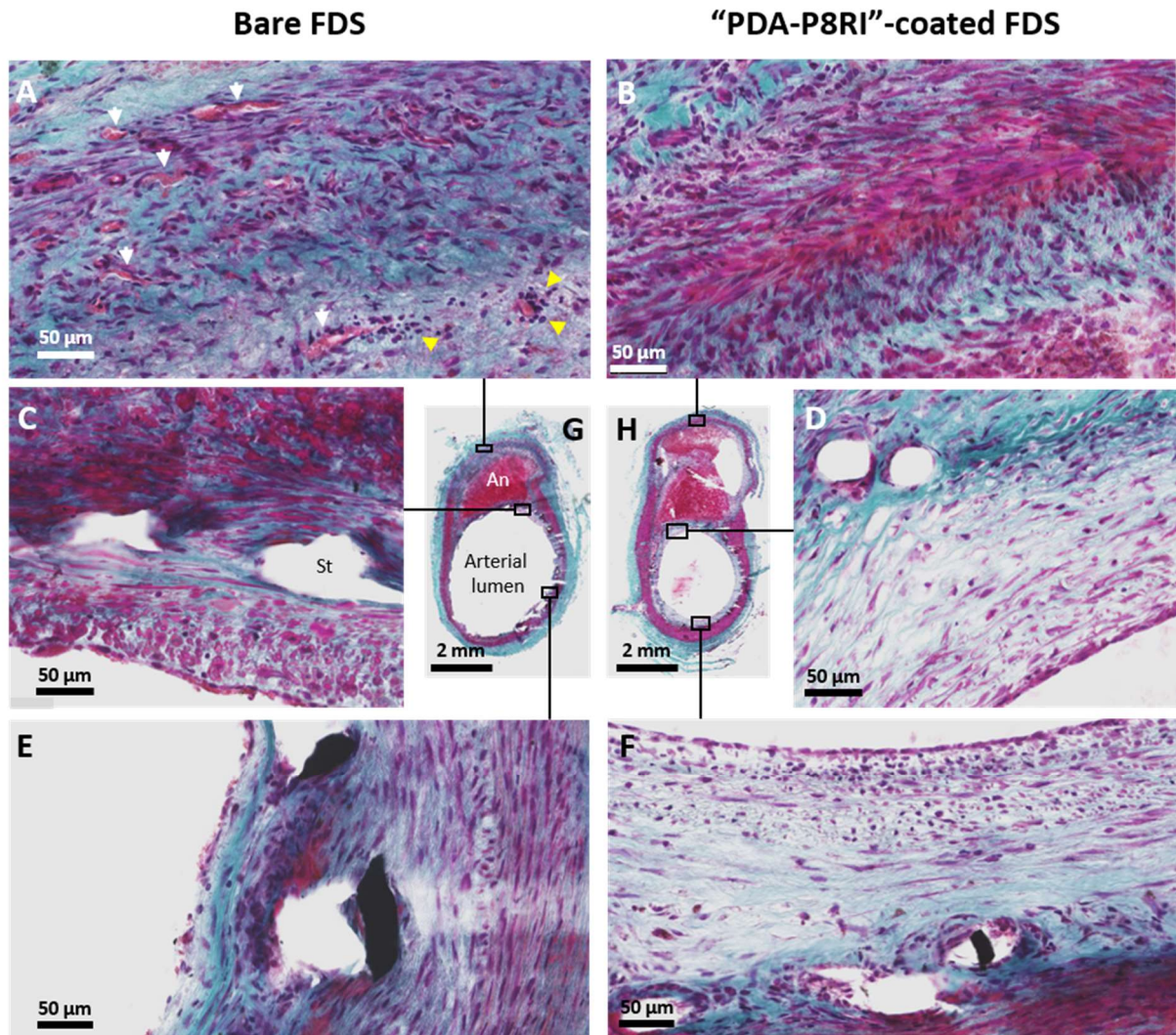


Figure 72. Histological sections of implanted FDSs stained with Masson's trichrome. Blue: connective tissue. Pink: cytoplasm. Purple: nuclei. *An*: aneurysm. *St*: position of a stent strut. Left (A, C, E, G): bare FDS. Right (B, D, F, H): "PDA-P8RI"-coated FDS. A, B: detail of the aneurysmal wall. C, D: detail of the tissue surrounding the stent struts in front of the aneurysm. E, F: detail of the arterial wall far from the aneurysm. G, H: global views of the sections. The white arrows highlight erythrocytes, identified by their pink color, small, round shape and absence of nucleus. The yellow arrows show infiltrated leukocytes, identified by their shape and their round nucleus.

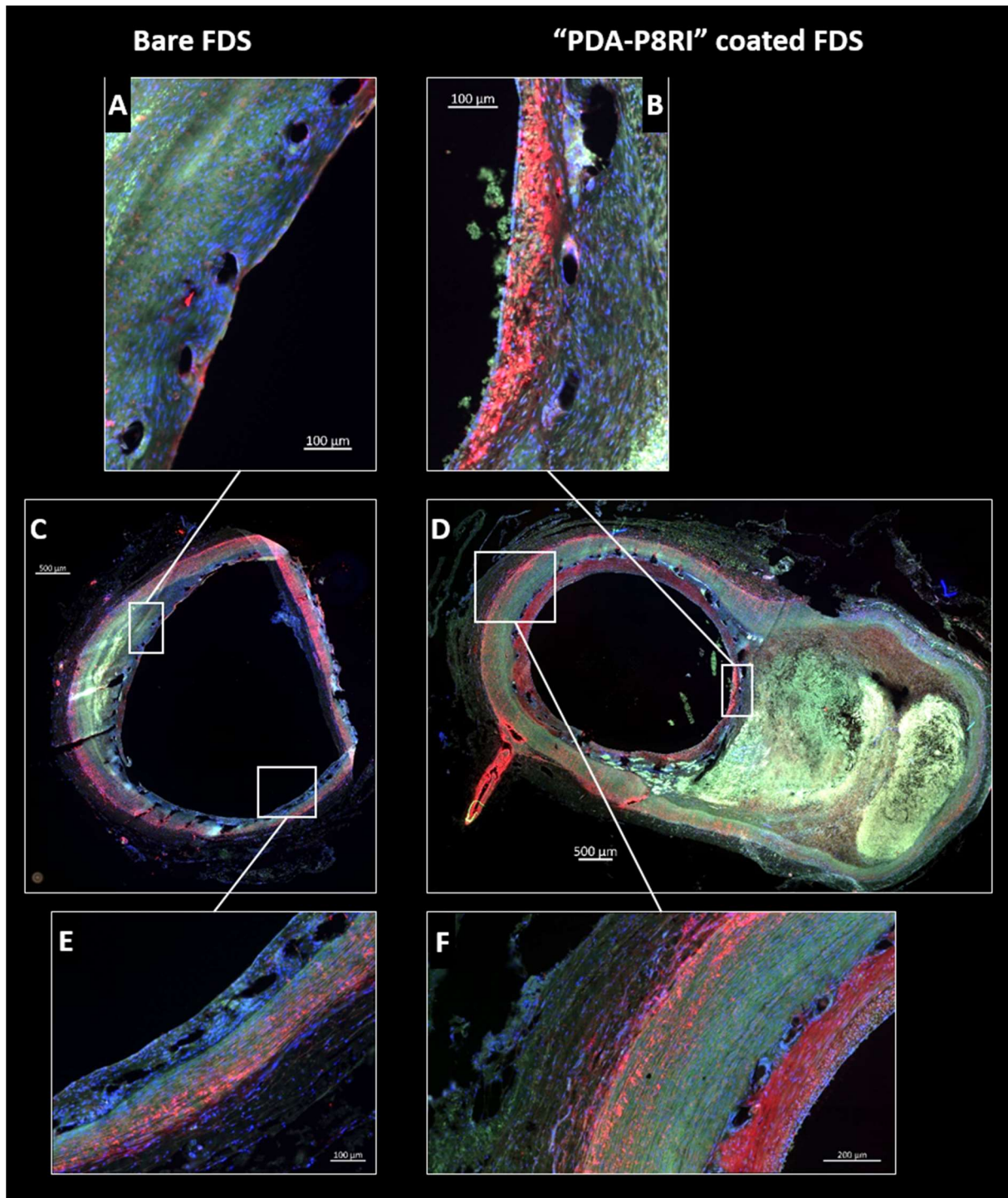


Figure 73. Histological sections of implanted FDSs immunostained for α SMA. Blue: Hoechst staining (nuclei). Red: α SMA (SMCs). Green: self-fluorescence (connective tissue). Left (A, C, E): bare FDS. Right (B, D, F): “PDA+P8RI”-coated FDS. A, B: detail of the arterial wall far from the aneurysm. C, D: global views of the sections. E, F: detail of the tissue surrounding the stent struts in front of the aneurysm. The tissue that covers the stent struts on the “PDA+P8RI”-coated stent is rich in SMCs (B, F), contrary to that of the bare stent (A, E).

Discussion

I. Strategic choices and characteristics of the P8RI coatings

I.1. Direct binding of P8RI on the alloy or use of an intermediate layer?

Concerns about the biocompatibility of stent polymer coatings have led to the recent development of polymer-free DESs: the Coroflex Isar stent manufactured by Braun and the Biofreedom by Biosensors, also sold under the name Lumeno Free by Cordis. On the Coroflex Isar stent, probucol is used as the drug matrix, whereas on the Biofreedom stent, the drug is adsorbed on the micro-structured surface of the stent. These approaches might be suitable for the controlled elution of drugs, but they do not allow the covalent and oriented grafting of bioactive molecules.

In the present work, the immobilization of P8RI on alloy surfaces, in a covalent and oriented manner, was performed both with the use of an intermediate PDA layer, and directly on plasma-aminated surfaces. The plasma-based method has the advantage of avoiding all polymer-related issues, but possesses neither the versatility of the PDA-based approach (since the plasma-assisted treatment of alloy surfaces is strongly dependent on the physico-chemical characteristics of the oxide layer (Lewis et al. 2011)) nor the scalability of a dip-coating process. Indeed, low-pressure plasma functionalization, contrary to the atmospheric-pressure treatments that we attempted to develop, requires the use of vacuum, which implies high maintenance and relatively expensive processes, and is therefore a hindrance for the potential industrial application of this method.

Thus, both the PDA-based and the plasma-based immobilization approaches have their strengths, but, considering the technical conditions of both strategies, we believe that the PDA-based approach is more reliable and suitable for a potential development on an industrial scale.

I.2. Why choose PDA rather than polymers already used for stents?

When it comes to the choice of a polymeric interface for the immobilization of bioactive molecules (such as P8RI) on stents, one could think that the most obvious options are the polymers already used in the coatings of commercially available stents. They have the advantage of having already been accepted for this use by the competent authorities (by FDA approval or CE marking), and they have presumably been selected for their satisfactory adhesion and biocompatibility properties.

However, there have been concerns about the biocompatibility of polymer coatings used in stents. Table 16 shows the polymers used for the coatings of drug-eluting stents reimbursed by

the French social security system. The non-degradable polymer coatings of first-generation DESs (Cypher and Taxus) were suspected to induce late neointimal hyperplasia (Carter et al. 2004), local inflammatory reactions (Virmani et al. 2004) and late stent thrombosis (McFadden et al. 2004; Virmani et al. 2004).

Inscription date	Manufacturer	Model	Alloy	Coating	Drug Matrix	Drug
2003	Cordis	Cypher	316L St. st.	Parylene C	PEVA + PBMA	Sirolimus
2004	Boston Scientific	Taxus	St. st.	-	SIBS	Paclitaxel
2006	Medtronic	Endeavor	MP35N CoCr	-	PC-based polymer	Zotarolimus
2008	Abbott/ Boston Scientific	Xience V/ Promus	L-605 CoCr	PBMA	PVDF-HFP	Everolimus
2010	Biosensors	Biomatrix	316L St. st.	-	PLA	Biolimus A9
2010	Boston Scientific	Promus Element	PtCr	PBMA	PVDF-HFP	Everolimus
2010	Terumo	Nobori	316L St. St.	Parylene C	PLA	Biolimus A9
2011	Medtronic	Resolute Integrity	MP35N CoCr	-	Mix of PBMA, PHMA, PVP, PVA	Zotarolimus
2014	Biotronik	Orsiro	L-605 CoCr	a-SiC:H	PLA	Sirolimus
2015	Boston Scientific	Synergy	PtCr	-	PLGA	Everolimus
2015	Braun	Coroflex Isar	L-605 CoCr	-	-	Sirolimus + Probuocol
2015	CID Vascular	Cre8	L-605 CoCr	Carbon	Sirolimus + fatty acids	Sirolimus
2015	Terumo	Ultimaster	L-605 CoCr	-	PLCL	Sirolimus
2016	Translumina	Yukon Choice PC	316L St. St.	-	PLA + shellac	Sirolimus
2017	Balton	Bioss Lim C	L-605 CoCr	-	PLGA	Sirolimus
2017	Biosensors/ Cordis	Biofreedom/ Lumeno Free	316L St. st.	-	-	Biolimus A9
2017	Cordis	Lumeno Alpha	CoCr	-	PLA	Biolimus A9

Table 16. Drug-eluting stents included in the list of products reimbursed by the French social security system. Similar models of the same line (e.g.: Xience V and Xience Alpine) have been omitted. St. st.: stainless steel. PtCr: Platinum-chromium alloy. PBMA: poly (n-butyl methacrylate). a-SiC:H: amorphous silicon carbide. PEVA: poly (ethylene-vinyl acetate). SIBS: poly(styrene-b-isobutylene-b-styrene). PC: phosphorylcoline. PVDF-HFP: poly(vinylidene fluoride-co-hexafluoropropylene). PLA: poly(lactic acid). PHMA: poly(hexylmethacrylate). PVP: polyvinylpyrrolidone. PVA: poly(vinyl alcohol). PLGA: poly(lactic-co-glycolic acid). PLCL: poly(DL-lactide-co-caprolactone).

As a consequence, a second generation of DESs (which eluted everolimus, zotarolimus and Biolimus A9 instead of sirolimus) was developed with different polymers. In particular, most recent DESs are coated with biodegradable polymers (pure poly-L-lactic acid or lactic acid-based copolymers), which are supposed to reduce the incidence of late thrombosis and restenosis. Yet, correlations between several biodegradable polymers and inflammatory reactions have been shown (Giessen et al. 1996; Lincoff et al. 1997), and, at this time, biodegradable polymer DESs have not demonstrated a clinical improvement compared to durable polymer DESs (Bundhun et al. 2017; Kalra et al. 2017). Thus, the search for more biocompatible polymers for stent coatings is not over yet. In this regard, PDA appears as a promising candidate. Our results, as well as those of other groups (Ku et al. 2010; Yang et al. 2012; Luo et al. 2013b), demonstrate that PDA coatings promote endothelial cell adhesion and proliferation and decrease platelet adhesion, and Huang's group showed that PDA reduced SMCs proliferation (Yang et al. 2012). Long-term *in vivo* studies are necessary to determine whether PDA-coated stents – and “PDA+P8RI”-coated stents – can decrease the incidence of late adverse events (thrombosis and restenosis) compared to existing stents polymeric coatings.

1.3. Choice of the strategy for the immobilization of P8RI on PDA

Ever since the first article on dopamine self-polymerization (Lee et al. 2007), PDA coatings have been used as an intermediate layer for the immobilization of numerous bioactive molecules. Most research groups have chosen the most direct possible method: a simple incubation of the PDA-coated substrates in a solution containing the molecules of interest. The covalent grafting of the molecules takes place thanks to the latent reactivity of PDA towards amines and thiols. Such an approach was used for the immobilization of bioactive molecules of various types: proteins (e.g. trypsin (Lee et al. 2009)), glycosaminoglycans (e.g. hyaluronic acid (Wu et al. 2016)), peptides (e.g. bivalirudin (Lu et al. 2012)), very small molecules (e.g. cystamine (Zhou et al. 2011)) and nanoparticles (e.g. VEGF-loaded heparin/poly-L-lysine nanoparticles (Liu et al. 2015b)). This is the method we first adopted for the immobilization of the P8RI peptide. Its extreme simplicity makes it low-cost and easily scalable, while ensuring a strong anchoring of the peptide to the coating through covalent bonding.

However, in order to better control the orientation of the grafted bioactive molecules and to make them more accessible to contacting cells, other studies have chosen to add a linker between the PDA coating and the immobilized molecule. Chen and colleagues (Chen et al. 2015a) grafted staphylococcal protein A on PDA before immobilizing anti-CD34 antibodies on the proteins, through their Fc constant region. Yuan and colleagues (Yuan et al. 2013) used a more conventional bifunctional linker for the grafting of chitosan: glutaraldehyde. In the present study,

we used a linker which combined the reaction efficiency and bioorthogonality of copper-free click chemistry with the availability and affordability of common commercial bifunctional linkers: the BCN-amine linker presented on Figure 46.

A third option exists for the immobilization of bioactive molecules on PDA coatings: the copolymerization of the molecules of interest with dopamine. The codeposition of dopamine and heparin, phosphorylcholine-based polymer or PEGylated poly(ethyleneimine) have been reported (Bae et al. 2012; Yao et al. 2012; Sin et al. 2016). However, this method does not allow the control of the orientation of the grafted molecules. Besides, it involves the use of much larger quantities of bioactive molecules than the surface immobilization techniques presented above. Therefore, it is better adapted to relatively inexpensive glycosaminoglycans or polymers than to proteins or peptides. Thus, this method was not considered fit for the present study.

1.4. Importance of the thickness of the coating in the “PDA-P8RI” strategy

During this project, we have not measured the thickness of the PDA coating. However, in the absence of personal experimental data, we can rely on the literature to provide estimates.

The first article on polydopamine (Lee et al. 2007) reported the measurement of the thickness of PDA coatings deposited in the same conditions that we used (2 mg/mL dopamine in Tris buffer, pH 8.5, at room temperature) on silicon substrates patterned by photolithography. The measurement was done by AFM, on coatings resulting from different deposition durations. The measured values are presented on Figure 74. The thickness of the coating resulting from the deposition duration we used (22h) was approximatively 45 nm.

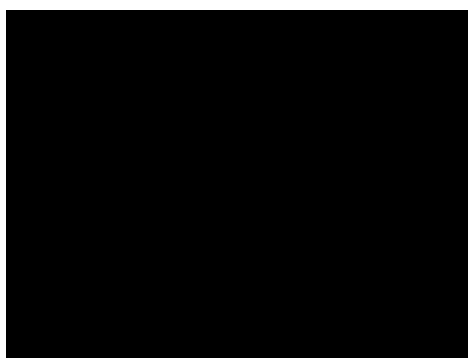


Figure 74. Thickness evolution of PDA coating on Si as measured by AFM of patterned surfaces. Adapted from Lee et al., 2007. The thickness of the coating after 22h of deposition is comprised between 45 and 50 nm.

Other research groups measured the thickness of PDA coatings deposited in identical conditions. Ellipsometry measurements on silicon substrates gave values around 45 nm (Zhu and Edmondson 2011) or 30 nm (Ball et al. 2012). Stylus profiler measurements on patterned silicon substrates (Li et al. 2009) resulted in higher values: around 100 nm. Bourmaud et al. (2009) reported a thickness of 150 nm of PDA coatings on poly(lactic acid), measured by AFM after scratching of the coating. Overall, the thickness of PDA coatings deposited in the conditions that we used can hence be considered to be between 30 and 150 nm.

The additional thickness of the immobilized linker and peptide can be roughly estimated as follows: the length of a C-C, C-N or C-O covalent bond is approximatively 0.15 nm. There are 25 bonds in the peptide backbone, and 12 in the BCN-amine linker. Thus, the size of a linear “linker + peptide” molecule is: $37 \times 0.15 = 5.6$ nm. Therefore, the immobilization of the linker and the peptide on the PDA coating adds only a few nanometers to the total thickness of the coating.

In summary, the thickness of the “PDA+P8RI” coating can be estimated to range between 30 and 160 nm. As discussed above for the PP-HMDSN coating, this low thickness is desirable in order to limit the amount of potentially toxic products released during *in vivo* coating degradation.

1.5. Adhesion and stability of the “PDA + P8RI” coating

Stent coatings are subjected to demanding conditions, first during the expansion of the stents, and secondly when they are exposed to arterial blood flow. Huang’s group (Yang et al. 2012) showed that PDA coated-stents (coated with the same protocol as the one we used) remained intact after balloon expansion. No delamination or degradation was observed. More generally, polydopamine is known for its excellent adhesive properties: Zhu and Edmonson (2011) showed that a PDA coating on polystyrene remained adherent after a tape peel test. Polydopamine has also been used as an intermediate adhesive layer, under zirconia and graphene oxide coatings (Ou et al. 2011, 2012), cyclodextrins based polymer coatings (Sobocinski et al. 2014), or polytetrafluoroethylene (PTFE) films (Beckford and Zou 2014). In their article, Beckford and Zou showed that the intermediate PDA layer drastically improved the friction and wear resistance of PTFE films on stainless steel.

As regards the stability of PDA-based coatings in aqueous medium, the “PDA-linker-P8RI” coating did not show any sign of degradation at the end of the one-month static ageing test in PBS that we performed. This is consistent with the results of other groups, which had demonstrated the stability of PDA coatings (deposited with the same protocol as the one we used) in static ageing tests carried out for one week in deionized water (Saidin et al. 2013), and for one month in PBS (Yang et al. 2012). These tests were carried out in static conditions, but pseudo-arterial

flow conditions would of course mimic more closely the *in vivo* environment of the stents. No report of *in vitro* stability tests in flow conditions has been found in the literature. We plan to perform ageing tests on the “PDA + P8RI” coating in the dynamic test bench presented on Figure 37, as we did on PP-HMDSN coatings.

In sum, the adhesion and stability studies carried out thus far in this thesis work and by other research groups all point to the conclusion that PDA coatings possess the adhesion and stability properties required for their use as stent coatings.

II. Technical consideration: cell-based assays on metallic samples

Similarly to the evaluation of the mechanical properties of the coating, the *in vitro* biocompatibility experiments on platelets and endothelial cells presented in this study were performed in static conditions. Here again, *in vitro* flow systems would reproduce more closely the *in vivo* environment of these cells. The phenotype of endothelial cells, in particular, is known to undergo significant changes depending on the applied shear stress. We have observed in our laboratory that endothelial cells cultivated in flow chambers align with the flow direction and form better-defined intercellular junctions than the same cells cultivated in static conditions. The effect of hemodynamic forces on the expression of several endothelial genes has also been proved (Resnick and Gimbrone 1995).

Flow systems for cell culture are commercially available, and our laboratory is equipped with one of them. However, flow chambers usually consist in transparent channels designed for the seeding of cells on the walls, and real-time observation by optical microscopy. They are not designed for the insertion of non-transparent biomaterial samples. We carried out several attempts to develop a flow system adapted to CoCr disks in the course of this study, using either commercial flow chambers (μ -Slide 3D Perfusion, Ibidi) or custom-made PDMS chambers. However, the imperfect fitting of the CoCr disks in the chambers induced artefacts and the experiments carried out with these chambers were flawed by poor reproducibility.

We met similar difficulties when we tried to develop an endothelial cell migration assay on coated CoCr disks. The cell migration assay would have been a closer model to the *in vivo* situation where endothelial cells progressively cover stent struts, compared to the direct seeding of endothelial cells on the disks. Unfortunately, it proved very difficult to ensure a good contact between the CoCr disks and the surrounding collagen gel on which the cells were cultivated, without contaminating the surface of the disks with collagen.

The technical limitations we encountered are inherent in the field of biomaterials, which stands at the crossroads of experimental biology (characterized by sub-millimeter-scale systems and stringent reproducibility and sterility requirements) and materials science (which generally involves custom-made, non-standard samples). There is today a range of commercial cell culture systems adapted to the testing of porous scaffolds such as hydrogels (Ebers' P3D chambers, Ibidi's μ -Slide 3D Perfusion, Cellego Biotek's U-Cup, Cellix's VenaT4, etc.). Maybe the next years will see the development and propagation of commercial flow systems adapted to solid, non-transparent biomaterials. This might go together with a standardization of the shape and dimensions of laboratory-made biomaterials samples.

III. Scientific and industrial context of the project

III.1. Alternative approaches to improve stents endothelialization

Ever since the association between late stent thrombosis and delay in endothelialization of DESs was shown (Joner et al. 2006), several coatings designed to improve stent endothelialization through the immobilization of bioactive molecules have been developed. Two main types of bioactive molecules can be distinguished: extracellular matrix (ECM)-derived molecules which promote the adhesion of endothelial cells, and antibodies or aptamers designed for the capture of circulating endothelial progenitor cells (EPCs).

As regards the first approach, either whole ECM glycoproteins such as fibronectin (Li et al. 2011; Montañó-Machado et al. 2017), or integrin-binding peptides derived from the proteins and glycoproteins of the ECM, such as RGDS, REDV, YIGSR or cyclic RGD (Joner et al. 2012; Castellanos et al. 2017), have been immobilized on metallic alloys and shown to improve endothelial cell adhesion and proliferation. However, the binding motifs of the ECM components are not specific to the integrins of endothelial cells. Integrin-binding peptides such as RGD or RGDS have been shown to improve the adhesion and spreading of vascular smooth muscle cells (SMCs) (Massia and Stark 2001; Mann and West 2002) and neutrophils (Kim et al. 2014). It is therefore questionable whether stents coated with these glycoproteins or peptides would result in reduced neointimal hyperplasia, and thus a lower restenosis rate, compared with BMSs. Long-term *in vivo* studies would be necessary to answer this question. At the present time, they have not yet been performed.

The second main strategy to improve stent endothelialization is the capture of circulating EPCs through the immobilization of anti-CD34 antibodies. An anti-CD34 antibody-coated stent, called Genous, is presently commercialized by OrbusNeich. Immobilized anti-CD34 antibodies have been shown to enhance EPCs adhesion *in vitro* (Chen et al. 2015a) and to promote rapid

stent endothelialization *in vivo* (Lin et al. 2010; van Beusekom et al. 2012). However, this promising approach has not fully solved the problem of stent biocompatibility, as clinical trials have found the Genous stent to be inferior to DESs in terms of restenosis prevention (Beijk et al. 2010; Klomp et al. 2011). This observation has led OrbusNeich to develop the Combo stent, which combines anti-CD34 antibodies with a sirolimus-eluting coating. A known limitation of anti-CD34 coatings is that CD34 positive cells represent a very small fraction of the PBMCs (0.002%), and that most CD34 positive cells (99.6%) are not EPCs. Some CD34 positive cells are also able to differentiate into vascular SMCs (Wendel et al. 2010). In order to address this concern, DNA aptamers which specifically target EPCs, rather than all CD34 positive cells, have recently been immobilized on stainless steel and proved to selectively promote the adhesion and proliferation of EPCs *in vitro* (Li et al. 2016). Short-term *in vivo* studies are needed to show whether these aptamers, which target such a small population of circulating cells (EPCs represent about 0.000008% of the PBMCs), result in an improvement of stent endothelialization.

In summary, the balance between stent endothelialization improvement and restenosis prevention appears difficult to achieve. Still, amongst the molecular targets considered for that purpose, CD31 presents the distinct advantage of being specifically expressed by cells of the blood/vessel interface, and not SMCs. Thus, P8RI, the CD31-agonist peptide on which this work is based, is not expected to promote SMC adhesion or proliferation, contrary to ECM glycoproteins, integrin-binding peptides or anti-CD34 antibodies. As for the alternative approaches presented here, long-term *in vivo* studies will be necessary to assess the effect of P8RI-based coatings on neointimal hyperplasia, and thus restenosis.

Besides the question of their specificity, the nature of the bioactive molecules used for improving stent endothelialization is also of primary importance. Peptides have often been preferred to whole proteins or antibodies because their biological activity does not require complex 3D folding or the exposition of particular binding sites, which could be compromised by non-oriented immobilization techniques. Peptides (and DNA aptamers) are also significantly less expensive than most proteins and antibodies, which is an important concern in the context of a highly competitive stent market.

III.2. Next generation stents: a highly competitive market

There is still a dire need for better vascular stents, despite the improvements in their successive generations, since they continue to provoke severe complications in a number of cases. The incidence of stent thrombosis at 3 years after the implantation of a BMS or a second-generation DES is of 1.0 to 1.5% (results from a study on 18334 patients (Tada et al. 2013)), and the incidence of angiographic restenosis is about 30% for BMSs and 12% for second generation

DESs (results from a study on 10004 patients (Cassese et al. 2013)). Flow diverters have been shown to cause in-stent thrombosis and thromboembolic events in a number of cases, despite treatment with dual antiplatelet therapy (Al-Mufti et al. 2016): the incidence of thromboembolic events in patients under DAPT has been reported to be between 2% and 7% (Saatci et al. 2012; Tan et al. 2014; Pierot et al. 2016).

The research on new coatings designed to improve the biocompatibility of vascular stents is therefore very active. However, researchers in this field must not ignore that appropriate biological effects, satisfactory adhesion and stability properties, and the absence of toxic degradation products are not the only requirements for a new stent coating. If it is to reach the market, the coating process reproducibility, scalability and cost should not be overlooked.

The requirements of reproducibility and scalability are common to all medical devices. The simplicity of the “PDA+P8RI” coating procedure is a great advantage in that respect: a dip-coating process can easily be adapted to industrial scale, and it has already been used for stent coating (Chen et al. 2015b). As for the base components, dopamine and custom peptides produced according to regulatory “Good Manufacturing Practices” (GMP) already exist (dopamine under the form of drugs such as Intropin, Dopastat or Dopastropin, and peptides as supplied by private companies). Thus, the deposition process of the “PDA+P8RI” coating is well suited to an adaptation to GMP-compliant industrial-scale production.

The issue of cost control is particularly relevant to the coronary stent industry. Indeed, the prices of BMSs and DESs have globally undergone a dramatic decrease over the last fifteen years. The evolution of the prices of the BMSs and DESs reimbursed by the French social security system is given on Figure 75 as an example. Today, a large number of similar BMSs and DESs are available. They often use the same alloys, polymers, and drugs as competitive models (as shown on Table 16), and show similar results in clinical trials. Thus, the competition between these products is strong and it drives the average selling prices down. Where prices are set by public authorities (in France for instance), the alignment of prices can even be legally mandatory. For these reasons, the control of the costs of any new stent coating is highly necessary. The most expensive component of the “PDA+P8RI” coating is the peptide, and its production cost is not prohibitive: it is inferior to that of proteins such as the anti-CD34 antibody immobilized on the Genous stent (manufactured by OrbusNeich). The coating process (dip-coating at room temperature) is very economical, since it does not require complex equipment or important quantities of energy.

In short, the development of new stent coatings must take into account the requirements of industrial production in a competitive market. The “PDA+P8RI” coating process is compatible with these exigencies.

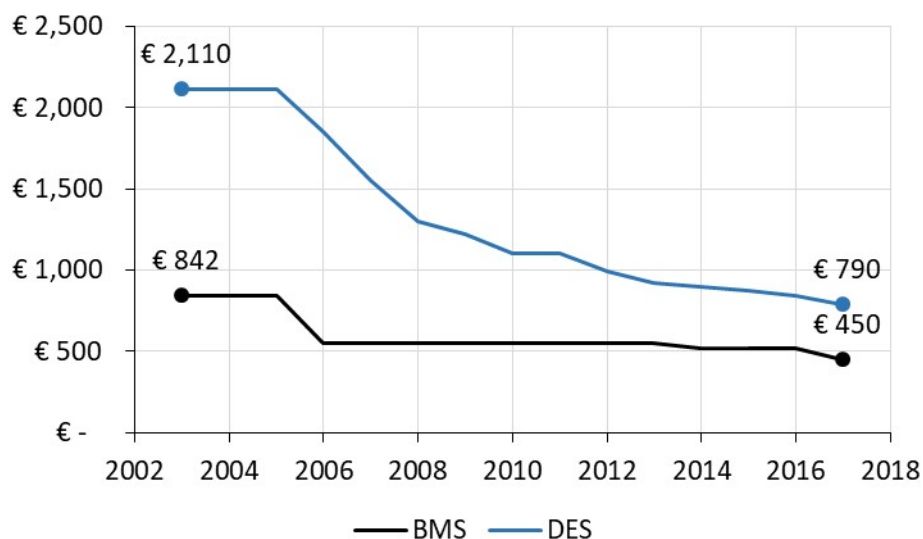


Figure 75. Evolution of the prices of the BMSs and DESs reimbursed by the French social security system between 2003 and 2017. Prices are set by the French state and are the same for all BMSs models and all DESs models.

IV. Perspectives

IV.1. “PDA+P8RI”-based dual stent coating

The approach we adopted to improve stents biocompatibility was the surface immobilization of P8RI, a CD31 agonist peptide. The main issue we wanted to address with this coating was stent strut endothelialization, because, as detailed in the introduction, it is a critical step of the complications that can arise after stenting. Still, “PDA+P8RI”-coated stents might benefit from additional anti-thrombotic properties (besides the not statistically significant decrease in platelet adhesion that we observed on “PDA+P8RI” coatings *in vitro*) during the first weeks after stent implantation, when the coating is not yet degraded. As PDA is a convenient platform for the immobilization of many types of biomolecules, the “PDA+P8RI” coating could easily be transformed into a dual coating, with the addition of a second bioactive molecule, with anti-thrombotic properties, such as heparin (heparin immobilization on PDA has already been reported by Jiang and colleagues (2010)).

The idea to co-immobilize two molecules with complementary effects on stents is not new: Huang’s group has developed a dual heparin/fibronectin coating in order to provide anti-thrombotic and pro-endothelialization properties to stents (Li et al. 2011); Montañó and colleagues have targeted the same objective with a phosphorylcholine/fibronectin coating (Montañó-Machado et al. 2017). Dual coatings with pro-endothelialization and anti-SMC proliferation effects have also been developed: a hyaluronic acid/sirolimus-in-polymer coating

by Kim and colleagues (2016), and the anti-CD34 antibody/sirolimus-in-polymer coating present on OrbusNeich's Combo stents.

In a nutshell, if the ongoing *in vivo* assessment of the "PDA+P8RI" coating yields encouraging results in terms of endothelialization, it might be interesting for the continuation of the project to test the effect of the co-immobilization of an anti-thrombotic bioactive molecule such as heparin.

IV.2. What will the stent of the future be?

Today, the stents commonly used for coronary artery disease treatment are either BMSs or DESs. Both types of stents are based on metallic alloys and are designed to stay in place during the lifetime of the patient. Hence the necessity to develop more biocompatible coatings to avoid long-term complications. However, a different type of stents has been developed, which could represent a breakthrough in the field: bioresorbable vascular stents (BVSs). These stents are designed to degrade in a few months, thus providing temporary scaffolding to the vessel (with the additional elution of antiproliferative drug) while avoiding neointimal hyperplasia and late stent thrombosis (Onuma and Serruys 2011). Around 20 models of BVSs are currently in clinical trials and some have already obtained CE marking (Tenekecioglu et al. 2016). In most cases, it is still too early to know whether they will perform better than DESs.

The Absorb BVS manufactured by Abbott has been the most tested in clinical trials (2008 patients were enrolled in the latest trial). However, it was withdrawn from the market earlier this year, after the 2-year results of the ABSORB III trial revealed its significantly higher target lesion failure and target vessel myocardial infarction incidence compared with the Xience DES (Ellis and Kereiakes 2015).

Despite this setback, the ongoing clinical trials on other models of BVSs might show better results. It must also be noted that, as the development of BVSs is very recent, the next years might bring considerable improvement in their design. In particular, because of the mechanical properties of the currently used bioresorbable materials, the strut thickness of existing BVSs is comprised between 100 and 175 μm (156 μm for the Absorb stent), whereas recent DESs have a strut thickness of about 80 μm (Foin et al. 2014). The correlation between stent strut thickness and neointimal hyperplasia is well known (Rittersma et al. 2004); thus, the development of biodegradable materials with better mechanical properties might bring a dramatic improvement in the clinical outcome of patients implanted with BVSs.

The future will tell us if BVSs can hold their promise to advantageously replace BMSs and DESs. Maybe BVSs will be added to the therapeutic arsenal of interventional cardiologists along with BMSs and DESs, each type of stent being more adapted to particular indications. This is

currently the case with DESs and BMSs: although most implanted coronary stents are DESs (74% in France in 2014, according to a report by the ANSM (Schapiro-Dufour et al. 2016)), BMSs are recommended for patients with high bleeding risk under anticoagulant treatment. As BVSs are best adapted to young patients with simple lesions, DESs and BMSs might remain the best option for complex lesions.

Future BVSs might benefit from a coating that promotes their fast endothelialization and thus helps prevent thrombosis while the stent is not fully degraded. Of course, such a coating can only be compatible with a BVS if it degrades faster than the stent. The “PDA+P8RI” coating is expected to fulfil this requirement, since melanin films (which have a chemical structure close to that of PDA) implanted *in vivo* were shown to be resorbed after 8 weeks (Bettinger et al. 2009). Still, we obviously need more time and experience with BVSs to determine fast endothelialization is really achieved with this type of stents.

Another type of progress might be made in the field of vascular stents in a more distant future, in the context of personalized medicine: the development of ‘smart’ stents, which would collect and send information about their *in vivo* environment. This information, monitored by a medical practitioner, should help diagnose potential complications such as in-stent thrombosis and restenosis, or indicate the progress of stent struts endothelialization. Several research projects have been published on smart stents equipped with pressure sensors (Menudet 2011; Chen et al. 2014; Park et al. 2016), mass sensors (Musick et al. 2010), or flow and temperature sensors (Son et al. 2015), but, to this day, they are still far from clinical application. A French start-up, Instent, was created in 2014 in order to develop a connected stent able to monitor thrombosis. However, it has recently changed the target application of its technology and is now developing a smart guidewire for ischemic stroke, under the name Sensome. Thus, it will be years before we know whether smart stents can significantly improve the follow-up of patients with stented arteries. However, one thing is certain: the development of real-time remote health monitoring will require a substantial change in the organization of medical practitioners’ work, so that they can efficiently adapt to their emerging new role.

In summary, the arterial stent of the future might be bioresorbable, and it might be later equipped with sensors and antennas; but its *in vivo* environment will be the same as that of current stents; thus, it might still benefit from the advances in bioactive coatings, such as those envisaged by my work, in order to ensure that the biomaterial is accepted as ‘peacefully’ as possible by the living cells of the patient’s vascular system.

General conclusion

The project of this thesis aims at reducing the complications associated with coronary stents and flow diverting stents. The objectives set for this thesis work were to immobilize the CD31 agonist peptide P8RI on the surface of coronary stents and FDSs, and to carry out the *in vitro* and *in vivo* evaluation of the biological properties of the resulting surfaces, in terms of anti-thrombotic, anti-inflammatory, and, above all, pro-endothelialization properties.

The immobilization of P8RI on alloy surfaces was successfully carried out with the use of an intermediary bio-inspired polydopamine layer. The covalent and oriented grafting of the peptide was realized through a series of simple dip-coating steps, in aqueous medium, thus rendering the coating process perfectly suitable for potential future applications at the industrial scale. The *in vitro* and *in vivo* evaluations of the coated surfaces yielded promising, although still preliminary, results, in terms of pro-endothelialization and anti-inflammatory effects.

The need for better coronary stents and FDSs is undisputed. Many different solutions are being investigated and developed all over the world. The scalability of the 'PDA-P8RI' coating process that we developed, associated with the known biocompatibility of PDA and the biological effects that were presented in this work, make the PDA-P8RI coating a plausible candidate amongst the numerous projects that compete to reach the bedside. Further studies will tell us whether it can live up to our expectations.

Bibliography

- Alam, A., Wan, C. and McNally, T. 2017. Surface amination of carbon nanoparticles for modification of epoxy resins: plasma-treatment vs. wet-chemistry approach. *European Polymer Journal* 87: 422–448.
- Albelda, S. M., Oliver, P. D., Romer, L. H. and Buck, C. A. 1990. EndoCAM: a novel endothelial cell-cell adhesion molecule. *The Journal of Cell Biology* 110 (4): 1227–1237.
- Albelda, S. M., Muller, W. A., Buck, C. A. and Newman, P. J. 1991. Molecular and cellular properties of PECAM-1 (endoCAM/CD31): a novel vascular cell-cell adhesion molecule. *The Journal of Cell Biology* 114 (5): 1059–1068.
- Al-Mufti, F., Amuluru, K., Gandhi, C. D. and Prestigiacomo, C. J. 2016. Flow Diversion for Intracranial Aneurysm Management: A New Standard of Care. *Neurotherapeutics* 13 (3): 582–589.
- Altes, T. A., Cloft, H. J., Short, J. G., DeGast, A., Do, H. M., Helm, G. A. and Kallmes, D. F. 2000. Creation of saccular aneurysms in the rabbit: a model suitable for testing endovascular devices. *American Journal of Roentgenology* 174 (2): 349–354.
- Amada, S. and Hirose, T. 1998. Influence of grit blasting pre-treatment on the adhesion strength of plasma sprayed coatings: fractal analysis of roughness. *Surface and Coatings Technology* 102 (1): 132–137.
- Artemenko, A., Kozak, H., Biederman, H., Choukourov, A. and Kromka, A. 2015. Amination of NCD Films for Possible Application in Biosensing. *Plasma Processes and Polymers* 12 (4): 336–346.
- Babaev, V. R., Bobryshev, Y. V., Sukhova, G. K. and Kasantseva, I. A. 1993. Monocyte/macrophage accumulation and smooth muscle cell phenotypes in early atherosclerotic lesions of human aorta. *Atherosclerosis* 100 (2): 237–248.
- Bae, I.-H., Park, I.-K., Park, D. S., Lee, H. and Jeong, M. H. 2012. Thromboresistant and endothelialization effects of dopamine-mediated heparin coating on a stent material surface. *Journal of Materials Science: Materials in Medicine* 23 (5): 1259–1269.
- Ball, V., Frari, D. D., Toniazzo, V. and Ruch, D. 2012. Kinetics of polydopamine film deposition as a function of pH and dopamine concentration: Insights in the polydopamine deposition mechanism. *Journal of Colloid and Interface Science* 386 (1): 366–372.
- de Barros Faria, M., Castro, R. N., Lundquist, J., Scrivano, E., Ceratto, R., Ferrario, A. and Lylyk, P. 2011. The role of the pipeline embolization device for the treatment of dissecting intracranial aneurysms. *AJNR. American journal of neuroradiology* 32 (11): 2192–2195.
- Bauters, C., Meurice, T., Hamon, M., McFadden, E., Lablanche, J. M. and Bertrand, M. E. 1996. Mechanisms and prevention of restenosis: From experimental models to clinical practice. *Cardiovascular Research* 31 (6): 835–846.
- Bayat, B., Werth, S., Sachs, U. J., Newman, D. K., Newman, P. J. and Santoso, S. 2010. Neutrophil transmigration mediated by the neutrophil-specific antigen CD177 is influenced by the endothelial S536N dimorphism of platelet endothelial cell adhesion molecule-1. *The Journal of Immunology* 184 (7): 3889–3896.
- Beckford, S. and Zou, M. 2014. Wear resistant PTFE thin film enabled by a polydopamine adhesive layer. *Applied Surface Science* 292 (Supplement C): 350–356.
- Beijk, M. A. M., Klomp, M., Verouden, N. J. W., van Geloven, N., Koch, K. T., Henriques, J. P. S., Baan, J., Vis, M. M., Scheunhage, E., Piek, J. J., Tijssen, J. G. P. and de Winter, R. J. 2010. Genous™ endothelial progenitor cell capturing stent vs. the Taxus Liberté stent in patients with de novo coronary lesions with a high-risk of coronary restenosis: a randomized, single-centre, pilot study. *European Heart Journal* 31 (9): 1055–1064.
- Berman, M. E. and Muller, W. A. 1995. Ligation of platelet/endothelial cell adhesion molecule 1 (PECAM-1/CD31) on monocytes and neutrophils increases binding capacity of leukocyte CR3 (CD11b/CD18). *The Journal of Immunology* 154 (1): 299–307.
- Bertrand, N., Drévilion, B., Gheorghiu, A., Sénémaud, C., Martinu, L. and Klemberg-Sapieha, J. E. 1998. Adhesion improvement of plasma-deposited silica thin films on stainless steel substrate studied by x-ray photoemission spectroscopy and in situ infrared ellipsometry. *Journal of Vacuum Science & Technology A* 16 (1): 6–12.

- Bettinger, C. J., Bruggeman, J. P., Misra, A., Borenstein, J. T. and Langer, R. 2009. Biocompatibility of biodegradable semiconducting melanin films for nerve tissue engineering. *Biomaterials* 30 (17): 3050–3057.
- van Beusekom, H. M. M., Ertaş, G., Sorop, O., Serruys, P. W. and van der Giessen, W. J. 2012. The genous™ endothelial progenitor cell capture stent accelerates stent re-endothelialization but does not affect intimal hyperplasia in porcine coronary arteries. *Catheterization and Cardiovascular Interventions* 79 (2): 231–242.
- Biswas, P., Canosa, S., Schoenfeld, D., Schoenfeld, J., Li, P., Cheas, L. C., Zhang, J., Cordova, A., Sumpio, B. and Madri, J. A. 2006. PECAM-1 affects GSK-3 β -mediated β -catenin phosphorylation and degradation. *The American journal of pathology* 169 (1): 314–324.
- Borris, J., Dohse, A., Hinze, A., Thomas, M., Klages, C.-P., Moebius, A., Elbick, D. and Weidlich, E.-R. 2009. Improvement of the Adhesion of a Galvanic Metallization of Polymers by Surface Functionalization Using Dielectric Barrier Discharges at Atmospheric Pressure. *Plasma Processes and Polymers* 6: S258–S263.
- Briguori, C., Sarais, C., Pagnotta, P., Liistro, F., Montorfano, M., Chieffo, A., Sgura, F., Corvaja, N., Albiero, R., Stankovic, G., Toutoutzas, C., Bonizzoni, E., Di Mario, C. and Colombo, A. 2002. In-stent restenosis in small coronary arteries: Impact of strut thickness. *Journal of the American College of Cardiology* 40 (3): 403–409.
- Brinjikji, W., Ding, Y. H., Kallmes, D. F. and Kadirvel, R. 2016. From bench to bedside: utility of the rabbit elastase aneurysm model in preclinical studies of intracranial aneurysm treatment. *Journal of NeuroInterventional Surgery* 8 (5): 521–525.
- Brinjikji, W., Murad, M. H., Lanzino, G., Cloft, H. J. and Kallmes, D. F. 2013. Endovascular Treatment of Intracranial Aneurysms With Flow Diverters A Meta-Analysis. *Stroke* 44 (2): 442–447.
- Brouillard, A. M., Sun, X., Siddiqui, A. H. and Lin, N. 2016. The Use of Flow Diversion for the Treatment of Intracranial Aneurysms: Expansion of Indications. *Cureus* 8 (1).
- Brown, S., Heinisch, I., Ross, E., Shaw, K. and others. 2002. Apoptosis disables CD31-mediated cell detachment from phagocytes promoting binding and engulfment. *Nature* 418 (6894): 200.
- Bundhun, P. K., Janoo, G., Yanamala, C. M. and Huang, F. 2017. Adverse cardiovascular events associated with biodegradable polymer drug-eluting stents and durable polymer everolimus-eluting stents A systematic review and meta-analysis of 10 randomized controlled trials. *Medicine* 96 (28): e7510.
- Caligiuri, G., Sayah, N. and Rasser, C. 2017. Revascularisation coronaire percutanée : progrès et nouveaux défis associés aux stents de dernière génération. *Archives des Maladies du Coeur et des Vaisseaux - Pratique* 2017 (260): 18–22.
- Cao, G., O'Brien, C. D., Zhou, Z., Sanders, S. M., Greenbaum, J. N., Makriganakis, A. and DeLisser, H. M. 2002. Involvement of human PECAM-1 in angiogenesis and in vitro endothelial cell migration. *American Journal of Physiology - Cell Physiology* 282 (5): C1181–C1190.
- Cao, M. Y., Huber, M., Beauchemin, N., Famiglietti, J., Albelda, S. M. and Veillette, A. 1998. Regulation of Mouse PECAM-1 Tyrosine Phosphorylation by the Src and Csk Families of Protein-tyrosine Kinases. *Journal of Biological Chemistry* 273 (25): 15765–15772.
- Caro, C. G., Fitz-Gerald, J. M. and Schroter, R. C. 1969. Arterial wall shear and distribution of early atheroma in man. *Nature* 223 (5211): 1159–1160.
- Caroff, J., Mihalea, C., Da Ros, V., Yagi, T., Iacobucci, M., Ikka, L., Moret, J. and Spelle, L. 2017. A computational fluid dynamics (CFD) study of WEB-treated aneurysms: Can CFD predict WEB 'compression' during follow-up? *Journal of Neuroradiology* 44 (4): 262–268.
- Carrell, T. W. G., Burnand, K. G., Booth, N. A., Humphries, J. and Smith, A. 2006. Intraluminal Thrombus Enhances Proteolysis in Abdominal Aortic Aneurysms. *Vascular* 14 (1): 9–16.
- Carter, A. J., Aggarwal, M., Kopia, G. A., Tio, F., Tsao, P. S., Kolata, R., Yeung, A. C., Llanos, G., Dooley, J. and Falotico, R. 2004. Long-term effects of polymer-based, slow-release, sirolimus-eluting stents in a porcine coronary model. *Cardiovascular Research* 63 (4): 617–624.
- Cassese, S., Byrne, R. A., Tada, T., Piniack, S., Joner, M., Ibrahim, T., King, L. A., Fusaro, M., Laugwitz, K.-L. and Kastrati, A. 2013. Incidence and predictors of restenosis after coronary stenting in 10 004 patients with surveillance angiography. *Heart: heartjnl-2013-304933*.

- Castellanos, M. I., Mas-Moruno, C., Grau, A., Serra-Picamal, X., Trepas, X., Albericio, F., Joner, M., Gil, F. J., Ginebra, M. P., Manero, J. M. and Pegueroles, M. 2017. Functionalization of CoCr surfaces with cell adhesive peptides to promote HUVECs adhesion and proliferation. *Applied Surface Science* 393: 82–92.
- Cebral, J. R., Mut, F., Raschi, M., Scrivano, E., Ceratto, R., Lylyk, P. and Putman, C. M. 2011. Aneurysm Rupture Following Treatment with Flow-Diverting Stents: Computational Hemodynamics Analysis of Treatment. *American Journal of Neuroradiology* 32 (1): 27–33.
- Chalouhi, N., Jabbour, P., Singhal, S., Drueding, R., Starke, R. M., Dalyai, R. T., Tjoumakaris, S., Gonzalez, L. F., Dumont, A. S., Rosenwasser, R. and Randazzo, C. G. 2013. Stent-Assisted Coiling of Intracranial Aneurysms Predictors of Complications, Recanalization, and Outcome in 508 Cases. *Stroke* 44 (5): 1348–1353.
- Chen, J., Li, Q., Xu, J., Zhang, L., Maitz, M. F. and Li, J. 2015a. Thromboresistant and rapid-endothelialization effects of dopamine and staphylococcal protein A mediated anti-CD34 coating on 316L stainless steel for cardiovascular devices. 3 (13): 2615–2623.
- Chen, W., Habraken, T. C. J., Hennink, W. E. and Kok, R. J. 2015b. Polymer-Free Drug-Eluting Stents: An Overview of Coating Strategies and Comparison with Polymer-Coated Drug-Eluting Stents. *Bioconjugate Chemistry* 26 (7): 1277–1288.
- Chen, X., Brox, D., Assadsangabi, B., Hsiang, Y. and Takahata, K. 2014. Intelligent telemetric stent for wireless monitoring of intravascular pressure and its in vivo testing. *Biomedical Microdevices* 16 (5): 745–759.
- Chen, Z., Li, Q., Chen, J., Luo, R., Maitz, M. F. and Huang, N. 2016. Immobilization of serum albumin and peptide aptamer for EPC on polydopamine coated titanium surface for enhanced in-situ self-endothelialization. *Materials Science & Engineering C-Materials for Biological Applications* 60: 219–229.
- Chevallier, P., Castonguay, M., Turgeon, S., Dubrulle, N., Mantovani, D., McBreen, P. H., Wittmann, J.-C. and Laroche, G. 2001. Ammonia RF- plasma on PTFE surfaces: Chemical characterization of the species created on the surface by vapor- phase chemical derivatization. *The Journal of Physical Chemistry B* 105 (50): 12490–12497.
- Chi, L., Li, Y., Stehno-Bittel, L., Gao, J., Morrison, D. C., Stechschulte, D. J. and Dileepan, K. N. 2001. Interleukin-6 production by endothelial cells via stimulation of protease-activated receptors is amplified by endotoxin and tumor necrosis factor-alpha. *Journal of Interferon & Cytokine Research: The Official Journal of the International Society for Interferon and Cytokine Research* 21 (4): 231–240.
- Choi, K., Ghosh, S., Lim, J. and Lee, C. M. 2003. Removal efficiency of organic contaminants on Si wafer by dry cleaning using UV/O₃ and ECR plasma. *Applied Surface Science* 206 (1): 355–364.
- Cicmil, M. 2002. Platelet endothelial cell adhesion molecule-1 signaling inhibits the activation of human platelets. *Blood* 99 (1): 137–144.
- Cicmil, M., Thomas, J. M., Sage, T., Barry, F. A., Leduc, M., Bon, C. and Gibbins, J. M. 2000. Collagen, Convulxin, and Thrombin Stimulate Aggregation-independent Tyrosine Phosphorylation of CD31 in Platelets EVIDENCE FOR THE INVOLVEMENT OF Src FAMILY KINASES. *Journal of Biological Chemistry* 275 (35): 27339–27347.
- Ciolan, M. A., Motrescu, I., Luca, D. and Nagatsu, M. 2014. Low temperature plasma functionalization of ZnO with amine groups for bioapplications. *Digest Journal of Nanomaterials and Biostructures* 9 (2): 483–491.
- Clement, M., Fornasa, G., Loyau, S., Morvan, M., Andreatta, F., Guedj, K., Khallou-Laschet, J., Larghi, P., Le Roux, D., Bismuth, G., Chiochia, G., Hivroz, C., Newman, D. K., Nicoletti, A. and Caligiuri, G. 2015. Upholding the T cell immune-regulatory function of CD31 inhibits the formation of T/B immunological synapses in vitro and attenuates the development of experimental autoimmune arthritis in vivo. *Journal of Autoimmunity* 56: 23–33.
- Cohen, J. E., Gomori, J. M., Moscovici, S., Leker, R. R. and Itshayek, E. 2014. Delayed complications after flow-diverter stenting: Reactive in-stent stenosis and creeping stents. *Journal of Clinical Neuroscience* 21 (7): 1116–1122.

- Colombo, A., Drzewiecki, J., Banning, A., Grube, E., Hauptmann, K., Silber, S., Dudek, D., Fort, S., Schiele, F., Zmudka, K., Guagliumi, G. and Russell, M. E. 2003. Randomized Study to Assess the Effectiveness of Slow- and Moderate-Release Polymer-Based Paclitaxel-Eluting Stents for Coronary Artery Lesions. *Circulation* 108 (7): 788–794.
- Constans, J. and Conri, C. 2006. Circulating markers of endothelial function in cardiovascular disease. *Clinica Chimica Acta* 368 (1–2): 33–47.
- Cruz, J. P., O’Kelly, C., Kelly, M., Wong, J. H., Alshaya, W., Martin, A., Spears, J. and Marotta, T. R. 2013. Pipeline embolization device in aneurysmal subarachnoid hemorrhage. *AJNR. American journal of neuroradiology* 34 (2): 271–276.
- Dai, D., Ding, Y. H., Kadirvel, R., Danielson, M. A., Lewis, D. A., Cloft, H. J. and Kallmes, D. F. 2006. A longitudinal immunohistochemical study of the healing of experimental aneurysms after embolization with platinum coils. *American Journal of Neuroradiology* 27 (4): 736–741.
- Deaglio, S., Morra, M., Mallone, R., Ausiello, C. M., Prager, E., Garbarino, G., Dianzani, U., Stockinger, H. and Malavasi, F. 1998. Human CD38 (ADP-ribosyl cyclase) is a counter-receptor of CD31, an Ig superfamily member. *The Journal of Immunology* 160 (1): 395–402.
- Debets, M. F., van Berkel, S. S., Dommerholt, J., Dirks, A. (Ton) J., Rutjes, F. P. J. T. and van Delft, F. L. 2011. Bioconjugation with Strained Alkenes and Alkynes. *Accounts of Chemical Research* 44 (9): 805–815.
- DeLisser, H. M., Christofidou-Solomidou, M., Strieter, R. M., Burdick, M. D., Robinson, C. S., Wexler, R. S., Kerr, J. S., Garlanda, C., Merwin, J. R., Madri, J. A. and others. 1997. Involvement of endothelial PECAM-1/CD31 in angiogenesis. *The American journal of pathology* 151 (3): 671.
- Dianzani, U., Funaro, A., DiFranco, D., Garbarino, G., Bragardo, M., Redoglia, V., Buonfiglio, D., De Monte, L. B., Pileri, A. and Malavasi, F. 1994. Interaction between endothelium and CD4+ CD45RA+ lymphocytes. Role of the human CD38 molecule. *The Journal of Immunology* 153 (3): 952–959.
- Dias, F. N., Ishii, M., Nogaroto, S. L., Piccini, B. and Penna, T. C. V. 2009. Sterilization of medical devices by ethylene oxide, determination of the dissipation of residues, and use of Green Fluorescent Protein as an indicator of process control. *Journal of Biomedical Materials Research. Part B, Applied Biomaterials* 91 (2): 626–630.
- Ding, Y., Yang, Z., Bi, C. W. C., Yang, M., Zhang, J., Xu, S. L., Lu, X., Huang, N., Huang, P. and Leng, Y. 2014. Modulation of protein adsorption, vascular cell selectivity and platelet adhesion by mussel-inspired surface functionalization. *Journal of Materials Chemistry B* 2 (24): 3819–3829.
- Dommerholt, J., Schmidt, S., Temming, R., Hendriks, L. J. A., Rutjes, F. P. J. T., van Hest, J. C. M., Lefeber, D. J., Friedl, P. and van Delft, F. L. 2010. Readily Accessible Bicyclononynes for Bioorthogonal Labeling and Three-Dimensional Imaging of Living Cells. *Angewandte Chemie International Edition* 49 (49): 9422–9425.
- Dzau, V. J., Braun-Dullaeus, R. C. and Sedding, D. G. 2002. Vascular proliferation and atherosclerosis: New perspectives and therapeutic strategies. *Nature Medicine* 8 (11): 1249–1256.
- Ellis, S. G. and Kereiakes, D. J. 2015. A Bioresorbable Everolimus-Eluting Scaffold Versus a Metallic Everolimus-Eluting Stent III. *Transcatheter Cardiovascular Therapeutics meeting 2015*.
- Eugenin, E. A., Gamss, R., Buckner, C., Buono, D., Klein, R. S., Schoenbaum, E. E., Calderon, T. M. and Berman, J. W. 2006. Shedding of PECAM-1 during HIV infection: a potential role for soluble PECAM-1 in the pathogenesis of NeuroAIDS. *Journal of Leukocyte Biology* 79 (3): 444–452.
- Evans, P. C., Taylor, E. R. and Kilshaw, P. J. 2001. Signaling through CD31 protects endothelial cells from apoptosis. *Transplantation* 71 (3): 457–460.
- Falati, S. 2006. Platelet PECAM-1 inhibits thrombus formation in vivo. *Blood* 107 (2): 535–541.
- Fedele, G., Frasca, L., Palazzo, R., Ferrero, E., Malavasi, F. and Ausiello, C. M. 2004. CD38 is expressed on human mature monocyte-derived dendritic cells and is functionally involved in CD83 expression and IL-12 induction. *European journal of immunology* 34 (5): 1342–1350.

- Ferrero, E., Ferrero, M. E., Pardi, R. and Zocchi, M. R. 1995. The platelet endothelial cell adhesion molecule-1 (PECAM1) contributes to endothelial barrier function. *FEBS letters* 374 (3): 323–326.
- Ferrero, E., Belloni, D., Contini, P., Foglieni, C., Ferrero, M. E., Fabbri, M., Poggi, A. and Zocchi, M. R. 2003. Transendothelial migration leads to protection from starvation-induced apoptosis in CD34+ CD14+ circulating precursors: evidence for PECAM-1 involvement through Akt/PKB activation. *Blood* 101 (1): 186–193.
- de Feyter, P. J., Serruys, P. W., v.d. Brand, M. and Hugenholtz, P. G. 1991. Percutaneous transluminal coronary angioplasty for unstable angina. *The American Journal of Cardiology* 68 (7): B125–B135.
- Fiorella, D., Kelly, M. E., Albuquerque, F. C. and Nelson, P. K. 2009. Curative reconstruction of a giant midbasilar trunk aneurysm with the pipeline embolization device. *Neurosurgery* 64 (2): 212–217; discussion 217.
- Fischer, S., Vajda, Z., Aguilar Perez, M., Schmid, E., Hopf, N., Bätzner, H. and Henkes, H. 2012. Pipeline embolization device (PED) for neurovascular reconstruction: initial experience in the treatment of 101 intracranial aneurysms and dissections. *Neuroradiology* 54 (4): 369–382.
- Fischman, D. L., Leon, M. B., Baim, D. S., Schatz, R. A., Savage, M. P., Penn, I., Detre, K., Veltri, L., Ricci, D., Nobuyoshi, M., Cleman, M., Heuser, R., Almond, D., Teirstein, P. S., Fish, R. D., Colombo, A., Brinker, J., Moses, J., Shaknovich, A., Hirshfeld, J., Bailey, S., Ellis, S., Rake, R. and Goldberg, S. 1994. A Randomized Comparison of Coronary-Stent Placement and Balloon Angioplasty in the Treatment of Coronary Artery Disease. *New England Journal of Medicine* 331 (8): 496–501.
- Foin, N., Lee, R. D., Torii, R., Guitierrez-Chico, J. L., Mattesini, A., Nijjer, S., Sen, S., Petraco, R., Davies, J. E., Di Mario, C., Joner, M., Virmani, R. and Wong, P. 2014. Impact of stent strut design in metallic stents and biodegradable scaffolds. *International Journal of Cardiology* 177 (3): 800–808.
- Fontaine, V., Jacob, M.-P., Houard, X., Rossignol, P., Plissonnier, D., Angles-Cano, E. and Michel, J.-B. 2002. Involvement of the Mural Thrombus as a Site of Protease Release and Activation in Human Aortic Aneurysms. *The American Journal of Pathology* 161 (5): 1701–1710.
- Fornasa, G., Groyer, E., Clement, M., Dimitrov, J., Compain, C., Gaston, A.-T., Varthaman, A., Khallou-Laschet, J., Newman, D. K., Graff-Dubois, S., Nicoletti, A. and Caligiuri, G. 2010. TCR Stimulation Drives Cleavage and Shedding of the ITIM Receptor CD31. *The Journal of Immunology* 184 (10): 5485–5492.
- Frostegård, J., Nilsson, J., Haegerstrand, A., Hamsten, A., Wigzell, H. and Gidlund, M. 1990. Oxidized low density lipoprotein induces differentiation and adhesion of human monocytes and the monocytic cell line U937. *Proceedings of the National Academy of Sciences* 87 (3): 904–908.
- Gao, C., Sun, W., Christofidou-Solomidou, M., Sawada, M., Newman, D. K., Bergom, C., Albelda, S. M., Matsuyama, S. and Newman, P. J. 2003. PECAM-1 functions as a specific and potent inhibitor of mitochondrial-dependent apoptosis. *Blood* 102 (1): 169–179.
- Gengenbach, T. R. and Griesser, H. J. 1999. Post-deposition ageing reactions differ markedly between plasma polymers deposited from siloxane and silazane monomers. *Polymer* 40 (18): 5079–5094.
- Gerrity, R. G. 1981. The role of the monocyte in atherogenesis: I. Transition of blood-borne monocytes into foam cells in fatty lesions. *The American Journal of Pathology* 103 (2): 181–190.
- Gerrity, R. G., Naito, H. K., Richardson, M. and Schwartz, C. J. 1979. Dietary Induced Atherogenesis in Swine. *The American Journal of Pathology* 95 (3): 775–792.
- Gheorghide, M., Ruzumna, P., Borzak, S., Havstad, S., Ali, A. and Goldstein, S. 1996. Decline in the rate of hospital mortality from acute myocardial infarction: Impact of changing management strategies. *American Heart Journal* 131 (2): 250–256.
- Giessen, W. J. van der, Lincoff, A. M., Schwartz, R. S., Beusekom, H. M. M. van, Serruys, P. W., Holmes, D. R., Ellis, S. G. and Topol, E. J. 1996. Marked Inflammatory Sequelae to Implantation of

- Biodegradable and Nonbiodegradable Polymers in Porcine Coronary Arteries. *Circulation* 94 (7): 1690–1697.
- van der Giessen, W. J., Serruys, P. W., van Beusekom, H. M., van Woerkens, L. J., van Loon, H., Soei, L. K., Strauss, B. H., Beatt, K. J. and Verdouw, P. D. 1991. Coronary stenting with a new, radiopaque, balloon-expandable endoprosthesis in pigs. *Circulation* 83 (5): 1788–1798.
- Gillespie, D. L., Villavicencio, J. L., Gallagher, C., Chang, A., Hamelink, J. K., Fiala, L. A., O'Donnell, S. D., Jackson, M. R., Pikoulis, E. and Rich, N. M. 1997. Presentation and management of venous aneurysms. *Journal of Vascular Surgery* 26 (5): 845–852.
- Gonzalez-Macia, L., Morrin, A., Smyth, M. R. and Killard, A. J. 2010. Advanced printing and deposition methodologies for the fabrication of biosensors and biodevices. *Analyst* 135 (5): 845–867.
- Goyert, S. M., Ferrero, E. M., Seremetis, S. V., Winchester, R. J., Silver, J. and Mattison, A. C. 1986. Biochemistry and expression of myelomonocytic antigens. *The Journal of Immunology* 137 (12): 3909–3914.
- Grimoldi, E., Zanini, S., Siliprandi, R. A. and Riccardi, C. 2009. AFM and contact angle investigation of growth and structure of pp-HMDSO thin films. *The European Physical Journal D-Atomic, Molecular, Optical and Plasma Physics* 54 (2): 165–172.
- Gruntzig, A. 1978. Trans-Luminal Dilatation of Coronary-Artery Stenosis. *Lancet* 1 (8058): 263–263.
- Guruvenket, S., Andrie, S., Simon, M., Johnson, K. W. and Sailer, R. A. 2012. Atmospheric-Pressure Plasma-Enhanced Chemical Vapor Deposition of a-SiCN:H Films: Role of Precursors on the Film Growth and Properties. *Acs Applied Materials & Interfaces* 4 (10): 5293–5299.
- Hay, S. I., Jayaraman, S. P., Truelsen, T., Sorensen, R. J. D., Millea, A., Giussani, G. and Beghi, E. 2017. Global, regional, and national incidence, prevalence, and years lived with disability for 310 diseases and injuries, 1990-2015: a systematic analysis for the Global Burden of Disease Study 2015. *Lancet* 389 (10064): E1–E1.
- Henriksen, T., Mahoney, E. M. and Steinberg, D. 1981. Enhanced macrophage degradation of low density lipoprotein previously incubated with cultured endothelial cells: recognition by receptors for acetylated low density lipoproteins. *Proceedings of the National Academy of Sciences* 78 (10): 6499–6503.
- Henshall, T. L., Jones, K. L., Wilkinson, R. and Jackson, D. E. 2001. Src Homology 2 Domain-Containing Protein-Tyrosine Phosphatases, SHP-1 and SHP-2, Are Required for Platelet Endothelial Cell Adhesion Molecule-1/CD31-Mediated Inhibitory Signaling. *The Journal of Immunology* 166 (5): 3098–3106.
- Hermanson, G. T. 2013. *Bioconjugate Techniques*. Academic Press, .
- Hody, H., Pireaux, J.-J., Choquet, P. and Moreno-Couranjou, M. 2010. Plasma functionalization of silicon carbide crystalline nanoparticles in a novel low pressure powder reactor. *Surface and Coatings Technology* 205 (1): 22–29.
- Hoh, B. L., Rabinov, J. D., Pryor, J. C. and Ogilvy, C. S. 2004. A modified technique for using elastase to create saccular aneurysms in animals that histologically and hemodynamically resemble aneurysms in human. *Acta neurochirurgica* 146 (7): 705–711.
- Hong, Y., Wang, Y.-J., Deng, Z., Wu, Q. and Zhang, J.-M. 2014. Stent-Assisted Coiling versus Coiling in Treatment of Intracranial Aneurysm: A Systematic Review and MetaAnalysis. *Plos One* 9 (1): e82311.
- Huang, C., Wu, S.-Y. and Chang, Y.-C. 2010. Synthesis of Organosilicon Film on Polycarbonate by Means of Low-Temperature Atmospheric-Pressure Plasma Jet. *IEEE Transactions on Plasma Science* 38 (5): 1101–1105.
- Huebsch, N., Gilbert, M. and Healy, K. E. 2005. Analysis of sterilization protocols for peptide-modified hydrogels. *Journal of Biomedical Materials Research. Part B, Applied Biomaterials* 74 (1): 440–447.
- Iannone, L. A., Anderson, S. M. and Phillips, S. J. 1993. Coronary angioplasty for acute myocardial infarction in a hospital without cardiac surgery. *Texas Heart Institute Journal* 20 (2): 99–104.

- Ijsselmuiden, A. J. J., Serruys, P. W., Scholte, A., Kiemeneij, F., Slagboom, T., v/d Wieken, L. R., Tangelder, G. J. and Laarman, G. J. 2003. Direct coronary stent implantation does not reduce the incidence of in-stent restenosis or major adverse cardiac eventsSix month results of a randomized trial. *European Heart Journal* 24 (5): 421–429.
- Ilan, N. and Madri, J. A. 2003. PECAM-1: old friend, new partners. *Current Opinion in Cell Biology* 15 (5): 515–524.
- Ilan, N., Cheung, L., Pinter, E. and Madri, J. A. 2000. Platelet-Endothelial Cell Adhesion Molecule-1 (CD31), a Scaffolding Molecule for Selected Catenin Family Members Whose Binding Is Mediated by Different Tyrosine and Serine/Threonine Phosphorylation. *Journal of Biological Chemistry* 275 (28): 21435–21443.
- Ilan, N., Mohsenin, A., Cheung, L. and Madri, J. A. 2001. PECAM-1 shedding during apoptosis generates a membrane-anchored truncated molecule with unique signaling characteristics. *FASEB journal: official publication of the Federation of American Societies for Experimental Biology* 15 (2): 362–372.
- Ivashchenko, V. I., Kozak, A. O., Porada, O. K., Ivashchenko, L. A., Sinelnichenko, O. K., Lytvyn, O. S., Tomila, T. V. and Malakhov, V. J. 2014. Characterization of SiCN thin films: Experimental and theoretical investigations. *Thin Solid Films* 569: 57–63.
- Jackson, D. E., Ward, C. M., Wang, R. G. and Newman, P. J. 1996. The protein tyrosine phosphatase, SHP-2, binds PECAM-1 and forms a distinct signaling complex during platelet aggregation: Evidence for a mechanistic link between PECAM-1 and integrin-mediated signal transduction. *Blood* 88: 1742–1742.
- Jiang, J.-H., Zhu, L.-P., Li, X.-L., Xu, Y.-Y. and Zhu, B.-K. 2010. Surface modification of PE porous membranes based on the strong adhesion of polydopamine and covalent immobilization of heparin. *Journal of Membrane Science* 364 (1): 194–202.
- John, S., Bain, M. D., Hui, F. K., Hussain, M. S., Masaryk, T. J., Rasmussen, P. A. and Toth, G. 2016. Long-term Follow-up of In-stent Stenosis After Pipeline Flow Diversion Treatment of Intracranial Aneurysms. *Neurosurgery* 78 (6): 862–867.
- Jonasson, L., Holm, J., Skalli, O., Bondjers, G. and Hansson, G. K. 1986. Regional accumulations of T cells, macrophages, and smooth muscle cells in the human atherosclerotic plaque. *Arteriosclerosis, Thrombosis, and Vascular Biology* 6 (2): 131–138.
- Joner, M., Finn, A. V., Farb, A., Mont, E. K., Kolodgie, F. D., Ladich, E., Kutys, R., Skorija, K., Gold, H. K. and Virmani, R. 2006. Pathology of Drug-Eluting Stents in Humans: Delayed Healing and Late Thrombotic Risk. *Journal of the American College of Cardiology* 48 (1): 193–202.
- Joner, M., Cheng, Q., Schönhofer-Merl, S., Lopez, M., Neubauer, S., Mas-Moruno, C., Laufer, B., Kolodgie, F. D., Kessler, H. and Virmani, R. 2012. Polymer-free immobilization of a cyclic RGD peptide on a nitinol stent promotes integrin-dependent endothelial coverage of strut surfaces. *Journal of Biomedical Materials Research. Part B, Applied Biomaterials* 100 (3): 637–645.
- Jones, C. I., Garner, S. F., Moraes, L. A., Kaiser, W. J., Rankin, A., Ouwehand, W. H., Goodall, A. H. and Gibbins, J. M. 2009. PECAM-1 expression and activity negatively regulate multiple platelet signaling pathways. *Febs Letters* 583 (22): 3618–3624.
- Jones, K. L., Hughan, S. C., Dopheide, S. M., Farndale, R. W., Jackson, S. P. and Jackson, D. E. 2001. Platelet endothelial cell adhesion molecule-1 is a negative regulator of platelet-collagen interactions. *Blood* 98 (5): 1456–1463.
- Kadirvel, R., Ding, Y.-H., Dai, D., Rezek, I., Lewis, D. A. and Kallmes, D. F. 2013. Cellular Mechanisms of Aneurysm Occlusion after Treatment with a Flow Diverter. *Radiology* 270 (2): 394–399.
- Kallmes, D. F., Hanel, R., Lopes, D., Boccardi, E., Bonafe, A., Cekirge, S., Fiorella, D., Jabbour, P., Levy, E., McDougall, C., Siddiqui, A., Szikora, I., Woo, H., Albuquerque, F., Bozorgchami, H., Dashti, S. R., Almandoz, J. E. D., Kelly, M. E., Turner, R., Woodward, B. K., Brinjikji, W., Lanzino, G. and Lylyk, P. 2015. International Retrospective Study of the Pipeline Embolization Device: A Multicenter Aneurysm Treatment Study. *American Journal of Neuroradiology* 36 (1): 108–115.

- Kalra, A., Rehman, H., Khera, S., Thyagarajan, B., Bhatt, D. L., Kleiman, N. S. and Yeh, R. W. 2017. New-Generation Coronary Stents: Current Data and Future Directions. *Current Atherosclerosis Reports* 19 (3): 14.
- Kim, H.-Y., Skokos, E. A., Myer, D. J., Agaba, P. and Gonzalez, A. L. 2014. $\alpha V\beta 3$ Integrin Regulation of Respiratory Burst in Fibrinogen Adherent Human Neutrophils. *Cellular and Molecular Bioengineering* 7 (2): 231–242.
- Kim, M. T. and Lee, J. 1997. Characterization of amorphous SiC:H films deposited from hexamethyldisilazane. *Thin Solid Films* 303 (1–2): 173–179.
- Kim, S. M., Park, K.-S., Lih, E., Hong, Y. J., Kang, J. H., Kim, I. H., Jeong, M. H., Joung, Y. K. and Han, D. K. 2016. Fabrication and characteristics of dual functionalized vascular stent by spatio-temporal coating. *Acta Biomaterialia* 38: 143–152.
- Kim, T. G., Lee, H., Jang, Y. and Park, T. G. 2009. Controlled release of paclitaxel from heparinized metal stent fabricated by layer-by-layer assembly of polylysine and hyaluronic acid-g-poly(lactic-co-glycolic acid) micelles encapsulating paclitaxel. *Biomacromolecules* 10 (6): 1532–1539.
- Klages, C.-P. and Grishin, A. 2008. Plasma amination of low-density polyethylene by DBD afterglows at atmospheric pressure. *Plasma Processes and Polymers* 5 (4): 368–376.
- Klomp, M., Beijik, M. A., Varma, C., Koolen, J. J., Teiger, E., Richardt, G., Bea, F., van Geloven, N., Verouden, N. J., Chan, Y. K., Woudstra, P., Damman, P., Tijssen, J. G. and de Winter, R. J. 2011. 1-Year Outcome of TRIAS HR (TRI-Stent Adjudication Study–High Risk of Restenosis): A Multicenter, Randomized Trial Comparing Genous Endothelial Progenitor Cell Capturing Stents With Drug-Eluting Stents. *JACC: Cardiovascular Interventions* 4 (8): 896–904.
- Klotz, O. and Manning, M. F. 1911. Fatty streaks in the intima of arteries. *The Journal of Pathology and Bacteriology* 16 (1): 211–220.
- Kondo, S., Scheef, E. A., Sheibani, N. and Sorenson, C. M. 2007. PECAM-1 isoform-specific regulation of kidney endothelial cell migration and capillary morphogenesis. *American Journal of Physiology-Cell Physiology* 292 (6): C2070–C2083.
- Krasteva, N., Hristova, K., Radeva, E., Pecheva, E., Dimitrova, R. and Pramatarova, L. 2009. Effect of Ammonia Plasma Treatment on the Biological Performance of Plasma Polymerized Hexamethyldisiloxane. In: Angelopoulos, A. and Fildisis, T. (eds.), *7th International Conference of the Balkan Physical Union Vols 1 and 2*, Vol. 1203, 688–+. Amer Inst Physics, Melville.
- Krings, T., Mandell, D. M., Kiehl, T.-R., Geibprasert, S., Tymianski, M., Alvarez, H., terBrugge, K. G. and Hans, F.-J. 2011. Intracranial aneurysms: from vessel wall pathology to therapeutic approach. *Nature Reviews Neurology* 7 (10): 547–559.
- Ku, S. H., Ryu, J., Hong, S. K., Lee, H. and Park, C. B. 2010. General functionalization route for cell adhesion on non-wetting surfaces. *Biomaterials* 31 (9): 2535–2541.
- Kulcsár, Z. and Szikora, I. 2012. The ESMINT Retrospective Analysis of Delayed Aneurysm Ruptures after flow diversion (RADAR) study. *EJMINT*.
- Kulcsár, Z., Houdart, E., Bonafé, A., Parker, G., Millar, J., Goddard, A. J. P., Renowden, S., Gál, G., Turowski, B., Mitchell, K., Gray, F., Rodriguez, M., Berg, R. van den, Gruber, A., Desal, H., Wanke, I. and Rüfenacht, D. A. 2011. Intra-Aneurysmal Thrombosis as a Possible Cause of Delayed Aneurysm Rupture after Flow-Diversion Treatment. *American Journal of Neuroradiology* 32 (1): 20–25.
- Kume, N., Cybulsky, M. I. and Gimbrone, M. A. 1992. Lysophosphatidylcholine, a component of atherogenic lipoproteins, induces mononuclear leukocyte adhesion molecules in cultured human and rabbit arterial endothelial cells. *Journal of Clinical Investigation* 90 (3): 1138–1144.
- Kuo, D. H. and Yang, D. G. 2000. Plasma-enhanced chemical vapor deposition of silicon carbonitride using hexamethyldisilazane and nitrogen. *Thin Solid Films* 374 (1): 92–97.
- Kutryk, M. J. B., Jr, R. J. C., Rowland, S. M. and Kuliszewski, M. A. 2008. Medical device with coating that promotes endothelial cell adherence and differentiation. .

- Lachmann, K., Michel, B. and Klages, C.-P. 2009. Density and Aging Behavior of Primary Amino Groups on Afterglow Plasma-Treated Low-Density Polyethylene (LDPE). *Plasma Processes and Polymers* 6: S401–S405.
- Lagerqvist, B., Carlsson, J., Fröbert, O., Lindbäck, J., Scherstén, F., Stenestrand, U., James, S. K. and Swedish Coronary Angiography and Angioplasty Registry Study Group. 2009. Stent thrombosis in Sweden: a report from the Swedish Coronary Angiography and Angioplasty Registry. *Circulation. Cardiovascular Interventions* 2 (5): 401–408.
- Lampugnani, M. G. and Dejana, E. 1997. Interendothelial junctions: structure, signalling and functional roles. *Current Opinion in Cell Biology* 9 (5): 674–682.
- Leclerc, J. R. 2002. Platelet glycoprotein IIb/IIIa antagonists: lessons learned from clinical trials and future directions. *Critical care medicine* 30 (5): S332–S340.
- Lee, H., Scherer, N. F. and Messersmith, P. B. 2006. Single-molecule mechanics of mussel adhesion. *Proceedings of the National Academy of Sciences of the United States of America* 103 (35): 12999–13003.
- Lee, H., Rho, J. and Messersmith, P. B. 2009. Facile Conjugation of Biomolecules onto Surfaces via Mussel Adhesive Protein Inspired Coatings. *Advanced materials (Deerfield Beach, Fla.)* 21 (4): 431–434.
- Lee, H., Dellatore, S. M., Miller, W. M. and Messersmith, P. B. 2007. Mussel-Inspired Surface Chemistry for Multifunctional Coatings. *Science (New York, N.Y.)* 318 (5849): 426–430.
- Lehr, H. A., Hübner, C., Nolte, D., Finckh, B., Beisiegel, U., Kohlschütter, A. and Meßmer, K. 1991. Oxidatively modified human low-density lipoprotein stimulates leukocyte adherence to the microvascular endothelium in vivo. *Research in Experimental Medicine* 191 (1): 85–90.
- Lewis, F. 2009. Etude sur les propriétés d'adhérence des revêtements fluorocarbonés déposés par plasma sur de l'acier inoxydable 316L pour les stents coronariens. Paris 6pp.
- Lewis, F., Cloutier, M., Chevallier, P., Turgeon, S., Pireaux, J.-J., Tatouljian, M. and Mantovani, D. 2011. Influence of the 316 L stainless steel interface on the stability and barrier properties of plasma fluorocarbon films. *ACS applied materials & interfaces* 3 (7): 2323–2331.
- Li, B., Liu, W., Jiang, Z., Dong, X., Wang, B. and Zhong, Y. 2009. Ultrathin and Stable Active Layer of Dense Composite Membrane Enabled by Poly(dopamine). *Langmuir* 25 (13): 7368–7374.
- Li, G., Yang, P., Qin, W., Maitz, M. F., Zhou, S. and Huang, N. 2011. The effect of coimmobilizing heparin and fibronectin on titanium on hemocompatibility and endothelialization. *Biomaterials* 32 (21): 4691–4703.
- Li, N. and Ho, C.-M. 2008. Photolithographic patterning of organosilane monolayer for generating large area two-dimensional B lymphocyte arrays. *Lab on a chip* 8 (12): 2105–2112.
- Li, X., Deng, J., Yuan, S., Wang, J., Luo, R., Chen, S., Wang, J. and Huang, N. 2016. Fabrication of endothelial progenitor cell capture surface via DNA aptamer modifying dopamine/polyethyleneimine copolymer film. *Applied Surface Science* 386: 138–150.
- Libby, P. 2002. Inflammation in atherosclerosis. *Nature* 420 (6917): 868–874.
- Limaye, V., Li, X., Hahn, C., Xia, P., Berndt, M. C., Vadas, M. A. and Gamble, J. R. 2005. Sphingosine kinase-1 enhances endothelial cell survival through a PECAM-1-dependent activation of PI-3K/Akt and regulation of Bcl-2 family members. *Blood* 105 (8): 3169–3177.
- Lin, Q., Ding, X., Qiu, F., Song, X., Fu, G. and Ji, J. 2010. In situ endothelialization of intravascular stents coated with an anti-CD34 antibody functionalized heparin-collagen multilayer. *Biomaterials* 31 (14): 4017–4025.
- Lincoff, A. M., Furst, J. G., Ellis, S. G., Tuch, R. J. and Topol, E. J. 1997. Sustained Local Delivery of Dexamethasone by a Novel Intravascular Eluting Stent to Prevent Restenosis in the Porcine Coronary Injury Model. *Journal of the American College of Cardiology* 29 (4): 808–816.
- Liu, T., Liu, Y., Chen, Y., Liu, S., Maitz, M. F., Wang, X., Zhang, K., Wang, J., Wang, Y., Chen, J. and Huang, N. 2014. Immobilization of heparin/poly-l-lysine nanoparticles on dopamine-coated surface to create a heparin density gradient for selective direction of platelet and vascular cells behavior. *Acta Biomaterialia* 10 (5): 1940–1954.

- Liu, X., Zhen, Z., Liu, J., Xi, T., Zheng, Y., Guan, S., Zheng, Y. and Cheng, Y. 2015a. Multifunctional MgF₂/Polydopamine Coating on Mg Alloy for Vascular Stent Application. *Journal of Materials Science & Technology* 31 (7): 733–743.
- Liu, Y., Zhang, J., Wang, J., Wang, Y., Zeng, Z., Liu, T., Chen, J. and Huang, N. 2015b. Tailoring of the dopamine coated surface with VEGF loaded heparin/poly-L-lysine particles for anticoagulation and accelerate in situ endothelialization. *Journal of Biomedical Materials Research Part A* 103 (6): 2024–2034.
- Lu, L., Li, Q.-L., Maitz, M. F., Chen, J.-L. and Huang, N. 2012. Immobilization of the direct thrombin inhibitor-bivalirudin on 316L stainless steel via polydopamine and the resulting effects on hemocompatibility in vitro. *Journal of Biomedical Materials Research Part A* 100A (9): 2421–2430.
- Lu, T. T., Barreuther, M., Davis, S. and Madri, J. A. 1997. Platelet Endothelial Cell Adhesion Molecule-1 Is Phosphorylatable by c-Src, Binds Src-Src homology 2 Domain, and Exhibits Immunoreceptor Tyrosine-based Activation Motif-like Properties. *Journal of Biological Chemistry* 272 (22): 14442–14446.
- Lundquist, J., Ferrario, A., Ceratto, R., Scrivano, E., Chudyk, J. and Lylyk, P. 2016. Buenos Aires Experience With Flow Diverter in our First 1000 Patients Safety, Efficacy and Long Term Follow-up. *Stroke* 47 (Suppl 1): A12–A12.
- Luo, R., Tang, L., Wang, J., Zhao, Y., Tu, Q., Weng, Y., Shen, R. and Huang, N. 2013a. Improved immobilization of biomolecules to quinone-rich polydopamine for efficient surface functionalization. *Colloids and Surfaces B-Biointerfaces* 106: 66–73.
- Luo, R., Tang, L., Zhong, S., Yang, Z., Wang, J., Weng, Y., Tu, Q., Jiang, C. and Huang, N. 2013b. In Vitro Investigation of Enhanced Hemocompatibility and Endothelial Cell Proliferation Associated with Quinone-Rich Polydopamine Coating. *ACS Applied Materials & Interfaces* 5 (5): 1704–1714.
- Mann, B. K. and West, J. L. 2002. Cell adhesion peptides alter smooth muscle cell adhesion, proliferation, migration, and matrix protein synthesis on modified surfaces and in polymer scaffolds. *Journal of Biomedical Materials Research* 60 (1): 86–93.
- Martin, A. R., Cruz, J. P., Matouk, C. C., Spears, J. and Marotta, T. R. 2012. The pipeline flow-diverting stent for exclusion of ruptured intracranial aneurysms with difficult morphologies. *Neurosurgery* 70 (1 Suppl Operative): 21–28; discussion 28.
- Martinez, A. W. and Chaikof, E. L. 2011. Microfabrication and Nanotechnology in Stent Design. *Wiley interdisciplinary reviews. Nanomedicine and nanobiotechnology* 3 (3): 256–268.
- Massia, S. P. and Stark, J. 2001. Immobilized RGD peptides on surface-grafted dextran promote biospecific cell attachment. *Journal of Biomedical Materials Research Part A* 56 (3): 390–399.
- Matsumura, T., Wolff, K. and Petzelbauer, P. 1997. Endothelial cell tube formation depends on cadherin 5 and CD31 interactions with filamentous actin. *The Journal of Immunology* 158 (7): 3408–3416.
- McAuliffe, W., Wycoco, V., Rice, H., Phatouros, C., Singh, T. J. and Wenderoth, J. 2012. Immediate and midterm results following treatment of unruptured intracranial aneurysms with the pipeline embolization device. *AJNR. American journal of neuroradiology* 33 (1): 164–170.
- McFadden, E. P., Stabile, E., Regar, E., Cheneau, E., Ong, A. T. L., Kinnaird, T., Suddath, W. O., Weissman, N. J., Torguson, R., Kent, K. M., Pichard, A. D., Satler, L. F., Waksman, R. and Serruys, P. W. 2004. Late thrombosis in drug-eluting coronary stents after discontinuation of antiplatelet therapy. *Lancet (London, England)* 364 (9444): 1519–1521.
- Menudet, J.-F. 2011. ENDOCOM: Implantable wireless pressure sensor for the follow-up of abdominal aortic aneurysm stented. *Irbm* 32 (3): 163–168.
- Miller, M., Sung, K.-L. P., Muller, W. A., Cho, J. Y., Roman, M., Castaneda, D., Nayar, J., Condon, T., Kim, J., Sriramarao, P. and others. 2001. Eosinophil tissue recruitment to sites of allergic inflammation in the lung is platelet endothelial cell adhesion molecule independent. *The Journal of Immunology* 167 (4): 2292–2297.
- Mitra, A. K. and Agrawal, D. K. 2006. In stent restenosis: bane of the stent era. *Journal of Clinical Pathology* 59 (3): 232–239.

- Molyneux, A. J., Birks, J., Clarke, A., Sneade, M. and Kerr, R. S. C. 2015. The durability of endovascular coiling versus neurosurgical clipping of ruptured cerebral aneurysms: 18 year follow-up of the UK cohort of the International Subarachnoid Aneurysm Trial (ISAT). *The Lancet* 385 (9969): 691–697.
- Montaño-Machado, V., Noël, C., Chevallier, P., Turgeon, S., Houssiau, L., Pauthe, E., Pireaux, J.-J. and Mantovani, D. 2017. Interaction of phosphorylcholine with fibronectin coatings: Surface characterization and biological performances. *Applied Surface Science* 396: 1613–1622.
- Moore, J., J. E., Ku, D. N., Zarins, C. K. and Glagov, S. 1992. Pulsatile Flow Visualization in the Abdominal Aorta Under Differing Physiologic Conditions: Implications for Increased Susceptibility to Atherosclerosis. *Journal of Biomechanical Engineering* 114 (3): 391–397.
- Moravej, M. and Hicks, R. F. 2005. Atmospheric plasma deposition of coatings using a capacitive discharge source. *Chemical vapor deposition* 11 (11–12): 469–476.
- Morel, D. W., DiCorleto, P. E. and Chisolm, G. M. 1984. Endothelial and smooth muscle cells alter low density lipoprotein in vitro by free radical oxidation. *Arteriosclerosis, Thrombosis, and Vascular Biology* 4 (4): 357–364.
- Morice, M.-C., Serruys, P. W., Sousa, J. E., Fajadet, J., Ban Hayashi, E., Perin, M., Colombo, A., Schuler, G., Barragan, P., Guagliumi, G., Molnàr, F. and Falotico, R. 2002. A Randomized Comparison of a Sirolimus-Eluting Stent with a Standard Stent for Coronary Revascularization. *New England Journal of Medicine* 346 (23): 1773–1780.
- Motrescu, I. and Nagatsu, M. 2016. Nanocapillary Atmospheric Pressure Plasma Jet: A Tool for Ultrafine Maskless Surface Modification at Atmospheric Pressure. *ACS Applied Materials & Interfaces* 8 (19): 12528–12533.
- Muller, W. A., Ratti, C. M., McDonnell, S. L. and Cohn, Z. A. 1989. A human endothelial cell-restricted, externally disposed plasmalemmal protein enriched in intercellular junctions. *Journal of Experimental Medicine* 170 (2): 399–414.
- Muller, W. A., Weigl, S. A., Deng, X. and Phillips, D. M. 1993. PECAM-1 is required for transendothelial migration of leukocytes. *Journal of Experimental Medicine* 178 (2): 449–460.
- Musick, K. M., Coffey, A. C. and Irazoqui, P. P. 2010. Sensor to detect endothelialization on an active coronary stent. *BioMedical Engineering OnLine* 9: 67.
- Napoli, C., D'Armiento, F. P., Mancini, F. P., Postiglione, A., Witztum, J. L., Palumbo, G. and Palinski, W. 1997. Fatty streak formation occurs in human fetal aortas and is greatly enhanced by maternal hypercholesterolemia. Intimal accumulation of low density lipoprotein and its oxidation precede monocyte recruitment into early atherosclerotic lesions. *Journal of Clinical Investigation* 100 (11): 2680–2690.
- Narata, A. P., Yilmaz, H., Schaller, K., Lovblad, K. O. and Pereira, V. M. 2012. Flow-diverting stent for ruptured intracranial dissecting aneurysm of vertebral artery. *Neurosurgery* 70 (4): 982-988; discussion 988-989.
- National Institutes of Health. 1985. *NIH Guide for Grants and Contracts, Vol. 14, No. 8, 25 Jun 1985. Special Edition: Laboratory Animal Welfare. - NLM Catalog - NCBI*. Downloaded from <https://www.ncbi.nlm.nih.gov/gate2.inist.fr/nlmcatalog/100950858> on 16 October 2017.
- Navarese, E. P., Tandjung, K., Claessen, B., Andreotti, F., Kowalewski, M., Kandzari, D. E., Kereiakes, D. J., Waksman, R., Mauri, L., Meredith, I. T., Finn, A. V., Kim, H.-S., Kubica, J., Suryapranata, H., Aprami, T. M., Di Pasquale, G., von Birgelen, C. and Kedhi, E. 2013. Safety and efficacy outcomes of first and second generation durable polymer drug eluting stents and biodegradable polymer biolimus eluting stents in clinical practice: comprehensive network meta-analysis. *Bmj-British Medical Journal* 347: f6530.
- Navasiolava, N. M., Dignat-George, F., Sabatier, F., Larina, I. M., Demiot, C., Fortrat, J.-O., Gauquelin-Koch, G., Kozlovskaya, I. B. and Custaud, M.-A. 2010. Enforced physical inactivity increases endothelial microparticle levels in healthy volunteers. *American Journal of Physiology - Heart and Circulatory Physiology* 299 (2): H248–H256.

- Nelson, P. K., Lylyk, P., Szikora, I., Wetzel, S. G., Wanke, I. and Fiorella, D. 2011. The pipeline embolization device for the intracranial treatment of aneurysms trial. *AJNR. American journal of neuroradiology* 32 (1): 34–40.
- Newman, D. K., Hamilton, C. and Newman, P. J. 2001. Inhibition of antigen-receptor signaling by Platelet Endothelial Cell Adhesion Molecule-1 (CD31) requires functional ITIMs, SHP-2, and p56lck. *Blood* 97 (8): 2351–2357.
- Newman, P. J. 1994. The Role of PECAM-1 in Vascular Cell Biology. *Annals of the New York Academy of Sciences* 714 (1): 165–174.
- Newman, P. J. 1999. Switched at birth: a new family for PECAM-1. *Journal of Clinical Investigation* 103 (1): 5–9.
- Newman, P. J. and Newman, D. K. 2003. Signal Transduction Pathways Mediated by PECAM-1: New Roles for an Old Molecule in Platelet and Vascular Cell Biology. *Arteriosclerosis, Thrombosis, and Vascular Biology* 23 (6): 953–964.
- Newman, P. J., Berndt, M. C., Gorski, J., White, G. C., Lyman, S., Paddock, C. and Muller, W. A. 1990. PECAM-1 (CD31) Cloning and Relation to Adhesion Molecules of the Immunoglobulin Gene Superfamily. *Science* 247 (4947): 1219–1222.
- Newman, P. J., Hillery, C. A., Albrecht, R., Parise, L. V., Berndt, M. C., Mazurov, A. V., Dunlop, L. C., Zhang, J. and Rittenhouse, S. E. 1992. Activation-dependent changes in human platelet PECAM-1: phosphorylation, cytoskeletal association, and surface membrane redistribution. *The Journal of Cell Biology* 119 (1): 239–246.
- Newton, J. P., Buckley, C. D., Jones, E. Y. and Simmons, D. L. 1997. Residues on Both Faces of the First Immunoglobulin Fold Contribute to Homophilic Binding Sites of PECAM-1/CD31. *Journal of Biological Chemistry* 272 (33): 20555–20563.
- Newton, J. P., Hunter, A. P., Simmons, D. L., Buckley, C. D. and Harvey, D. J. 1999. CD31 (PECAM-1) Exists as a Dimer and Is Heavily N-Glycosylated. *Biochemical and Biophysical Research Communications* 261 (2): 283–291.
- Newton-Nash, D. K. and Newman, P. J. 1999. A New Role for Platelet-Endothelial Cell Adhesion Molecule-1 (CD31): Inhibition of TCR-Mediated Signal Transduction. *The Journal of Immunology* 163 (2): 682–688.
- Nieuwkamp, D. J., Setz, L. E., Algra, A., Linn, F. H., de Rooij, N. K. and Rinkel, G. J. 2009. Changes in case fatality of aneurysmal subarachnoid haemorrhage over time, according to age, sex, and region: a meta-analysis. *The Lancet Neurology* 8 (7): 635–642.
- Nivelstein, P. F., Fogelman, A. M., Mottino, G. and Frank, J. S. 1991. Lipid accumulation in rabbit aortic intima 2 hours after bolus infusion of low density lipoprotein. A deep-etch and immunolocalization study of ultrarapidly frozen tissue. *Arteriosclerosis, Thrombosis, and Vascular Biology* 11 (6): 1795–1805.
- Nowling, G. R., Yajima, M., Babayan, S. E., Moravej, M., Yang, X., Hoffman, W. and Hicks, R. F. 2005. Chamberless plasma deposition of glass coatings on plastic. *Plasma Sources Science and Technology* 14 (3): 477.
- Ochi, H., Kume, N., Nishi, E., Moriwaki, H., Masuda, M., Fujiwara, K. and Kita, T. 1998. Tyrosine Phosphorylation of Platelet Endothelial Cell Adhesion Molecule-1 Induced by Lysophosphatidylcholine in Cultured Endothelial Cells. *Biochemical and Biophysical Research Communications* 243 (3): 862–868.
- Ohto, H., Maeda, H., Shibata, Y., Chen, R. F., Ozaki, Y., Higashihara, M., Takeuchi, A. and Tohyama, H. 1985. A novel leukocyte differentiation antigen: two monoclonal antibodies TM2 and TM3 define a 120-kd molecule present on neutrophils, monocytes, platelets, and activated lymphoblasts. *Blood* 66 (4): 873–881.
- Onuma, Y. and Serruys, P. W. 2011. Bioresorbable Scaffold: The Advent of a New Era in Percutaneous Coronary and Peripheral Revascularization? *Circulation* 123 (7): 779–797.
- Osawa, M., Masuda, M., Harada, N., Lopes, R. B. and Fujiwara, K. 1997. Tyrosine phosphorylation of platelet endothelial cell adhesion molecule-1 (PECAM-1, CD31) in mechanically stimulated vascular endothelial cells. *European journal of cell biology* 72 (3): 229–237.

- Otsuka, F., Finn, A. V., Yazdani, S. K., Nakano, M., Kolodgie, F. D. and Virmani, R. 2012. The importance of the endothelium in atherothrombosis and coronary stenting. *Nature Reviews Cardiology* 9 (8): 439–453.
- Ou, J., Wang, J., Qiu, Y., Liu, L. and Yang, S. 2011. Mechanical property and corrosion resistance of zirconia/polydopamine nanocomposite multilayer films fabricated via a novel non-electrostatic layer-by-layer assembly technique. *Surface and Interface Analysis* 43 (4): 803–808.
- Ou, J., Liu, L., Wang, J., Wang, F., Xue, M. and Li, W. 2012. Fabrication and tribological investigation of a novel hydrophobic polydopamine/graphene oxide multilayer film. *Tribology Letters* 48 (3): 407–415.
- Oude Nijhuis, C. S. M., Vellenga, E., Daenen, S. M. G. J., Kamps, W. A. and De Bont, E. S. J. M. 2003. Endothelial cells are main producers of interleukin 8 through Toll-like receptor 2 and 4 signaling during bacterial infection in leukopenic cancer patients. *Clinical and Diagnostic Laboratory Immunology* 10 (4): 558–563.
- Pache, J. ürgen, Kastrati, A., Mehilli, J., Schühlen, H., Dotzer, F., Hausleiter, J. örg, Fleckenstein, M., Neumann, F.-J., Sattelberger, U., Schmitt, C., Müller, M., Dirschinger, J. and Schömig, A. 2003. Intracoronary stenting and angiographic results: strut thickness effect on restenosis outcome (ISAR-STEREO-2) trial. *Journal of the American College of Cardiology* 41 (8): 1283–1288.
- Paddock, C., Zhou, D., Lertkiatmongkol, P., Newman, P. J. and Zhu, J. 2016. Structural basis for PECAM-1 homophilic binding. *Blood* 127 (8): 1052–1061.
- Palinski, W., Rosenfeld, M. E., Ylä-Herttuala, S., Gurtner, G. C., Socher, S. S., Butler, S. W., Parthasarathy, S., Carew, T. E., Steinberg, D. and Witztum, J. L. 1989. Low density lipoprotein undergoes oxidative modification in vivo. *Proceedings of the National Academy of Sciences* 86 (4): 1372–1376.
- Pandya, B., Gaddam, S., Raza, M., Asti, D., Nalluri, N., Vazzana, T., Kandov, R. and Lafferty, J. 2016. Biodegradable polymer stents vs second generation drug eluting stents: A meta-analysis and systematic review of randomized controlled trials. *World Journal of Cardiology* 8 (2): 240–246.
- Park, J., Kim, J.-K., Patil, S. J., Park, J.-K., Park, S. and Lee, D.-W. 2016. A Wireless Pressure Sensor Integrated with a Biodegradable Polymer Stent for Biomedical Applications. *Sensors* 16 (6): 809.
- Pasquier, E., Carré, M., Pourroy, B., Camoin, L., Rebaï, O., Briand, C. and Braguer, D. 2004. Antiangiogenic activity of paclitaxel is associated with its cytostatic effect, mediated by the initiation but not completion of a mitochondrial apoptotic signaling pathway. *Molecular Cancer Therapeutics* 3 (10): 1301–1310.
- Patil, S., Newman, D. K. and Newman, P. J. 2001. Platelet endothelial cell adhesion molecule-1 serves as an inhibitory receptor that modulates platelet responses to collagen. *Blood* 97 (6): 1727–1732.
- Pekkarinen, T., Hietalala, O., Jämsä, T. and Jalovaara, P. 2005. Gamma irradiation and ethylene oxide in the sterilization of native reindeer bone morphogenetic protein extract. *Scandinavian journal of surgery: SJS: official organ for the Finnish Surgical Society and the Scandinavian Surgical Society* 94 (1): 67–70.
- Pérez de Prado, A., Pérez-Martínez, C., Cuellas-Ramón, C., Gonzalo-Orden, J. M., Regueiro-Purriños, M., Martínez-Fernández, B., Diego-Nieto, A. and Fernández-Vázquez, F. 2011. Scanning Electron Microscopy Analysis of Luminal Inflammation Induced by Different Types of Coronary Stent in an Animal Model. *Revista Española de Cardiología (English Edition)* 64 (2): 159–162.
- Peyvandi, F., Garagiola, I. and Baronciani, L. 2011. Role of von Willebrand factor in the haemostasis. *Blood Transfusion* 9 (Suppl 2): s3–s8.
- Pfisterer, M., Brunner-La Rocca, H. P., Buser, P. T., Rickenbacher, P., Hunziker, P., Mueller, C., Jeger, R., Bader, F., Osswald, S. and Kaiser, C. 2006. Late Clinical Events After Clopidogrel Discontinuation May Limit the Benefit of Drug-Eluting Stents: An Observational Study of

- Drug-Eluting Versus Bare-Metal Stents. *Journal of the American College of Cardiology* 48 (12): 2584–2591.
- Pierot, L. 2011. Flow diverter stents in the treatment of intracranial aneurysms: Where are we? *Journal of Neuroradiology* 38 (1): 40–46.
- Pierot, L., Spelle, L. and Vitry, F. 2008. Immediate Clinical Outcome of Patients Harboring Unruptured Intracranial Aneurysms Treated by Endovascular Approach: Results of the ATENA Study. *Stroke* 39 (9): 2497–2504.
- Pierot, L., Spelle, L., Molyneux, A. and Byrne, J. 2016. Clinical and Anatomical Follow-up in Patients With Aneurysms Treated With the WEB Device: 1-Year Follow-up Report in the Cumulated Population of 2 Prospective, Multicenter Series (WEBCAST and French Observatory). *Neurosurgery* 78 (1): 133–139.
- Pigott, R., Dillon, L. P., Hemingway, I. H. and Gearing, A. J. H. 1992. Soluble forms of E-selectin, ICAM-1 and VCAM-1 are present in the supernatants of cytokine activated cultured endothelial cells. *Biochemical and Biophysical Research Communications* 187 (2): 584–589.
- Piotin, M., Blanc, R., Spelle, L., Mounayer, C., Piantino, R., Schmidt, P. J. and Moret, J. 2010. Stent-Assisted Coiling of Intracranial Aneurysms: Clinical and Angiographic Results in 216 Consecutive Aneurysms. *Stroke* 41 (1): 110–115.
- Poole, J. C. F. and Florey, H. W. 1958. Changes in the endothelium of the aorta and the behaviour of macrophages in experimental atheroma of rabbits. *The Journal of Pathology and Bacteriology* 75 (2): 245–251.
- Prager, E., Staffler, G., Majdic, O., Säemann, M. D., Godár, S., Zlabinger, G. J. and Stockinger, H. 2001. Induction of hyporesponsiveness and impaired T lymphocyte activation by the CD31 receptor: ligand pathway in T cells. *The Journal of Immunology* 166 (4): 2364–2371.
- Prasad, C. K., Resmi, K. R., Krishnan, L. K. and Vaishnav, R. 2005. Survival of endothelial cells in vitro on Paclitaxel-loaded coronary stents. *Journal of Biomaterials Applications* 19 (4): 271–286.
- Privratsky, J. R. and Newman, P. J. 2014. PECAM-1: regulator of endothelial junctional integrity. *Cell and Tissue Research* 355 (3): 607–619.
- Pumphrey, N. J., Taylor, V., Freeman, S., Douglas, M. R., Bradfield, P. F., Young, S. P., Lord, J. M., Wakelam, M. J. O., Bird, I. N., Salmon, M. and Buckley, C. D. 1999. Differential association of cytoplasmic signalling molecules SHP-1, SHP-2, SHIP and phospholipase C- γ 1 with PECAM-1/CD31. *FEBS Letters* 450 (1–2): 77–83.
- Quinn, M. T., Parthasarathy, S. and Steinberg, D. 1988. Lysophosphatidylcholine: a chemotactic factor for human monocytes and its potential role in atherogenesis. *Proceedings of the National Academy of Sciences* 85 (8): 2805–2809.
- Radeva, E., Pramatarova, L., Pecheva, E., Hikov, T., Iacob, E., Vanzetti, L., Dimitrova, R., Krasteva, N., Spassov, T. and Fingarova, D. 2009. Study of Organosilicon Plasma Polymer Used in Composite Layers with Biomedical Application. In: Angelopoulos, A. and Fildisis, T. (eds.), *7th International Conference of the Balkan Physical Union Vols 1 and 2*, Vol. 1203, 949–+. Amer Inst Physics, Melville.
- Rajah, G., Narayanan, S. and Rangel-Castilla, L. 2017. Update on flow diverters for the endovascular management of cerebral aneurysms. *Neurosurgical Focus* 42 (6): E2.
- Rathore, V., Stapleton, M. A., Hillery, C. A., Montgomery, R. R., Nichols, T. C., Merricks, E. P., Newman, D. K. and Newman, P. J. 2003. PECAM-1 negatively regulates GPIIb/IIIa signaling in murine platelets. *Blood* 102 (10): 3658–3664.
- Ravetch, J. V. and Lanier, L. L. 2000. Immune Inhibitory Receptors. *Science* 290 (5489): 84–89.
- RayChaudhury, A., Elkins, M., Koziem, D. and Nakada, M. T. 2001. Regulation of PECAM-1 in endothelial cells during cell growth and migration. *Experimental Biology and Medicine* 226 (7): 686–691.
- Reineke, D. C., Müller-Schweinitzer, E., Winkler, B., Kunz, D., Konerding, M. A., Grussenmeyer, T., Carrel, T. P., Eckstein, F. S. and Grapow, M. T. R. 2015. Rapamycin impairs endothelial cell function in human internal thoracic arteries. *European Journal of Medical Research* 20 (1).

- Resnick, N. and Gimbrone, M. A. 1995. Hemodynamic forces are complex regulators of endothelial gene expression. *The FASEB Journal* 9 (10): 874–882.
- Rinkel, G. J. E., Djibuti, M., Algra, A. and van Gijn, J. 1998. Prevalence and risk of rupture of intracranial aneurysms - A systematic review. *Stroke* 29 (1): 251–256.
- Rittersma, S. Z. H., de Winter, R. J., Koch, K. T., Bax, M., Schotborgh, C. E., Mulder, K. J., Tijssen, J. G. P. and Piek, J. J. 2004. Impact of strut thickness on late luminal loss after coronary artery stent placement. *The American Journal of Cardiology* 93 (4): 477–480.
- Rouchaud, A., Brinjikji, W., Lanzino, G., Cloft, H. J., Kadirvel, R. and Kallmes, D. F. 2016a. Delayed hemorrhagic complications after flow diversion for intracranial aneurysms: a literature overview. *Neuroradiology* 58 (2): 171–177.
- Rouchaud, A., Johnson, C., Thielen, E., Schroeder, D., Ding, Y.-H., Dai, D., Brinjikji, W., Cebral, J., Kallmes, D. F. and Kadirvel, R. 2016b. Differential Gene Expression in Coiled versus Flow-Diverter-Treated Aneurysms: RNA Sequencing Analysis in a Rabbit Aneurysm Model. *American Journal of Neuroradiology* 37 (6): 1114–1121.
- Rui, Y., Liu, X., Li, N., Jiang, Y., Chen, G., Cao, X. and Wang, J. 2007. PECAM-1 ligation negatively regulates TLR4 signaling in macrophages. *The Journal of Immunology* 179 (11): 7344–7351.
- Ruigrok, Y. M., Elias, R., Wijmenga, C. and Rinkel, G. J. E. 2008. A comparison of genetic chromosomal loci for intracranial, thoracic aortic, and abdominal aortic aneurysms in search of common genetic risk factors. *Cardiovascular Pathology* 17 (1): 40–47.
- Saatci, I., Yavuz, K., Ozer, C., Geyik, S. and Cekirge, H. S. 2012. Treatment of Intracranial Aneurysms Using the Pipeline Flow-Diverter Embolization Device: A Single-Center Experience with Long-Term Follow-Up Results. *American Journal of Neuroradiology* 33 (8): 1436–1446.
- Sabbah, H. N., Khaja, F., Hawkins, E. T., Brymer, J. F., McFarland, T. M., van der Bel-Kahn, J., Doerger, P. T. and Stein, P. D. 1986. Relation of atherosclerosis to arterial wall shear in the left anterior descending coronary artery of man. *American Heart Journal* 112 (3): 453–458.
- Sachs, U. J., Andrei-Selmer, C. L., Maniar, A., Weiss, T., Paddock, C., Orlova, V. V., Choi, E. Y., Newman, P. J., Preissner, K. T., Chavakis, T. and others. 2007. The neutrophil-specific antigen CD177 is a counter-receptor for platelet endothelial cell adhesion molecule-1 (CD31). *Journal of Biological Chemistry* 282 (32): 23603–23612.
- Sagawa, K., Swaim, W., Zhang, J., Unsworth, E. and Siraganian, R. P. 1997. Aggregation of the High Affinity IgE Receptor Results in the Tyrosine Phosphorylation of the Surface Adhesion Protein PECAM-1 (CD31). *Journal of Biological Chemistry* 272 (20): 13412–13418.
- Saidin, S., Chevallier, P., Abdul Kadir, M. R., Hermawan, H. and Mantovani, D. 2013. Polydopamine as an intermediate layer for silver and hydroxyapatite immobilisation on metallic biomaterials surface. *Materials Science and Engineering: C* 33 (8): 4715–4724.
- Schaffner, T., Taylor, K., Bartucci, E. J., Fischer-Dzoga, K., Beeson, J. H., Glagov, S. and Wissler, R. W. 1980. Arterial foam cells with distinctive immunomorphologic and histochemical features of macrophages. *The American Journal of Pathology* 100 (1): 57–80.
- Schapiro-Dufour, E., Tricotel, A., Rudnichi, A., Emery, G. and Dray-Spira, R. 2016. *Utilisation des endoprothèses (stents) coronaires en France en 2014: Étude à partir des données du SNIIRAM*. ANSM, HAS, .
- Schievink, W. I. 1997. Intracranial Aneurysms. *New England Journal of Medicine* 336 (1): 28–40.
- Schmidt, M., Jacobsen, J. B., Lash, T. L., Botker, H. E. and Sorensen, H. T. 2012. 25 year trends in first time hospitalisation for acute myocardial infarction, subsequent short and long term mortality, and the prognostic impact of sex and comorbidity: a Danish nationwide cohort study. *British Medical Journal* 344: e356.
- Schoenhagen, P., Ziada, K. M., Vince, D. G., Nissen, S. E. and Tuzcu, E. M. 2001. Arterial remodeling and coronary artery disease: the concept of ‘dilated’ versus ‘obstructive’ coronary atherosclerosis. *Journal of the American College of Cardiology* 38 (2): 297–306.
- Schwartz, R. S., Edelman, E., Virmani, R., Carter, A., Granada, J. F., Kaluza, G. L., Chronos, N. A. F., Robinson, K. A., Waksman, R., Weinberger, J., Wilson, G. J. and Wilensky, R. L. 2008. Drug-Eluting Stents in Preclinical Studies: Updated Consensus Recommendations for Preclinical Evaluation. *Circulation: Cardiovascular Interventions* 1 (2): 143–153.

- Schwenke, D. C. and Carew, T. E. 1989. Initiation of atherosclerotic lesions in cholesterol-fed rabbits. I. Focal increases in arterial LDL concentration precede development of fatty streak lesions. *Arteriosclerosis, Thrombosis, and Vascular Biology* 9 (6): 895–907.
- Sekhar, L. N. and Heros, R. C. 1981. Origin, growth, and rupture of saccular aneurysms: a review. *Neurosurgery* 8 (2): 248–260.
- Serruys, P. W., Kutryk, M. J. B. and Ong, A. T. L. 2006. Coronary-Artery Stents. *New England Journal of Medicine* 354 (5): 483–495.
- Serruys, P. W., de Jaegere, P., Kiemeneij, F., Macaya, C., Rutsch, W., Heyndrickx, G., Emanuelsson, H., Marco, J., Legrand, V., Materne, P., Belardi, J., Sigwart, U., Colombo, A., Goy, J. J., van den Heuvel, P., Delcan, J. and Morel, M. 1994. A Comparison of Balloon-Expandable-Stent Implantation with Balloon Angioplasty in Patients with Coronary Artery Disease. *New England Journal of Medicine* 331 (8): 489–495.
- Sharma, H. and Mutharasan, R. 2012. A novel pulsed-plasma approach for protein immobilization by grafting reactive amine groups on polyurethane-coated biosensors. *Sensors and Actuators B-Chemical* 173: 569–574.
- Short, J. G., Fujiwara, N. H., Marx, W. F., Helm, G. A., Cloft, H. J. and Kallmes, D. F. 2001. Elastase-induced saccular aneurysms in rabbits: comparison of geometric features with those of human aneurysms. *American journal of neuroradiology* 22 (10): 1833–1837.
- Sigwart, U., Puel, J., Mirkovitch, V., Joffre, F. and Kappenberg, L. 1987. Intravascular Stents to Prevent Occlusion and Re-Stenosis after Transluminal Angioplasty. *New England Journal of Medicine* 316 (12): 701–706.
- Silva, R. M., Elvira, C., Mano, J. F., San Román, J. and Reis, R. L. 2004. Influence of beta-radiation sterilisation in properties of new chitosan/soybean protein isolate membranes for guided bone regeneration. *Journal of Materials Science. Materials in Medicine* 15 (4): 523–528.
- Sin, M.-C., Lin, W.-L., Chen, J. C.-H., Higuchi, A., Zheng, J., Chinnathambi, A., Alharbi, S. A. and Chang, Y. 2016. Hemocompatible interface control via thermal-activated bio-inspired surface PEGylation. *International Journal of Polymeric Materials and Polymeric Biomaterials* 65 (8): 409–420.
- Sobocinski, J., Laure, W., Taha, M., Courcot, E., Chai, F., Simon, N., Addad, A., Martel, B., Haulon, S., Woisel, P., Blanchemain, N. and Lyskawa, J. 2014. Mussel Inspired Coating of a Biocompatible Cyclodextrin Based Polymer onto CoCr Vascular Stents. *ACS Applied Materials & Interfaces* 6 (5): 3575–3586.
- Société Française de Neuroradiologie. 2016. Registre diversion. *Journal of Neuroradiology* 43 (2): 69–70.
- Son, D., Lee, J., Lee, D. J., Ghaffari, R., Yun, S., Kim, S. J., Lee, J. E., Cho, H. R., Yoon, S., Yang, S., Lee, S., Qiao, S., Ling, D., Shin, S., Song, J.-K., Kim, J., Kim, T., Lee, H., Kim, J., Soh, M., Lee, N., Hwang, C. S., Nam, S., Lu, N., Hyeon, T., Choi, S. H. and Kim, D.-H. 2015. Bioresorbable Electronic Stent Integrated with Therapeutic Nanoparticles for Endovascular Diseases. *Acs Nano* 9 (6): 5937–5946.
- Song, C.-L., Li, Q., Yu, Y.-P., Wang, G., Wang, J.-P., Lu, Y., Zhang, J.-C., Diao, H.-Y., Liu, J.-G., Liu, Y.-H., Liu, J., Li, Y., Cai, D. and Liu, B. 2015. Study of novel coating strategy for coronary stents: simultaneous coating of VEGF and anti- CD34 antibody. *Revista Brasileira De Cirurgia Cardiovascular: Órgão Oficial Da Sociedade Brasileira De Cirurgia Cardiovascular* 30 (2): 159–163.
- Starbuck, W. and Busch, H. 1963. Hydroxyethylation of Amino Acids in Plasma Albumin with Ethylene Oxide. *Biochimica Et Biophysica Acta* 78 (4): 594-.
- Sтары, H. C. 2001. The development of calcium deposits in atherosclerotic lesions and their persistence after lipid regression. *The American Journal of Cardiology* 88 (2, Supplement 1): 16–19.
- Stefanini, G. G., Taniwaki, M. and Windecker, S. 2014. Coronary stents: novel developments. *Heart* 100 (13): 1051–1061.
- Steinberg, D. 1983. Lipoproteins and atherosclerosis. A look back and a look ahead. *Arteriosclerosis, Thrombosis, and Vascular Biology* 3 (4): 283–301.

- Steinberg, D. 1997. Low Density Lipoprotein Oxidation and Its Pathobiological Significance. *Journal of Biological Chemistry* 272 (34): 20963–20966.
- Steinberg, D., Parthasarathy, S., Carew, T. E., Khoo, J. C. and Witztum, J. L. 1989. Beyond cholesterol. Modifications of low-density lipoprotein that increase its atherogenicity. *The New England Journal of Medicine* 320 (14): 915–924.
- Stockinger, H., Gadd, S., Eher, R., Majdic, O., Schreiber, W., Kasinrerck, W., Strass, B., Schnabl, E. and Knapp, W. 1990. Molecular Characterization and Functional-Analysis of the Leukocyte Surface Protein Cd31. *Journal of Immunology* 145 (11): 3889–3897.
- Stone, G. W., Ellis, S. G., Colombo, A., Grube, E., Popma, J. J., Uchida, T., Bleuit, J. S., Dawkins, K. D. and Russell, M. E. 2011. Long-Term Safety and Efficacy of Paclitaxel-Eluting Stents: Final 5-Year Analysis From the TAXUS Clinical Trial Program. *JACC: Cardiovascular Interventions* 4 (5): 530–542.
- Sun, Q.-H., DeLisser, H. M., Zukowski, M. M., Paddock, C., Albelda, S. M. and Newman, P. J. 1996. Individually Distinct Ig Homology Domains in PECAM-1 Regulate Homophilic Binding and Modulate Receptor Affinity. *Journal of Biological Chemistry* 271 (19): 11090–11098.
- Szikora, I., Berentei, Z., Kulcsar, Z., Marosfoi, M., Vajda, Z. S., Lee, W., Berez, A. and Nelson, P. K. 2010. Treatment of intracranial aneurysms by functional reconstruction of the parent artery: the Budapest experience with the pipeline embolization device. *AJNR. American journal of neuroradiology* 31 (6): 1139–1147.
- Tabas, I. 2005. Consequences and therapeutic implications of macrophage apoptosis in atherosclerosis - The importance of lesion stage and phagocytic efficiency. *Arteriosclerosis Thrombosis and Vascular Biology* 25 (11): 2255–2264.
- Tada, T., Byrne, R. A., Simunovic, I., King, L. A., Cassese, S., Joner, M., Fusaro, M., Schneider, S., Schulz, S., Ibrahim, T., Ott, I., Massberg, S., Laugwitz, K.-L. and Kastrati, A. 2013. Risk of Stent Thrombosis Among Bare-Metal Stents, First-Generation Drug-Eluting Stents, and Second-Generation Drug-Eluting Stents Results From a Registry of 18,334 Patients. *Jacc-Cardiovascular Interventions* 6 (12): 1267–1274.
- Takabe, W., Kanai, Y., Chairoungdua, A., Shibata, N., Toi, S., Kobayashi, M., Kodama, T. and Noguchi, N. 2004. Lysophosphatidylcholine Enhances Cytokine Production of Endothelial Cells via Induction of L-Type Amino Acid Transporter 1 and Cell Surface Antigen 4F2. *Arteriosclerosis, Thrombosis, and Vascular Biology* 24 (9): 1640–1645.
- Takahara, N., Kashiwagi, A., Maegawa, H. and Shigeta, Y. 1996. Lysophosphatidylcholine stimulates the expression and production of MCP-1 by human vascular endothelial cells. *Metabolism* 45 (5): 559–564.
- Tan, L. A., Keigher, K. M., Munich, S. A., Moftakhar, R. and Lopes, D. K. 2014. Thromboembolic complications with Pipeline Embolization Device placement: impact of procedure time, number of stents and pre-procedure P2Y12 reaction unit (PRU) value. *Journal of neurointerventional surgery: neurintsurg*–2014.
- Tenekecioglu, E., Farooq, V., Bourantas, C. V., Silva, R. C., Onuma, Y., Yilmaz, M. and Serruys, P. W. 2016. Bioresorbable scaffolds: a new paradigm in percutaneous coronary intervention. *BMC Cardiovascular Disorders* 16.
- Terzian, Z., Gasser, T. C., Blackwell, F., Hyafil, F., Louedec, L., Deschildre, C., Ghodbane, W., Dorent, R., Nicoletti, A., Morvan, M., Nejjari, M., Feldman, L., Pavon-Djavid, G. and Michel, J.-B. 2017. Peristrut microhemorrhages: a possible cause of in-stent neoatherosclerosis? *Cardiovascular Pathology* 26 (Supplement C): 30–38.
- Thom, T., Haase, N., Rosamond, W., Howard, V. J., Rumsfeld, J., Manolio, T., Zheng, Z.-J., Flegal, K., O'Donnell, C., Kittner, S., Lloyd-Jones, D., Goff, D. C., Hong, Y., Subcommittee, M. of the S. C. and S. S., Adams, R., Friday, G., Furie, K., Gorelick, P., Kissela, B., Marler, J., Meigs, J., Roger, V., Sidney, S., Sorlie, P., Steinberger, J., Wasserthiel-Smoller, S., Wilson, M. and Wolf, P. 2006. Heart Disease and Stroke Statistics—2006 Update: A Report From the American Heart Association Statistics Committee and Stroke Statistics Subcommittee. *Circulation* 113 (6): e85–e151.
- Tiwari, A. and Nordin, A. N. 2014. *Advanced Biomaterials and Biodevices*. John Wiley & Sons, .

- Tsang, C. K., Qi, H., Liu, L. F. and Zheng, X. F. S. 2007. Targeting mammalian target of rapamycin (mTOR) for health and diseases. *Drug Discovery Today* 12 (3–4): 112–124.
- Tugyi, R., Uray, K., Iván, D., Fellingner, E., Perkins, A. and Hudecz, F. 2005. Partial D-amino acid substitution: Improved enzymatic stability and preserved Ab recognition of a MUC2 epitope peptide. *Proceedings of the National Academy of Sciences of the United States of America* 102 (2): 413–418.
- Unger, J., Filippi, G. and Patsch, W. 2007. Measurements of Free Hemoglobin and Hemolysis Index: EDTA- or Lithium-Heparinate Plasma? *Clinical Chemistry* 53 (9): 1717–1718.
- Unkeless, J. C. and Jin, J. 1997. Inhibitory receptors, ITIM sequences and phosphatases. *Current Opinion in Immunology* 9 (3): 338–343.
- Vaporciyan, A. A., DeLisser, H. M., Yan, H.-C., Mendiguren, I. I., Thom, S. R., Jones, M. L., Ward, P. A. and Albelda, S. M. 1993. Involvement of platelet-endothelial cell adhesion molecule-1 in neutrophil recruitment in vivo. *Science* 262 (5139): 1580–1583.
- Varon, D., Jackson, D. E., Shenkman, B., Dardik, R., Tamarin, I., Savion, N. and Newman, P. J. 1998. Platelet/Endothelial Cell Adhesion Molecule-1 Serves as a Costimulatory Agonist Receptor That Modulates Integrin-Dependent Adhesion and Aggregation of Human Platelets. *Blood* 91 (2): 500–507.
- de Villiers, W. J. and Smart, E. J. 1999. Macrophage scavenger receptors and foam cell formation. *Journal of Leukocyte Biology* 66 (5): 740–746.
- Virmani, R. and Farb, A. 1999. Pathology of in-stent restenosis. *Current Opinion in Lipidology* 10 (6): 499.
- Virmani, R., Guagliumi, G., Farb, A., Musumeci, G., Grieco, N., Motta, T., Mihalcsik, L., Tespili, M., Valsecchi, O. and Kolodgie, F. D. 2004. Localized hypersensitivity and late coronary thrombosis secondary to a sirolimus-eluting stent: should we be cautious? *Circulation* 109 (6): 701–705.
- Wang, I.-S., Lin, Y.-T., Huang, C.-H., Lu, T.-F., Lue, C.-E., Yang, P., Pijanswska, D. G., Yang, C.-M., Wang, J.-C., Yu, J.-S., Chang, Y.-S., Chou, C. and Lai, C.-S. 2012. Immobilization of enzyme and antibody on ALD-HfO₂-EIS structure by NH₃ plasma treatment. *Nanoscale Research Letters* 7 (1): 179.
- Wang, J., Li, B., Li, Z., Ren, K., Jin, L., Zhang, S., Chang, H., Sun, Y. and Ji, J. 2014. Electropolymerization of dopamine for surface modification of complex-shaped cardiovascular stents. *Biomaterials* 35 (27): 7679–7689.
- Wang, R., Paddock, C., Augustine, J. A. and Newman, P. J. 1998. Oxidative stress triggers PECAM-1-mediated signaling pathways. *Blood* 92: 548A–548A.
- Watanabe, T. 2004. *Nano-plating: Microstructure Control Theory of Plated Film and Data Base of Plated Film Microstructure*. Elsevier, .
- Wendel, H. P., Avci-Adali, M. and Ziemer, G. 2010. Endothelial progenitor cell capture stents — hype or hope? *International Journal of Cardiology* 145 (1): 115–117.
- Wiebers, D. O. 2003. Unruptured intracranial aneurysms: natural history, clinical outcome, and risks of surgical and endovascular treatment. *The Lancet* 362 (9378): 103–110.
- Wilkinson, R., Lyons, A. B., Roberts, D., Wong, M.-X., Bartley, P. A. and Jackson, D. E. 2002. Platelet endothelial cell adhesion molecule-1 (PECAM-1/CD31) acts as a regulator of B-cell development, B-cell antigen receptor (BCR)-mediated activation, and autoimmune disease. *Blood* 100 (1): 184–193.
- Wong, M.-X., Roberts, D., Bartley, P. A. and Jackson, D. E. 2002. Absence of platelet endothelial cell adhesion molecule-1 (CD31) leads to increased severity of local and systemic IgE-mediated anaphylaxis and modulation of mast cell activation. *The Journal of Immunology* 168 (12): 6455–6462.
- Wong, M.-X., Harbour, S. N., Wee, J. L., Lau, L.-M., Andrews, R. K. and Jackson, D. E. 2004. Proteolytic cleavage of platelet endothelial cell adhesion molecule-1 (PECAM-1/CD31) is regulated by a calmodulin-binding motif. *FEBS Letters* 568 (1–3): 70–78.
- Wong, S. S. 1991. *Chemistry of Protein Conjugation and Cross-Linking*. CRC Press, .
- Wu, F., Li, J., Zhang, K., He, Z., Yang, P., Zou, D. and Huang, N. 2016. Multifunctional Coating Based on Hyaluronic Acid and Dopamine Conjugate for Potential Application on Surface

- Modification of Cardiovascular Implanted Devices. *ACS Applied Materials & Interfaces* 8 (1): 109–121.
- Wu, J. and Sheibani, N. 2003. Modulation of VE-cadherin and PECAM-1 mediated cell–cell adhesions by mitogen-activated protein kinases. *Journal of cellular biochemistry* 90 (1): 121–137.
- Wu, Y., Stabach, P., Michaud, M. and Madri, J. A. 2005. Neutrophils lacking platelet-endothelial cell adhesion molecule-1 exhibit loss of directionality and motility in CXCR2-mediated chemotaxis. *The Journal of Immunology* 175 (6): 3484–3491.
- Xi, Z.-Y., Xu, Y.-Y., Zhu, L.-P., Wang, Y. and Zhu, B.-K. 2009. A facile method of surface modification for hydrophobic polymer membranes based on the adhesive behavior of poly(DOPA) and poly(dopamine). *Journal of Membrane Science* 327 (1): 244–253.
- Yang, S.-H., Liu, C.-H., Su, C.-H. and Chen, H. 2009. Atmospheric-pressure plasma deposition of SiO_x films for super-hydrophobic application. *Thin Solid Films* 517 (17): 5284–5287.
- Yang, Y.-W., Wu, J.-Y., Liu, C.-T., Liao, G.-C., Cheng, K.-Y., Chiang, M.-H. and Wu, J.-S. 2015. An Optimized Two-Step Nitrogen-Based Plasma Treatment Procedure under Atmospheric-Pressure Condition and its Surface Amination Mechanism. *Plasma Processes and Polymers* 12 (7): 678–690.
- Yang, Z., Tu, Q., Zhu, Y., Luo, R., Li, X., Xie, Y., Maitz, M. F., Wang, J. and Huang, N. 2012. Mussel-Inspired Coating of Polydopamine Directs Endothelial and Smooth Muscle Cell Fate for Re-endothelialization of Vascular Devices. *Advanced Healthcare Materials* 1 (5): 548–559.
- Yao, Y., Fukazawa, K., Ma, W., Ishihara, K. and Huang, N. 2012. Platelet adhesion-resistance of titanium substrate with mussel-inspired adhesive polymer bearing phosphorylcholine group. *Applied Surface Science* 258 (14): 5418–5423.
- Yu, F., Chen, S., Chen, Y., Li, H., Yang, L., Chen, Y. and Yin, Y. 2010. Experimental and theoretical analysis of polymerization reaction process on the polydopamine membranes and its corrosion protection properties for 304 Stainless Steel. *Journal of Molecular Structure* 982 (1): 152–161.
- Yuan, S., Yin, J., Jiang, W., Liang, B., Pehkonen, S. O. and Choong, C. 2013. Enhancing antibacterial activity of surface-grafted chitosan with immobilized lysozyme on bioinspired stainless steel substrates. *Colloids and Surfaces B-Biointerfaces* 106: 11–21.
- Zarins, C. K., Giddens, D. P., Bharadvaj, B. K., Sottiurai, V. S., Mabon, R. F. and Glagov, S. 1983. Carotid bifurcation atherosclerosis. Quantitative correlation of plaque localization with flow velocity profiles and wall shear stress. *Circulation research* 53 (4): 502–514.
- Zehnder, J. L., Shatsky, M., Leung, L. L., Butcher, E. C., McGregor, J. L. and Levitt, L. J. 1995. Involvement of CD31 in lymphocyte-mediated immune responses: importance of the membrane-proximal immunoglobulin domain and identification of an inhibiting CD31 peptide. *Blood* 85 (5): 1282–1288.
- Zhou, Y., Weng, Y., Zhang, L., Jing, F., Huang, N. and Chen, J. 2011. Cystamine immobilization on TiO₂ film surfaces and the influence on inhibition of collagen-induced platelet activation. *Applied Surface Science* 258 (5): 1776–1783.
- Zhou, Z., Christofidou-Solomidou, M., Garlanda, C. and DeLisser, H. M. 1999. Antibody against murine PECAM-1 inhibits tumor angiogenesis in mice. *Angiogenesis* 3 (2): 181–188.
- Zhu, B. and Edmondson, S. 2011. Polydopamine-melanin initiators for Surface-initiated ATRP. *Polymer* 52 (10): 2141–2149.
- Zijlstra, F. 1995. Primary angioplasty is the most effective treatment for an acute myocardial infarction. *British Heart Journal* 73 (5): 403–404.

Annex

Revascularisation coronaire percutanée : progrès et nouveaux défis associés aux stents de dernière génération



Percutaneous coronary revascularisation: Progress and challenges with last generation stents

G. Caligiuri^{a,b}
N. Sayah^{a,b}
C. Rasser^b

^aService de cardiologie, hôpital universitaire Xavier-Bichat, 46, rue Henri-Huchard, 75018 Paris, France
^bInserm U 1148, hôpital universitaire Xavier-Bichat, 46, rue Henri-Huchard, 75018 Paris, France

Disponible en ligne sur ScienceDirect le 24 août 2017

L'ANGIOPLASTIE

La revascularisation coronaire endoluminale percutanée est devenue la procédure de référence pour la prise en charge de la cardiopathie ischémique. La technique de base a vu le jour dans un centre hospitalier suisse où le Dr Andreas Gruentzig a effectué la première angioplastie dans une artère coronaire en 1976, chez le chien, et en 1977 chez l'homme [1]. En France, les premières angioplasties coronaires ont été réalisées en 1979 par Jean-Léon Guermontez à Versailles, puis par Jean Marco à Toulouse. Le nombre d'angioplasties réalisées en France est de l'ordre de 125 000/an et ne cesse de croître avec le temps [2]. Plusieurs études multicentriques permettant de colliger les résultats des équipes françaises ont été initialement réalisées par la Société française de cardiologie et se poursuivent actuellement dans le « Groupe Athérome et Cardiologie Interventionnelle » (GACI).

Alors que l'angioplastie coronaire permet de rétablir une lumière suffisante pour permettre un bon flux en aval d'une sténose, la procédure implique une agression mécanique contre la paroi vasculaire et la mise à nu (dénudation jusqu'à la dissection) de l'intima qui provoque l'exposition de facteurs pro-thrombotiques sous-endothéliaux (risque de thrombose de l'ordre de 8 % malgré l'utilisation d'antiagrégants plaquettaires), ainsi qu'une réponse inflammatoire locale inhérente au processus de cicatrisation qui, s'il est excessif, conduit au rétrécissement du segment traité

(phénomène de « resténose »), lequel survient dans 20 à 57 % des cas. Ainsi, au milieu des années 1980, la thrombose et la resténose sont devenues les cibles d'intérêt pour les chercheurs dans ce domaine.

LES STENTS

La pose d'une prothèse à la fin de la procédure d'angioplastie s'oppose au retour élastique des parois coronaires. Elle devait permettre de maintenir un flux coronaire stable et de réduire le risque de resténose à court et moyen terme. Le premier stent coronaire a été posé en France par Jacques Puel à Toulouse le 28 mars 1986 mais il a fallu presque 10 ans pour faire accepter l'idée, a priori aberrante, d'insérer une structure métallique rigide dans une artère coronaire souple et perpétuellement en mouvement. C'est après la publication des études Benestent [3] et Stress [4] que l'utilisation des stents s'est intensifiée et n'a pas cessé de croître.

Cependant, l'avantage apporté par le stent vis-à-vis du risque de retour élastique immédiat après l'angioplastie a été nuancé par un taux de thrombose de stent important (40 % sur les 17 premiers patients implantés) et le taux de resténose (remodelage constrictif) intrastent n'était pas réduit de façon drastique et demeurait de l'ordre de 20 à 30 % [5]. C'est pour limiter l'incidence de cette complication que les stents actifs ont été conçus.

Auteur correspondant :

G. Caligiuri,
Inserm U 1148, hôpital universitaire Xavier-Bichat, 46, rue Henri-Huchard, 75018 Paris, France.
Adresse e-mail :
giuseppina.caligiuri@inserm.fr

Revascularisation coronaire percutanée : progrès et nouveaux défis associés aux stents de dernière génération

LES STENTS ACTIFS

Le stent coronaire dit « actif » est recouvert d'un polymère imbibé d'un agent pharmacologique antimitotique ou cytostatique, capable de contrer le processus inflammatoire local et la prolifération des cellules musculaires lisses qui conduisent à la resténose. La première génération de stents actifs (Cypher[®], au sirolimus, et Taxus[®] avec le paclitaxel) est parue en décembre 1999. L'étude Ravel, présentée par Marie-Claude Morice, a généré de très grands espoirs en faisant entrevoir la possibilité d'éradiquer la resténose (le taux de resténose à 6 mois passe de 26 % avec un stent métallique à 0 % avec le Cypher[®]) [6].

Cet enthousiasme initial a cependant été contrebalancé par la publication des résultats de l'étude BASKET LATE en décembre 2006 : la survenue de complications (thrombose intrastent, infarctus, décès, nécessité de revascularisation de la lésion traitée) à l'arrêt des antiagrégants à 6 mois était bien plus importante avec les stents actifs (4,9 %) par rapport aux stents « nus » (1,3 %) [7] et ce risque s'est avéré encore plus grand avec le Taxus[®] [8].

En sus des facteurs mécaniques comme le sous-déploiement et la malapposition (possibles également avec les stents « nus »), l'augmentation du risque de complications avec les stents actifs est également due aux facteurs chimiques, dérivés du polymère et des principes actifs, qui peuvent, de façon inattendue, aggraver la réaction locale. D'autre part, la libération des médicaments cytostatiques non vectorisée vers la média mais impactant aussi l'endothélium peut également être mise en cause. En effet, alors que la libération abluminale de ces médicaments vers la média est souhaitable parce qu'elle empêche la croissance des cellules musculaires lisses (responsable de la resténose), la libération de ces médicaments du côté luminal empêche le recouvrement des mailles du stent par l'endothélium (« endothélialisation ») à cause de leur effet cytostatique qui s'exerce aussi sur les cellules endothéliales. Ceci peut rendre compte de la persistance du risque thrombogène dû au contact du métal avec le sang circulant, notamment lorsque les stents présentent des montages complexes.

DE LA PREMIÈRE À LA TROISIÈME GÉNÉRATION DE STENTS ACTIFS

Quels que soient leur génération et leur type, tous les stents actifs sont composés d'une plateforme (structure métallique) recouverte complètement (contour) ou partiellement (côté abluminal seulement) d'un polymère et d'une substance pharmacologique « active ». Afin de pallier les problèmes mécaniques, les fabricants ont fait varier la composition de l'alliage métallique. Dans les stents de deuxième génération, l'acier (alliage 316L) a été remplacé par le Cobalt Chrome (CoCr, Alliage L-605) qui facilite l'accès aux sites d'occlusion (profil de franchissement plus performant et meilleure radio-opacité), permet une grande flexibilité tout en maintenant une force radiale suffisante et permet aussi de diviser par deux l'épaisseur des mailles (Tableau I). Enfin, puisque la composition du polymère est l'un des facteurs impliqués dans la « neoathérosclérose » qui se développe dans la lumière des artères implantées avec des stents actifs [9], la composition chimique des polymères a changé pour la rendre davantage

Physiopathologie cardiovasculaire

« biocompatible ». Les stents de troisième génération sont caractérisés par l'utilisation de polymères à base d'acide polylactique, biodégradable.

Au vu du coût plus élevé (68 % de plus qu'un stent nu) et du potentiel de complications plus dangereuses par rapport aux stents nus, sur la base des données de la littérature médicale et médico-économique et des données cliniques fournies par les fabricants, la Haute Autorité de santé (HAS) a établi que devant une indication cliniquement justifiée de revascularisation myocardique, le choix de la technique (pontage ou angioplastie) et, le cas échéant, le choix du stent (nu ou actif) et de la gamme de matériel dépendent des caractéristiques cliniques et lésionnelles. La pose d'un stent actif doit en tout cas être écartée si le traitement antiagrégant est contre-indiqué (par exemple, intervention chirurgicale programmée à bref délai présentant un risque hémorragique) ou si son observance par le patient est incertaine. Les stents actifs ont un intérêt chez des patients sélectionnés, à haut risque de resténose : lésions supérieures à 15 mm, diamètre du vaisseau atteint inférieur à 3 mm, présence de diabète et/ou insuffisance rénale chronique, resténose intrastent, occlusion coronaire totale, sténose du tronc commun gauche non protégé. La sténose d'un greffon veineux n'est pas une indication des stents actifs.

À partir des données nationales de remboursement des soins par l'Assurance maladie reliées aux données d'hospitalisation, une étude de 2014 a cependant montré qu'en France, la grande majorité des stents coronaires mis en place sont des stents actifs. Les seules maladies qui ne reçoivent pas de stents actifs sont ceux avec un risque hémorragique élevé et/ou à faible espérance de vie. Dans les années à venir, il est à prévoir que l'utilisation de stents actifs va continuer à progresser, les dernières données rapportant qu'en 2015 seuls 16 % des stents posés à l'hôpital étaient des stents nus.

À ce jour, cinq gammes de stents actifs, avec indications et bénéfices variables, sont ouvertes au remboursement en France. Ceux recouverts de biolimus (Biomatrix[®] et Nobori[®]), d'évérolimus (Promus[®] et Xience[®]), de paclitaxel (Taxus[®]), de sirolimus (Cypher[®]), et de zotarolimus (Endeavor[®], Endeavor Resolute[®] et Resolute Integrity[®]). Les plus implantés en 2014 étaient le Xience (58,5 %), le Resolute (21,7 %) et le Nobori (12 %). L'utilisation de ce dernier, dont l'accès au marché est plus récent et qui est recouvert par un polymère biorésorbable, réduirait le risque de thrombose tardive associée à l'utilisation des stents actifs [10]. Il est toutefois important de noter que toutes les études cliniques évaluant les dernières générations de stents ont été des études dites de « non infériorité » et ne permettent donc pas de conclure quant à leur supériorité par rapport aux générations précédentes. En réalité, une méta-analyse récente conclut à l'absence de différence, en termes de complications, entre les stents de seconde génération et les stents de troisième génération, à polymère biodégradable [11].

LES STENTS BIORÉSORBABLES

L'utilisation du métal pour fabriquer les stents était justifiée par la nécessité d'exercer une force radiale suffisante pour contre-carrer le retour élastique de l'artère traitée. Cependant, la pérennité des structures métalliques au contact avec les cellules de la paroi vasculaire et du sang génère une réaction inflammatoire vasculaire à ce « corps étranger » qui est

Physiopathologie cardiovasculaire

G. Caligiuri et al.

Tableau I. Les cinq gammes de stents actifs.

Génération	1 ^{re}	1 ^{re}	2 ^e	2 ^e	3 ^e
Abréviation	PES	SES	ZES	EES	BP-EES
Principe actif	Paclitaxel	Sirolimus	Zotarolimus	Éverolimus	Biolimus = éverolimus + polymère biodégradable
Nom commercial	Taxus [®]	Cypher [®]	Endeavor [®] , Resolute [®] et Integrity [®]	Promus [®] et Xience [®]	Biomatrix [®] et Nobori [®]
Design					
Plateforme	Acier	Acier	CoCr	CoCr	Acier
Épaisseur (µm)	132	140	91	81	120
Polymère	Durable	Durable	Durable	Durable	Dégradable
Épaisseur (µm)	22 (contour)	13 (contour)	6 (contour)	8 (contour)	10 (abluminal)

X « ES » = X « Eluting Stent ».

persistante et qui est à l'origine des complications associées à l'utilisation des stents. De plus, la libération des médicaments associés aux stents actifs est limitée dans le temps. De ces constatations est née l'idée d'un stent fait d'un matériel biorésorbable : les caractéristiques physicochimiques du matériau devaient permettre son expansion et son maintien dans la forme voulue pendant un temps limité. La « disparition » des stents permettrait une cicatrisation « physiologique » et ainsi non seulement de limiter les processus de remodelage mais aussi de restaurer la vasomotricité de la paroi artérielle. Les travaux de plusieurs chercheurs académiques et industriels ont permis aux premiers stents résorbables de voir le jour au cours des 10 dernières années.

Les stents Absorb[®] (Abbott, plateforme en acide poly L-lactique directement imbibé avec de l'éverolimus) et les stent Magmaris[®] (Biotronik, plateforme en magnésium recouvert d'un polymère en acide poly L-lactique imbibé avec du sirolimus) ont été les premiers stents biorésorbables actifs mis sur le marché. Le bénéfice clinique étant très limité, l'HAS ne les a pas inscrits sur la liste des prestations prises en charge par la Sécurité sociale et en a restreint considérablement les indications : l'utilisation des stents biorésorbables doit être limitée au traitement des lésions de novo des artères coronaires natives à haut risque de resténose (lésions > 15 mm, diamètre du vaisseau atteint < 3 mm ou patients diabétiques). L'utilisation est clairement contre-indiquée en cas de sténose du tronc commun gauche non protégé, lésions pluritronculaires, lésions présentant des calcifications ne pouvant être prédilatées par ballon, après échec de l'angioplastie au ballon, (pourcentage de sténose résiduelle > 40 % ou un flux TIMI de grade < 3), lésions situées à moins de 3 mm de l'origine de l'artère interventriculaire antérieure, de l'artère circonflexe, ou de l'ostium de la coronaire droite, présence de thrombus dans le vaisseau cible. Plusieurs critères d'exclusion sur la base des caractéristiques cliniques ont aussi été établis : les patients ayant un infarctus du myocarde datant de moins de 72 heures et enzymes cardiaques non normalisées et/ou une fraction d'éjection ventriculaire gauche inférieure à 30 %, ayant bénéficié d'une angioplastie de moins de 12 mois sur le même vaisseau coronaire, présentant une intolérance au traitement

antiagrégant plaquettaire, à l'héparine, ou un haut risque hémorragique ou une insuffisance rénale. Dès 2015, l'alerte a été donnée sur le risque accru d'événements indésirables associés à l'usage des stents biorésorbables [12]. L'incidence de survenue des infarctus du myocarde et de thrombose après pose des stents de type Absorb s'est avérée plus élevée (jusqu'à 11 % contre 7 % avec Xience[®], c'est-à-dire le stent métallique imbibé du même éverolimus) à 2 ans, dans au moins 5 études [13]. La limite principale était certainement liée à la nature de la plateforme qui définit les caractéristiques mécaniques du stent. Dans les modèles in vitro, les performances mécaniques (force radiale, expansion) des stents biorésorbables semblaient comparables à celles des stents métalliques de deuxième génération [14] mais aucune étude ne les avait évaluées in vivo. À l'inverse, comparés aux informations concernant les stents actifs de deuxième génération dans la littérature, les indices de performance des stents biorésorbables sont moins bons, avec un taux d'asymétrie lésionnelle et de persistance de plaque excentrique plus élevé [15].

Le futur des stents biorésorbables doit donc passer par l'amélioration de leurs caractéristiques physicochimiques. Les nouveaux stents biorésorbables en acide polylactique sont faits de mailles plus fines (MeRes100[®], Meril LifeSciences, Inde et Firesorb[®], MicroPort, Chine) et comportent des marqueurs radio-opaques aux extrémités ou bien sont faits en polycarbonate de désaminoxyrosine mélangé à des atomes d'iode, qui rendent tout le stent radio-opaque (stent Fantom II[®], reva Medical) afin d'en faciliter le suivi sous scopie au moment de la pose. Le taux d'événements cardiovasculaires majeurs serait assez faible avec ces nouveaux stents biorésorbables (2,1 % avec le Fantom II[®] et 2,2 % avec le Firesorb[®] selon les données présentées au dernier congrès « Transcatheter Cardiovascular Therapeutics » à Washington en novembre 2016). L'amélioration des résultats pourrait aussi résulter de l'introduction, dans la pratique clinique des cardiologues interventionnels, de la postdilatation sous contrôle par OCT à la fin de la procédure, dans le but d'optimiser le déploiement du stent et réduire ainsi la survenue des événements liés au sous-déploiement [16].

Revascularisation coronaire percutanée :
 progrès et nouveaux défis associés aux
 stents de dernière génération

ENDOTHÉLIALISATION PRÉCOCE : LE DÉFI ULTIME POUR TOUS LES STENTS

Les complications biologiques (autres que celles dues à la malapposition ou au sous-déploiement) des stents sont dues à l'exposition du matériau qui les constitue aux composants du sang circulant. Ainsi, au contact avec les mailles du stent, l'activation des plaquettes et des facteurs de la coagulation est à l'origine des complications thrombotiques et l'activation des leucocytes et la prolifération des cellules musculaires lisses, qui reflètent une sorte de « rejet » de ce corps étranger, sont à l'origine de la resténose. À l'heure actuelle, pour contenir ces processus, il faut accepter les effets secondaires liés :

- à la libération des médicaments anti-inflammatoires/cytostatiques en local (retard de l'endothélialisation) ;
- à l'utilisation par voie systémique d'une double anti-agrégation plaquettaire au long cours (à cause du retard de l'endothélialisation qui prolonge le temps au cours duquel les mailles du stent restent exposées au sang circulant).

En effet, l'imagerie ex- ou in vivo des artères stentées indique que la survenue des complications est inversement proportionnelle au degré d'endothélialisation des mailles du stent [17]. Ainsi, les stratégies capables de favoriser l'endothélialisation des stents ont été mises en avant au cours des dernières années.

En 2009, OrbusNeich Medical a mis sur le marché le stent Genous[®], un stent métallique en acier inoxydable (316L) recouvert d'un polymère fixant des anticorps monoclonaux dirigés contre la molécule CD34 qui est enrichie à la surface des cellules endothéliales, permettant ainsi de capturer des progéniteurs circulants de cellules endothéliales. Sur la base de deux études et registres non comparatifs, les indications proposées étaient très larges : sténoses, jusqu'à 100 %, des vaisseaux de calibre supérieur ou égal à 3 mm et d'une longueur pouvant aller jusqu'à 40 mm, y compris les greffons veineux et les sténoses produites par des accidents peropératoires de l'angioplastie (dissections/occlusions aiguës). Cependant, en l'absence d'études comparatives avec les stents nus et actifs déjà disponibles, la HAS a conclu que l'intérêt clinique du stent Genous[®] n'était pas prouvé et ne l'a pas inscrit sur la liste des prestations prises en charge par la Sécurité sociale.

Dans notre laboratoire (Inserm U1148, Laboratory for Vascular Translational Science) et en collaboration avec le Pr Laurent Feldman, dans le département de cardiologie à l'hôpital Bichat, nous mettons au point un stent en cobalt chrome recouvert d'un polymère de dopamine (une molécule extra-adhésive en milieu aqueux dérivée des protéines utilisées par la moule pour se fixer aux surfaces de contact sous-marines) sur lequel est fixé, de façon covalente et orientée dans l'espace, une molécule agoniste du CD31, un récepteur trans-homophile exprimé par les cellules de l'interface sang-vaisseaux et qui joue un rôle clé dans l'homéostasie de la circulation. Elle est notamment présente au niveau des jonctions des cellules endothéliales et participe à la fonction essentielle de barrière endothéliale. Cette molécule induit des signaux intracellulaires opposés en fonction du type cellulaire : elle active des signaux de survie et de prolifération des cellules endothéliales et des signaux d'inhibition d'activation des plaquettes et des leucocytes. Le greffage de cette molécule répondrait donc aux problématiques actuelles de défaut de ré-endothélialisation en améliorant la cicatrisation endothéliale et de survenue

Physiopathologie cardiovasculaire

d'accidents thrombotiques en inhibant l'activation plaquettaire et leucocytaire survenant après l'angioplastie. Ainsi, l'obtention d'un meilleur profil de tolérance biologique pourrait permettre de réduire la durée de double anti-agrégation plaquettaire, limitant ainsi les événements indésirables hémorragiques. Ce projet fait l'objet d'un financement de l'Agence nationale de la recherche et de la Fondation pour la recherche médicale. Les résultats précliniques sont très encourageants et offrent de réelles perspectives d'implantation chez l'homme.

PERSPECTIVES À L'ÈRE DU NUMÉRIQUE : LES STENTS CONNECTÉS

Les événements cellulaires et moléculaires qui peuvent entraver l'intégration d'un dispositif médical dans notre organisme sont très complexes, non seulement dans l'espace mais aussi, et peut-être surtout, dans le temps. Ainsi, nos connaissances des causes de thrombose/resténose intrastent demeurent fragmentaires parce que l'histologie mais aussi les technologies les plus modernes pour l'imagerie in vivo demeurent des moyens d'analyse à un temps donné et ne peuvent pas rendre compte de la dynamique ni des liens de cause à effet des différents processus biologiques qui se mettent en place après la pose d'un stent. Dans l'ère naissante de la e-médecine, un nouveau champ d'intérêt pour les industriels des stents a vu le jour en 2014 : celui des stents dits « connectés ». La start-up française Sensome (ex. Instent) est née suite à la conception d'un guide connecté à combiner avec le « stent-retrieveur », dispositif utilisé de plus en plus dans la revascularisation des artères intracrâniennes après un accident vasculaire cérébral ischémique. Les microsenseurs appliqués sur le guide permettent l'analyse en temps réel des composants qui entrent en contact avec le stent (qualité du thrombus, de l'endothélium vasculaire, du sang en aval de l'occlusion). L'ambition d'un service médical rendu directement au patient traité grâce à ce type de guide est l'offre d'un traitement personnalisé où le choix du traitement (thrombo-aspiration ± injection locale de t-PA ± utilisation d'un *stent-retrieveur*) serait basé sur l'évidence. Les études précliniques sont en cours et la première utilisation chez l'homme est envisagée fin 2017. De tels renseignements, appliqués directement aux stents implantés, permettraient la prise en charge à un stade précoce des événements aigus tels que la thrombose intrastent. L'analyse des données télétransmises est en train de faire une vraie percée dans la e-médecine et plusieurs géants de l'informatique s'y mettent aux États-Unis. Medable, une société localisée à Palo Alto, développe la plateforme d'analyse médicale à distance ainsi que les applications associées comme par exemple « Cerebrum », la première application de « machine learning » réalisée sur des données de santé enregistrées et transmises par les objets connectés (<http://hitconsultant.net/2017/04/04/medable-launches-machine-learning-solution-specifically-healthcare-apps/>). Pour passer aux stents coronaires connectés, plusieurs défis technologiques doivent être relevés, notamment ceux afférents à la transmission à distance et dans le temps d'un dispositif médical implanté en profondeur et à demeure (source énergétique, mode de transmission sans fil, sécurité des transferts...).

Si ces défis technologiques peuvent être résolus, les senseurs tels que ceux conçus par Sensome pourraient très prochainement être montés sur les stents coronaires déjà validés cliniquement pour relever, en temps réel, l'état du revêtement

Physiopathologie cardiovasculaire

G. Caligiuri et al.

vasculaire au contact des mailles ainsi que le dépôt de fibrine, de plaquettes ou encore de leucocytes. La possibilité d'étudier la séquence d'événements qui conduit à (ou qui empêche) la cicatrisation endothéliale, selon le type de stents et de patients, contribuerait à accélérer de façon spectaculaire la conception des stents du futur.

Déclaration de liens d'intérêts

Les auteurs déclarent ne pas avoir de liens d'intérêts.

RÉFÉRENCES

- [1] Gruntzig AR, Senning A, Siegenthaler WE. Nonoperative dilatation of coronary-artery stenosis: percutaneous transluminal coronary angioplasty. *N Engl J Med* 1979;301:61–8.
- [2] Utilisation des endoprothèses (stents) coronaires en France en 2014 : Étude à partir des données du SNIIRAM; 2016, http://ansm.sante.fr/var/ansm_site/storage/original/application/235e5f608d757c81db055c84e61b7463.pdf.
- [3] Erruys PW, de Jaegere P, Kiemeneij F, et al. A comparison of balloon-expandable-stent implantation with balloon angioplasty in patients with coronary artery disease. Benestent Study Group. *N Engl J Med* 1994;331:489–95.
- [4] Fischman DL, Leon MB, Baim DS, et al. A randomized comparison of coronary-stent placement and balloon angioplasty in the treatment of coronary artery disease. Stent Restenosis Study Investigators. *N Engl J Med* 1994;331:496–501.
- [5] Ijsselmuiden AJ, Serruys PW, Scholte A, et al. Direct coronary stent implantation does not reduce the incidence of in-stent restenosis or major adverse cardiac events: six month results of a randomized trial. *Eur Heart J* 2003;24:421–9.
- [6] Morice MC, Serruys PW, Sousa JE, et al. A randomized comparison of a sirolimus-eluting stent with a standard stent for coronary revascularization. *N Engl J Med* 2002;346:1773–80.
- [7] Pfisterer M, Brunner-La Rocca HP, Buser PT, et al. Late clinical events after clopidogrel discontinuation may limit the benefit of drug-eluting stents: an observational study of drug-eluting versus bare-metal stents. *J Am Coll Cardiol* 2006;48:2584–91.
- [8] Stone GW, Ellis SG, Colombo A, et al. Long-term safety and efficacy of paclitaxel-eluting stents final 5-year analysis from the TAXUS Clinical Trial Program. *JACC Cardiovasc Interv* 2011;4:530–42.
- [9] Nakazawa G, Otsuka F, Nakano M, et al. The pathology of neoatherosclerosis in human coronary implants bare-metal and drug-eluting stents. *J Am Coll Cardiol* 2011;57:1314–22.
- [10] Lupi A, Gabrio Secco G, Rognoni A, et al. Meta-analysis of bioabsorbable versus durable polymer drug-eluting stents in 20,005 patients with coronary artery disease: an update. *Catheter Cardiovasc Interv* 2014;83:E193–206.
- [11] Pandya B, Gaddam S, Raza M, et al. Biodegradable polymer stents vs second generation drug eluting stents: A meta-analysis and systematic review of randomized controlled trials. *World J Cardiol* 2016;8:240–6.
- [12] Cassese S, Byrne RA, Ndrepepa G, et al. Everolimus-eluting bioresorbable vascular scaffolds versus everolimus-eluting metallic stents: a meta-analysis of randomised controlled trials. *Lancet* 2016;387:537–44.
- [13] Polimeni A, Anadol R, Munzel T, Indolfi C, De Rosa S, Gori T. Long-term outcome of bioresorbable vascular scaffolds for the treatment of coronary artery disease: a meta-analysis of RCTs. *BMC Cardiovasc Disord* 2017;17:147.
- [14] Foin N, Lee R, Bourantas C, et al. Bioresorbable vascular scaffold radial expansion and conformation compared to a metallic platform: insights from in vitro expansion in a coronary artery lesion model. *EuroIntervention* 2016;12:834–44.
- [15] Suwannasom P, Sotomi Y, Ishibashi Y, et al. The Impact of post-procedural asymmetry, expansion, and eccentricity of bioresorbable everolimus-eluting scaffold and metallic everolimus-eluting stent on clinical outcomes in the ABSORB II trial. *JACC Cardiovasc Interv* 2016;9:1231–42.
- [16] Maggio S, Zanetti C, Pesarini G, et al. Immediate and long-term clinical performance of bioresorbable vascular scaffolds in a real world population. *Minerva Cardioangiol* 2016;64:404–10.
- [17] Otsuka F, Finn AV, Yazdani SK, Nakano M, Kolodgie FD, Virmani R. The importance of the endothelium in atherothrombosis and coronary stenting. *Nat Rev Cardiol* 2012;9:439–53.

Résumé

Au cours des dernières décennies, les stents coronaires et les stents déviateurs de flux intracrâniens ont révolutionné le traitement endovasculaire de deux pathologies artérielles différentes : la maladie coronarienne et les anévrismes intracrâniens. Ces deux types d'endoprothèses métalliques ont des mécanismes de fonctionnement différents, mais ils sont tous deux associés à des complications qui découlent de problèmes de biocompatibilité. En particulier, la couverture rapide de ces endoprothèses par des cellules endothéliales présentant un phénotype anti-inflammatoire et anti-thrombotique est cruciale pour leur intégration à l'interface vaisseau/sang. Par conséquent, le développement de solutions visant à améliorer l'endothélialisation et l'intégration de ces deux types de stents dans la paroi vasculaire représenterait un progrès majeur dans leur domaine respectif.

Dans ce contexte, cette thèse porte sur l'immobilisation d'une molécule bioactive à la surface de stents coronaires et de stents déviateurs de flux, afin de résoudre leurs problèmes de biocompatibilité. La molécule bioactive utilisée est un peptide synthétique, appelé P8RI, qui promeut les fonctions régulatrices de la glycoprotéine transmembranaire CD31 : l'inhibition de l'activation des plaquettes et des leucocytes, ainsi que l'amélioration de la survie, de la migration et de la fonction de barrière des cellules endothéliales.

La première partie de ce travail de thèse a consisté à développer un procédé d'immobilisation du P8RI sur des stents métalliques. Nous avons successivement adopté trois approches : l'immobilisation directe du peptide sur des surfaces d'alliage fonctionnalisées par plasma ; le dépôt chimique en phase vapeur assisté par plasma d'une couche intermédiaire de polymère ; et le dépôt d'une couche de polydopamine par auto-polymérisation, suivi de l'immobilisation d'un bras d'ancrage et de la liaison du P8RI par chimie click sans cuivre.

Nous avons ensuite réalisé une évaluation *in vitro* de la biocompatibilité des surfaces d'alliage ainsi revêtues, en termes de propriétés anti-thrombotiques, anti-inflammatoires et pro-endothélialisation. Les surfaces sur lesquelles le P8RI avait été immobilisé ont montré une tendance à diminuer l'adhésion plaquettaire, à améliorer l'adhérence et la fonction de barrière de cellules endothéliales vasculaires humaines, et à promouvoir un phénotype anti-inflammatoire et anti-thrombotique chez ces dernières.

Enfin, nous avons évalué *in vivo* des stents coronaires et déviateurs de flux recouverts de P8RI. Les stents coronaires ont été implantés dans des artères coronaires de porcs, et les résultats préliminaires ont montré une endothélialisation plus complète et une moindre densité de leucocytes adhérents sur les stents recouverts de P8RI que sur les témoins. Quant aux stents déviateurs de flux recouverts de P8RI, implantés dans un modèle d'anévrisme carotidien induit par incubation d'élastase chez le lapin, ils ont été associés à la formation d'une néointima plus épaisse et mieux organisée que sur les témoins, en particulier au niveau du collet anévrisimal, ce qui implique de moindres risques de persistance du flux sanguin et de rupture d'anévrisme.